INTEGRATED MODELLING OF WHOLE-PLANT METABOLISM AND GROWTH

Tarit Konuntakiet

St Edmund Hall
University of Oxford



A thesis submitted for the degree of
Doctor of Philosophy

Trinity Term 2020

Abstract

Source-sink interactions describe the relationship between different plant organs and the division of labour in relation to source activity (resource uptake and assimilation) and sink activity (resource utilisation). Recently, multiscale growth models have been proposed as a tool to investigate unresolved aspects of whole-plant level processes, including source-sink interactions. In particular, constraint-based modelling using stoichiometric biochemical models has been shown to generate accurate predictions of metabolic fluxes and fine-grained, quantitative descriptions of plant biochemistry. The aim of this work was to develop a computational framework that captures the interactions between different organs during plant growth and the metabolic activity of each organ.

Two main modelling approaches are presented in this work. The first approach consists of stoichiometric metabolic models integrated into a previously established multiscale Arabidopsis growth model. However, exploration of the resulting model revealed that the model's structure was unable to account for the effects of non-carbon resources on growth, which led to poor predictions of growth rates.

The second modelling approach was developed to overcome this issue. I generated a whole-plant stoichiometric network of tomato metabolism by connecting organ-specific models via a common metabolite pool. Vegetative growth simulations produced predictions for metabolic fluxes that were in good agreement with known biochemistry (e.g. phototrophism in leaves and heterotrophism in stems and roots) and accurate growth patterns. Relaxing model constraints for metabolite flow between organs revealed optimal patterns of resource partitioning and utilisation for improved growth, including leaf-based nitrate assimilation, increased amino acid transport in the phloem, threonine catabolism as a carbon-efficient route for acetyl-CoA production, and branch-chain amino acids as a respiratory substrate. Additionally, simulations of reproductive growth with altered biomass partitioning patterns between organs identified reduced stem growth as being highly beneficial for increasing fruit yield. As individual biochemical reactions are represented in the model, specific molecular targets for improving plant growth and crop yield were deduced from model predictions.

Overall, the results presented in this work indicate that multiscale whole-plant models are useful tools for generating insight into plant biology. Future explorations using these models should be pursued.

Acknowledgements

First and foremost, I would like to thank Lee for your guidance and advice throughout this project. Your encyclopaedic knowledge of plant metabolism continues to amaze me. Equally, I would like to thank Sanu for letting me consult you on countless occasions. Your creative approach to coding, amazing work ethic, and patience with me were instrumental to the success of this thesis.

I would also like to thank various members of the Department of Plant Sciences. Thank you Nick for always giving me a fresh perspective on the project. Thank you Gem for always reminding me to keep the big picture in mind and to celebrate the small wins; countless DPhil students owe their sanity to you. Thank you Gla and Pedro for your advice on GC-MS. And thank you Tim and Yuan for your help with hydroponics.

Most importantly, the friends that I made throughout the DPhil have made my time in Oxford more than enjoyable. These include, and are not limited to, members of the Sweetlove Group and the biochemistry floor, Hertford College MCR, Lilly Dining Society, Teddies, and the Pierrehumbert Group. Great memories of holidays, dog walks, squash, dinners, punting, balls, parties, office chats, and general antics will undoubtedly be the parts of the DPhil that I will remember most fondly.

Much of my appreciation goes to the E.P.A. Cephalosporin Fund and St Edmund Hall for providing financial support throughout this project.

Lastly, thank you to my mother and siblings for constantly pulling me away for much needed breaks and holidays. To my mother, thank you for your constant love and support. I aspire to be as equally carefree and driven as you. To Mark, thank you for putting up with my anger on the squash court, keeping me appropriately insane, and always lending me an ear.

Abbreviations

AAP	Amino acid permease
AGPase	ADP-glucose pyrophosphorylase
BCAA	Brain-chain amino acid
CAM	Crassulacean acid metabolism
C	Carbon
CBB	Calvin-Benson-Bassham
CDM	Carbon Dynamic Model
CUpE	Carbon uptake efficiency
DAS	Days after sowing
DAE	Days after emergence
ddH_2O	Double distilled water
DW	Dry weight
dFBA	Dynamic flux balance analysis
EDTA	Ethylenediaminetetraacetic acid
ETC	Electron transport chain
FBA	Flux balance analysis
FM	Framework Model
FSPM	Functional-structural plant model
FW	Fresh weight
G3P	Glycerate-3-phosphate
GOGAT	Glutamate synthase
GS	Glutamine synthetase
GSM	Genome-scale model
LAI	Leaf area index

LUpE	Light uptake efficiency
MS	Murashige and Skoog
MSTFA	*N*-methyl-*N*-trimethylsilyl-trifluoroacetamide
MTBSTFA	*N*-*tert*-Butyldimethylsilyl-*N*-methyltrifluoroacetamide
N	Nitrogen
NGAM	Non-growth associated maintenance
NiR	Nitrite reductase
NR	Nitrate reductase
NSC	Non-structural carbohydrate
NUE	Nitrogen use efficiency
NUpE	Nitrogen uptake efficiency
OPPP	Oxidative pentose phosphate pathway
pFBA	Parsimonious flux balance analysis
P_i	Inorganic phosphate
PPFD	Photosynthetic photon flux density
QTL	Quantitative trait locus
RMA	Reduced major axis
RMSE	Root-mean-square error
RuBisCO	Ribulose-1,5-bisphosphate carboxylase oxygenase
SBPase	Sedoheptulose-1,7-bisphosphatase
SD	Standard deviation
SLA	Specific leaf area
SuSy	Sucrose synthase
TCA	Tricarboxylic acid
WT	Wild type

Contents

1 Introduction **1**
- 1.1 Source and sink metabolism . . . 1
- 1.2 Regulation of source-sink interactions . . . 6
- 1.3 Co-limitation and manipulation experiments . . . 9
- 1.4 Source-sink interactions in growth models . . . 14
- 1.5 Source-sink interactions in metabolic models . . . 18
- 1.6 Project justification . . . 24

2 Materials and methods **26**
- 2.1 Model construction . . . 26
- 2.2 Constraint-based modelling . . . 30
- 2.3 Reagents . . . 32
- 2.4 Plant growth experiment . . . 32
- 2.5 Phloem exudate metabolite profiling . . . 34
- 2.6 Statistical analysis . . . 36

3 Coupling metabolic models to a multiscale model of Arabidopsis **37**
- 3.1 Introduction . . . 37
- 3.2 Results . . . 41
- 3.3 Discussion . . . 54
- 3.4 Conclusions . . . 58

4 Constructing a whole-plant model of primary metabolism **60**
- 4.1 Introduction . . . 60
- 4.2 Results . . . 62
- 4.3 Discussion . . . 88
- 4.4 Conclusions . . . 94

5 Optimal resource partitioning of carbon and nitrogen **95**
- 5.1 Introduction . . . 95
- 5.2 Results . . . 98
- 5.3 Discussion . . . 117
- 5.4 Conclusions . . . 126

6 Optimal biomass partitioning for improved fruit yield **128**
6.1 Introduction 128
6.2 Results 130
6.3 Discussion 144
6.4 Conclusions 150

7 General discussion **152**
7.1 Summary of results 152
7.2 Metabolic models as a tool for studying source-sink interactions . 153
7.3 Limitations of the modelling approach 157
7.4 Future directions in whole-plant growth modelling 160
7.5 Closing remarks 163

References **164**

A Supplementary data **201**

B Model code **207**

1 | Introduction

Source-sink interactions are major determinants of plant growth and underlie a wide array of processes, ranging from photosynthesis to protein synthesis, through to phloem transport and cell maintenance. The principal aim of the work described in this thesis is to improve our understanding of source-sink interactions with the aid of computational models, not only to advance basic plant sciences, but also to apply this knowledge to optimise plant growth in the agricultural setting.

1.1 Source and sink metabolism

Nearly a century ago, Mason and Maskell (1928) first proposed the idea of classifying plant organs as sources and sinks. Source organs are net exporters of a specific resource, whereas sink organs are net importers. For example, mature leaves are sources of carbon but sinks for inorganic nitrogen, whereas roots are the sole source of inorganic nitrogen but act as a sink for carbon. Table 1.1 lists the source/sink status of the major plant organs in Arabidopsis and tomato (the two main species of focus in this study) in relation to carbon and nitrogen. It also shows that source/sink status depends on the resource under consideration and the developmental stage of the organ.

Source organs often acquire external resources from the environment, though stored resources can be remobilised from sink organs, turning them into sources. For example, storage organs, such as seeds, are sink organs during their development, but are source organs during the initial phase of germination. On the other

Table 1.1: Major plant organs in Arabidopsis and tomato categorised as either sources or sinks of carbon (C), inorganic nitrogen (N_i), and organic nitrogen (N_o). Immature leaves refer to those that are still growing, whereas mature leaves have fully expanded.

Status	Immature leaves	Mature leaves	Fruits	Roots	Stems
Source	-	C, N_o,	-	N_i	-
Sink	C, N_i, N_o	N_i	C, N_i, N_o	C, N_o	C, N_i, N_o

hand, sink organs take up resources from source organs for the production of new biomass and the maintenance of existing tissues. The sink strength of an organ is defined as the net rate of import of a specific resource, which is determined by the organ's size and sink activity (capacity for utilisation of the import resource; Chang and Zhu, 2017). Source strength can also be similarly defined as the net rate of export of a specific resource (Chang and Zhu, 2017).

1.1.1 Carbon metabolism

C_3 photosynthesis is the most common metabolic pathway for fixing carbon in plants (Stitt et al., 2010). In illuminated leaves, carbon dioxide is converted into triose phosphates by ribulose-1,5-bisphosphate carboxylase/oxygenase (RuBisCO), a constituent enzyme of the plastidial Calvin-Benson-Bassham (CBB) cycle. Assimilated carbon can remain in the leaf to be respired to generate energy for growth, used to synthesise biomass components, or stored as a polymer (e.g. starch or fructans) for future use (Stitt et al., 2010).

Alternatively, assimilated carbon can be exported from the leaf via the phloem. To support this, triose phosphates from the CBB cycle are exported out of the chloroplast to the cytosol and used to produce sucrose (Stein and Granot, 2019). Sucrose is the main form of carbon transported from source organs towards sink organs, where it can be respired to provide energy or used to provide carbon skeletons for biomass production (Liu et al., 2012).

Following uptake into cells in sink organs, sucrose is either hydrolysed by

cytosolic invertase to produce glucose and fructose, transported to the vacuole for storage, or catabolised by sucrose synthase (SuSy) to produce fructose and UDP-glucose (Stein and Granot, 2019). A vacuolar isoform of invertase is also present to allow for hexose storage in the organelle (Ruan, 2014). Alternatively, sucrose can be hydrolysed by extracellular invertase in the apoplast, allowing for hexose uptake across the plasma membrane (Ruan, 2014).

1.1.2 Nitrogen metabolism

Plants grown in well-fertilised soils take up nitrogen through the root mainly as nitrate, although ammonium and amino acids can also be taken up (Wang et al., 2006). A notable exception to this are legumes, which host nitrogen-fixing rhizobia in root nodules, which provide the plants with ammonium. Within the plant, nitrate is reduced to nitrite by nitrate reductase (NR), and then further reduced to ammonium via nitrite reductase (NiR). Ammonium can then be assimilated into amino acids via the glutamine synthetase/glutamate synthase (GS/GOGAT) pathway (Xu et al., 2012).

The site of nitrate assimilation varies between species and environmental conditions. For example, temperate, perennial species mostly limit nitrate assimilation to the root in low nitrate soils, whereas tropical species mostly assimilate nitrate in the shoot (Andrews, 1986). In this thesis, I focus on Arabidopsis and tomato, which both show higher NR activity within leaves, compared to roots (Park et al., 2011; Flores et al., 2004; Brewitz et al., 1996). This suggests that following uptake into the root, nitrate is transported to leaves for assimilation into amino acids. Generally, the ultimate fate of amino acids is to be used as a substrate for protein synthesis. Source leaves can partition a portion of their amino acid pool into their own growth, while the rest can be transported to sink organs to support growth (Tegeder and Hammes, 2018). Leaves have a notably high demand for

nitrogen for use in assembling and maintaining photosynthetic enzymes, with RuBisCO accounting for up to 50% of the leaf's nitrogen content (White et al., 2016). RuBisCO also provides an example of how carbon and nitrogen metabolism are highly interconnected: it mediates carbon source activity, but is dependent on nitrogen sink activity.

1.1.3 Plant vasculature

In vascular plants, the flow of metabolites between source and sink tissues is mediated by the xylem and the phloem. The xylem is formed of non-living hollow lignified cells that provide a low-resistance pathway for water and nutrient transport from the root to the shoot. The movement of water through the column is driven by the negative pressure generated in leaves as a result of transpiration via stomata and thus requires no energetic expenditure. Mineral macronutrients that are commonly transported via the xylem following uptake into the root include calcium, chlorine, magnesium, nitrate, phosphate, potassium, and sulphate (Grünzweig et al., 1998; Bialczyk and Lechowski, 1995). Ion loading from root xylem parenchyma cells into the xylem vessel is mediated by voltage-dependent ion channels (Köhler and Raschke, 2007; Gilliham and Tester, 2005). Following transport to the shoot, nutrients are unloaded from the xylem into the apoplast. Energy-dependent cellular uptake mechanisms then facilitate transport into the symplast (Reid and Hayes, 2003).

In contrast to the dead cells that make up the xylem, the phloem consists of a network of living sieve tube elements, connected by extensive plasmodesmata to form a symplastic highway (Omid et al., 2008). Metabolite transport through the phloem is driven by pressure flow, where the high concentration of organic solutes in source leaf phloem cells draws in water from adjacent xylem vessels along osmotic gradients (de Schepper et al., 2013). This increases the hydrostatic

pressure within the phloem, driving the movement of phloem contents towards sinks, where the pressure is lower due to the unloading of metabolites into the sink tissues. In principle, this allows mass flow through the phloem to be bidirectional, in contrast to the xylem's unidirectional upward flow.

Though in most plants sucrose constitutes the major transport metabolite in the phloem, the composition of phloem sap varies significantly between species and plant developmental status (Wilkinson and Douglas, 2003; Karley et al., 2002; Valle et al., 1998). For example, Wilkinson and Douglas (2003) reported that the sugar content of 16 plant species ranged between 50–90% of the phloem. In source leaves, mesophyll cells export sucrose into the extracellular space via SWEET proteins, where it is actively taken up by phloem companion cells via SUT sucrose/proton symporters for subsequent symplastic transfer into sieve tube elements (Braun et al., 2014). In sink organs, sucrose can either be unloaded from the phloem via the symplast or apoplast (Osorio et al., 2014). In tomato fruits, for example, sucrose is unloaded symplastically under low to intermediate carbon demand. Whereas under high demand, apoplastic unloading is preferred as extracellular invertase can cleave sucrose into hexoses to maintain a strong osmotic pressure gradient between source and sink cells (Ruan and Patrick, 1995).

A significant amount of amino acids are also transported via the phloem; all 20 proteinogenic amino acids have been detected in phloem sap, with glutamate, glutamine, asparagine, aspartate, and serine being the most abundant (Wilkinson and Douglas, 2003; Karley et al., 2002; Valle et al., 1998). Relatively few studies have attempted to characterise leaf amino acid export but it is thought that the apoplastic route is taken in most crop plants and Arabidopsis (Tegeder and Masclaux-Daubresse, 2018). Several transporters have been proposed to facilitate amino acid export from mesophyll cells, including UmamiT18 (glutamine exporter) and SIAR1 (bidirectional transporter of several amino acids; Tegeder

and Masclaux-Daubresse, 2018; Ladwig et al., 2012). And several members of the amino acid permease (AAP) family (proton-coupled symporters), cationic amino acid transporters, and proline and compatible solute transporters (ProTs) have been shown to import amino acids into the phloem (Tegeder and Hammes, 2018; Perchlik and Tegeder, 2017).

1.2 Regulation of source-sink interactions

The dynamic balance between source and sink activities ensures that a plant can appropriately adapt its growth to the resources available. Plants can assimilate carbon in excess to its growth requirement and store it for future use, but this can only happen if the plant has sufficient sink strength. Sinks must therefore exert some control on source activity (White et al., 2016). Conversely, sources control the growth and development of new sinks to allow for resources to be used (White et al., 2016). There is thus a large network of mechanisms regulating source-sink interactions.

1.2.1 Carbon regulation

Leaf carbon source activity is regulated via the control of photosynthesis at multiple points throughout central metabolism. It is well-established that the accumulation of non-structural carbohydrates (NSCs), which is influenced by carbon sink activity and leaf carbon export, represses photosynthetic activity. NSCs have been found to generate various redox signals that downregulate the expression of photosynthetic genes (Paul and Foyer, 2001). Excessive starch accumulation in leaf chloroplasts can also result in organelle damage, reducing photosynthetic activity (Delucia et al., 1985). High levels of glucose sensed by hexokinase in the leaf leads to stomatal closure, limiting the supply of atmospheric carbon dioxide (Kelly et al., 2013). Over a longer time-scale, NSC accumulation ultimately affects leaf development and

senescence (Pourtau et al., 2006).

At shorter timescales, photosynthesis is regulated by inorganic phosphate (P_i). ATP production via the light-dependent reactions requires a supply of P_i. However, under high photosynthetic flux, the rate of P_i recycling to the chloroplast becomes limited by the rate of sucrose synthesis, which determines the release of P_i from photosynthates (Stitt, 1986).

Low leaf carbon source activity also exerts control of carbon sink activity. The protein kinase SnRK1 and C/S1 bZIP transcription factors have both been reported to repress growth in response to reduced carbon source activity (Lastdrager et al., 2014). The activities of these regulators are downregulated by increased sucrose and triose phosphate pool sizes resulting from an increase in photosynthetic activity.

1.2.2 Nitrogen regulation and carbon-nitrogen interactions

Similarly to carbon in leaves, feedback regulation acts on nitrogen source activity in the root. High nitrate levels in root tissues result in a reduction in nitrogen transporter activity, the repression of nitrate uptake genes, and the inhibition of lateral root meristem growth (Zhang et al., 2007; Vidmar et al., 2000; Glass et al., 2002; Vidmar et al., 2000). High root nitrate concentrations also upregulate NR expression (Stitt and Krapp, 1999). Conversely, nitrogenous end-products, such as glutamine, can repress NR transcription (Klein et al., 2000). Additional, external nitrate in soil can promote lateral root elongation to increase nitrogen uptake capacity (Zhang et al., 2007).

The regulation of source-sink interactions extends beyond mechanisms governing carbon and nitrogen metabolism in isolation. A high degree of control arises from the crosstalk between the two networks. Ultimately, nitrogen metabolism is dependent on carbon, and vice versa. An elevated nitrogen status has been reported to promote both carbon source and sink activity, via photosynthesis and

a higher shoot:root ratio (Stitt and Krapp, 1999). The reciprocal increase in carbon activity allows the plant to use more of the available nitrogen.

Some processes are co-regulated by both carbon and nitrogen substrates. For example, starch accumulation in leaves is regulated via allosteric activation by triose phosphates and repression by nitrate of ADP-glucose pyrophosphorylase (AGPase), a constituent enzyme in the starch synthesis pathway (Stitt and Krapp, 1999). Reducing the amount of carbon stored as starch allows for a higher sucrose export rate from source leaves for co-utilisation with nitrogen in sink tissues. Nitrate assimilation is also upregulated by both sugars and nitrate in the root (Klein et al., 2000; Stitt and Krapp, 1999). In fact, the regulation of NR expression and post-translational modification by carbohydrates becomes more critical than nitrate at low carbon status (Reda, 2015; Kaiser et al., 2002; Klein et al., 2000; Stitt and Krapp, 1999).

Recently, the TOR protein complex has been identified as a master regulator of plant metabolism in response to carbon/nitrogen (C/N) status. Under high nutrient availability conditions (carbohydrates and amino acids) and an elevated energy status, the TOR complex promotes growth, protein synthesis, and cell proliferation (Bakshi et al., 2019). Conversely, under abiotic stress conditions and nutrient limitation, the TOR complex activates the transcription of stress responsive genes, promotes root growth to increase nutrient uptake capacities, and decreases the rate of chlorophyll degradation to maintain a high carbon source capacity (Bakshi et al., 2019). Many aspects of the specific molecular mechanisms underlying TOR signalling still remain unresolved, but recent progress has provided some insight. For example, O'Leary et al. (2020) reported that the TOR complex inactivates proline dehydrogenase, a constituent enzyme in the proline catabolism pathway, via phosphorylation. Additionally, S6 kinase is also a substrate of the TOR complex's kinase activity and promotes protein translation at the ribosome when

activated by phosphorylation. Consequently, the activation of TOR signalling by amino acids and carbohydrates (through unknown nutrient sensing mechanisms) shifts the role of amino acids as a respiratory substrate in catabolic pathways towards anabolic pathways via protein synthesis under nutrient-rich conditions.

Various phytohormones also play an important role in mediating the crosstalk between carbon and nitrogen metabolism at the whole-plant level. A high nitrogen status in the root promotes the transport of cytokinins to the shoot (Stitt and Krapp, 1999). In the shoot, cytokinins promote photosynthetic activity via RuBisCO and the upregulation of various photosynthetic genes, delay leaf senescence, and stimulate cell division and shoot sink strength (Cortleven and Schmülling, 2015; Paul and Foyer, 2001; Jordi et al., 2000). The last of these effects increases the shoot:root ratio, allowing for more carbon to be captured to match the increase in nitrogen availability (Ghanem et al., 2011; Kuiper, 1993). Throughout the plant, NR activity is increased by cytokinins (Stitt and Krapp, 1999). Other important signalling molecules include ethylene, abscisic acid, and various transcription factors; these have been found to control grain filling, fruit development, leaf carbon transport, and nutrient uptake from the soil (Chen et al., 2016; Wang et al., 2012; Yang et al., 2001).

1.3 Co-limitation and manipulation experiments

Significant increases in food production are required in response to the predicted growth in human populations in the face of shifting environmental conditions (Alexandratos and Bruinsma, 2012). The importance of understanding source-sink interactions thus stems from the potential to optimise resource allocation in plants for greater crop yields. This requires mechanistic knowledge of whether plant growth is controlled by source or sink limitation. The presence of the vast network of regulatory mechanisms would suggest that plants constantly adapt so that their

source-sink balances can be dynamically optimised (Chang and Zhu, 2017). Results from the experimental manipulation of source or sink activities suggest that both source and sink activity exert a degree of control on growth.

1.3.1 Manipulating source activity

Much interest has been placed on optimising photosynthesis for increased crop yields; this assumes that carbon source activity limits growth (Fernie et al., 2020). Faster growth rates have been consistently reported for various plant species grown in elevated CO_2, which increases source capacity (Nguyen et al., 2017; Leakey et al., 2009; Ainsworth et al., 2006; Ainsworth and Long, 2005; Fangmeier et al., 2000; Nicolas et al., 1993). Increasing pot size to improve the source strength for both nitrogen and carbon also results in greater yields (Poorter et al., 2012a).

More recently, targeting potential bottlenecks in photosynthesis through genetic engineering experiments has identified multiple approaches for improving source efficiency, including engineering C_4 in C_3 plants, minimising carbon loss through photorespiration, improving the catalytic efficiency of RuBisCO and the CBB cycle, reducing water loss through stomata, and reducing adjustment times to light fluctuations (Fernie et al., 2020; López-Calcagno et al., 2020; Papanatsiou et al., 2019; South et al., 2019; Sharwood et al., 2016; Kromdijk et al., 2016; Nölke et al., 2014). For example, the regeneration of ribulose-1,5-bisphosphate by sedoheptulose-1,7-bisphosphatase (SBPase) in the CBB cycle was predicted by computational modelling to be rate-limiting under elevated CO_2 (Long et al., 2015). Transgenic overexpression of SBPase has been reported to significantly increase plant biomass and photosynthetic efficiency in wheat, tobaco, Arabidopsis, and rice (López-Calcagno et al., 2020; Driever et al., 2017; Simkin et al., 2017; Gong et al., 2015; Simkin et al., 2015; Lefebvre et al., 2005). In another example, the introduction of transgenic bypasses to minimise carbon loss and energy expenditure through

photorespiration has also been shown to increase shoot biomass by up to 40% in field-grown tobacco (South et al., 2019).

Explicitly improving nitrogen source capacity also results in improved growth and nitrogen use efficiency (NUE). Overexpressing cytosolic GS leads to faster growth in various species, and overexpressing AMT1 (an ammonium membrane transporter) leads to higher grain yields and increased filled grain number in rice (Ranathunge et al., 2014; Thomsen et al., 2014).

Nevertheless, plant growth models have highlighted that the observed increases in growth under elevated CO_2 do not match predicted theoretical improvements, suggesting a degree of sink limitation (Leakey et al., 2009; Ainsworth et al., 2008; Long et al., 2006). Further, decreasing source strength by defoliation has been shown to increase photosynthetic activity in the remaining leaves (Eyles et al., 2013; von Caemmerer and Farquhar, 1984). The source potential of each leaf was therefore not maximised prior to manipulation, providing evidence of sink limitation.

1.3.2 Manipulating sink activity

As with source metabolism, much interest has also been dedicated to manipulating sink strength. Typically, these studies are carried out in plants with large sink organs, including tomato, potato, and cereal crops (Sonnewald and Fernie, 2018). Increased starch content and final yield have been reported in many species following sink-specific engineering of starch metabolism. In wheat, seed mass increased by 38% in lines expressing a transgenic version of AGPase less susceptible to allosteric inhibition by P_i, and a similar increase of 23% was reported in rice (Smidansky et al., 2003, 2002). In potato, upregulating SuSy in tubers to promote sucrolytic activity to provide precursors for starch synthesis resulted in increases in tuber dry weight and starch content (Baroja-Fernández et al., 2009).

Impressive yield increases have been reported in studies increasing energy availability for starch synthesis in sink organs. For example, a 16% increase in tuber yield was reported when plastidial glucose-6-phosphate and adenylate translocators were upregulated in potato (Zhang et al., 2008). Additionally, downregulating plastidial adenylate kinase to increase the pool size of adenylates for starch synthesis increased tuber starch content by 16% and tuber yield by 86% (Regierer et al., 2002). Using the same rationale, similar increases were reported in lines with reduced uridine monophosphate synthase activity (Geigenberger et al., 2005).

Recently, Amthor et al. (2019) provided suggestions for improving growth by minimising carbon loss through respiration, many of which affect sink efficiency. For example, slowing protein and membrane turnover should reduce the cost of degrading and resynthesising them; as should suppressing futile cycles and reducing ion transport costs (Ishihara et al., 2017; Cairns and Gallagher, 2004; Whitlow et al., 1992). Specific molecular targets were suggested by Amthor et al. (2019) and remain to be tested.

1.3.3 *Push and pull* approaches

It is evident from manipulation experiments that target source and sink activity in isolation that both source and sink strength can co-limit plant growth. Yield increases can arise from increasing one or the other. It is therefore rational to assume that when source strength is increased, sink activity becomes more limiting, and vice versa (Sonnewald and Fernie, 2018). The simultaneous engineering of both sources and sinks, so called *push and pull* approaches, should therefore result in the largest yield improvements. Evidence of this is provided by various wheat cultivars grown in elevated CO_2. Increases in source carbon activity was only observed in cultivars with a high harvest index, indicating a dependency on high sink strength (Aranjuelo et al., 2013). Similarly, species-specific sink size was a

determining factor for increased biomass production in various *Brassica* species grown in elevated CO_2 (Reekie et al., 1998).

Increasing tuber sink strength in potato by overexpressing plastidial glucose-6-phosphate and adenylate translocators to promote starch synthesis has been coupled to improving source strength to great success in triple transgenic experiments. In one example, the antisense expression of leaf AGPase to reduce shoot starch accumulation resulted in the doubling of tuber starch content (Jonik et al., 2012). Similar increases were reported when soluble pyrophosphatase was overexpressed in mesophyll tissue to enhance sucrose production in leaves (Jonik et al., 2012). In both examples, carbon transport to sinks was promoted at the expense of leaf starch storage. The yield increases reported were larger than when each genetic target was engineered in isolation, showing the promising potential of *push and pull* approaches.

1.3.4 Manipulating source-to-sink transport

Though much less well-explored compared to source and sink activity, the transport of nutrients and metabolites between source and sink organs is also fundamental to growth. Transport resistance within the phloem has been shown to not be limiting to long-distance metabolite flow between organs. Wheat plants forced to grow with only one seminal root showed very high rates of flow through the root base phloem and exhibited no detrimental effects on growth (Passioura and Ashford, 1974). The removal of significant portions of the phloem area by girdling in four different tropical tree species also had no effect on leaf carbohydrate accumulation and photosynthesis, suggesting that assimilate export from source leaves was unaffected (Asao and Ryan, 2015).

In contrast, phloem loading and unloading, which both rely on transmembrane transporters, have been identified as potential areas for significant improvement.

For example, the simultaneous overexpression of SUT1, a sucrose transporter, in both leaf phloem and seed cotyledon epidermal tissues resulted in higher rates of sucrose flow from leaves to seeds in *Pisum sativum* (Lu et al., 2019). SUT1 mediated both the loading of sucrose into the phloem and also the import of sucrose into developing pea seeds. Compared to the WT, the transgenic peas had increased levels of sucrose and starch, and a higher seed yield.

Amino acid transporters have also been targeted for enhanced loading into the phloem and developing seeds. AAP1, a broad-specificity amino acid permease, was overexpressed in both leaf phloem and seed cotyledon tissues, leading to improved amino acid translocation, seeds with higher protein content, and increased seed yield (Zhang et al., 2015). Under a range of soil nitrate conditions, the transgenic pea plants also displayed better NUE as a result of a positive feedback effect by AAP1 overexpression on root nitrate uptake and nitrate assimilation (Perchlik and Tegeder, 2017).

1.4 Source-sink interactions in growth models

The optimisation of source-sink interactions clearly presents an attractive target for improving plant growth. However, the factors underlying a plant's response to environmental and molecular intervention are complex, multivariate, and often also non-linear. As a result, many of the potential targets for manipulation may be non-intuitive and difficult to predict without the aid of mechanistic models of plant growth. A systems approach to studying source-sink interactions has a long history that can be traced back to early models of shoot-root interactions and photosynthate partitioning in vegetative plants (Thornley, 1972a,b).

Compared to sink metabolism, there is a much larger body of literature modelling source metabolism. Many highly detailed and mechanistic models of photosynthesis are available and have historically proven to be powerful at analysing

source behaviour (Bernacchi et al., 2013; von Caemmerer, 2013; Zhu et al., 2013; Farquhar et al., 1980). These models require precise knowledge of kinetic parameters and take environment conditions as inputs, including radiation, internal leaf CO_2 concentration, and temperature. Many of the strategies proposed by these models have been applied *in planta* to confirm yield increases, including overexpressing SBPase, increasing the carboxylation rate of RuBisCO, and reducing flux through photorespiration (South et al., 2019; Driever et al., 2017; Sharwood et al., 2016).

In contrast, models of sink activity are much more limited in number and are often highly simplified, though a few relatively mechanistic models are available (Amthor, 2000; Cannell and Thornley, 2000). Yet, to model source-sink interactions, both resource assimilation and growth have to be accounted for. Many models address this by connecting a well-established source model to a highly reductive sink model. Non-growth associated maintenance (NGAM) is often just a function of temperature or leaf carbon status and growth respiration is reduced to a single coefficient expressed as a fraction of total carbon assimilated (Wu et al., 2019; Rasse and Tocquin, 2006). Although an ecosystem-level model recently showed the importance of factoring temperature on sink growth in alpine trees growing across an attitudinal gradient, very few models have attempted to account for mechanisms of sink control, such as the repression of photosynthesis by low sink strength (Leuzinger et al., 2013). The lack of detail on sink activity (e.g. the cost of assimilate transport, protein synthesis, biomass production, and protein turnover) limits the predictive power of these models.

An important class of whole-plant growth models is functional-structural plant models (FSPMs; Sievänen et al., 2014). In these models, plant organs are divided into modular units and both the topology and geometry of organs are accounted for (Yan et al., 2004). Growth is simulated using ecophysiological principles, whereby physiological (e.g. photosynthesis) and physical (e.g. stem branching and elon-

gation) processes are driven by environmental factors, including temperature, water, light, and atmospheric CO_2 concentration. Given the importance of plant architecture in FSPMs, they are powerful tools for analysing carbon partitioning and resource allocation dynamics between different organs. FSPMs have been used to determine the effect of source:sink ratios on tomato fruit-setting, phenotypic plasticity in response to plant spacing, resource competition between sinks, and kernel filling in maize (Ma et al., 2018; Kang et al., 2011; Dong et al., 2008; Christophe et al., 2008). However, FSPMs rely heavily on parameter fitting and require a larger amount of empirical data as inputs to predict growth accurately. FSPMs also contain no molecular detail, leading to limitations in predicting genetic targets for manipulation. For example, the entirety of the plant metabolic network was reduced to two equations in an FSPM of Arabidopsis (Christophe et al., 2008).

A common limitation of all aforementioned modelling methods is that growth is often solely driven by carbon availability. But the availability of other elemental resources clearly also exerts some control on growth. Some models have attempted to account for the effect of nitrogen and phosphorus, but an ideal model would be able to consider the limiting effect of all key resources and their metabolic interactions (Brown et al., 2019; Caldararu et al., 2020; Feller et al., 2015; Guilbaud et al., 2015; Verkroost and Wassen, 2005; Bijlsma and Lambers, 2000).

1.4.1 Multiscale whole-plant growth models

There is a strong consensus within the plant modelling community that there needs to be a framework for establishing multiscale plant growth models (Benes et al., 2020; Peng et al., 2020; Millar et al., 2019; Chew et al., 2017b; Marshall-Colon et al., 2017; Zhu et al., 2016). This refers to models that integrate biological knowledge at various spatial and temporal scales, ranging from genetics to metabolism, through to physiology, anatomy, structure, and ecosystems. Many different aspects

of plant biology have been modelled, including photosynthesis, tree branching patterns, assimilate transport, the genetic regulation of anthesis, and field management strategies (Koch et al., 2018; Seleznyova and Hanan, 2018; Zhang et al., 2018; Peyhardi et al., 2017; Brown et al., 2013; Zhu et al., 2013; Migue et al., 2012). A multiscale model would combine these pre-existing models to increase its potential to identify unknown mechanistic details and provide a more comprehensive depiction of plant growth.

Many obstacles are present that make developing a multiscale model difficult, including the lack of transparency and access to data and software/code, and the lack of both computational (e.g. scripting language) and biological (e.g. units of measurements) standardisation. However, guidelines set out by initiatives like the *Crops in silico* consortium should facilitate collaboration between different research groups in the future (Benes et al., 2020; Millar et al., 2019; Marshall-Colon et al., 2017).

Of the few examples available, a multiscale growth model of Arabidopsis provides an excellent example of how model integration can aid us in studying source-sink interactions. In the Framework Model (FM), Chew et al. (2014) connected an FSPM to models of source carbon metabolism, photoperiodism, and photothermal development. By accounting for both the gene regulation of the circadian clock and leaf carbon metabolism, the model was able to predict photosynthetic adaptation and flexible leaf starch metabolism under different day length regimes (Chew et al., 2017a, 2014). More recent work using the FM identified that growth repressors exert control on leaf development, affecting source capacity and sink strength to regulate plant growth rates (Pullen et al., 2019). These examples show that the use of multiscale models is clearly an attractive approach for exploring source-sink interactions.

1.5 Source-sink interactions in metabolic models

The need for molecular detail of the biochemical processes underlying source and sink activity in whole-plant models is evident from the perspective of predicting specific targets for yield improvements. This can be achieved by constructing metabolic models, of which there are two main approaches (Kruger and Ratcliffe, 2015). Kinetic modelling provides a powerful framework for analysing metabolic networks and consists of reactions described by their chemical stoichiometry and rate equation (Baghalian et al., 2014; Rohwer, 2012). Using specified initial concentrations of metabolites, kinetic models can predict changes in metabolite concentrations and reaction rates over time, whilst also accounting for allosteric regulation. However, kinetic models require a large number of empirically-derived kinetic parameters, often limiting their scope to smaller subsystems within the wider plant metabolic network. For example, even though *e-Photosynthesis*, a kinetic model of carbon source activity in C_3 plants, provided several important insights into improving photosynthetic efficiency, the network of 100 reactions presented a considerable challenge to parameterise and analytically solve, and several key aspects of leaf photosynthesis (e.g. the export of triose phosphates from the chloroplast and their utilization in the cytosol) remain poorly described in the model (Zhu et al., 2013).

1.5.1 Stoichiometric modelling

The alternative approach is stoichiometric modelling, in which reactions are defined solely by their chemical stoichiometry. With the advent of better sequencing technologies and computing power, genome-scale models (GSMs) of species-specific metabolic networks can be generated with relative ease (Chiewchankaset et al., 2019; Yuan et al., 2016a; Cheung et al., 2014; Poolman et al., 2013; de Oliveira

Dal'Molin et al., 2010a; Mintz-Oron et al., 2012; Radrich et al., 2010; Poolman et al., 2009). As there is no requirement for kinetic parameters as inputs, networks with thousands of reactions are common in GSMs. Further curation of these models can include specifying subcellular compartmentalisation, metabolite charge states, and energetic costs (Shameer et al., 2019; Shaw and Cheung, 2019; Cheung et al., 2014, 2013).

The most common method for identifying biologically relevant flux distributions in such models is flux balance analysis (FBA). A stoichiometric model is represented by a matrix (**S**) of size m x n, where columns represent reactions and rows represent compounds (Orth et al., 2010). The entries in **S** equate to the reaction stoichiometries of the network. Vector **v** represents the fluxes through reactions, which can each be assigned lower (l) and upper (u) bounds. The solution space of the network thus has to satisfy the following two conditions: $\mathbf{S} \cdot \mathbf{v} = 0$ and $l_i < \mathbf{v_i} < u_i$, where i is a reaction. The first equation describes the matrix **S**'s mass balance constraint, where any compound produced in the system has to be consumed in an equal amount and assumes the model to be at steady-state. Most large-scale stoichiometric models are underdetermined, meaning that there are more reactions in the network than there are metabolites. The consequence of this is that there is often more than one flux distribution that can satisfy the model constraints. FBA uses linear programming to identify optimal points within the solution space by seeking to maximise or minimise a predefined objective function, which is often chosen to reflect specific biological assumptions.

As GSMs contain all the reactions needed to sustain life in all plant tissues (the so-called *reactome*), they can be used to simulate a range of metabolic behaviours. The simplest approach is to model a single cell type by imposing tissue-specific constraints. For example, sink metabolism can be simulated by allowing for assimilate uptake into the model (representing the supply of resources from source

tissues), and specifying the objective function to maximising biomass production. By providing tissue-specific biomass compositions, sink models have been constructed for seeds, fruits, roots, root nodules, stems, and heterotrophic cell culture in a variety of species (DiCenzo et al., 2020; Shameer et al., 2020; Chiewchankaset et al., 2019; Scheunemann et al., 2018; Yuan et al., 2016a; Colombié et al., 2015; Cheung et al., 2013; de Oliveira Dal'Molin et al., 2010a; Grafahrend-Belau et al., 2009; Poolman et al., 2009). These models have been used to elucidate the role of climacteric crises and transitory starch storage in developing tomato fruits, C/N balances on cassava storage root yield, and NGAM in Arabidopsis cell culture under stress (Shameer et al., 2020; Chiewchankaset et al., 2019; Colombié et al., 2015; Cheung et al., 2013).

Similarly, source metabolism in leaves can be simulated by allowing for light uptake into the model and specifying the objective function to maximising the export of photosynthates to the phloem. To this end, source leaf models have been used to explore the role of photorespiration in energy dissipation at high light intensities, metabolic plasticity in response to gene deletions, the importance of mitochondrial respiration on leaf energy balances, the energetic efficiencies of Crassulacean acid metabolism (CAM), and the role of transient organic acid accumulation in providing carbon skeletons for leaf exports (Shameer et al., 2019, 2018; Shaw and Kundu, 2015; Cheung et al., 2014; Poolman et al., 2013).

Cheung et al. (2014) devised an important framework for simulating the relationship between the light and dark phases of source metabolism. A diel model can be constructed by duplicating a stoichiometric model, constraining each copy of the model to represent each phase, and specifying linker reactions between the two models to represent metabolite accumulation over each phase. This multiphase set-up has been reported to generate more accurate predictions of leaf activity compared to a constant light model, with daytime autotrophic behaviour inter-

acting with night-time heterotrophic behaviour via transient starch, organic acid, and amino acid accumulation (Cheung et al., 2014) . This framework also allowed for an analysis of CAM, for which temporal resolution is critical (Shameer et al., 2018; Cheung et al., 2014). Additionally, this approach has been used to simulate interactions at the spatial-scale between different tissue types. For example, malate transport between mesophyll and bundle sheath cells is an important part of C_4 photosynthesis. Various multi-cell models of C_4 metabolism have shed light on metabolite shuttling for proton balancing, the effect of CO_2 leakage, and the role of secondary metabolism in various grass species (Shaw and Cheung, 2019; Saha et al., 2011; de Oliveira Dal'Molin et al., 2010b).

1.5.2 Whole-plant metabolic models

To model whole-plant processes like source-sink interactions, the same framework used to model interactions between different cell types can be expanded to simulate relationships between different plant organs (Shaw and Cheung, 2020). Compartments linking these organs facilitating metabolite flow can either constitute a common pool or explicitly state the linkages between organs. Whole-plant stoichiometric modelling makes a particularly attractive platform for modelling source-sink interactions as equal importance can be given to all elemental resources, preventing the model from being driven purely by carbon (a common issue in plant growth models). Additionally, equal importance can be given to source and sink activity, where the same level of fine-grain molecular detail can be accounted for in all organs, allowing for the effect of precise genetic perturbations to be characterised.

Though the field is relatively nascent, several whole-plant metabolic models have been constructed for Arabidopsis, barley, soybean, *Medicago truncatula*, and *Setaria viridis* (Table 1.2). These studies have explored various aspects of

source-sink interactions, including grain filling, sink-to-source shifts in storage organs, the division of energy expenditure between organs, herbivory-induced source limitation, and seedling germination (Shaw and Cheung, 2018; de Oliveira Dal'Molin et al., 2015; Grafahrend-Belau et al., 2013).

Of particular note is the earliest example of a whole-plant stoichiometric model, where barley leaf, stem, seed, and root metabolic models were connected via a phloem compartment and coupled to an FSPM (Grafahrend-Belau et al., 2013). The model provided novel insights into the importance of resource remobilisation from stem tissue for grain filling in the face of reduced source capacity resulting from leaf senescence. These predictions could only be generated by a model that accounted for the metabolism of all major plant organs. However, Grafahrend-Belau et al. (2013) only included a trivial three-reaction root compartment, limiting the analysis of root metabolism severely. Furthermore, dynamic constraints for carbon partitioning between organs were supplied from the FSPM to the stoichiometric models without any fluxes being relayed back to the FSPM after model optimisation. This meant that metabolic flux predictions exerted no control on growth

Table 1.2: Published whole-plant metabolic models of plant growth that use stoichiometric modelling. Keys for model limitations are as follows: (a) growth is not driven by metabolism, (b) growth is static and only provides a snapshot of metabolism (c) major plant organs are missing from the model, and (d) growth predictions were not validated against growth data. dFBA, dynamic flux balance analysis; FBA, flux balance analysis; FSPM, functional-structural plant model.

Reference	Species (organs)	Driver of growth	Scope of analysis	Limitations
Shaw and Cheung (2018)	Arabidopsis (leaf, root)	dFBA	Environmental and physiological perturbations	d
Zakhartsev et al. (2016)	Arabidopsis (leaf, root)	FBA	Sucrose translocation	b,d
de Oliveira Dal'Molin et al. (2015)	Arabidopsis (leaf, root, stem)	FBA	The division of labour between organs	b,d
Grafahrend-Belau et al. (2013)	Barley (leaf, root, seed, stem)	FSPM	Source-sink interactions over development	a,c,d
DiCenzo et al. (2020)	*Medicago truncatula* (shoot, root, root nodule)	FBA	Symbiotic nitrogen fixation in legumes	b,d
Shaw and Cheung (2019)	*Setaria viridis* (leaf, stem)	FBA	Proton balancing in C_4 plants	b,c,d
Moreira et al. (2019)	Soybean (cotyledon, hypocotyl)	FBA	Seed germination	b,d

and that the model was solely driven by carbon; the model thus cannot be used to predict the effects of metabolic manipulations on growth over development. Other whole-plant stoichiometric models that suffer from this limitation are those that optimise for fluxes at a single growth stage, restricting their potential to only providing snapshots of metabolism (DiCenzo et al., 2020; Moreira et al., 2019; Shaw and Cheung, 2019; Zakhartsev et al., 2016; de Oliveira Dal'Molin et al., 2015).

Shaw and Cheung (2018) circumnavigated this problem by using dynamic FBA (dFBA) in a model of Arabidopsis leaf and root growth, where flux predictions at previous time steps and shifting environmental conditions are relayed forward as model constraints. This allowed for growth to be driven by metabolism. The shifting control of nitrogen and carbon was analysed under a range of soil nitrate concentrations, resulting in novel predictions on the differential efficiencies of nitrate assimilation in the shoot and root, and C/N balances in assimilate transport. The control of source sucrose and glutamine output towards sinks by leaf NR and NiR activity was also identified. However, model predictions for plant growth were not validated against measured growth data. In fact, this limitation is common to all whole-plant metabolic models to date, bringing their accuracy into question. For example, resource allocation in Shaw and Cheung (2018) was dictated by an equation based on optimal partitioning theory, but the authors made no attempts at experimentally-informed parametrisation, and the form of the function was devised on weak theoretical grounds (Shipley and Meziane, 2002). Integration with a well-established model of resource allocation, such as an FSPM, would prevent this (Christophe et al., 2008). The case for coupling metabolic models to models at other biological scales in a multiscale framework is therefore highly desirable, both to improve the scope of analysis possible and also to increase the accuracy of model mechanisms outside the control of metabolism (Section 1.4.1).

1.6 Project justification

Our understanding of source-sink interactions is clearly far from complete. However, lessons learnt from manipulation experiments have shown us that source-sink interactions exert strong control on plant growth and have the potential to be optimised further for improved crop yields. Given the complex nature of the processes underlying source-sink interactions, computational models have been proposed as a tool to decipher the gaps in our knowledge. Much progress has been made with previous models, with whole-plant stoichiometric models of metabolism proving to be particularly promising. However, major limitations restrict the applicability, flexibility, and accuracy of these models (Table 1.2).

To this end, I constructed multiscale whole-plant growth models of Arabipdosis and tomato with integrated stoichiometric models for all major plant organs (Chapters 3 and 4). The choice of tomato reflects its status as an important crop plant (182.3 million tonnes of tomato fruits is produced each year using 4.9 million hectares of agricultural land) and its use as a model organism for fleshy fruit biology (FAO, 1997; Kimura and Sinha, 2008). In addition to its economic importance, its close relation to other economically-important plants in the Solanaceae family (potato, tobacco, aubergine, pepper, and petunia), short generation times, ease of cultivation, and the availability of complete genome sequences for an inbred cultivar and a wild ancestor also make tomato particularly attractive for study (Schwarz et al., 2014; Sato et al., 2012).

The model building process took particular care to avoid the limitations of previously established models. Namely, these were the use of a carbon-centric focus on growth, an incomplete consideration of all major plant organs, and a static framework that can only provide insight into snapshots of metabolism. Importantly, growth in glasshouse-grown tomato plants was characterised to

generate a detailed dataset with which model growth predictions could be assessed. These considerations facilitated the construction of a model that could simulate the effect on growth by all major plant nutrients, allowing for the optimal allocation of resources within a plant over development to be explored. Consequently, the model was applied to investigate optimal C/N balances for source to sink transport under different environmental conditions (Chapter 5). Finally, the model was used to investigate metabolism during reproductive growth and was used to identify optimal sink strength balances between organs for maximised fruit production in tomato (Chapter 6).

2 | Materials and methods

2.1 Model construction

All simulations and computational tasks were completed using the Python 3 programming language through the Jupyter Notebook environment (https://www.jupyter.org) or using MATLAB software version R2017a (The MathWorks, Inc., Natick, US).

2.1.1 FM-SoFBA-SiFBA

I constructed a whole-plant multiscale model of Arabidopsis with integrated stoichiometric models representing metabolic networks (FM-SoFBA-SiFBA) by connecting the FM to PlantCoreMetabolism v1.2 (Chapter 3). The FM was obtained from Chew et al. (2014) as MATLAB files, whereas PlantCoreMetabolism was obtained from Shameer et al. (2018) as an xml file in SBML format. Detailed descriptions of the construction process for FM-SoFBA-SiFBA are provided in Chapter 3, and the relevant code to simulate plant growth using FM-SoFBA-SiFBA is provided in Appendix B.

Briefly, I devised custom Python scripts to adapt PlantCoreMetabolism into a diel model of leaf source metabolism (SoFBA) and a non-diel model of sink metabolism (SiFBA). The day and night phases are represented separately in SoFBA according to the framework described by Cheung et al. (2014), whereby the diel cycle is divided into two phases, day and night, with each phase assumed to be

at steady-state. To achieve this, the PlantCoreMetabolism model was duplicated, with the compartment, metabolite, and reaction identifiers in each phase being suffixed with either a `_day` or `_night` suffix. Linker reactions were added to allow for metabolites and storage compounds to be transferred between the two phases.

In FM-SoFBA-SiFBA, SoFBA and SiFBA are provided to the FM model as xml files to the top-level script in the FM (`frameworkmodel.m`), which enacts model initialisation and hourly growth simulations. Metabolic activity is dictated by a carbon partitioning module in the FM (`plant_carbon_balance.m` and associated files); this was selected as the connection point between FBA flux predictions and the FM. Flux predictions by SoFBA for daytime and night-time sucrose output rates to the phloem from the leaf and the daytime starch accumulation rate are used to replace the following variables in `assimilation.m`: `al_suc`, `sta_use`, and `suc_sta_base`, which are respectively the variables in the carbon partitioning module of the FM assigned to the corresponding flux values. Unit conversions between SoFBA and the FM are required for model compatibility (μmol m^{-2} s^{-1} to g C^{-1} $plant^{-1}$ h^{-1}). Flux predictions by SiFBA for respiratory carbon loss for growth in the leaf and root are provided to the FM in `organdemand.m` and are used to replace the variables `rlc_pt` (leaf growth respiration cost variable in the FM) and `rrc_pt` (root growth respiration cost variable in the FM), respectively. Unit conversions between SiFBA and the FM are also required for model compatibility (μmol m^{-2} s^{-1} to g C^{-1} $plant^{-1}$ h^{-1}). The starch overflow mechanism in FM-SoFBA-SiFBA was disabled by setting `suc_sta` (excess starch variable in the FM) in the `allocation.m` module to always be zero.

The experimental conditions modelled in Chapter 3 were in reference to an Arabidopsis growth dataset provided by (Chew et al., 2014) and were as follows: 21.3 °C, 12h:12h day/night cycle, 110 μmol m^{-2} s^{-1} photosynthetic photon flux density (PPFD), and 375 parts-per-million mean atmospheric CO_2 concentration.

2.1.2 WholePlantMetabolism v1

I constructed a whole-plant model of tomato metabolism and growth (WholePlantMetabolism v1) using the Python 3 programming language. The model was built by connecting organ-specific stoichiometric models of core metabolism to drive growth. Detailed descriptions of the construction process for WholePlantMetabolism v1 are provided in Chapter 4. Briefly, `core.py` in Appendix B contains all of the functions required to construct and run WholePlantMetabolism v1. Model initialisation is enacted in `WholePlantMetabolism.py` using `initialisation()`, which calls functions from `core.py`. This includes loading input parameters (`loadParams()`), generating organ-specific models for the leaf (diel set-up), root, and stem (`generateStoichiometricModels()`), and generating the whole-plant network by defining the connections between organ-specific models (`generateModelAtEmergence()`). Identifiers for reactions, metabolites, and compartments in the leaf (day), leaf (night), root, and stem are suffixed with the following tags: `_LD`, `_LN`, `_R`, and `_ST`, respectively. The organ-specific models are connected to each other via phloem (suffixed with `_ph`) and xylem (suffixed with `_xy`) compartments. All reactions allowed to proceed in the forward direction are assigned flux upper bounds of 1,000,000, and all reactions allowed to proceed in the backward direction are assigned flux lower bounds of -1,000,000.

The `simulateGrowth()` function in `WholePlantMetabolism.py` enacts the daily growth simulations in WholePlantMetabolism v1. Model constraints for the maximum root nitrate uptake rate, maximum leaf light uptake and carbon assimilation rates, and NGAM requirements are updated during growth by `maxNitrateUptake()`, `maxLightUptakeCarbonAssimilation()`, and `maintRespirationConstraint()`, respectively. The nitrate uptake rate is constrained according to the concentration of nitrate available to the plant in the soil/growth solution us-

ing a Michaelis-Menten function to account for root nitrate transport kinetics. The carbon assimilation rate is constrained at the level of RuBisCO carboxylase activity and is determined by light availability using an empirically-derived relationship between PPFD and net carbon assimilation. Biomass partitioning between organs is dictacted by a model based on allometric growth theory. The code for this model is included directly in the `simulateGrowth()` function and is described in detail in Chapter 4.

It should also be noted that PlantCoreMetabolism v1.2 contains the degradation reactions for amino acids with resolved pathways. However, inspection of the model revealed that two reactions were missing from the leucine catabolism pathway. These were the reactions for mitochondrial acetoacetate-CoA ligase and cytosolic acetyl-CoA acetyltransferase (Hildebrandt et al., 2015). Equation 2.1 states the reaction stoichiometry for the former, and Equation 2.2 for the latter. These reactions were added to the version of PlantCoreMetabolism v1.2 used in WholePlantMetabolism v1.

$$\text{3-Ketobutyrate} + \text{CoA} + \text{ATP} \rightarrow \text{Acetoacetyl-CoA} + \text{AMP} + \text{PP}_\text{i} \tag{2.1}$$

$$2\text{Acetyl-CoA} \leftrightarrow \text{Acetoacetyl-CoA} + \text{CoA} \tag{2.2}$$

2.1.3 WholePlantMetabolism v2

WholePlantMetabolism v2 was constructed using the same framework generated for WholePlantMetabolism v1 and includes significant model improvements for plant development and reproductive growth compared to the earlier model version. The relevant code for simulating WholePlantMetabolism v2 is presented in Appendix B. Detailed descriptions of the construction process for WholePlantMetabolism v2 are provided in Chapter 6. Briefly, a mask file (a table of boolean values stating the presence or absence of an organ type at each phytomer rank) is

provided as an input to the `readStrucutrefromMask()` function during model initialisation to determine the aboveground structure of the plant. During daily growth simulations in `simulateGrowth()`, new organs are added to the whole-plant stoichiometric network according to thermal time and a specified organ appearance rate using the `createNewOrgansAlongAxis()` function. In addition to the suffix denoting organ-type added to reaction, metabolite, and compartment identifiers in each organ-specific model, these attributes are also suffixed with the phytomer rank number to allow for different models of the same organ-type to be distinguishable. For example, the suffix `_LD1` is used for the daytime leaf model at the first phytomer position along the plant main stem, whereas the suffix `_LD2` is used for the daytime leaf model at the second phytomer position.

WholePlantMetabolism v2 also accounts for reproductive growth and generates fruit-specific metabolic models (using `_FR` as a suffix). To reflect the significant re-programming of fruit metabolism over organ development, WholePlantMetabolism v2 uses a dynamic constraint for the composition of biomass demands in fruits. Using time series data of fruit content in tomato cv. Moneymaker provided by Shameer et al. (2020), daily biomass compositions were generated following the method described by Colombié et al. (2015). Third-order polynomial and sigmoidal functions were fitted to data for each metabolite or compound detected in fruits, and the function that fitted the data best was selected as judged by its root-mean-square error (RMSE) value. The first-order derivative of each chosen function is used to dictate fruit biomass demand of each metabolite as a function of organ age in days in WholePlantMetabolism v2 (Appendix A).

2.2 Constraint-based modelling

Constraint-based modelling was performed using COBRApy in Python 3 and the COBRA v3.0 toolbox in MATLAB (Schellenberger et al., 2011; Ebrahim et al., 2013).

2.2.1 Flux balance analysis

Inbuilt parsimonious FBA (pFBA) functions within COBRA(py) were used to perform linear optimisation of stoichiometric models with the CPLEX solver (IBM Corporation, Armonk, US). pFBA is a specific type of FBA where the minimisation of the total sum of fluxes is used as an objective function. This reflects the assumption that biological systems have evolved to minimise their investment in the cellular machinery that mediate metabolism (enzymes and transporters), whilst still sustaining growth. It is important to note that the model output has to first be defined before pFBA can be performed, otherwise no fluxes through the system will be predicted. pFBA was thus used alongside other objective functions, such as the biomass objective (WholePlantMetabolism and SiFBA) or maximising export to the phloem from source leaves (SoFBA).

2.2.2 Flux ratio constraints

Some reactions required for their fluxes to be constrained to a fixed ratio. The steady-state assumption of the system can be used to implement this (Shameer et al., 2018). If P and Q are two non-zero sets of reactions whose sum of fluxes are to be constrained in the ratio m:n, then a pseudometabolite M is added to all reactions in P and Q such that the coefficient of M in all reactions in P and Q are n and -m, respectively. Given the steady-state assumption, this resulted in an additional constraint to the solution space in the form of

$$n \cdot f_{p1} + n \cdot f_{p2} + \ldots + n \cdot f_{pr} + (-m) \cdot f_{q1} + (-m) \cdot f_{q2} + \ldots + (-m) \cdot f_{qs} = 0, \quad (2.3)$$

where $p1, p2 \ldots pr = P$, $q1, q2 \ldots qs = Q$, and f_a is the flux through reaction a. Rewriting the equation, it is evident that sum of fluxes of reactions in sets P and Q

were now constrained to the m:n ratio:

$$n\left(f_{p1} + f_{p2} + \ldots + f_{pr}\right) = m\left(f_{q1} + f_{q2} + \ldots + f_{qs}\right), \tag{2.4}$$

$$\frac{\left(f_{\mathrm{p}1} + f_{\mathrm{p}2} + \ldots + f_{\mathrm{pr}}\right)}{\left(f_{\mathrm{q}1} + f_{\mathrm{q}2} + \ldots + f_{\mathrm{q}s}\right)} = \frac{m}{n}. \tag{2.5}$$

2.3 Reagents

Agar, ethylenediaminetetraacetic acid (EDTA), inorganic salts, ribitol, *N*-*tert*-butyldimethylsilyl-*N*-methyltrifluoroacetamide (MTBSTFA), and solvents were purchased from Sigma-Aldrich Co. Ltd., Gillingham, UK. Murashige and Skoog (MS) basal salt mixture was purchased from Duchefa Biochemie B.V., Haarlem, The Netherlands. *N*-methyl-*N*-trimethylsilyl-trifluoroacetamide (MSTFA) was purchased from Regis Technologies, Inc., Morton Grove, US.

2.4 Plant growth experiment

2.4.1 Plant material

Solanum lycopersicum cv. Moneymaker seeds were kindly provided by José Vallarino (Max Planck Institute of Molecular Plant Physiology, Potsdam, Germany). Seeds were surface sterilised with 8.5% w/v sodium hypochlorite solution for 15 minutes at room temperature with occasional agitation before being washed in sterile double distilled water (ddH_2O) six times. Seeds were sown on half strength MS medium (0.7% w/v agar, pH 5.8) and kept in the dark at room temperature. After three days, sown seeds were allowed to germinate under illumination, with a diurnal cycle of 16 hours light at 22 °C and 8 hours dark at 14 °C.

After 12 days, seedlings were transferred to 1.5 L opaque hydroponic growth tanks, holding 10 plants each, and placed in a climate-controlled glasshouse (University of Oxford, Oxford, UK). Plants were supported by foam padding at the

base of the main stem to ensure that they remained upright. Artificial lights supplemented sunlight to maintain a 16 hour photoperiod. Throughout the growth period, light intensity and temperature were recorded using a Quantum PAR meter (Hydrofarm LLC., Petaluma, US) and a RC-4 Data Logger (Elitech Ltd., London, UK), respectively; these measurements are reported in Chapter 4. Each tank was supplemented with 1.3 L half strength Hoagland's solution (pH 5.8), with the solution being replaced every two days. At 22 days after sowing (DAS), each plant was individually placed into a 3 L opaque growth tank and supplemented with 2.7 L full strength Hoagland's solution every three days. Hoagland's solution is composed of 4 mM $Ca(NO_3)_2{\cdot}4H_2O$, 6 mM KNO_3, 1 mM KH_2PO_4, 2 mM $MgSO_4{\cdot}7H_2O$, 46.2 µM H_3BO_3, 9.1 µM $MnCl_2{\cdot}4H_2O$, 0.8 µM $ZnSO_4{\cdot}7H_2O$, 0.3 µM $CuSO_4{\cdot}5H_2O$, 0.08 µM $Na_2MoO_4{\cdot}2H_2O$, 20 µM $FeSO_4{\cdot}7H_2O$, and 20 µM Na_2-EDTA.

Plants were pruned at the shoot apical bud to limit development to 13 leaves. Leaf number was recorded approximately every four days to follow organ initiation. Side shoots were regularly removed upon emergence to maintain plants with a single main stem.

2.4.2 Plant mass

Plants were harvested at 12, 20, 33, 45, 57, 70, 78, 87, and 96 DAS and separated into individual organs. Roots were considered as a single sample. Stem samples included the subtending internode, node, peduncles, pedicels, petiole, petiolules, and rachis. Immediately after harvest, fresh weight measurements were taken. Leaves were scanned on an Epson Expression 1600 Pro flatbed scanner (Epson Ltd., Hemel Hempstead, UK), and the resulting images were analysed using ImageJ to determine the leaf area (Schneider et al., 2012). All samples were dried at 80 °C to constant weight for dry mass measurements.

2.5 Phloem exudate metabolite profiling

2.5.1 Plant material

S. lycopersicum cv. Moneymaker seeds were sown and germinated on MS medium as described in Section 2.4.1. At 12 DAS, seedlings were transferred onto an equal mixture of fine horticultural sand and vermiculite. Regular watering was supplemented three times a week with 100 mL of Hoagland's solution per plant. A week before harvest, half of the plants were subjected to low nitrate treatment and supplemented with reduced-nitrate Hoagland's solution (nitrogenous compounds replaced with 0.1 mM $Ca(NO_3)_2$, 6 mM KCl_2, and 3.8 mM $CaCl_2{\cdot}2H_2O$). Plant height was measured at 45 DAS.

2.5.2 Phloem exudate collection

Phloem exudates were collected following the method described by Tetyuk et al. (2013) for EDTA-facilitated collection. At 45 DAS, leaves at the third, fourth, and fifth phytomer positions were cut at the base of the petiole and submerged in 20 mM EDTA-Na_2. Leaves were then recut along the rachis while submerged and transferred into 800 µL 20 mM EDTA-Na_2. After one hour incubation under illumination (320 µmol m^{-2} s^{-1} PPFD) in a sealed humidified chamber, leaves were washed in running distilled water to remove EDTA and transferred into 700 µL sterile ddH_2O placed in the chamber. Phloem exudates were collected for one hour under illumination (320 µmol m^{-2} s^{-1} PPFD) and leaves were removed at the end of the collection period.

2.5.3 Sample preparation and derivatisation

400 µL methanol and 250 µL chloroform were added to each sample and heated at 70 °C for 15 minutes whilst shaking at 1000 rpm. Samples were then centrifuged at 4500 x *g* for 10 minutes and supernatants (the polar phase) were transferred into a

fresh tube, pooling together groups of seven samples. Methanol and water were removed by freeze-drying overnight at -80 °C.

To each dried sample, 25 µL pyridine was added and incubated at 37 °C for 30 minutes whilst shaking at 1000 rpm. 12.5 µL sample was mixed with 17.5 µL MSTFA and incubated at 37 °C for 30 minutes whilst shaking at 1000 rpm. The remaining 12.5 µL was mixed with 17.5 µL MTBSTFA and incubated at 60 °C for 40 minutes whilst shaking at 1000 rpm. Blank samples were prepared with just pyridine and a derivatisation agent. All samples were transferred to glass vials and sealed with septum caps.

2.5.4 Gas chromatography/mass spectrometry

Metabolite profiles were determined using a 5977B GC/MS (gas chromatography/mass spectrometry) machine (Agilent Technologies, Inc., Santa Clara, US). Machine calibration was carried out using the inbuilt autotune method before use.

1 µL of each MSTFA-derived sample was loaded onto an Agilent 122 column (15 m x 0.25 mm x 0.25 µm) via splitless mode injection with gas flow through the column set to 1.2 mL He min^{-1}. The column temperature was programmed to start at 70 °C for 5 minutes, before increasing to 330 °C at a rate of 7.5 °C min^{-1}. The total run time was 40 minutes, inclusive of a solvent delay (7.5 minutes).

For MTBSTFA-derived samples, 1 µL of each sample was loaded onto an Agilent 122 column (15 m x 0.25 mm x 0.25 µm) via splitless mode injection with gas flow through the column set to 1.2 mL He min^{-1}. The column temperature was programmed to start at 120 °C for 5 minutes , before increasing to 310 °C for 3 minutes at a rate of 20 °C min^{-1}. The total run time was 47.5 minutes, inclusive of a solvent delay (7.5 minutes).

2.5.5 Gas chromatography/mass spectrometry analysis

Mass Hunter Qualitative Analysis (Agilent Technologies, Inc., Santa Clara, US) was used to extract and integrate chromatographic peaks (using the ChemStation Integrator algorithm with baseline correction). Peaks were identified by comparing their retention times and mass spectra to known standards for major phloem sugars, organic acids, and amino acids. Relative abundances were calculated from peak areas. Comparisons of mass spectra against the National Institute of Standards and Technology database with a 80% similarity threshold was performed to identify unassigned peaks and for further validation of known peaks (Linstrom and Mallard, 2020).

2.6 Statistical analysis

All statistical analyses were executed with custom Python 3 scripts and the Scipy package (https://www.scipy.org). The Barlett's test was used to determine homoscedasticity. Significant differences in the means of two samples with equal variances were determined using the Student's t-test. Under heteroscedasticity, the Welch's t-test was used. One-way analysis of variance (ANOVA) was used to determine differences in the means of three or more samples.

Linear and nonlinear regression models were fitted to bivariate data using the least squares method. In exceptions where both variables are assumed to have a degree of error, the reduced major axis (RMA) method was used.

RMSE measures the differences between predicted and observed values and was used to measure model performance. RMSE is defined as

$$\text{RMSE} = \sqrt{\sum_{i=1}^{n} \frac{(\hat{y}_i - y_i)^2}{n}}, \tag{2.6}$$

where n is the sample size, $\hat{y}_i$ is a predicted value, and y_i is an observed value.

3 | Coupling metabolic models to a multiscale model of Arabidopsis

3.1 Introduction

The Framework Model (FM) is one of the most advanced multiscale models of plant growth and incorporates a host of molecular-level signalling and decision mechanisms (Chew et al., 2014). The FM was constructed by combining pre-existing models of Arabidopsis at four different biological scales. A major consideration in the construction process was modularity and flexibility, allowing other models to be added in a true *plug-and-play* manner in future model applications. In its current form, the FM consists of the following models:

- The Carbon Dynamic Model (CDM) represents carbon assimilation through photosynthesis and carbon partitioning between sugars and starch (Rasse and Tocquin, 2006)
- The GREENLAB FSPM computes individual organ growth, phenology, and resource allocation (Christophe et al., 2008)
- The photothermal model uses thermal time to compute flowering time, representing photoperiod-sensing pathways (Chew et al., 2012)
- The photoperiodism model simulates circadian regulatory pathways (Chew et al., 2014)

To ensure compatibility between each model, hourly time steps were imple-

mented in all the models in the FM, allowing for hourly environmental data as inputs. The model integration process entailed the identification of connection points; where there is redundancy between the models, the more mechanistic option was retained and used to replace the simpler alternative. For example, the dynamic growth demand for each organ calculated by the FSPM replaced the carbon growth allocation mechanism computed by the CDM.

The FM has been used to accurately predict fresh mass, dry mass, rosette area, and net ecosystem production of CO_2 in three different Arabidopsis accessions and various other mutant lines (Pullen et al., 2019; Chew et al., 2017a, 2014). The model has also been applied to analyse a range of source-sink interaction processes. This includes the role of leaf development and leaf thickness on modulating source efficiency, the regulation of starch storage in leaves for night-time source activity by circadian rhythms, and the effect of increasing leaf initiation rates on source capacity (Pullen et al., 2019; Chew et al., 2017a, 2014).

However, metabolism is represented in the FM in a relatively simplistic manner by the CDM. The model considers the status of only four carbon pools: sucrose, starch, leaf biomass, and root biomass (Rasse and Tocquin, 2006). Source activity is represented by a classical biochemical model of photosynthesis that requires light intensity, temperature, and CO_2 levels as inputs (Farquhar et al., 1980). Two rate-limiting steps in photosynthesis are considered: RuBisCO carboxylase flux and plastidial electron transport. The maximum rates of these two processes are critical parameters for model performance, and were measured experimentally using gas exchange experiments. Photoassimilates are partitioned into either starch or sucrose pools. During the day, starch is synthesised at a fixed baseline rate and stored for use as an energy source for night-time growth, and at night, starch is degraded into sucrose at a linear rate (Gibon et al., 2004, 2009). Growth respiration is calculated as a fixed proportion of the growth rate. On the other hand, NGAM

is computed from the model's sucrose status, where NGAM increases linearly in response to increases in the sucrose pool size (Ögren, 2000). This mechanism is based on observations in starchless Arabidopsis mutants, where higher NGAM rates are reported in leaves with high soluble sugar contents. This is hypothesised to result from the cost of maintaining concentration gradients (Rasse and Tocquin, 2006). The model can grow if there is sucrose remaining after respiration and starch production have been considered. By limiting its scope to just four stores of carbon, the CDM is also unable to model the control exerted by other elemental resources, such as nitrogen (Reich et al., 2014; Nunes-Nesi et al., 2010; Stitt et al., 2002; Stitt, 1999).

In the CDM, growth demand cannot exceed a specified maximum leaf growth rate and excess carbon is instead diverted into a starch store (van der Kooij and de Kok, 1996; Gibeaut et al., 2001). No strong experimental support for this starch overflow mechanism has been reported so far (Streb and Zeeman, 2012; Sun et al., 1999). Importantly, the mechanism does not reflect the regulatory network coordinating starch accumulation in leaves under illumination. When grown in short photoperiods, Arabidopsis leaves increase their rate of starch synthesis during the day and decrease their rate of starch degradation at night (Smith and Stitt, 2007). This concerted response allows the plant to support growth throughout the long dark phase, avoiding the depletion of carbon stores. Additionally, Mugford et al. (2014) found that mutants lacking components of the photoperiod-signalling pathway were unable to adjust their starch synthesis rate in response to changes in day length, indicating that the circadian clock may also be involved. Overall, the literature does not support the starch overflow mechanism as a key determinant of leaf starch biosynthesis.

In contrast to the limited network size of enzyme kinetic models, the wider scope of stoichiometric models is likely to capture sufficient aspects of metabolism

to address the deficiencies of the CDM. The integration of the CDM in the FM with metabolic models is therefore appealing. For example, the steady-state requirement of FBA ensures that no resources are assimilated in excess of growth demands, meaning that the model will not predict any unused carbon that needs to be diverted to an overflow store. Recently, Shameer et al. (2018) constructed a stoichiometric model of central metabolism in a generalised plant. The model was constructed from a previously published GSM of Arabidopsis, and contains 641 reactions and 555 metabolites that can produce all major biomass components (Cheung et al., 2014). As central plant metabolism is highly conserved, the model can be applied to study any plant species. All the reactions in the model were verified to be present in every species-specific metabolic network in the PlantCyc database, which includes various C_3, C_4, and CAM species (Schläpfer et al., 2017). Importantly, the size of the model facilitated manual model curation, allowing for metabolite charge-balancing, reaction compartmentation, and the addition of energy costs to reaction stoichiometries (Shameer et al., 2018). PlantCoreMetabolism has been applied to model a range of metabolic scenarios in a range of species and tissues, and has proven itself to be a reliable tool for analysing metabolic behaviour. Examples include the role of the carbon-concentrating effect of malate decarboxylation in CAM efficiency, energy balances between chloroplasts and mitochondria in C_3 photosynthesis, and dynamic patterns of metabolite accumulation during fruit development (Shameer et al., 2019, 2018). The high level of versatility and flexibility shown by PlantCoreMetabolism make it an attractive choice for integration with the FM. The small model size also makes the manual analysis of flux predictions more manageable.

The FM presents itself as an appealing foundation for developing an advanced multiscale whole-plant growth model. However, major model limitations at the metabolic level leave much room for improvement. The aim of this chapter was

thus to improve the metabolic scope of the FM, with a particular focus on removing the limitations imposed by the CDM's model structure. To this end, PlantCoreMetabolism was constrained to represent source and sink metabolic modes and was coupled to the FM through various connection points to the CDM. This produced an improved model version with the capacity to generate fine-grained metabolic predictions.

3.2 Results

3.2.1 Metabolic model construction

This section explains how I constructed stoichiometric models for source and sink metabolism in Arabidopsis. Separate models for each metabolic mode were developed, as opposed to a single integrated whole-plant model (Figure 3.1). Table 3.1 lists the names and descriptions of the various models that are used and discussed in this chapter.

Source leaf metabolism

PlantCoreMetabolism v1.2 was constrained to represent an Arabidopsis source leaf (Shameer et al., 2018). The model was named SoFBA and was solved by maximising

Table 3.1: Descriptions of the Framework model (FM), stoichiometric metabolic models, and coupled models used in Chapter 3.

Model	Description
FM	A multiscale model of whole-plant growth in Arabidopsis
SoFBA	A diel stoichiometric model of source leaf metabolism
SiFBA	A stoichiometric model of sink metabolism that is either constrained for leaf or root growth
FM-SoFBA	The FM integrated with a source stoichiometric model representing the leaf
FM-SiFBA	The FM integrated with sink stoichiometric models representing the leaf and root
FM-SoFBA-SiFBA	The FM integrated with both source and sink stoichiometric models

metabolite export from the source leaf to the phloem, whilst also minimizing the sum of all fluxes as objective functions. Metabolite export to the phloem was constrained to consist solely of sucrose to reflect the composition of the phloem in the CDM (Rasse and Tocquin, 2006). Chloroplastic NADPH dehydrogenase and plastoquinol oxidase fluxes were constrained to zero as these enzymes have been reported to contribute minimally to photosynthesis (Josse et al., 2000; Yamamoto et al., 2011). ATP transport between the chloroplast and the cytosol has been reported to occur minimally in mature chloroplasts so ATP transport between the two compartments was not permitted (Voon et al., 2018). Photorespiration was simulated by constraining the ratio of carboxylation to oxygenation by RuBisCO to 3:1 (Gutteridge and Pierce, 2006).

To construct a diel version of SoFBA that accounts for the integrated metabolism of a leaf during the day and night, the method described by Cheung et al. (2014) was followed. The model was divided into day and night phases by duplicating the model (Figure 3.1). Both phases were simulated simultaneously as a single optimisation problem. The phototrophic nature of daytime metabolism was captured by allowing photon uptake during the day. Heterotrophic metabolism during the night phase was captured by constraining photon uptake to zero. Additionally, linker reactions that allow metabolites to pass between the day and night phases were included to represent the accumulation and consumption of storage metabolites and macromolecules. Molecules that were allowed to accumulate included starch, glucose, fructose, nitrate, malate, citrate, and fumarate. All twenty amino acids were also allowed to accumulate, but this was limited only to the day to reflect our current understanding of leaf nitrogen metabolism (Scheible et al., 2000). All linker reactions were otherwise unconstrained, allowing the model to freely choose which storage molecules to accumulate and the rates of their accumulation.

Phloem output during the day and night phases was constrained to a 3:1 ratio according to measurements in Arabidopsis rosettes, and nitrate uptake to 3:2 according to measurements in a variety of plant species (Gibon et al., 2004; Macduff and Bakken, 2003; Siebrecht et al., 2003; Delhon et al., 1995). Nitrate was also selected as the sole source of nitrogen as it has been reported that 80% of the nitrogen provided to the leaf is in this form (Macduff and Bakken, 2003). The route of nitrate transport from the soil to leaves requires two active transport steps: (1) transport into the root symplast prior to xylem loading, and (2) transport into leaf cells following xylem unloading. Both of these steps are mediated by plasma membrane-localised nitrate-proton symporters, which have been found to mediate the co-transport of one molecule of nitrate per two protons (Parker and Newstead, 2014). Consequently, the stoichiometry of nitrate import in SoFBA was updated to four protons per molecule of nitrate transported.

Reactions representing NGAM were removed from the model as the CDM already accounts for the process. Namely, these were the reactions representing the oxidation of NAD(P)H and the hydrolysis of ATP that fuels the maintenance of cellular machinery (Cheung et al., 2013).

Sink metabolism

The sink metabolic model, named SiFBA, was constructed in a similar manner to SoFBA but with the exception that a non-diel set-up was used (Figure 3.1). Furthermore, the objective function of the model was the maximisation of biomass production, whilst the minimisation of the sum of fluxes still remained the secondary objective. The biomass reaction was constrained according to metabolite profiles and biomass composition reported for Arabidopsis heterotrophic cell cultures (Poolman et al., 2009). The stoichiometries of protein amino acids, soluble carbohydrates, starch, lipids, and cell wall components were included (Appendix

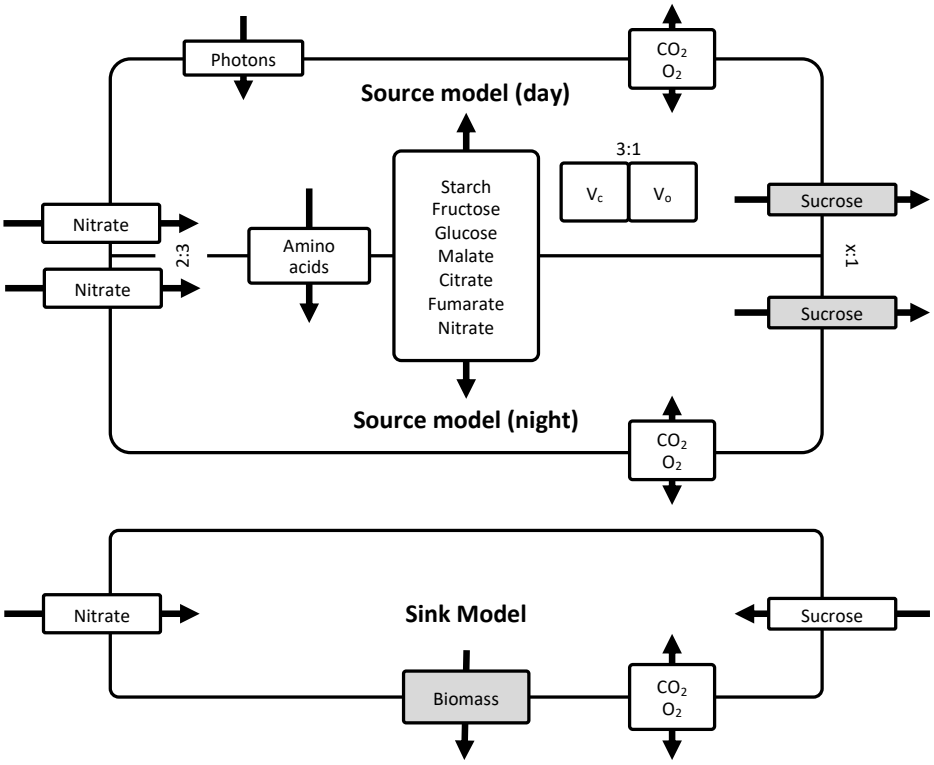

Figure 3.1: Schematic of stoichiometric models representing source (SoFBA) and sink (SiFBA) metabolism. Grey boxes indicate the model objective function. Specified ratios indicate flux ratio constraints between reaction pairs. Various flux ratio constraints were applied to sucrose export to the phloem in SoFBA over the diel cycle throughout the model integration process, as indicated by *x*:1. Linker reactions between the day and night phases in the source model allow for metabolite storage over the diel cycle. Flux distributions through the source and sink models are simulated as two separate optimisation problems. V_C, RuBisCO carboxylase activity; V_O, RuBisCO oxygenase activity.

A). The direction of the phloem output reaction was reversed to reflect metabolite uptake from the vasculature. Photon uptake was not allowed in SiFBA.

3.2.2 Integrating source metabolism

As the CDM computes carbon supply and demand in separate modules, the source and sink metabolic models were incorporated as separated models (Figure 3.2). This section describes the model integration process underlying the coupling of SoFBA to the CDM to generate FM-SoFBA.

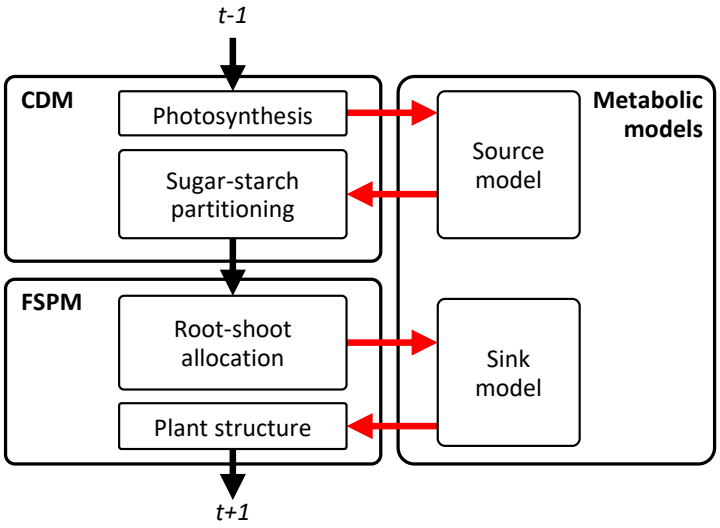

Figure 3.2: Schematic illustrating the integration of stoichiometric metabolic models with the FM. Red arrows indicate new connections made between the FM and metabolic models. The CDM and the FSPM are constituent parts of the FM and the metabolic models are as outlined in Figure 3.1. The CDM relays the carbon assimilation rate to the source model (SoFBA), which uses it to calculate the sucrose export rate and daytime starch accumulation rate. The FSPM relays the demand for growth to the sink model (SiFBA), which then calculates the rate of growth over day *t*. CDM, Carbon Dynamic Model; FM, Framework Model; FSPM, functional-structural plant model.

Constraining the source metabolic model

The CDM computes rates for net carbon assimilation and photon uptake for each hour of growth. These variables were selected as connection points and were relayed from the FM to SoFBA to constrain the appropriate reactions. However, when reactions representing CO_2 and photon uptake in SoFBA were constrained to values provided by the CDM, SoFBA predicted CAM-like behaviour, which manifested as nocturnal carbon fixation and the accumulation of organic acids (malate and citrate) in the vacuole for decarboxylation during the day (Table 3.2). When SoFBA was constrained with only the photon uptake rate, the model was able to predict C_3 behaviour, as expected of Arabidopsis, with carbon assimilation being restricted to the day and net carbon loss occurring at night arising from respiration. However, the net CO_2 assimilation rate predicted by SoFBA was nearly double the value computed by the CDM (7.96 µmol m^{-2} s^{-1} versus 4.44 µmol

m^{-2} s^{-1}, respectively). This highlights one of the issues with FBA's linear nature: non-linear processes, such as saturation kinetics, are not intrinsically accounted for without the addition of specific constraints. To address this, the non-linear response of photosynthesis to light intensity was instead captured by varying the daytime carboxylase flux of RuBisCO in SoFBA until the predicted daytime net CO_2 uptake flux matched that predicted by the CDM (Shameer et al., 2019). With both photon uptake and RuBisCO carboxylase fluxes constrained, SoFBA successfully predicted C_3 photosynthesis, and a CO_2 uptake flux in agreement with predictions by the CDM (Table 3.2). Additionally, transient organic accumulation patterns were consistent with the current understanding of diel leaf metabolism. Daytime malate storage fuels the tricarboxylic acid (TCA) cycle during the night, and citrate storage during the night provides carbon skeletons for amino acid synthesis during the day (Cheung et al., 2014). Under all simulation conditions, starch was chosen by SoFBA as the main carbon storage molecule to supply energy to fuel night-time metabolism, which is also in agreement with known leaf biochemistry in Arabidopsis.

In contrast to applying a daytime CO_2 uptake constraint, which gives the model a higher degree of freedom to choose between different routes of carbon assimilation and utilisation, constraining the model using a daytime RuBisCO carboxylase constraint comparatively reduces SoFBA's choice of potential photosynthetic routes. This potentially explains why CAM-like behaviour was not predicted by using the final choice of constraints.

Time step compatibility

SoFBA computes flux distributions over a complete diel cycle, effectively giving it a time step of 24 hours. In contrast, the FM simulates growth using hourly time steps. To avoid compatibility issues between the two models in FM-SoFBA, flux

Table 3.2: Flux predictions for source carbon activity by SoFBA when simulated to maximise sucrose output towards the phloem. Flux constraints for daytime photon uptake and CO_2 uptake were provided by the Carbon Dynamic Model. The constraint for daytime RubisCO carboxylase flux was estimated from the provided CO_2 uptake rate. Storage reactions are listed as transfers from the day to the night.

Process	Flux (μmol m^{-2} s^{-1})		
Constraints			
Photon uptake (day)	110	110	110
CO_2 uptake (day)	3.70	-	-
RuBisCO carboxylase (day)	-	-	4.44
Predictions			
CO_2 uptake (day)	3.70	7.96	3.70
CO_2 uptake (night)	2.92	-0.0251	-0.00750
Starch storage	2.18	0.335	0.158
Malate storage	-2.92	0	0.00750
Citrate storage	-0.450	0	-0.00750

distributions are generated by SoFBA during model initialisation before hourly simulations are enacted. Owing to the linear nature of FBA, predicted fluxes respond linearly to the limiting reaction in the network, which in this case is the net carbon assimilation rate during the day (A), and the starch degradation rate during the night (q'). During hourly simulations, flux distributions generated during the model initialisation stage are scaled relative to values for A (during the day) or q' (during the night) generated by the CDM in that hour of growth. Predicted daytime starch accumulation (q), daytime sucrose export (r), and nighttime sucrose export (r') fluxes from SoFBA are thus scaled (including conversions from μmol m^{-2} s^{-1} to μmol $plant^{-1}$ h^{-1}) and relayed onto the CDM as

$$q_j = 3600 \cdot q_o \cdot z_j \cdot \frac{A_j}{A_o}, \tag{3.1}$$

$$r_j = 3600 \cdot r_o \cdot z_j \cdot \frac{A_j}{A_o}, \tag{3.2}$$

$$r'_k = 3600 \cdot r'_o \cdot z_k \cdot \frac{q'_k}{q'_o}, \tag{3.3}$$

where z is the leaf surface area, j is the hour of the day and k is the hour of the night, and o denotes the fluxes predicted during the initial optimisation. With time step scaling rules applied, FM-SoFBA was able to predict the growth of Arabidopsis shoot accurately and displayed minimal differences compared to the FM's predictions (Figure 3.3).

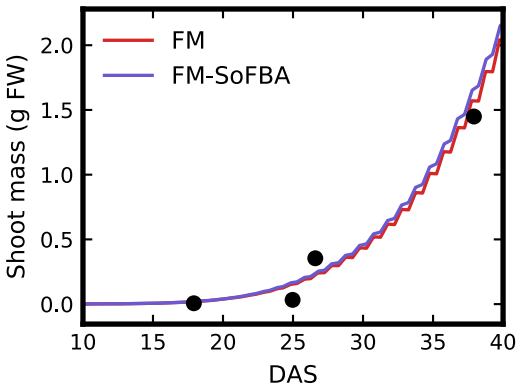

Figure 3.3: Shoot growth predictions by the FM and FM-SoFBA (coloured lines) compared to experimental data (black symbols). SoFBA was coupled to the FM via the daytime RuBisCO carboxylation rate (estimated from the daytime net carbon assimilation rate) and daytime photon uptake rate as calculated by the FM. Data are the mean±SD (n = 5) from Chew et al. (2014) — symbols are larger than error bars. DAS, days after sowing; FW, fresh weight.

The starch overflow mechanism

One of the goals of integrating SoFBA into the FM was to remove the starch overflow mechanism from the CDM as little experimental evidence has been reported to support its role in source metabolism. The starch overflow mechanism diverts any assimilated carbon that is left after the demands for plant growth and maintenance have been met. When the starch overflow mechanism was disabled in FM-SoFBA, the model predicted highly underestimated growth rates (Figure 3.4a). This indicates that FM-SoFBA had insufficient assimilated carbon to support growth. Reviewing flux predictions by SoFBA more closely revealed that it generated starch accumulation rates that fell below the demand for night-time growth during early development. In SoFBA, the daytime starch accumulation rate

is determined largely by the demand for sucrose export to the phloem during the night. The leaf daytime-to-night-time phloem export rate was constrained to 3:1, following observed carbon export rates from Arabidopsis leaves calculated from the difference between the net rate of carbon exchange and the net change in carbon content (Gibon et al., 2004). A more recent study characterising phloem exudate extracted from Arabidopsis over the diel cycle reported a lower phloem export ratio of 1.5:1 (Brauner et al., 2018). A range of other values have also been reported in other plant species, including 1.7:1 in *Gossypium hirsutum* (Hendrix and Huber, 1986), and 5:1 in *Zea mays* (Kalt-Torres and Huber, 1987). This variation suggests that phloem export rates over the diel cycle may differ significantly between species and growth conditions. FM-SoFBA was thus simulated with a range of phloem day:night export ratios and its effect on the accuracy in predicting shoot growth was evaluated. Figure 3.4b shows that a ratio of 1.5:1, as observed by Brauner et al. (2018), results in growth predictions that fitted the experimental growth data best. With this lower ratio, the model predicted a higher daytime starch accumulation rate, supplementing night-time growth and enabling a predicted shoot growth rate that was a close match to experimental data (Figure 3.4a).

3.2.3 Integrating sink metabolism

SiFBA was integrated into the FM to model the metabolism of growing leaves (leaf sink) and growing roots (root sink). Leaf sink activity was modelled by using the maximum leaf growth rate generated by the CDM component of the FM to constrain the biomass production rate in SiFBA. FM-SiFBA was then optimised using the minimisation of sum of fluxes as the objective, and the predicted rate of sucrose uptake from the phloem by SiFBA was used to replace the leaf growth demand value generated by the CDM. A similar approach was applied to model root growth: the root growth demand value generated by the CDM component

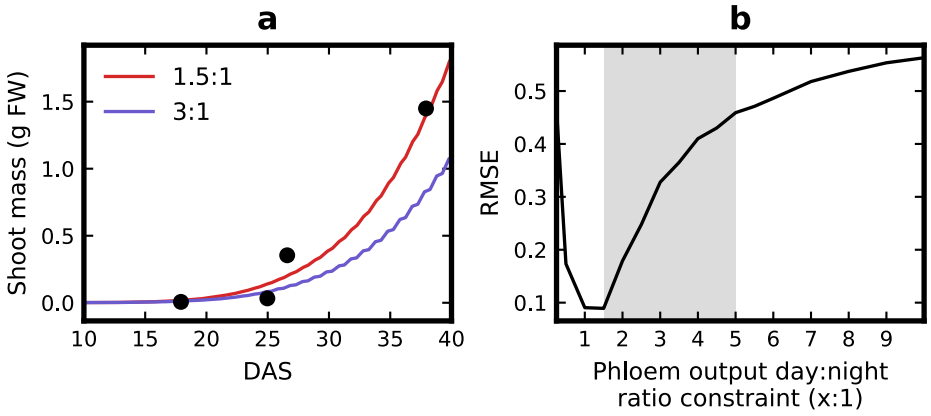

Figure 3.4: Shoot growth predictions by FM-SoFBA with different phloem output day:night ratio constraints applied in the absence of the starch overflow mechanism. **(a)** Shoot growth predictions by FM-SoFBA with two phloem output day:night ratio observed in Arabidopsis (coloured lines). Data (black symbols) are the mean±SD (n = 5) from Chew et al. (2014) — symbols are larger than error bars. **(b)** Goodness of fit of shoot growth predictions by FM-SoFBA with different phloem output day:night ratios constraints. Shading highlights the range of phloem output ratios estimated from experimental measurements. DAS, days after sowing; FW, fresh weight; RMSE, root-mean-square error.

of the FM was used to constrain the biomass demand in SiFBA, and the resulting phloem sucrose uptake rate following the minimisation of the sum of fluxes was used to replace the root growth demand parameter in the FM.

The CDM calculates whole-plant growth respiration as a proportion of total growth (proportion of gross carbon assimilation lost as carbon dioxide), which is set to 19.5% according to empirical observations (Rasse and Tocquin, 2006). However, SiFBA directly accounts for the energetic costs of reactions and transports in terms of ATP, protons, and reducing power stoichiometries (Cheung et al., 2014). In FM-SiFBA, the net CO_2 output fluxes generated by the integrated SiFBA models are relayed onto the CDM to replace the equivalent parameters for both leaf and root growth respiration. SiFBA predicted growth respiration to proportionally contribute to 19.2% of total growth.

Biomass composition

Simulating growth using FM-SiFBA resulted in overestimated shoot growth predictions (RMSE = 0.73; Figure 3.5). The biomass composition in SiFBA was constrained according to measurements made on Arabidopsis heterotrophic cell cultures (Poolman et al., 2009). However, upon comparing reported characterisations from multiple studies, major differences between the biomass compositions of cell cultures and whole-plant tissues were apparent (Figure 3.6). Arnold and Nikoloski (2014) characterised the metabolite profile of Arabidopsis leaves, whereas de Oliveira Dal'Molin et al. (2015) provided compositions for both the leaf and root. Leaves and roots have distinctive high protein contents, whereas cell wall content was much higher in cell cultures (Figure 3.6). Roots were also reported to have higher cell wall and starch contents compared to leaves.

As FM-SiFBA simulates the growth of whole Arabidopsis plants, biomass compositions from whole plants may describe sink activity in the model more accurately, compared to cell culture data. Two different datasets were used to constrain the biomass objective in SiFBA instead: organ-specific compositions were applied

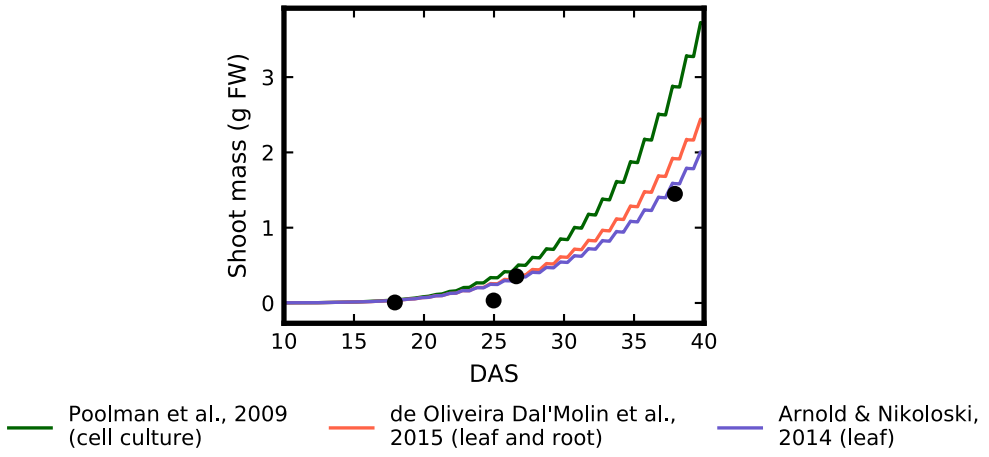

Figure 3.5: Shoot growth predictions by FM-SiFBA with different biomass compositions applied as constraints (coloured lines). Data (black symbols) are the mean±SD (n = 5) from Chew et al. (2014) — symbols are larger error bars. Biomass compositions are shown in Figure 3.6. DAS, days after sowing; FW, fresh weight.

to leaf and root SiFBA using data from de Oliveira Dal'Molin et al. (2015), whereas data from Arnold and Nikoloski (2014) contained no organ-specific information so the leaf composition was applied to both the leaf and root models. The accuracy of shoot mass predictions improved greatly when whole-plant biomass constraints were applied to FM-SiFBA, with data from Arnold and Nikoloski (2014) yielding the best fit to observed values (RMSE = 0.13; Figure 3.5).

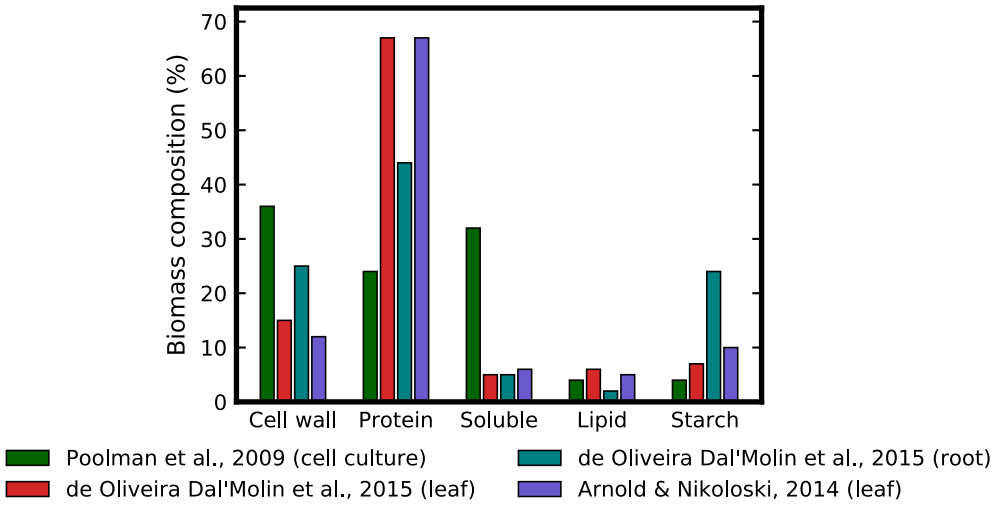

Figure 3.6: The biomass composition of different Arabidopsis tissue types categorised by biochemical groups. Data are from de Oliveira Dal'Molin et al. (2015), Arnold and Nikoloski (2014), and Poolman et al. (2009).

3.2.4 Amino acid translocation

As Figures 3.4b and 3.5 show, source and sink metabolic models were successfully integrated into the FM separately without significant decreases in model performance and the accuracy of shoot growth predictions. However, these simulations were limited to a carbon-only flow between organs as only sucrose translocation was modelled. However, amino acids are commonly detected in plant phloem sap and exudates and contribute significantly to long-distance assimilate transport (Wilkinson and Douglas, 2003; Valle et al., 1998; Riens et al., 1991; Walker and Ho, 1977). Implementing nitrogen flow from sources to sinks is clearly desirable and

would greatly increase the predictive power of FM-SoFBA-SiFBA, especially in relation to analysing the control of nitrogen availability on growth.

To this end, phloem output in SoFBA and phloem uptake by SiFBA were defined according to experimentally observed relative concentrations of sucrose, glucose, fructose, and amino acids in Arabidopsis petiole phloem exudates (Wilkinson and Douglas, 2003). Figure 3.7 shows shoot growth predictions by FM-SoFBA-SiFBA both before and after metabolites other than sucrose were included in the phloem composition. Model predictions using only sucrose in the phloem were in good agreement with growth data. However, the inclusion of other metabolites into the phloem significantly reduced growth and a highly underestimated plant mass was predicted. SoFBA predicted a lower sucrose export rate as more photosynthates were now being used to synthesis amino acids and other sugars. As the CDM still remained a carbon-based model, only sucrose fluxes could be relayed from SoFBA. This equates to a reduction in the amount of photosynthate available for growth as a proportion of assimilated carbon in SoFBA was allocated to the phloem amino acids. In fact, the scale of the reduction in sucrose export corresponded exactly to the reduction in the contribution to the phloem by sucrose (31%; Wilkinson and Douglas, 2003).

The CDM also has mechanisms adjusting the size of the four carbon pools in the model to account for processes such as NGAM and the minimum sugar content requirement in leaves (Rasse and Tocquin, 2006). Adjustments made to the sucrose pool would lead to equivalent changes in the amount of amino acids supplied to SiFBA, further reducing the amount of assimilates transported from source to sink. The results here show that the CDM's carbon-centric approach, with sucrose being considered as the only driver of growth, inherently makes integrating the metabolism of other elemental resources difficult. A major redesign of the CDM's architecture would be required to achieve such an aim.

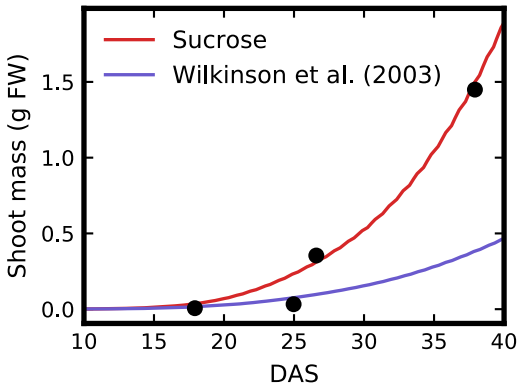

Figure 3.7: Shoot growth predictions by FM-SoFBA-SiFBA with different phloem compositions applied as constraints (coloured lines). The phloem composition determined by Wilkinson and Douglas (2003) included sugars and amino acids. Data (black symbols) are the mean±SD (n = 5) from Chew et al. (2014) — symbols are larger error bars. DAS, days after sowing; FW, fresh weight.

3.3 Discussion

3.3.1 Model improvements

FM-SoFBA-SiFBA constitutes a significant improvement to the FM, and its construction led to a multiscale whole-plant model that considers growth at the genetic, metabolic, phenological, and structural levels with the capacity to generate fine-grained flux predictions through central metabolism. The improved model can do so without any significant reduction in the accuracy of major model outputs, such as shoot fresh weight (Figure 3.7). More importantly, metabolism is the major driver of growth in FM-SoFBA-SiFBA, allowing for the effects of precise genetic perturbations to be modelled. For instance, future applications of the model could be used to explore the effects of reducing the rate of protein turnover to reduce respiratory carbon loss through NGAM or the effect of improving the catalytic efficiency of RuBisCO under different environmental conditions and photoperiods (Amthor et al., 2019; Sharwood et al., 2016). In comparison, another multiscale model of barley, comprising of an FSPM connected to organ-specific stoichiometric models, could also generate metabolic predictions. However, the control of growth

remained with the FSPM and the model structure did not allow for flux predictions to inform plant growth (Grafahrend-Belau et al., 2013).

Several emergent properties of SoFBA and SiFBA were used to replace empirical input parameters in the FM, which are often difficult to quantify experimentally. Decreasing the number of model parameters also reduces the problem of overfitting parameters to specific datasets (Hawkins, 2004). For instance, the CDM synthesises starch during the day in leaves according to a fixed starch accumulation rate as a proportion of total carbon fixed (Rasse and Tocquin, 2006). In contrast, the diel modelling framework, which has previously been shown to accurately predict C_3 behaviour over complete day-night cycles, can predict the starch accumulate rate without explicit constraints; the model only seeks to satisfy the objective of sucrose output to the phloem throughout the diel cycle (Cheung et al., 2014). The same applies to the night-time starch degradation rate. The cost of growth was accounted for in SiFBA by including ATP and reducing power stoichiometries in reactions that required energetic input (Cheung et al., 2013). Once again, the CDM requires an empirically-derived parameter to dictate the ratio of carbon respired to carbon assimilated. The CO_2 output flux predicted by SiFBA could thus be used to replace the growth respiration parameter in the CDM. SiFBA predicted the cost of growth to be nearly identical to that observed experimentally, suggesting that the sink model accounts for cellular energetics accurately (19.2% vs 19.5% as a proportion of growth; Rasse and Tocquin, 2006).

Another significant model improvement was the removal of the starch overflow mechanism in the CDM, whereby excess photoassimilates were diverted into starch stores when source activity exceeded growth demands (Rasse and Tocquin, 2006). This mechanism was constructed based on the hypothesis that starch is an overflow product of photosynthesis in plants with low sink capacities (Sun et al., 1999). AGPase, which catalyses the first dedicated step in the starch synthesis pathway,

has been shown to be allosterically activated by glycerate-3-phosphate (G3P) and inhibited by P_i (Stitt, 1990; Ballicora et al., 2004). Whilst high G3P:P_i ratios can be indicative of sucrose accumulation arising from excessive photosynthetic activity, the regulatory mechanism alone fails to explain how leaves can coordinate starch accumulation rates to match the carbon demand of night-time metabolism (Stitt et al., 2010). Other lines of evidence have been provided that support much more well-established models of starch regulation (Thormählen et al., 2013; Hendriks et al., 2003; Stitt, 1990).

3.3.2 Effect of biomass composition

The composition of plants has been reported to vary markedly between different tissue types, species, and growth conditions (Yuan et al., 2016a; Hay and Schwender, 2011b; Colombié et al., 2015; de Oliveira Dal'Molin et al., 2015; Arnold and Nikoloski, 2014; Poolman et al., 2009; Poorter and Bergkotte, 1992). Focusing on Arabidopsis, Figure 3.6 shows that there is a marked difference between the composition of heterotrophic cell cultures and whole-plant tissues. The principal constituent of leaf and root mass was protein, whereas cell cultures had a higher contribution from cellulose.

The effect of biomass composition on FBA predictions for growth has been recently assessed using the same datasets used in this study (Yuan et al., 2016b). The authors concluded that central metabolism is highly robust to changes in biomass composition. Instead, internal network structure was determined to be the critical factor affecting model behaviour and growth rate predictions. In constrast, Figure 3.5 shows that the biomass composition has a significant effect on the growth rate in FM-SiFBA. This indicates that what Yuan et al. (2016b) concluded to be minor differences in model behaviour under a static FBA framework can result in much stronger responses under a dynamic framework. The FM simulates exponential

growth, making it more sensitive to cumulative effects of minor variations in the energetic costs of producing the various components of biomass.

FM-SiFBA predicted the best fit to data when simulated using Arabidopsis leaf biomass constraints for both the leaf and root sink models (Figure 3.5). This composition was determined using photosynthetic rosettes grown under optimal conditions with no nutrient limitations, closely reflecting the simulation conditions (Arnold and Nikoloski, 2014). In contrast, de Oliveira Dal'Molin et al. (2015) provided compositions for the leaf, stem and root. Applying organ-specific biomass constraints allows SiFBA to predict the effect of different growth demands and modes of resource utilisation. However, constraining growth in FM-SiFBA using these compositions resulted in overestimated growth rates (Figure 3.5). Reviewing the data more closely revealed that the compositions were determined using 24 different European C_3 species (Poorter and Bergkotte, 1992). These included both monocots and dicots but notably excluded Arabidopsis, suggesting that species-specific data are required for accurate growth predictions. Future model versions should attempt to use organ-specific biomass composition for Arabidopsis as model constraints.

3.3.3 Model limitations

Throughout the model construction process, it became apparent that the CDM's carbon-centric view of metabolism presented significant obstacles to its coupling with stoichiometric models that account for all elemental resources. At its core, the CDM functions by updating four carbon stores (Rasse and Tocquin, 2006). Any adjustments made to these stores also affected other metabolic predictions within the network in SoFBA and SiFBA (Section 3.2.4). For example, nitrogen is also essential for plant metabolism and exerts strong control on growth (Stitt et al., 2002). On a whole-plant level, many aspects of nitrogen metabolism remain uncertain.

Recent constraint-based models have shown that it is energetically preferable to assimilate nitrate in illuminated leaves and to then transport assimilates as amino acids to other organs compared to root-based assimilation (Shaw and Cheung, 2018; Cheung et al., 2014; Andrews et al., 2013). This implicates a role for amino acid transport from source tissues to sinks via the phloem (Wilkinson and Douglas, 2003). However, attempts to integrate nitrogen flow between source and sink organs within FM-SoFBA-SiFBA significantly worsened model performance, limiting its applicability for analysing nitrogen metabolism (Figure 3.7).

Extending the scope beyond nitrogen, the CDM's limitations also make FM-SoFBA-SiFBA unsuitable for modelling other resources. For example, calcium, magnesium, phosphorus, potassium, and sulphur have been shown to affect growth and development in plants and are already accounted for in PlantCoreMetabolism (Péret et al., 2011; Osakabe et al., 2013; Ostaszewska et al., 2014; Guo et al., 2015).

The FM was originally developed to model whole-plant growth with the aim of maintaining a modular structure to allow for additional models at different biological scales to be integrated into the framework (Chew et al., 2014). However, the issues described here prove that the FM may not be as flexible and versatile as its authors intended for it to be. The CDM's rigid architecture presents just one example of this. Other aspects of the model that also present potential obstacles to future development include hard-coded model properties (e.g. a fixed time step of one hour), unintuitive coding practices, and the use of proprietary software (MATLAB).

3.4 Conclusions

This chapter aimed to improve the predictive power of the FM at the metabolic level. This was achieved by coupling stoichiometric models of central plant metabolism to the FM. The updated model was able to accurately predict Arabidopsis

shoot growth and provide detailed predictions for fluxes through central metabolism, representing one of the most advanced multiscale whole-plant models to be constructed to date. Other significant model improvements included an improved mechanism for simulating starch metabolism and a reduction in the number of input parameters required. However, significant model limitations were still present, with the main issue being FM-SoFBA-SiFBA's inability to model the interactions and flow of nitrogen between sources and sinks. As the scope of this thesis extends far beyond considering carbon metabolism in isolation, I conclude that FM-SoFBA-SiFBA is an unsuitable modelling framework for adequately addressing the questions posed in this study. The rest of the thesis will therefore focus on the development of an alternative approach to modelling whole-plant metabolism that explicitly avoids the limitations described here.

4 | Constructing a whole-plant model of primary metabolism

4.1 Introduction

Many lessons were learnt from the model integration process between the FM and PlantCoreMetabolism, particularly with respect to the restrictions model structure can impose on modularity and flexibility (Chapter 3). Hard-coded parameters and a carbon-centric focus are highly undesirable model properties. The aim of this chapter was to develop a framework for modelling metabolism at the whole-plant level that explicitly avoids such limitations. The framework should also avoid limitations common to other whole-plant metabolic models, including the lack of validation against growth data, a static approach to metabolism, and an incomplete consideration of all major plant organs (Table 1.2).

A stoichiometric model employing dFBA to simulate growth would provide the appropriate model structure that fulfils these requirements. Organ-specific metabolic models can be connected by common assimilate pools representing the vasculature contents to create a single optimisation problem at the whole-plant level. The control exerted by elemental resources and the environment, such as carbon and nitrogen, can be assessed by imposing uptake and availability constraints.

However, biomass partitioning between organs, which is the mechanism dictating the ultimate destination of assimilates within the plant, cannot be explicitly

accounted for by stoichiometric models. The biology underlying this process and its regulation remain poorly understood due to the complex integration of a host of signals and information cues, including those from genetically-imposed ontogenetic programmes and responses to environment and stress. As a result, many plant growth models instead use empirical relationships to dictate the partitioning of resources within the model. These empirical relationships are formulated from data either in the form of assimilate partitioning coefficients or organ sink strengths, and are provided to models as lookup tables (Kang et al., 2011; Marcelis and Heuvelink, 2007; Marcelis, 1993; Yan et al., 2004). However, this approach is inherently dataset-specific and does not allow for any flexibility in simulating different partitioning patterns under varying environmental conditions and genotypes. I thus sought to establish an improved method for modelling resource partitioning based on theory.

Two main competing theories have been proposed to explain biomass partitioning within a plant. The first, optimal partitioning theory, states that plants will preferentially grow organs that acquire the limiting resource (e.g. the growth of leaves is preferred in a carbon-limited plants; Shipley and Meziane, 2002; Müller et al., 2000). However, when growth patterns in different environments were normalised by accounting for variations in plant size, the apparent control of external resources on partitioning is significantly reduced (Poorter et al., 2012b). The second theory states that biomass partitioning patterns results in allometry, which describes the size-dependent relationship between the growth of different organs (Niklas and Enquist, 2002). Allometric models have shown that canonical allocation rules for vegetative mass can be identified across phylogenies and a ten-order magnitude range in plant size using the following equation:

$$\ln M_Y = \alpha \ln M_X + \ln \beta, \tag{4.1}$$

where M_Y and M_X are the masses of two organs, α is the scaling exponent, and β is the allometric constant (Enquist and Niklas, 2002; Niklas and Enquist, 2002). These relationships are thought to reflect underlying the biophysical constraints that restrict the growth of organs in relation to each other. For example, the mass of water being transported from the roots through the stem for transpiration out of leaf stomata has to be conserved, which imposes limits on the relative cross-sectional area of these organs. Overall, the literature supports allometric scaling laws as a reliable model of biomass partitioning.

In this chapter, I present WholePlantMetabolism v1, a whole-plant metabolic model of growth. The PlantCoreMetabolism stoichiometric model was replicated, and adapted to model metabolic networks in the leaf, stem, and root. These were integrated into a single optimisation problem to represent whole-plant metabolism. A biomass partitioning model was devised according to allometric growth theory and was coupled to the metabolic model. In this instance, WholePlantMetabolism v1 was constrained to simulate vegetative growth in tomato cv. Moneymaker, an important crop plant. To capture the non-linear responses of plant growth to key environmental inputs (light, carbon, and nitrogen), maximum flux constraints derived from kinetic rate equations were applied to the model. Model predictions for both plant growth and metabolic activity were validated against greenhouse tomato growth data and known plant biochemistry.

4.2 Results

4.2.1 Plant growth measurements

I undertook some tomato growth experiments to support the development of the WholePlantMetabolism v1 model. These provided key data that were used as input parameters for the model. The detailed dataset also allowed model predictions to be

tested by comparison to data that was not used to constrain the model. Throughout this thesis, the data from these growth experiments are referred to as the *validation dataset*.

Environmental conditions

Environmental conditions in climate-controlled greenhouses (Department of Plant Sciences, University of Oxford, UK) were monitored throughout the growth period. The daily mean temperature was 23.9 °C, the mean light intensity was 320 µmol m^{-2} s^{-1}, and the day length was 16 hours.

Phytomer appearance rate

Plant development can be followed by observing the rate of organ appearance. In tomato, organs are organised along the main stem in phytomer units, each composed of a leaf attached to the main stem at a node and a subtending stem internode. Reproductive phytomers also include peduncles and fruits. The rate of phytomer appearance is controlled largely by temperature and responds linearly to thermal time (Fleisher et al., 2006). Thermal time is defined as the cumulative mean daily temperature and represents the sum of heat energy provided to the plant.

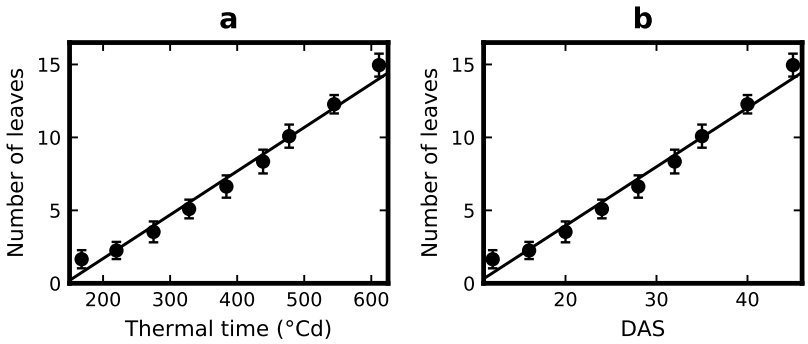

Figure 4.1: The appearance rate of new leaves in tomato cv. Moneymaker grown hydroponically over **(a)** thermal time and **(b)** absolute time. Thermal time is expressed in degree days (°Cd) with a base temperature of 10 °C. Data (symbols) are the mean±SD (n = 22–40) and the line shows a linear regression of the data. DAS, days after sowing.

As there is a leaf in every phytomer unit, the leaf appearance rate can be used as a proxy for phytomer development. A new leaf appeared approximately every 33.4 °Cd during the first 45 days of growth (r^2 = 0.98; Figure 4.1a). This falls within the range of values (28 – 40 °Cd) reported in other studies observing development in tomato plants (Kang et al., 2011; Dong et al., 2008). Additionally, as the plants were grown under constant temperature, the leaf appearance rate also showed a linear response to absolute time, with a new leaf appearing every 2.5 days (r^2 = 0.98; Figure 4.1b).

Plant development was limited to 13 phytomers by removing the shoot apical bud at 45 DAS. If left unpruned, the plants would have continued to produce more vegetative and reproductive phytomers as Moneymaker is an indeterminate variety of tomato.

Fresh and dry mass

Leaves, stems, and roots increased in dry mass throughout the experiment, indicating continual vegetative growth (Figure 4.2a–c). Flowers first appeared on the 10th phytomer at 45 DAS, marking the transition into the reproductive growth phase (Figure 4.2d). An additional truss appeared at the 13th phytomer. Anthesis occurred approximately 10 days after phytomer appearance.

Fresh mass measurements were also recorded at each harvest. However, given that the water content of plant tissues is highly variable, using dry mass ensures more consistency within the data and also between different studies. The fruit (F = 5.77, p = 0.005), root (F = 4.36, p = 0.003), and stem (F = 127.17, p < 0.001) all showed significant differences in water content between each harvest (Appendix A). Only leaf water content remained constant throughout growth (F = 2.12, p = 0.08; Appendix A).

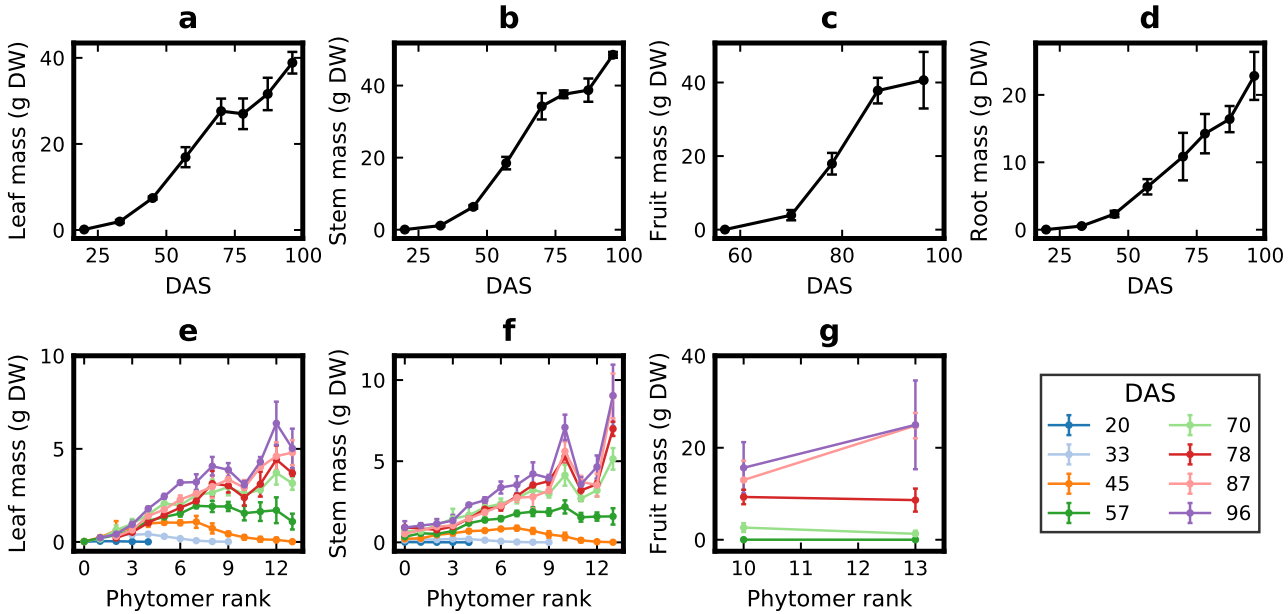

Figure 4.2: Organ growth in tomato cv. Moneymaker categorised by **(a–d)** organ type and **(e–g)** phytomer rank. Data are the mean±SD (n = 3–6 plants per harvest). DAS, days after sowing; DW, dry weight.

The dry mass distribution among organs along the main stem at the phytomer level was also recorded. Leaf and stem dry masses showed bell-shaped distributions across phytomer ranks in younger plants (20 – 57 DAS), with peaks at middle-tier phytomers (Figure 4.2e-f). This pattern has also been observed in several other tomato glasshouse growth experiments (Kang et al., 2011; Dong et al., 2008). In older plants (57 – 96 DAS), the relationship between leaf and stem mass and phytomer rank became increasingly more linear, with positionally higher phytomers being heavier than lower ones. However, stems at the 10th and 13th phytomers had proportionally increased mass and leaves had decreased mass. Both of these phytomers were reproductive and required more stem mass to support fruit growth in the form of peduncles (Figure 4.2g). The decrease in leaf mass may arise from the load-bearing limitations of the main stem at particular phytomer positions (Niklas and Enquist, 2002).

A significantly different number of fruits set on each truss (t = 2.17, p = 0.04), with more fruits setting at the 13th phytomer (Figure 4.3a). However, no significant difference in mature fruit mass, whether at the truss level (t = 1.68, p = 0.16) or at the individual fruit level (t = 0.02, p = 0.99), was found (Figure 4.3b-c).

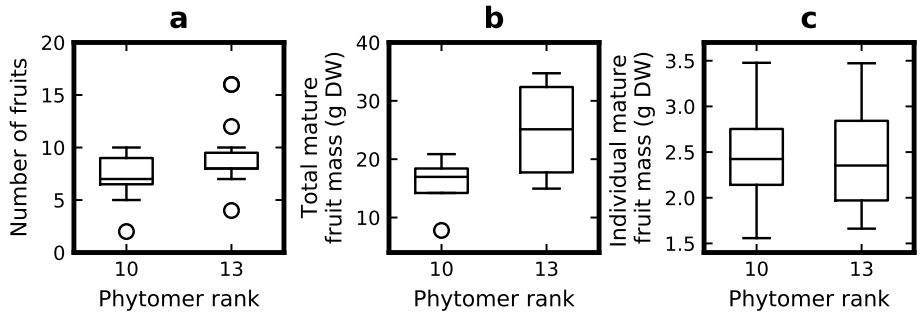

Figure 4.3: (a) Fruit number, **(b)** total mature fruit mass per truss, and **(c)** mean individual mature fruit mass on each truss in tomato cv. Moneymaker. n = 19 plants for fruit number and n = 4 for mature fruit mass (96 days after sowing). DW, dry weight.

Leaf surface area

Figure 4.4a shows that total leaf surface area increased over growth, reflecting increases in leaf mass. The specific leaf area (SLA) of a leaf is a measure of its thickness. Figure 4.4b shows that there was a significant difference between the SLA during vegetative and reproductive growth ($t = 7.38, p < 0.001$). The mean vegetative SLA was 369 ± 29 cm^2 g dry weight^{-1} (DW) and the mean reproductive SLA was 279 ± 23 cm^2 g DW^{-1}, indicating that leaves in younger plants were thinner. Similarly, Heuvelink (1995c) observed that the SLA of tomato decreases over development and ranged between 200–400 cm^2 g DW^{-1}.

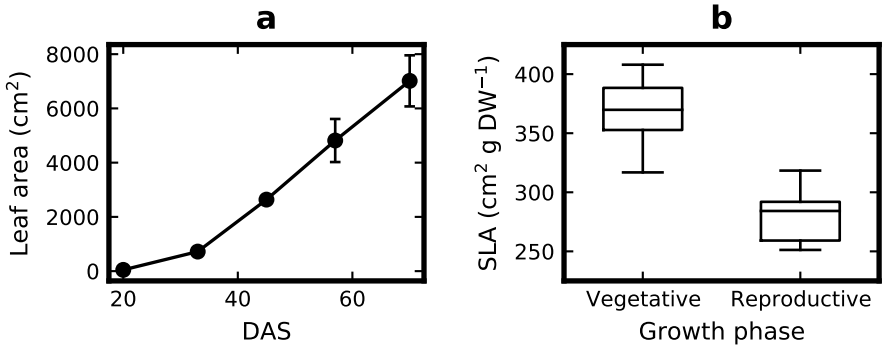

Figure 4.4: (a) Total plant leaf area in tomato cv. Moneymaker over a period of growth. Data are the mean±SD (n = 3–6 plants per harvest). **(b)** The SLA of tomato cv. Moneymaker in two growth phases. n = 14 plants for vegetative growth and n = 8 plants for reproductive growth. DAS, days after sowing; DW, dry weight; SLA, specific leaf area.

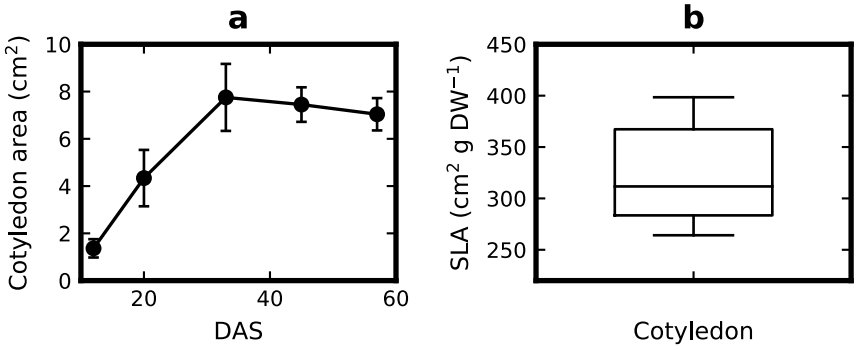

Figure 4.5: (a) Cotyledon surface area in tomato cv. Moneymaker over a period of growth. Data are the mean±SD (n = 3–6 plants per harvest). **(b)** The SLA of cotyledons in tomato cv. Moneymaker (n = 18). DAS, days after sowing; DW, dry weight, SLA, specific leaf area.

Figure 4.5a shows the growth of cotyledons in tomato. Cotyledons were fully expanded by 33 DAS and remained on tomato plants up until 57 DAS. The mean SLA for cotyledons was 322 $\pm$ 46 cm^2 g DW^{-1}(Figure 4.5b). This indicated that cotyledons were thicker than leaves during early development, as also observed by various other studies in a range of species (Pullen et al., 2019; Kitajima, 1992).

4.2.2 Model construction

This section describes how I constructed a whole-plant model of metabolism in tomato during vegetative growth (WholePlantMetabolism v1). In total, the model contained more than 3,300 reactions representing compartmentalised central metabolism in the leaf, root, and stem. Figure 4.6a shows a simplified schematic of the final metabolic network of the whole-plant model.

Tissue-specific models

As in Section 3.2.1, a model of diel leaf metabolism was generated from PlantCoreMetabolism v1.2. Additional copies of PlantCoreMetabolism v.1.2 were constructed to represent the root and the stem. The biomass composition of each organ was constrained according to experimental values (Appendix A). Principally, cellulose, fatty acids, proteinogenic amino acids, soluble sugars, and starch were considered. Species-specific data were available for tomato leaves (Yuan et al., 2016a). However, interspecies averages from 24 C_3 species were applied to the root and stem models as no equivalent data could be found (Poorter and Bergkotte, 1992).

Photon uptake was only permitted in the leaf during the day. This assumes that photosynthetic activity in the stem is negligible compared to that in the leaf. Hetherington et al. (1998) report that only 4% of the photosynthetic activity at each phytomer unit happens in the stem.

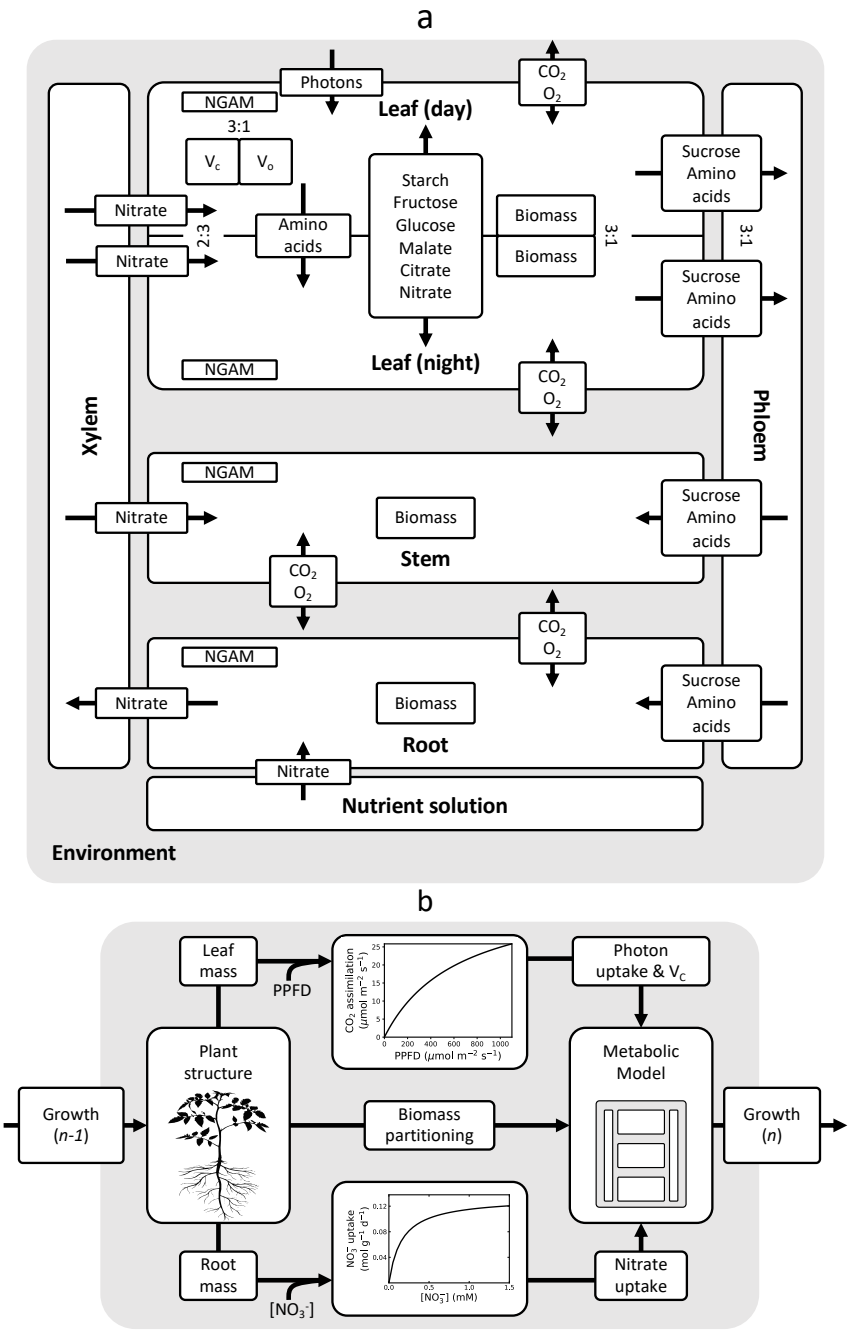

Figure 4.6: Schematic of WholePlantMetabolism v1 model structure. **(a)** Stoichiometric models for diel leaf, root, and stem metabolism are connected via common metabolite pools representing plant vasculature (the phloem and xylem). The model is optimised for biomass production. Linker reactions between the leaf day and night phases allow for metabolite storage over the diel cycle. Specified ratios indicate flux ratio constraints between reaction pairs. **(b)** Modelling framework for constraining and simulating growth on day *n*. The plant structure records model predictions for the mass of organs at the start of each day, which is used to scale the maximum leaf CO_2 assimilation rate, leaf photon uptake rate, and root nitrate uptake rate observed empirically under specified environmental conditions. NGAM, non-growth associated maintenance; PPFD, photosynthetic photon flux density; V_C, RuBisCO carboxylase rate; V_O, RuBisCO oxygenase rate.

Mineral nutrients from the hydroponic solution could only be taken up by the root (calcium, magnesium, nitrate, phosphate, potassium, and sulphate). As the hydrophobic Casparian strip within root endodermal tissues forces all nutrients bound for the xylem to enter the symplast, transport costs were imposed onto all root nutrient uptake reactions (Cheung et al., 2013). Metabolite transport in plants often rely on proton gradients established across a membrane through energy-dependent processes (Gaxiola et al., 2007). In the model, proton-pumping ATPases are localised to the plasma membrane and tonoplast, allowing for metabolite transport into the cytosol and vacuole, respectively, using proton co-transport. A new compartment was added to the model to represent the hydroponic growth solution, allowing for apoplastic metabolite pools either side of the Casparian strip to be distinguishable.

Plant vasculature

The diel leaf, root, and stem models were integrated into a single framework through two compartments representing plant vasculature (Figure 4.6a). Neither the phloem or the xylem were metabolically active and both were functionalised solely for transport. Observations of growth patterns in tomato support the hypothesis that transport resistance and the effect of physical distance between organs do not significantly affect resource partitioning (Heuvelink, 1995a). This supports the model assumption that the plant vasculature forms a single common metabolite pool, equally accessible to all organs.

Xylem loading by the root and xylem unloading by the leaf and stem were permitted to allow for nutrient transport (calcium, magnesium, nitrate, phosphate, potassium, and sulphate). As xylem loading is thought to be a largely passive process, no transport costs were included in the model (Köhler, 2007). On the other hand, xylem unloading in the leaf and stem models was constrained to only proceed

with proton co-transport to represent cellular uptake cost. The stoichiometry of each uptake reaction was defined according to values specified in Cheung et al. (2014).

Phloem loading by the leaf and unloading in the root and stem were allowed to support sugar and amino acid transport. The metabolite composition of the phloem was constrained according to values observed in tomato cv. Kingley Cross and Platense through phloem exudate experiments (Valle et al., 1998; Walker and Ho, 1977). Sucrose forms the majority of this composition (76%), with hexose sugars and amino acids forming the remaining proportion (Appendix A). The model was allowed to load and unload metabolites from the phloem in these fixed ratios only. Both phloem loading and unloading had associated transport costs to represent import into companion cells and import into sink cells, respectively. The stoichiometry of each reaction was defined according to values specified in Cheung et al. (2014).

4.2.3 Simulating growth

WholePlantMetabolism v1 models growth from the seedling to the mature vegetative stage (12 to 45 DAS) using dFBA (Figure 4.6b). The diel framework can easily be adapted to model metabolism at various timescales: flux predictions can simply be scaled to shorter or longer time intervals, as shown in Chapter 3. WholePlantMetabolism therefore does not have a fixed time step. In this work, a daily time step was chosen as the diel model simulates growth over a 24 hour period by default.

Maximising whole-plant biomass production was chosen as the primary objective function in FBA optimisations, with total flux minimisation acting as an additional constraint. The decision to use a biomass objective was made on the assumption that crops bred for yield have been selected for maximised growth.

After a period of growth, the masses of each organ are updated and relayed onto the next time step as

$$M_X(t) = M_X(t-1) + G_X(t-1), \tag{4.2}$$

where $M_X(t)$ is the dry mass of organ X at the start of day t and $G_X(t-1)$ is the growth of organ X over the preceding day. Updated organ masses are used to scale constraints for growth over the day in two ways: (1) maximum uptake rates are scaled according to organ size (e.g. the maximum root nitrate uptake rate is scaled according to root mass) and (2) allometric exponents for the growth of different organs are scaled using leaf, root, and stem mass to reflect changes in resource partitioning patterns.

The model simulates growth post-germination and does not account for seed metabolism. Simulations begin at 12 DAS, meaning that initial organ masses need to be provided as input parameters. In the validation dataset, seedlings have the following mass distribution at this developmental stage: 1.4 mg DW leaves, 2.5 mg DW roots, and 1.2 mg DW stems (Figure 4.2).

Carbon assimilation

Carbon assimilation relies on energy generated by light-dependent photosynthetic processes. Canopy effects can significantly reduce photosynthetic activity as a result of the attenuation of light through the canopy (Hirose, 2005). This includes the effect of self-shading by leaves of the same plant, leaf angle relative to the source of light, and also shading between plants grown in the same vicinity. The Monsi-Saeki model quantifies the light received within the canopy (PPFD′) relative to light received above the plant on the horizontal plane (PPFD) as

$$\text{PPFD}' = \frac{\text{PPFD} \cdot k \cdot e^{-kF}}{1-m}, \tag{4.3}$$

where k is the extinction coefficient of leaves, F is the leaf area index (LAI) and m is the transmittance of leaves (Monsi and Saeki, 1953). For tomato, de Oliveira Pereira et al. (2019) reports that k = 0.8 and Acock et al. (1976) reports that m = 0.1. Figure 4.7 shows the reduction in light levels within the canopy of tomato over a range of values for LAI, which measures the density of plant leaf area, when provided with 320 µmol m^{-2} s^{-1} of light. The Monsi-Saeki model predicts an exponential reduction in canopy photosynthesis as a function of LAI.

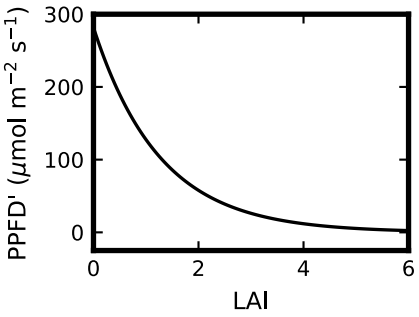

Figure 4.7: Light intensity within a tomato plant canopy (PPFD') predicted by the Monsi-Seki model as a function of LAI when provided with 320 µmol m^{-2} s^{-1} PPFD above the plant on the horizontal plane. LAI, leaf area index; PPFD, photosynthetic photon flux density.

Carbon assimilation also exhibits a non-linear response to light availability, with saturation kinetics at high light intensity. By fitting a non-rectangular hyperbola function to data reported by Nunes-Nesi et al. (2005), I derived the following relationship between net carbon assimilation (A) and PPFD′ in tomato cv. Moneymaker:

$$A = \frac{40.9 \cdot \text{PPFD}'}{644 + \text{PPFD}'}, \tag{4.4}$$

where both A and PPFD′ are expressed in µmol m^{-2} s^{-1}.

As shown before in Chapter 3, directly constraining the net carbon assimilation rate in a diel set-up results in CAM-like behaviour. To avoid this, I varied the RuBisCO carboxylation rate (V_C) in the model until the net carbon assimilation rate predicted by the model matched that derived from Equation 4.4 for the mean

growth light intensity (Nunes-Nesi et al., 2005). For model compatibility, V_C and PPFD′ were scaled from µmol m^{-2} s^{-1} to mmol g DW^{-1} day^{-1} by

$$\frac{3600 \cdot V_C \cdot \text{SLA} \cdot p}{1000}, \tag{4.5}$$

$$\frac{3600 \cdot \text{PPFD}' \cdot \text{SLA} \cdot p}{1000}, \tag{4.6}$$

respectively, where p is the photoperiod.

Cotyledons also contribute to photosynthetic activity during early development. In the validation dataset, the mean surface area of fully expanded tomato cotyledons (c) was 7.46 ± 1.07 cm^2 and cotyledons remained on plants up until 57 DAS before senescing and dropping off (Figure 4.5). Leaf carbon assimilation on days of growth where cotyledons are still photosynthetically active is thus modelled by constraining the maximum RuBisCO carboxylase ($V_{C\,\text{max}}$) and the maximum photon uptake fluxes (P_{max}) as

$$V_{C\,\text{max}}(t) = V_C(t) \cdot (M_L(t) + \frac{c}{\text{SLA}}), \tag{4.7}$$

$$P_{\text{max}}(t) = \text{PPFD}'(t) \cdot (M_L(t) + \frac{c}{\text{SLA}}), \tag{4.8}$$

where M_L is the leaf dry mass. Leaf carbon assimilation was modelled on days without photosynthetic activity in cotyledons as

$$V_{C\,\text{max}}(t) = V_C(t) \cdot M_L(t), \tag{4.9}$$

$$P_{\text{max}}(t) = \text{PPFD}'(t) \cdot M_L(t). \tag{4.10}$$

Nitrogen uptake

Root nitrate uptake is mediated by both low and high affinity transport systems (Parker and Newstead, 2014). To date, few nitrate transporters in tomato have been characterised, though five genes in the *Le*NRT family have been identified (Fu et al., 2015). Albornoz et al. (2018) and Smart and Bloom (1988) show that nitrate

uptake in tomato exhibits biphasic Michaelis-Menten kinetics, with high affinity transporters operating in the micromolar range and low affinity transporters at higher concentrations. WholePlantMetabolism v1 thus constrains maximum root nitrate uptake (N_{max}) as

$$N_{\text{max}}(t) = \frac{V_{\text{max}} \cdot [NO_3^-]}{K_M + [NO_3^-]} \cdot M_R(t), \tag{4.11}$$

$$V_{\text{max}} = \begin{cases} 133 \text{ mmol g DW}^{-1} \text{ day}^{-1}, & [NO_3^-] > 1\text{mM} \\ 4.51 \text{ mmol g DW}^{-1} \text{ day}^{-1}, & \text{otherwise} \end{cases}, \tag{4.12}$$

$$K_M = \begin{cases} 0.16 \text{ mM}, & [NO_3^-] > 1\text{mM} \\ 43 \text{ µM}, & \text{otherwise} \end{cases}, \tag{4.13}$$

where V_{max} is the maximum rate of uptake, K_M is the Michaelis-Menten constant, $[NO_3^-]$ is the nitrate concentration in the root growth media, and M_R is the root dry mass.

Plants in the validation dataset were provided with 14 mM nitrate, yielding a nitrate uptake rate of 132 mmol g DW^{-1} day^{-1}. Given that the hydroponic nutrient solution was regularly replaced and that a saturating concentration of nitrate was supplied, the model assumes that the nitrate concentration in the medium was constant (i.e. it was not significantly depleted from the large excess present in the hydroponic growth solution).

Non-growth associated maintenance respiration

Different NGAM demands have been reported for leaf, stem and root tissues in tomato. Heuvelink (1995b) reported that NGAM requirements are highest in the leaf (3.24 mmol ATP g DW^{-1} day^{-1}) and lower in roots and stems (1.08 and 1.62 mmol ATP g DW^{-1} day^{-1}, respectively). For the root and stem, NGAM demands are applied to the model by scaling according to the organ mass (e.g. $1.08 \cdot M_R$ for the root) and distributing a quarter of the flux to generic NADPH oxidase reactions, and

the rest to a generic ATPase reaction. For the leaf, daytime and night-time NGAM demands are assumed to be equal per unit time and requires scaling according to the photoperiod. Leaf NGAM demands over each phase (NGAM_L) are calculated at each daily time step as

$$\mathrm{NGAM}_L(t) = \begin{cases} 3.24 \cdot M_L(t) \cdot \frac{p}{24}, & P_{\max} > 0 \\ 3.24 \cdot M_L(t) \cdot \frac{(24-p)}{24}, & \text{otherwise} \end{cases}. \tag{4.14}$$

4.2.4 Biomass partitioning

As explained in Section 4.1, allometric models can accurately capture the relationships between the growth of different organs and its size-dependency (Poorter et al., 2012b). This section describes the results of applying an allometric biomass partitioning function to WholePlantMetabolism v1.

Allometric growth

Figure 4.8a-c shows the relationship between log-transformed leaf, root, and stem mass measurements in the validation dataset. Fitting RMA linear regression models to these, I derived the scaling exponent (α) from the slope and the allometric constant (β) from the y-intercept. Tomato growth data was also provided by Niklas and Enquist (2002). These measurements were made on plants grown in diverse environments, ranging in size by many magnitudes and of various ages (Figure 4.8d-f). Combining all the mass data for tomato from these two datasets together (*combined dataset*), Figure 4.8g-i shows that the validation dataset and data from Niklas and Enquist (2002) express similar trends at the species level.

The scaling exponent is equal to the ratio of the relative growth rates between two organs:

$$\alpha_{M_Y/M_X} = \frac{\ln M_Y(t) - \ln M_Y(t)}{\ln M_X(t) - \ln M_X(t)}, \tag{4.15}$$

where $M_X(t)$ and $M_Y(t)$ are the masses of organs X and Y at time t, respectively. If $\alpha = 1$, the relative growth of two organs is said to be isometric. Hyperallometric and hypoallometric growth are achieved when $\alpha > 1$ or $\alpha < 1$, respectively.

Additional mass datasets for angiosperms and spermatophytes were provided by Niklas and Enquist (2002). Table 4.1 shows α and β parameters derived from each dataset. Angiosperm- and spermatophyte-specific datasets generated allometric

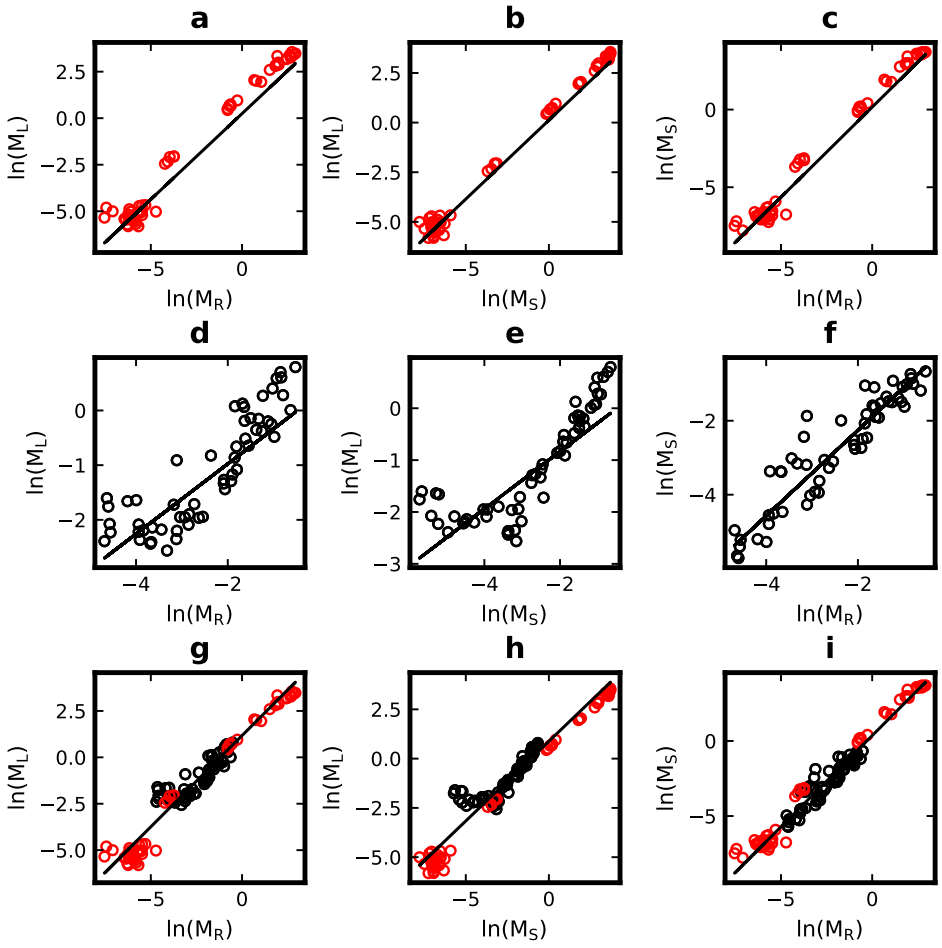

Figure 4.8: Allometric relationships between log-transformed leaf (M_L), root (M_R), and stem (M_S) mass over vegetative growth in tomato derived from **(a-c)** the validation dataset (red), **(d-f)** tomato-specific data from Niklas and Enquist (2002, black), and **(g-i)** the two datasets combined. Solid lines indicate RMA linear regression models fitted to the data. $n = 55$ plants for the validation dataset and $n = 114$ for the Niklas and Enquist (2002) dataset. RMA, reduced major axis.

relationships similar to the canonical rules derived by Niklas and Enquist (2002): $M_L \propto M_S^{3/4} \propto M_R^{3/4}$, such that $M_S \propto M_R$. Tomato-specific datasets expressed similar trends qualitatively. However, in the validation dataset, the hypoallometric relationship between leaf and root growth verged closer to isometry, as did the hypoallometric relationship between leaf and stem growth. Contrastingly, the hyperallometric relationship between stem and root growth verged further away from isometry. Expanding the analysis to include tomato data from Niklas and Enquist (2002) in the combined dataset enhanced these quantitative differences between species-specific scaling exponents for tomato and interspecific values further.

Allometric relationships as partitioning constraints

WholePlantMetabolism v1 uses scaling exponents to calculate the ratio of absolute growth rates (i.e. biomass partitioning) by accounting for the size of each organ present. The stoichiometry of the whole-plant biomass reaction is constrained at each time step as

$$\begin{aligned}(M_L(t) \cdot \alpha_{M_L/M_R}) \cdot \text{Biomass}_L + M_R(t) \cdot \text{Biomass}_R \\ + (M_S(t) \cdot \alpha_{M_S/M_R}) \cdot \text{Biomass}_S \rightarrow ,\end{aligned} \tag{4.16}$$

where Biomass_X is a pseudometabolite produced by the biomass reaction of organ X in a 1:1 ratio, and M_S is the stem dry mass. For leaf growth, biomass production has to be partitioned between the day and the night phases. To reflect the relative demand for phloem output over the diel cycle, leaf growth was constrained to 3:1 between the day and the night (Gibon et al., 2004).

Table 4.1: Scaling exponents (α)and allometric constants (β) derived from various log-transformed leaf (M_L), root (M_R), and stem (M_S) mass datasets. RMSE values indicate the goodness of fit to the validation dataset by WholePlantMetabolism v1 predictions when simulated with different scaling exponents. RMSE, root-mean-square error.

Dataset	Species	M_X v M_Y	n	$\alpha \pm$ SD	$\beta \pm$ SD	RMSE		
						Leaf	Root	Stem
Validation dataset	Tomato	M_R v M_L	55	0.92 ± 0.016	0.25 ± 0.041	1.17	0.20	0.93
		M_S v M_L	55	0.79 ± 0.007	0.12 ± 0.020			
		M_R v M_S	55	1.16 ± 0.012	0.15 ± 0.032			
Validation dataset & Niklas and Enquist (2002)	Tomato	M_R v M_L	169	0.98 ± 0.020	1.17 ± 0.069	0.67	0.23	0.42
		M_S v M_L	169	0.81 ± 0.017	$0.88 \pm 0.0.68$			
		M_R v M_S	169	1.22 ± 0.019	0.36 ± 0.065			
Niklas and Enquist (2002)	Angiosperms	M_R v M_L	396	0.80 ± 0.008	-	3.16	0.6	2.22
		M_S v M_L	692	0.72 ± 0.005	-			
		M_R v M_S	389	1.13 ± 0.007	-			
Niklas and Enquist (2002)	Spermatophytes	M_R v M_L	568	0.84 ± 0.008	-	2.65	0.37	1.84
		M_S v M_L	1042	0.76 ± 0.004	-			
		M_R v M_S	560	1.12 ± 0.006	-			

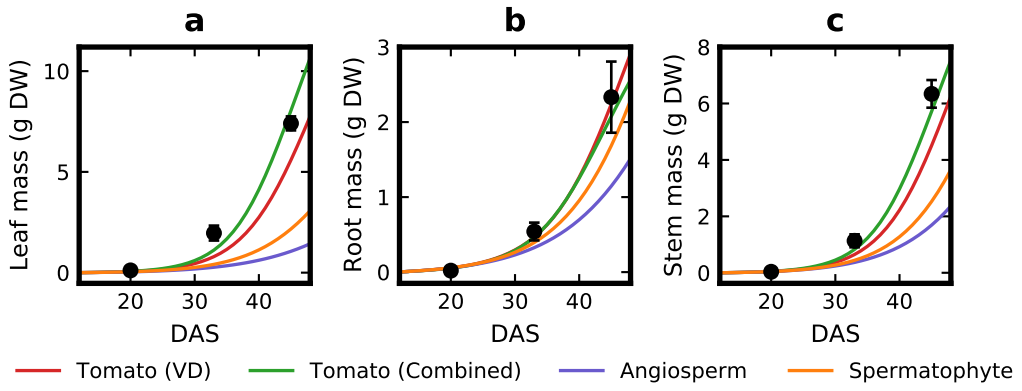

Figure 4.9: Growth predictions (coloured lines) for **(a)** leaf, **(b)** root, and **(c)** stem by WholePlantMetabolism v1 during the vegetative growth stage using scaling exponents derived from different datasets. Tomato-specific data were provided from two different sources: the validation dataset (VD) and Niklas and Enquist (2002) . Data (black symbols) are the mean±SD mass of tomato cv. Moneymaker in the validation dataset (n = 3–6 at each harvest). The goodness of fit of model predictions to the data are listed in Table 4.1. DAS, days after sowing; DW, dry weight.

Table 4.1 shows the accuracy of growth predictions made by the model when different allometric rules were applied to the biomass partitioning function, and Figure 4.9 shows organ growth predictions in comparison to growth data. Simulations using scaling exponents derived from angiosperm and spermatophyte datasets resulted in poor fits to the validation dataset. Underinvestment in leaf growth hampered total plant growth by limiting the plant's capacity to assimilate carbon (Figure 4.9a). This arose from the more strongly hypoallometric relationship between leaf and both root and stem growth reported for angiosperms and spermatophytes. In contrast, using scaling exponents derived from tomato datasets unsurprisingly resulted in the best model behaviour. Using data from the validation data resulted in good growth predictions, though leaf and stem mass were slightly underestimated (Figure 4.9a,c). Simulations using scaling exponents derived from the combined dataset predicted very good fits to growth data for all three organs, with predictions for leaf, stem, and root mass at the end of the vegetative growth phase (45 DAS) falling within experimental error (Figure 4.9). Taking model performance into account, biomass partitioning in WholePlantMetabolism v1 was

modelled using scaling exponents from the combined tomato dataset.

4.2.5 Metabolic flux predictions

This section describes the metabolic flux predictions for vegetative growth in tomato generated by WholePlantMetabolism v1 when simulated under reference environmental conditions. Aspects of both whole-plant metabolism and organ-specific flux distributions for the leaf, root, and stem are considered.

Carbon and nitrogen assimilation

Plant growth in the model was principally controlled by three environmental inputs: light, carbon, and nitrogen availability. Table 4.2 shows that both light and nitrate were being provided to the system in excess, and that growth was carbon limited — the leaf model assimilated the maximum amount of carbon possible throughout development.

Table 4.2: Maximum metabolic capacities calculated from the availability of resources in the environment (upper bound) and flux predictions at 45 days after sowing by WholePlantMetabolism v1 for growth in tomato cv. Moneymaker. Values are provided in mmol g DW^{-1} day^{-1}, and the upper bounds for RuBisCO carboxylase, photon uptake, and nitrate uptake reactions were calculated according to Equations 4.7, 4.8, and 4.11, respectively. DW, dry weight.

Reaction	Organ	Upper bound	Flux
RuBisCO carboxylase	Leaf (day)	97.3	97.3
Photon uptake	Leaf (day)	1962.6	1204.2
Nitrate uptake	Root	251.4	5.3

The model predicted carbon assimilation by RuBisCO to only occur in the leaf during the day. Figure 4.10a–b shows that both light uptake and carbon assimilation in the leaf increased exponentially throughout development, reflecting increases in leaf surface area.

Similarly, nitrate uptake from the hydroponic growth solution increased with plant age (Figure 4.10c). Following import into the root, the majority of the nitrate was loaded into the xylem for transport to the leaf and stem models. In all organs,

nitrate was assimilated via NR and NiR to generate ammonium for amino acid synthesis. The model predicted that the percentage of total nitrate assimilation taking place in the shoot ranged between 56–87%, with an increase throughout development (Figure 4.10d).

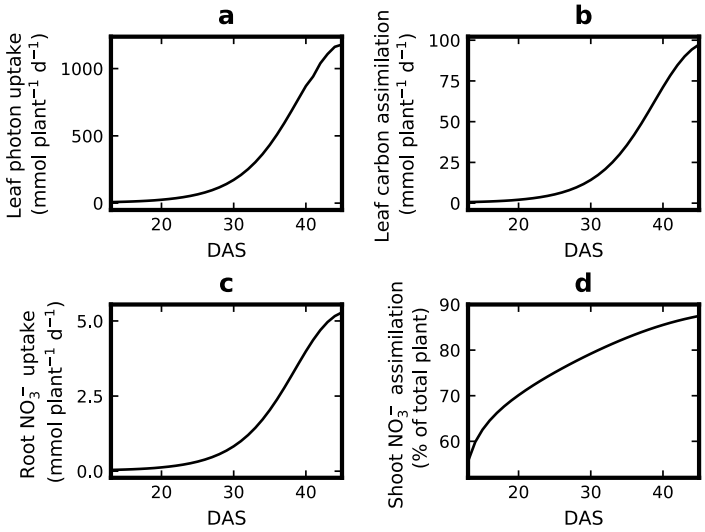

Figure 4.10: Flux predictions for light, carbon, and nitrogen assimilation by WholePlantMetabolism v1 over vegetative growth in tomato cv. Moneymaker. DAS, days after sowing.

Leaf metabolism

Figure 4.11 summarises the major fluxes predicted for leaf metabolism during vegetative growth. Metabolic activity in the leaf during the day was dominated by the photosynthetic light-dependent reactions, with the plastidial electron transport chain (ETC) contributing to 88% of daytime ATP synthesis via plastidial ATP synthase and daytime reducing power synthesis via ferredoxin-NADP+ reductase (Figures 4.12 and 4.13). The mitochondrial ETC generated the remaining 12% of ATP.

The majority of the ATP (85%) and the reducing power (80%) was used to assimilate carbon via the CBB cycle in the chloroplast. As RuBisCO oxygenase flux was constrained to be active in relation to its carboxylase flux, photorespiratory

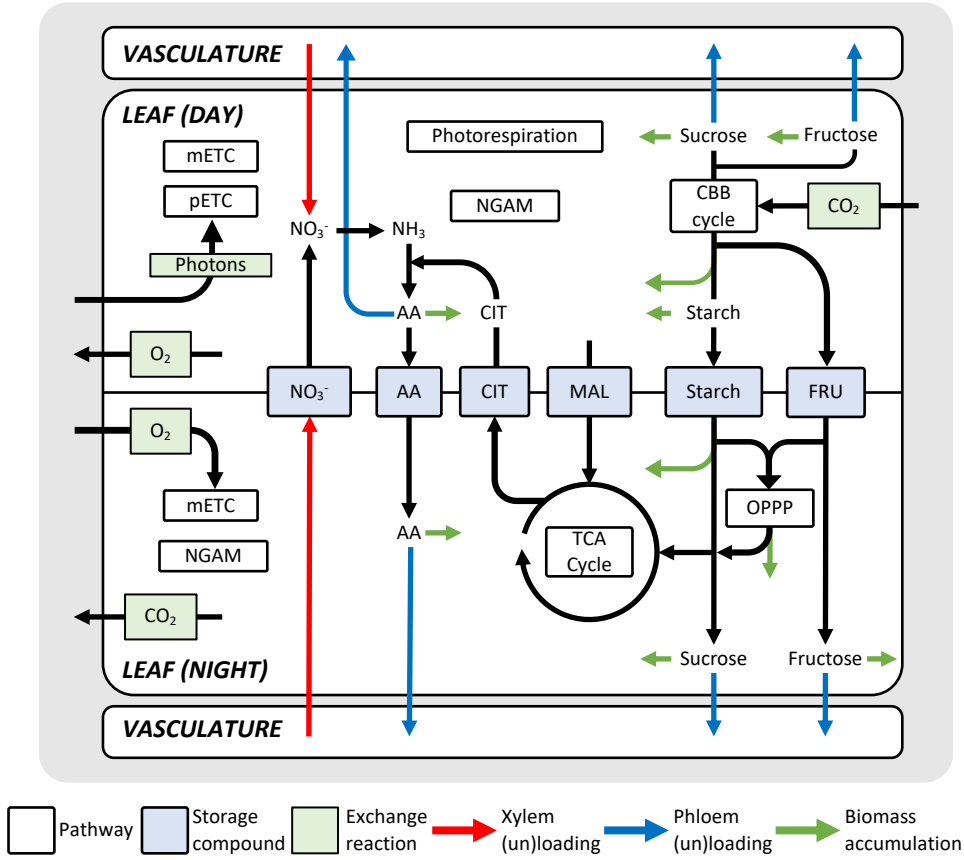

Figure 4.11: Flux predictions for leaf metabolism during vegetative growth in tomato cv. Moneymaker. Phototrophic growth was predicted during the day, with large fluxes though photosynthetic pathways. Heterotrophic growth was predicted during the night, with starch stored over the preceding day being the ultimate source of energy. AA, amino acids; CBB, Calvin-Benson-Bassham; CIT, citrate; FRU, fructose; MAL, malate; mETC, mitochondrial electron transport chain; NGAM, non-growth associated maintenance; OPPP, oxidative pentose phosphate pathway; pETC plastidial electron transport chain; TCA, tricarboxylic acid.

pathways were active and consumed 4% of the daytime ATP pool and 6% of the NAD(P)H pool. The oxidation of photorespiratory glycine by mitochondrial glycine decarboxylase generated a substantial amount of NADH that was used exclusively for mitochondrial ETC activity to generate ATP. The photorespiratory demand for NADH in the peroxisome (for hydroxypyruvate reductase) was met via the chloroplast-cytosol and cytosol-peroxisome malate-oxaloacetate shuttles, which were used to transfer reducing power from the chloroplast to the peroxisome. NGAM requirements contributed to only 2% of daytime ATP usage (Figure 4.12)

The remainder of the daytime ATP pool was used in biosynthetic processes to generate biomass and phloem export components (Figure 4.11). The model predicted that nitrate assimilation in the leaf occurred exclusively during the day through the GS/GOGAT pathway, with nitrate taken up from the xylem being accumulated during the night in the vacuole and released into the cytosol during the day. Some citrate accumulation during the night was also predicted, providing carbon skeletons for amino acid synthesis during the day. A select collection of amino acids were accumulated during the day to support phloem export and biomass demands during the night. 6% of daytime ATP consumption was dedicated to growth-related protein synthesis.

The model predicted starch as the main energy storage compound that was accumulated during the day to fuel night-time metabolism (Figure 4.11). During the night, starch was degraded via hydrolysis to generate sucrose for growth and also for export to the phloem. The model also predicted some fructose accumulation during the day, which contributed directly to growth and phloem export during the night.

The TCA cycle was predicted to operate cyclically during the night, generating reducing power for ATP production via the mitochondrial ETC, which contributed to 94% of the leaf's night-time ATP pool (Figure 4.12). Malate stored during the day was transported from the vacuole to mitochondria to fuel the TCA cycle. The mitochondrial ETC consumed 57% of the leaf's night-time NAD(P)H pool (Figure 4.13). Another 23% was consumed by NGAM.

ATP consumption during the night was principally shared between NGAM (33%), plasma membrane proton-ATPase pump flux (25%), and GTP synthesis (14%; Figure 4.12). Proton pump activity into the apoplast provided energy for nitrate uptake from the xylem and also for the export of metabolites to the phloem. On the other hand, GTP provided energy for protein and cellulose synthesis required

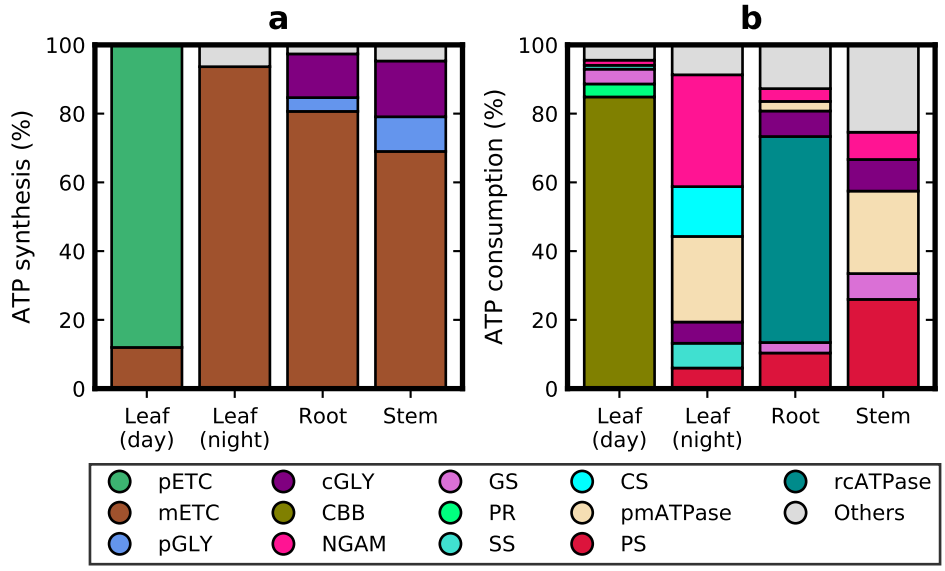

Figure 4.12: Model predictions for **(a)** ATP synthesis and **(b)** ATP consumption during vegetative growth in tomato cv. Moneymaker at 45 days after sowing. CBB, Calvin–Benson–Bassham cycle; CS, cellulose synthase; GS, glutamine synthetase; NGAM, non-growth associated maintenance; PR, photorespiration; PS, protein synthesis; SS, sucrose synthesis; cGLY, cytosolic glycolysis; mETC, mitochondrial ETC; pETC, plastidial ETC; pGLY, plastidial glycolysis; pmATPase, plasma membrane proton pump; rcATPase, root cortical proton pump.

for growth.

In total, 68% of metabolic activity in the leaf was dedicated to producing metabolites for export to the phloem (Figure 4.11). The rest constituted processes for biomass production for leaf growth. This remained constant throughout the diel cycle due to the flux ratio constraints imposed on both biomass accumulation and phloem export.

Root metabolism

Figure 4.14a summarises the metabolic flux predictions for the root, which was characterised by the degradation of sucrose provided by the phloem into fructose and UDP-glucose via cytosolic sucrose synthase for biomass production. Fructose entered glycolysis via fructose-1,6-bisphosphate, ultimately providing acetyl-CoA in the mitochondrion to the TCA cycle via pyruvate dehydrogenase. Combined, cytosolic glycolysis and the TCA cycle produced a total of 60% of the root's NAD(P)H

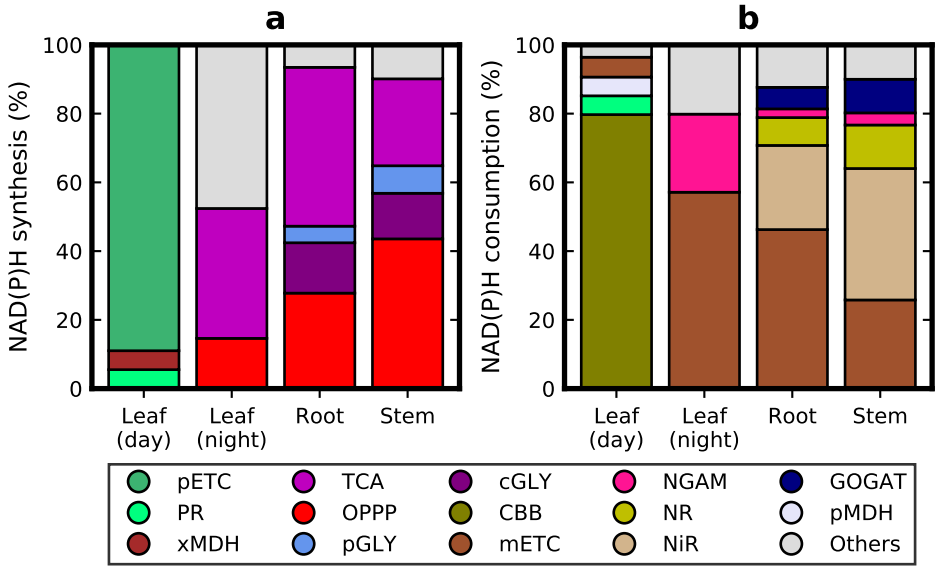

Figure 4.13: Model predictions for **(a)** reducing power synthesis and **(b)** reducing power consumption during vegetative growth in tomato cv. Moneymaker at 45 days after sowing. Abbreviations are as for Figure 4.12, as well as: GOGAT, glutamate synthase; NR, nitrate reductase; NiR, nitrite reductase; OPPP, oxidative pentose phosphate pathway; pMDH, plastidial malate dehydrogenase; TCA, tricaboxylic acid cycle; xMDH, peroxisomal malate dehydrogenase.

supply and 13% of the ATP pool (Figures 4.12 and 4.13). 46% of the reducing power pool was used to generate ATP via the mitochondrial ETC, which provided 80% of the root's ATP supply.

On the other hand, 39% of UDP-glucose was used as a precursor for cellulose synthesis. The remaining 61% was directed into the oxidative pentose phosphate pathway (OPPP) in the plastid to generate NADPH (Figure 4.14a). Ultimately, this produced triose phosphates, which entered the plastidial glycolysis pathway to generate more reducing power. Overall, the OPPP and plastidial glycolysis generated 35.5% of the root's reducing power pool and 4% of the ATP pool. Further, acetyl-CoA synthesis in the plastid was used to produce fatty acids as a biomass component.

Root metabolic activity was also dominated by the active uptake of nutrients from the hydroponic growth solution, with proton-ATPase powering the export of protons at the root surface consuming 59% of the organ's ATP pool (Figure 4.12).

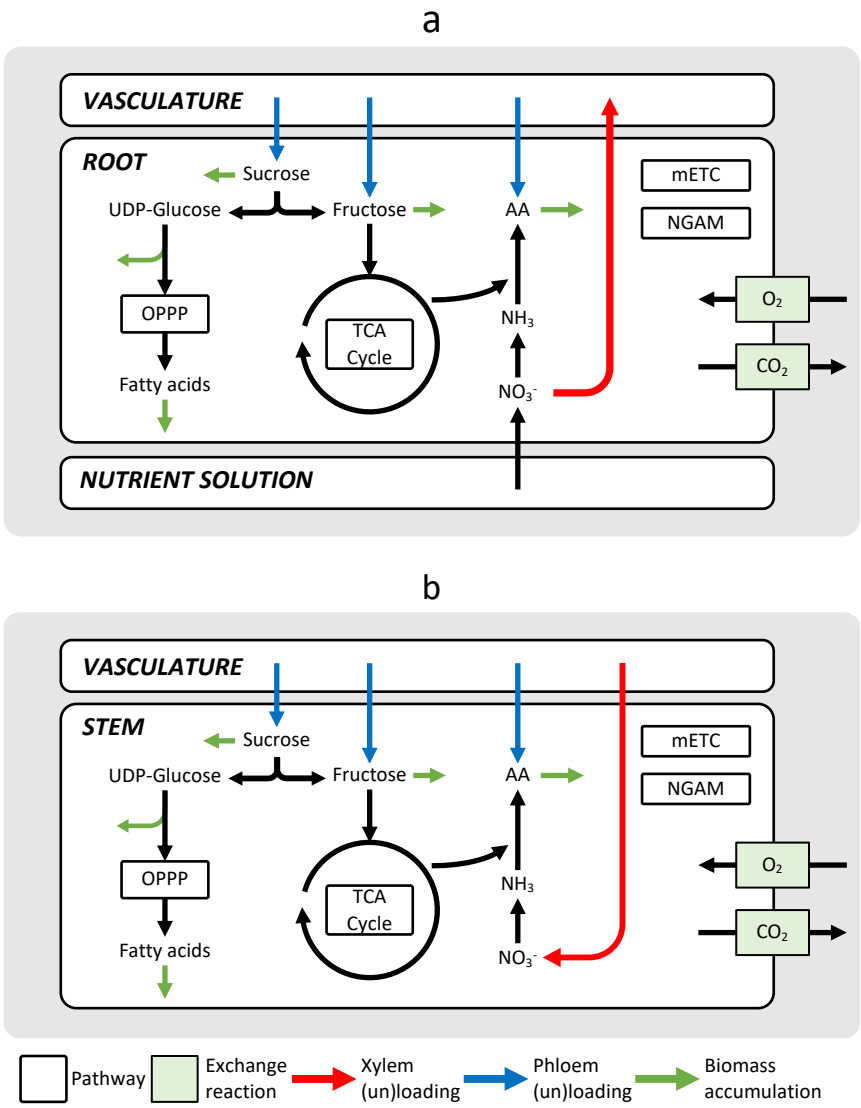

Figure 4.14: Flux predictions for **(a)** root and **(b)** stem metabolism during vegetative growth in tomato cv. Moneymaker. Heterotrophic growth using sucrose provided from the leaf via the phloem was the ultimate source of energy in both the root and stem. Abbreviations are as for Figure 4.11, as well as: OPPP, oxidative pentose phosphate pathway; UDP, uracil-diphosphate.

Nitrate assimilation constituted a large energetic cost to the root, with NR, NiR, GS, GOGAT collectively making up 40% of demand for reducing power and 3% of ATP demand. Only 14% of the nitrate taken up from the environment was assimilated in the root, with the remainder being exported to the shoot via the xylem. As a result of the constraint on phloem composition, amino acid uptake from the phloem accompanying sucrose uptake was predicted. However, the majority of

the nitrate contributing to protein synthesis in the root was assimilated in the root itself (86%).

Stem metabolism

The model predicted similar metabolic behaviour for the stem compared to the root (Figure 4.14b). Sucrose imported from the phloem was degraded to produce ATP and reducing power via glycolysis, the mitochondrial ETC, and the OPPP to fuel the production of biomass components. Once again, glycolytic pathways were active in both the cytosol and the plastid.

Amino acids imported from the phloem contributed to protein synthesis. However, this was not sufficient to fulfil the biomass requirements of the stem and additional nitrate from the xylem was imported, making up 89% of the total nitrogen input into the organ. Uptake costs from the vasculature consumed 24% of the stem's ATP pool (Figure 4.12). As with the root, nitrate assimilation demanded a large proportion of the stem's reducing power (61%) and ATP pool (8%). The conversion of nitrite to ammonium via plastidial NiR was predicted to be the most energetically costly step; it alone required 38% of the stem's reducing power. Protein synthesis also was energetically demanding in the stem (27% of the stem's ATP pool).

NGAM only demanded 8% of the stem's ATP pool and 4% of the NAD(P)H pool (Figure 4.12 and Figure 4.13). This is comparable to the maintenance cost associated with the root, but significantly lower than in the leaf during the night.

4.3 Discussion

WholePlantMetabolism v1 presents a modelling framework that is capable of predicting both detailed metabolic fluxes through multiple plant tissues and resource partitioning between organs over vegetative growth. By using a minimal number

of environmental, physiological, and kinetic parameters, the model was able to predict growth in tomato accurately when compared to a reference dataset (Figure 4.9).

In this particular instance, WholePlantMetabolism v1 was parameterised for tomato growth. However, an advantage of using PlantCoreMetabolism, a generic model which contains no species-specific information, as the foundation for generating organ-specific models is that it can be applied to model any plant species. The framework presented here can thus be expanded to model many other important plant species, provided that the minimal set of parameters required is readily available. In comparison, other whole-plant metabolic models employ the use of species-specific GSMs (Shaw and Cheung, 2018; de Oliveira Dal'Molin et al., 2015; Grafahrend-Belau et al., 2013; Zakhartsev et al., 2016). Furthermore, these studies did not compare their growth predictions against experimental data, bringing into question the accuracy of their models. The exception to this is the model developed by Grafahrend-Belau et al. (2013), which was able to predict growth in barley accurately. However, growth was not dictated by FBA optimisations but was instead controlled by the FSPM coupled to the metabolic models.

4.3.1 Allometric biomass partitioning

The biomass partitioning mechanism in WholePlantMetabolism v1 is based on allometric growth theory and uses a large dataset of tomato plants grown in diverse environments to derive scaling exponents. It must be noted though that accurate predictions were not achieved using large interspecies datasets (Table 4.1). Using tomato-specific data greatly improved the accuracy of growth predictions, suggesting that generic allometric relationships derived from large interspecies datasets do not closely capture species-specific adaptations and life histories well (Niklas, 2006).

A major advantage of the biomass partitioning mechanism adopted in this study is that it reflects the biophysical constraints imposed on the growth of each organ in relation to each other, whilst also accounting for their respective physiological functions (Niklas and Enquist, 2002). These relationships are independent of time, and this allows the model to make predictions about growth under different environmental conditions without violating the integrity of the predicted plant structure. This is in contrast to assimilate partitioning coefficients, commonly used in plant growth models, which are strictly dependent on organ and plant age (Kang et al., 2011; Marcelis, 1993; Yan et al., 2004). For example, if growth is simulated under nutrient-limited conditions compared to the reference environment used to calculate a set of partitioning coefficients, the model would incorrectly allocate resources between organs to reflect the pattern observed in reference plants of a larger size at an equivalent age. Using allometric scaling exponents would instead partition biomass according to existing organ masses. This allows the model to simulate growth under different nutrient and light regimes without the need for reparameterisation, an aspect of the model that I make use of to explore differences in nitrogen- and carbon- limited growth in the next chapter (Chapter 5).

4.3.2 Whole-plant metabolic predictions

By accounting for the structure and function of both leaves and roots, WholePlant-Metabolism v1 was able to predict the balance between the limiting effects of light, carbon, and nitrogen on growth (Table 4.2). Intuitively, the prediction that growth is carbon-limited is unsurprising given that the plants were grown under moderate light (320 μmol m^{-2} s^{-1}) and high nitrate treatment (14 mM). Furthermore, only 61% of the incident photons was used by the leaf for photosynthetic activity, with the rest not being taken up by the system. This is in line with well-established knowledge of light energy dissipation mechanisms used by plants to ensure that

the production of ATP and reducing power is in keeping with plastidial demands. An example of such a mechanism is non-photochemical quenching, which is regulated by the energetic state of chloroplasts (Müller et al., 2001). Light availability can also be reduced by reflectance from and transmission through the leaf (Zhu et al., 2010).

With regards to nitrogen metabolism, only 8% of the nitrate provided in the hydroponic growth solution was taken up by the plant. However, leaf vacuoles are known to have substantial nitrate storage capacities. In *Brassica campestris*, *Brassica chinensis*, and *Spinacia oleracea*, it has been reported that leaf NR flux and leaf nitrate storage pools increased with nitrate supply (Chen et al., 2004). But above a certain concentration threshold, NR activity saturates, resulting in an increased proportion of nitrate being diverted to storage pools. This is not reflected in the modelling approach used here as a result of FBA's steady-state constraint, so nitrate uptake predictions should be interpreted as a measure of the growth demand for nitrogen in the absence of long-term storage pools.

The model predicted that the majority of nitrogen assimilation occurred in the shoot (Figure 4.10d). This is in agreement with Flores et al. (2004) and Brewitz et al. (1996), who reported shoot NR flux to be between 7–9 times higher than in the root in young tomato plants. As with other diel leaf models, nitrate taken up by the leaf was exclusively assimilated during the day (Cheung et al., 2014; Shaw and Cheung, 2018). Increased NR and GS fluxes in tobacco leaves under illumination support this prediction, though nitrate reduction does continue at a reduced rate in darkness (Stitt et al., 2002; Lillo, 2008). Recently, it has been hypothesized that limiting nitrate assimilation to the daytime is more energetically efficient due to the energy excess provided by the light-dependent reactions (Shaw and Cheung, 2018; Cheung et al., 2014). This also suggests that the translocation of amino acids from leaves to sink tissues is a product of economising energetic investments in

nitrogen metabolism.

4.3.3 Leaf, root, and stem metabolic predictions

The leaf model was able to predict many of the experimentally-verified diel metabolic behaviour first reported by Cheung et al. (2014). For example, the model chose starch as the main carbon storage compound to fuel night-time metabolism, which is in accordance with observations that tomato plants leaves accumulate starch during the day (Yuan et al., 2016a). The model also predicted citrate storage during the night, which provided carbon skeletons for amino acid assimilation during the day, and malate storage during the day, which supported the TCA cycle during the night (Gauthier et al., 2010).

The significant contribution of the mitochondrial ETC to the leaf's daytime ATP supply has also been predicted by Shameer et al. (2019). Under low light conditions, mitochondrial respiration is required to support mitochondrial and cytosolic ATP demands. Only when light input was increased to more than 400 $\mu mol\ m^{-2}\ s^{-1}$ did chloroplastic ATP synthase flux become sufficient to fulfil cytosolic ATP demand. The importance of the mitochondrial ETC to phototrophic growth in barley protoplasts has been observed *in planta* (Gardeström and Igamberdiev, 2016). Using respiratory inhibitors, the study also supported the prediction that the majority of the mitochondrial NADH pool is generated by glycine decarboxylase as product of photorespiration. Shameer et al. (2019) theorise that the use of mitochondrial respiration facilitates higher energy use efficiency under energy limitation, as the plastidial ETC generates approximately half as much ATP per photon as its mitochondrial equivalent (Kramer and Evans, 2011).

Additionally, mitochondrial glycine decarboxylase produces cytotoxic ammonium as result of daytime photorespiration. The subcellular location of ammonium reassimilation remains unresolved experimentally but hypothesised routes include

direct reassimilation by GS in mitochondria or plastidial reassimilation following export from the mitochondria. The model predicted that the former principally mediated this process; in fact, 88% of the leaf's daytime GS flux was localised to mitochondria. This prediction is supported by the identification of an Arabidopsis GS isoform that is localised to both the chloroplast and mitochondria (Taira et al., 2004). The study also found that the light-adapted leaves exhibited 3.9-times more GS in mitochondria than in chloroplasts.

The ultimate source of carbon and energy in both the stem and root was sucrose provided by the leaf. The model assumed that photosynthetic activity in stem tissues makes up a negligible contribution to growth based on estimates that leaves assimilate 96% of the carbon at each phytomer unit in tomato (Hetherington et al., 1998). Cytosolic sucrose synthase carried the entirety of the sucrose degradation flux, yielding fructose and UDP-glucose. However, sucrose can also be catabolised via invertase to produce fructose and glucose (Roitsch and González, 2004). Though less energetically efficient when compared to sucrose synthase, there is a large body of evidence supporting the role of invertase in the regulation of sucrose translocation and as a signalling molecule during pathogen response (Chang et al., 2017). As such, invertase activity has been reported to be 2.2-times higher than sucrose synthase in 25 day old tomato roots (Shi et al., 2008). The model's failure to capture this dynamic highlights one of the major limitations of stoichiometric modelling: regulation and signalling cannot be accounted for.

Significant flux predictions through both the cytosolic and plastidial glycolytic pathways in sink tissues are supported by observations that root growth is greatly reduced when plastidial glyceraldehyde-3-phosphate dehydrogenase activity is repressed in heterotrophic tissues in Arabidopsis (Anoman et al., 2015). Isotopic labelling experiments have also revealed that both the cytosol and plastid contribute significantly to carbohydrate oxidation in Arabidopsis cell cultures fed with

labelled glucose (Masakapalli et al., 2014). Plastidial glycolysis plays an important role in connecting carbon and nitrogen metabolism together through amino acid biosynthesis. The generation of acetyl-CoA as an end product also contributes to fatty acid biosynthesis.

In the model, NGAM demand was constrained according to experimentally observed values in specific tissues in tomato (Heuvelink, 1995b). WholePlant-Metabolism v1 predicted comparably low demands for ATP and reducing power for NGAM between the root and the stem given that both organs have been observed to have low maintenance requirements (Figure 4.12 and 4.13). However, a lower carbon use efficiency was predicted for root growth (64%) compared to stem growth (82%), where carbon use efficiency is defined as the proportion of gross carbon assimilation that contributes to net carbon gain. Carbon use efficiencies of 55–69% have been reported for Arabidopsis heterotrophic cell cultures grown on glucose (Masakapalli et al., 2013). The lower efficiency reported for the root can be explained by its function as a source for nitrate uptake. To power nutrient uptake from the environment, 59% of the roots ATP supply was dedicated to root surface proton-ATPase flux (Figure 4.12); this significantly raises the respiration cost of root growth compared to stem growth.

4.4 Conclusions

In this chapter, I described the development of a whole-plant metabolic model for vegetative growth in tomato, and demonstrated its accuracy in predicting growth patterns using an allometric model of resource partitioning. I also verified that metabolic predictions were biologically relevant and reflected known plant biochemistry. In the next chapter, I will show how WholePlantMetabolism v1 can be used to predict potential targets for improving yield by manipulating source-sink interactions.

5 | Optimal resource partitioning of carbon and nitrogen

5.1 Introduction

It is reasonable to assume that many crops species do not optimally partition resources between organs as the environment that the progenitors to modern crops evolved in differs significantly from that found in the agricultural setting. The selection pressures driving evolution in the two scenarios are also likely to have differed significantly: where wild plants are selected for fitness (reproductive success), crops are selected for the increased production of a harvestable plant component (e.g. leaves in tobacco, fruits in tomato, and tubers in potato). The improvements in plant growth observed following the experimental manipulation of source or sink activities support the notion that crop growth may be further optimised (Section 1.3). These findings suggest that resource partitioning between organs is an attractive target for improving crop yield.

Recently, a whole-plant metabolic model of Arabidopsis identified optimal modes of nitrogen source/sink activity (Shaw and Cheung, 2018). In particular, flux predictions indicated that leaf-based nitrate assimilation is energetically more efficient than root-based assimilation as an excess of light energy is available in the leaf during the day (i.e. the amount of light provided to the leaf exceeds the energetic demands for leaf metabolism). Energy-intensive nitrate assimilation pathways can thus proceed in the leaf without incurring major respiratory costs

(as is the case in roots). Leaf-based nitrate assimilation also implicates a role for organic nitrogen transport through the phloem from source leaves to sink organs (Okumoto and Pilot, 2011).

Furthermore, various experimental studies have reported improved growth for plants with increased sucrose transport through the phloem, achieved by overexpressing sucrose transporters for phloem loading or tuber/embryo loading (Yadav et al., 2015; Sun et al., 2011; Weichert et al., 2010; Rosche et al., 2002). Similarly, increased amino acid transport through the phloem has also been reported to increase total plant growth and crop yield (Tegeder and Masclaux-Daubresse, 2018; Perchlik and Tegeder, 2017; Zhang et al., 2015). Importantly, in studies targeting carbon transport, there is often an unintended complementary effect on nitrogen metabolism, and vice versa (Lu et al., 2019; Zhang et al., 2015; Weichert et al., 2010).

Overall, these findings suggest that the partitioning of carbon and nitrogen and the interactions between their respective metabolic networks can be further optimised. However, little effort has been made to characterise the metabolic behaviours underlying the improved phenotypes. A solution to this would be to apply FBA to conduct a systematic analysis of optimal flux modes of carbon and nitrogen metabolism at the whole-plant level. FBA is a suitable platform for this type of investigation as the optimality constraint forms a core aspect of FBA: flux distributions are generated to either maximise or minimise a specified objective function (Orth et al., 2010). This feature of FBA allows modellers to explore the potential flux solution space in response to environmental and genetic perturbations. Most commonly, FBA has been applied to microbial systems to identify optimal routes for the production of commercially-important chemicals. For example, the OptKnock algorithm is a powerful extension of FBA that allows the effects of combinatorial gene deletions on both growth and metabolite production to be assessed (Burgard et al., 2003). Optknock and other similar approaches

have been used to identify optimal deletions for increased biofuel, amino acid, vanillin, lycopene, and organic acid production (among others) in bacteria and yeasts (Chen and Henson, 2016; Choon et al., 2014; Cautha et al., 2013; Yin et al., 2013; Alper et al., 2005; Pharkya et al., 2003). In plant systems, FBA has been used to assess metabolic behaviour in response to light availability, herbivory, osmotic stress, high temperature, and nutrient limitation (Shameer et al., 2019; Shaw and Cheung, 2018; Cheung et al., 2013; Luo et al., 2009). Many studies focus on finding targets for improving metabolic efficiency, and consequently plant growth (Sweetlove and Ratcliffe, 2011). For example, Bar-Even et al. (2010) compared the efficiencies of six carbon assimilation pathways using a stoichiometric model containing the metabolic reactions found in the three domains of life. The model identified a synthetic pathway that could fix carbon three times faster than the CBB cycle, as judged by energetic efficiency, favourable thermodynamics, topological compatibility, and superior kinetics. In another example, the metabolic plasticity of rice leaves was assessed by simulating growth with various gene deletions in central metabolism (Shaw and Kundu, 2015). This allowed for the identification of enzymes essential for growth. More importantly, alternative routes for biomass production were identified in simulations with non-lethal deletions, allowing for a comparison of the energetic efficiencies of the pathways.

In this chapter, I use the optimality requirement of FBA to explore possible routes of carbon and nitrogen partitioning between plant organs for improved growth. Various constraints were applied to vascular transport in WholePlant-Metabolism v1, and vegetative growth was simulated under two different nitrogen regimes. The analysis focuses on carbohydrate and amino acid transport in the phloem from source leaves to sink organs. Model predictions generated novel modes of resource assimilation and utilisation, providing promising strategies for improving growth *in planta*.

5.2 Results

The WholePlantMetabolism v1 model as described in the previous chapter uses a fixed composition for the phloem contents. To explore optimal patterns of resources partitioning in tomato, I applied various constraints to phloem transport reactions in WholePlantMetabolism v1 and simulated vegetative growth over 45 DAS. In order of increasing model flexibility, the phloem composition was constrained as follows: (1) fixed to only sucrose, (2) fixed to the composition observed in tomato (Valle et al., 1998; Walker and Ho, 1977), (3) the minimum proportion of sucrose fixed to the experimental reported value for sucrose (76%; Valle et al., 1998), and (4) completely unconstrained. For convenience, I refer to constraint 1 as *SUC*, constraint 2 as the fixed composition, constraint 3 as *mSUC*, and constraint 4 as the free composition throughout this chapter. With mSUC, except for the minimum sucrose requirement, the model was free to transport any metabolites commonly detected in tomato phloem (the twenty proteinogenic amino acids, GABA, glucose, fructose, and sucrose), including transporting more sucrose than the minimum requirement. Simulations with free compositions were given the same choice of metabolites. The effect of carbon limitation versus nitrogen limitation on resource partitioning patterns was also analysed by simulating growth under two different nutrient regimes: moderate light availability (320 µmol m^{-2} s^{-1}) with either high (14 mM) or low (0.1 mM) nitrate treatments.

5.2.1 General model predictions

Figure 5.1 shows the model predictions for total plant mass after 45 days of growth. The environmental conditions used in the validation dataset, where a final plant mass of 16.10 $\pm$ 0.43 g DW was reported, match that of the high nitrate treatment. When only sucrose was allowed in the phloem, a final plant mass of 15.01 g DW was

predicted, a decrease of 6% compared to the validation dataset. On the other hand, using the fixed phloem composition resulted in growth predictions that fell within experimental error (refer to Chapter 4 for detailed descriptions of model behaviour under this set-up). Relaxing the constraints applied to the phloem composition significantly improved plant growth under high nitrate treatment. Applying a minimum sucrose constraint resulted in an increase of 34% in final plant mass compared to the validation dataset, and allowing the model total freedom to dictate assimilate transport resulted in an impressive yield increase of 47% relative to the validation dataset, with the final plant mass predicted to be 23.75 g DW.

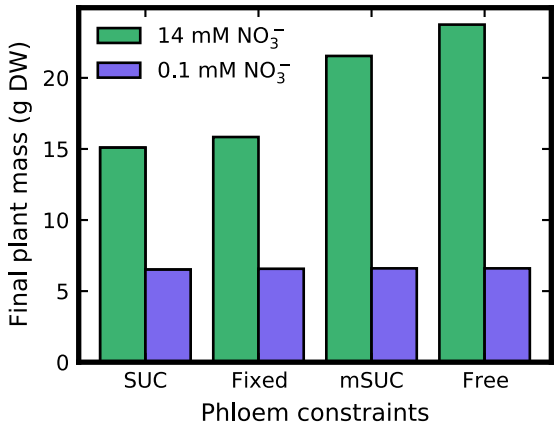

Figure 5.1: Model predictions for final plant mass after 45 days of vegetative growth under two different nitrate regimes and 320 μmol m^{-2} s^{-1} PPFD. Various constraints were applied to assimilate transport from source leaves to sink organs via the phloem: only sucrose (SUC), fixed to a composition reported in tomato (fixed), the minimum proportion of sucrose fixed to an experimentally reported value but the remaining composition remained unconstrained (mSUC), and a completely unconstrained composition (free). DW, dry weight.

Figure 5.1 also shows that the model successfully predicted the limiting effect of a low nutrient regime on growth, with all simulations using low nitrate returning lower growth rates than under high nitrate treatment, regardless of the phloem constraint. Applying different phloem composition constraints under this treatment also resulted in an increased growth rate in response to increasing model freedom. However, the scale of this response was comparatively reduced, with

the difference between the lowest and highest predicted yields being only 0.09 g DW, an increase of 1%. Given the nature of exponential growth, where subtle differences can become amplified over time, the limiting effect of low nutrient availability on growth explains some of the differences in the responses to relaxing model constraints between the two treatments.

To investigate the response of the model under the different nutrient regimes in more detail, a range of parameters related to the emergent properties of model resource partitioning and utilisation were calculated (Table 5.1). Carbon uptake efficiency (CUpE) is defined as the ratio between carbon assimilation via photosynthesis and the maximum carboxylation rate by RuBisCO at a given atmospheric carbon dioxide concentration and light input. Light uptake efficiency (LUpE) and nitrogen uptake efficiency (NUpE) are defined as the ratio between light absorbed by leaves and light available, and the ratio between nitrate taken up by roots and nitrate provided in growth media, respectively. Table 5.1 shows that growth under high nitrate treatment was predicted to be carbon-limited (CUpE = 1), with the model using all of the carbon provided to it, and that nitrate and light were under-utilised (NUpE < 1, LUpE < 1). In contrast, growth under low nitrate was predicted to be nitrate-limited (NUpE = 1), with light and carbon now being provided in excess instead (LUpE < 1, CUpE < 1). These modes of control by carbon and nitrogen were true for all simulations in each nitrate regime, regardless of the phloem constraint.

Quantum yield is a measure of photosynthetic efficiency and is defined as the moles of carbon dioxide fixed per mole of photon absorbed, and values between 0.04 and 0.09 have been reported for tomato (Frantz and Bugbee, 2005). The model predicted a quantum yield of 0.08, regardless of the nutrient regime and phloem constraints (Table 5.1). The lack of variation in quantum yield between simulations suggests that the differences in growth predictions did not arise from

Table 5.1: Summary of general predictions for source/sink capacities and respiration at 45 DAS by WholePlantMetabolism v1 for growth under two different nitrate regimes. Various constraints were applied to assimilate transport from source leaves to sink organs via the phloem: only sucrose (SUC), fixed to a composition reported in tomato (fixed), the minimum proportion of sucrose fixed to an experimentally reported value but the remaining composition remained unconstrained (mSUC), and a completely unconstrained composition (free). CUpE, LUpE, and NUpE are expressed as the ratio between resource uptake and availability (carbon, light, and nitrogen, respectively). Quantum yield is expressed as moles carbon dioxide fixed per photon absorbed. Stem and root respiration are listed in mmol CO_2 g DW^{-1} day^{-1}. NR/NiR fluxes are listed in mmol g DW^{-1} day^{-1}. CUpE, carbon uptake efficiency; LUpE, light uptake efficiency; NR, nitrate reductase; NiR, nitrite reductase; NUpE, nitrogen uptake efficiency.

Parameter	14 mM NO_3^-				0.1 mM NO_3^-			
	SUC	Fixed	mSUC	Free	SUC	Fixed	mSUC	Free
CUpE	1.00	1.00	1.00	1.00	0.79	0.78	0.70	0.69
LUpE	0.61	0.61	0.64	0.65	0.48	0.47	0.44	0.44
NUpE	0.02	0.02	0.02	0.02	1.00	1.00	1.00	1.00
Quantum yield	0.08	0.08	0.08	0.08	0.08	0.08	0.08	0.08
Stem respiration	2.39	2.20	0.96	0.88	2.75	2.57	1.17	1.17
Root respiration	2.25	2.11	1.73	1.08	2.54	2.42	2.32	1.53
Leaf NR/NiR fluxes (day)	0.13	0.19	0.47	0.48	0.16	0.24	0.72	0.82
Leaf NR/NiR fluxes (night)	0.00	0.00	0.00	0.00	0.00	0.00	0.00	0.00
Root NR/NiR fluxes	0.39	0.32	0.22	0.00	0.46	0.39	0.35	0.00
Stem NR/NiR fluxes	0.62	0.54	0.00	0.00	0.74	0.65	0.00	0.00
C/N ratio of phloem content	-	92.35	11.16	9.40	-	92.35	11.16	9.08

significant modulation of source activity. On the other hand, sink activity showed significantly different behaviour between simulations. In both high and low nitrate treatments, relaxing phloem compositional constraints resulted in decreasing respiration costs in sink organs (both root and stem; Table 5.1). Additionally, nitrogen-limited growth appeared to exhibit higher respiration costs compared to carbon-limited growth using equivalent phloem constraints. This indicated that nutrient availability exerted an effect on the model's tolerance for carbon loss through high respiration costs.

To decipher the specific metabolic behaviours underlying these diverse modelling predictions, I analysed metabolite flow through the phloem. In both treatments, relaxing phloem compositional constraints decreased the C:N ratio of the phloem composition (Table 5.1). Simulations using mSUC decreased this ratio by 88% compared to the experimentally observed value. Using the free phloem

composition constraint, this reduction was decreased further to 90%, indicating a strong preference for organic nitrogen transport within the vasculature. This was further supported by an increase in nitrate assimilation in the leaf during the day and a reciprocal decrease of nitrate assimilation in sink organs (Table 5.1). In fact, simulations using the free phloem composition predicted NR and NiR fluxes to be restricted exclusively to the leaf during the day. The preference for leaf-based nitrate assimilation is explored later in this chapter.

Figures 5.2 shows the composition of metabolites in the phloem. The fixed composition was predominantly composed of sugars, with a large sucrose pool (76%) being supplemented with fructose (8%) and glucose (7%; Walker and Ho, 1977). Amino acids only made up 8% of the phloem (Valle et al., 1998). In contrast, growth using mSUC under both carbon and nitrogen limitation predicted a phloem composed of 76% sucrose and 24% arginine, with no other metabolites being transported (Figure 5.2). Note that the model was given the option to transport sucrose at levels above the minimum requirement but did not do so. Using a free phloem constraint resulted in two different compositions for carbon-limited and nitrogen-limited growth. For the former, the abundance of sucrose was greatly reduced to 31% of the phloem, whereas the transport of threonine (37%) and isoleucine (24%) was strongly preferred (Figure 5.2). Trace amounts of five other metabolites (< 3% each) were also predicted. Other the other hand, nitrogen-limited growth using a free phloem composition predicted a phloem consisting mainly of sucrose (41%), aspartate (14%), isoleucine (8%), asparagine (8%), and trace amounts of twelve other metabolites (< 6% each; Figure 5.2).

The next sections will focus on determining the fates of these metabolites following after their uptake into sink organs. A particular interest will be paid to how their modes of utilisation can result in improved growth. Note that these model predictions relate to stoichiometric optima and do not consider factors such

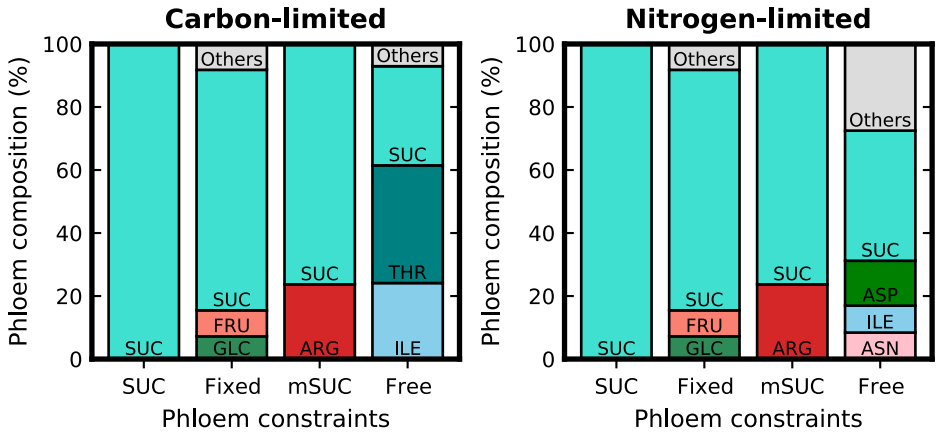

Figure 5.2: Model predictions for the composition of assimilates transported through the phloem from source leaves to sink organs under two different modes of resource limitation, imposed by varying the nitrate supply to the root. Others indicate metabolites transported in trace amounts. Various constraints were applied to assimilate transport from source leaves to sink organs via the phloem: only sucrose (SUC), fixed to a composition reported in tomato (fixed), the minimum proportion of sucrose fixed to an experimentally reported value but the remaining composition remained unconstrained (mSUC), and a completely unconstrained composition (free). Amino acids are abbreviated using their respective standard three-letter codes. FRU, fructose; GLC, glucose; SUC, sucrose.

as thermodynamic and kinetic limitations and toxicity issues that may limit their operation *in planta*. In exploring these metabolic flux modes, the aim was to make an initial explanation of why the different phloem compositions and resulting fluxes make such an impact on plant growth.

5.2.2 Arginine as an efficient nitrogen carrier

Following uptake from the phloem, sucrose and arginine were predicted to follow the same metabolic fates in sink organs using the mSUC constraint in both carbon- and nitrogen-limited conditions. To avoid repetition, I report only the findings for growth under carbon-limitation here.

Applying the minimum sucrose requirement constraint resulted in a high proportion of sucrose import into sink organs. Though some flux through invertase was predicted, the majority of the sucrose degradation flux was carried by SuSy, which produced UDP-glucose and fructose. Sucrose acted as the main source of

energy in the root and stem, being catabolised through glycolysis, the TCA cycle, and the OPPP to generate ATP and reducing power (NAD(P)H). Mitochondrial ATP synthase constituted the largest source of ATP, using reducing power generated by glycolysis and the TCA cycle. Additionally, downstream products of sucrose degradation were also used to generate cellulose, sugars, starch, and fatty acids for biomass production.

Compared to the fixed composition model, there was a marked increase in the preference for leaf-based nitrate assimilation when imposing the mSUC constraint. NR and NiR fluxes in the leaf were increased by 144%, and decreased by 74% in sink organs relative to the fixed composition model (Table 5.1). In the model, energy is abundant in the leaf during the day as LUpE < 1 (i.e. more energy is available than required). The predictions here suggest that it is energetically more beneficial to transport nitrate taken up from the growth media to the leaf for assimilation, and to subsequently transport fixed nitrogenous compounds to sink organs, compared to fixing nitrate *in situ* in sink organs using transported sugars as an energy source (Shaw and Cheung, 2018).

Figure 5.3 shows the fate of arginine following uptake from the phloem into sink organs. It was first degraded into urea and ornithine by mitochondrial arginase. Using 2-oxoglutarate as a carbon skeleton, ornithine was used to generate glutamate through the action of ornithine aminotransferase and 1-pyrroline-5-carboxylate dehydrogenase. Urea was hydrolysed by cytosolic urease, yielding ammonium and carbamate, which rapidly decayed to produce another molecule of ammonium and carbon dioxide (Witte, 2011). With glutamate and ammonium, sink organs were able to synthesise all other 18 proteinogenic amino acids for protein synthesis through their known biosynthetic pathways (Figure 5.3). Ammonium was reassimilated through asparagine production from aspartate via asparagine synthetase, and glutamine production from glutamate via GS.

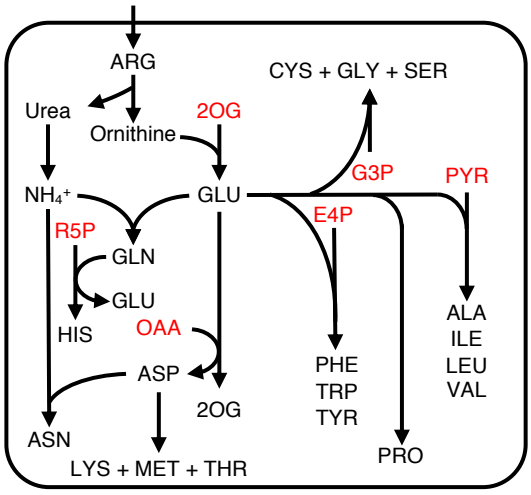

Figure 5.3: Model predictions for the fate of arginine through amino acid catabolism and biosynthesis pathways in sink organs (root and stem) following import from the phloem using the minimum sucrose content requirement phloem constraint (mSUC). Carbon skeletons provided by sucrose degradation through the oxidative pentose phosphate pathway, glycolysis, and the tricarboxylic acid cycle are highlighted in red. Amino acids are abbreviated using their respective standard three-letter codes. 2OG, 2-oxoglutarate; E4P, erythrose-4-phosphate; G3P, glycerate-3-phosphate; OAA, oxaloacetate; PYR, pyruvate; R5P, ribose-5-phosphate.

Another role for sucrose in sink organs was to provide carbon skeletons for amino acid biosynthesis (Figure 5.3). For example, the TCA cycle generated 2-oxoglutarate and oxaloacetate for glutamate and aspartate production. The OPPP provided erythrose-4-phosphate for aromatic amino acid biosynthetic via the shikimate pathway, and ribose-5-phosphate for histidine biosynthesis. Glycolysis provided pyruvate and glycerate-3-phosphate for the production of various other amino acids.

By constraining the phloem to be dominated by sucrose, sink organs were provided with high levels of energy and carbon. The main selection criteria for optimal phloem transport was thus to maximise nitrogen transport from sources to sinks, as indicated by the prediction to only transport the minimum amount of sucrose required and maximise amino acid transport. This is further supported by the choice of amino acid. Arginine contains a three-nitrogen guanidine group on its side chain and is the most nitrogen rich out of all of the proteinogenic amino

acids. Overall, the model suggests that the vegetative plant could be made more nutrient-use efficient by increasing the capability to transport nitrogen-rich amino acids and catabolise them in sink organs.

5.2.3 Optimal resource partitioning under carbon limitation

Free phloem compositional constraints led to the highest growth rates in the model. Under both carbon-limited and nitrogen-limited growth, NR and NiR fluxes were limited exclusively to the leaf during the day, providing further evidence of the energetic benefits of leaf-based nitrogen assimilation (Table 5.1). The phloem in both simulations was characterised by a lower sucrose content compared to physiologically observed levels and a higher amino acid content. The choice of amino acids, however, differed significantly between the two conditions. In this section, I will first focus on predictions under carbon limitation, where threonine, sucrose, and isoleucine transport was preferred (Figure 5.2). The transport of six other metabolites was also predicted in trace amounts, including arginine, cysteine, glucose, histidine, lysine, and proline. However, these were directly used for biomass production in sink organs and served no other function.

Isoleucine as an energy and nitrogen carrier

Following uptake into sink organs, isoleucine was transported into mitochondria to enter branch-chain amino acid (BCAA) catabolism pathways (Figure 5.4). Through the action of BCAA transaminase and branched-chain α-ketoacid dehydrogenase, isoleucine was used to generate 2-methylbutanoyl-CoA, glutamate, and NADH. Isovaleryl-CoA dehydrogenase then oxidised 2-methylbutanoyl-CoA, providing electrons to the mitochondrial ETC via ubiquinone using electron transfer flavoprotein and ETF:ubiquinone oxidoreductase (Araújo et al., 2011; Däschner et al., 2001). The oxidation of isoleucine proceeded further, ending with the production

of two molecules of acetyl-CoA and four molecules of NADH through an eight-step pathway (Hildebrandt et al., 2015). Acetyl-CoA then entered the TCA cycle, generating more reducing power for ATP production via the mETC.

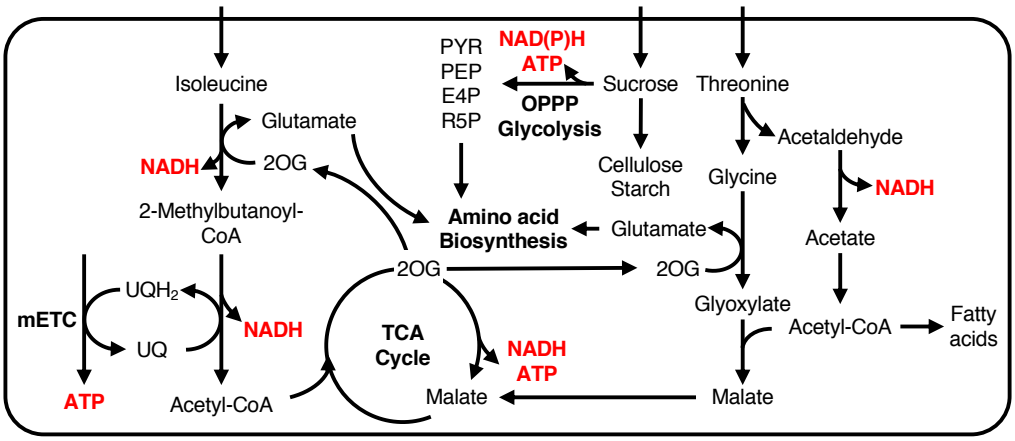

Figure 5.4: Model predictions for the fate of isoleucine, sucrose, and threonine in sink organs (root and stem) following import from the phloem using the free phloem constrain under carbon-limited growth conditions. Isoleucine and threonine entered amino acid catabolism pathways to generate energy, carbon skeletons, and other amino acids. Processes generating ATP and reducing power are highlighted in red. Carbon skeletons for amino acid biosynthesis were also provided by sucrose degradation through the OPPP and glycolysis. 2OG, 2-oxoglutarate; E4P, erythrose-4-phosphate; mETC, mitochondrial electron transport chain; OPPP, oxidative pentose phosphate pathway; PEP, phosphoenolpyruvate; PYR, pyruvate; R5P, ribose-5-phosphate; TCA, tricarboxylic acid; UQ, ubiquinone; UQH_2, ubiquinol.

Figure 5.5 shows that BCAA catabolism contributed to 22% of total reducing power production in sink organs. The provision of acetyl-CoA to the TCA cycle supplied another 40% of the reducing power pool and also 6% of the ATP pool (Figure 5.5). Additionally, the direct transfer of electrons to the mETC, along with consumption of NADH, contributed to the production of ATP by mitochondrial ATP synthase, providing 91% of ATP supply. Overall, these results suggest that the role of isoleucine within sink organs was to provide energy. Though marginally lower, the potential energy yield from the complete oxidation of isoleucine is comparable to that of glucose (29 ATP and 32 ATP, respectively; Hildebrandt et al., 2015). However, isoleucine can also act as a nitrogen carrier, generating glutamate, a precursor for the biosynthesis of other amino acids, via mitochondrial BCAA

transaminase (Figure 5.4). This dual capacity as both an energy and nitrogen carrier potential makes isoleucine a more efficient metabolite to fuel sink metabolism and protein synthesis than sugars.

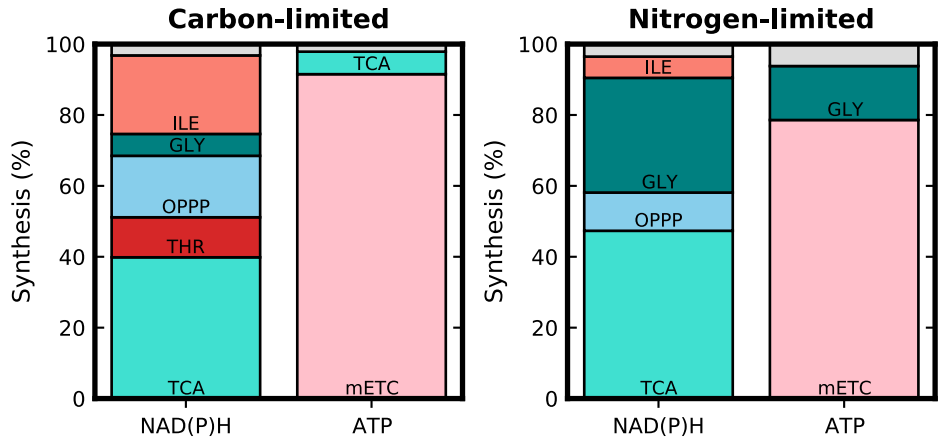

Figure 5.5: Model predictions for ATP and reducing power synthesis under two different modes of resource limitation in sink organs (root and stem) using the free phloem composition constraint. Fluxes through pathways that generate trace amounts of reducing power or ATP are shown in grey. GLY, glycolysis; ILE, isoleucine catabolism; mETC, mitochondrial electron transport chain; OPPP, oxidative pentose phosphate pathway; TCA, tricarboxylic acid cyle; THR, threonine catabolism.

Threonine as an energy, carbon, and nitrogen carrier

Following uptake into sink organs, threonine was catabolised to produce glycine and acetaldehyde via cytosolic threonine aldolase (Figure 5.4). Some glycine was transported into mitochondria for serine biosynthesis via serine hydroxymethyltransferase and glutamine biosynthesis through GS and glycine decarboxylase complex-mediated ammonium production. Glycine was also transported into the peroxisome for transamination to glutamate and glyoxylate using glycine transaminase. Glutamate was used to generate various other amino acids for protein synthesis.

On the other hand, acetaldehyde generated from threonine aldolase was oxidised by aldehyde dehydrogenase to produce acetate, also generating reducing power (Figure 5.4). Acetyl-CoA was generated by acetate-CoA ligase and trans-

ported into both the plastid and peroxisome. Within the plastid, acetyl-CoA was used as precursors for fatty biosynthesis and amino acid synthesis (methionine and leucine). Within the peroxisome, acetyl-CoA was used to acetylate glyoxlate to produce malate via malate synthase. The source of glyoxylate was also from the catabolism of threonine via threonine aldolase and glycine transaminase. Malate was transported into mitochondria to fuel the TCA cycle in conjunction with mitochondrial acetyl-CoA generated by BCAA catabolism.

The TCA cycle also provided other organic acids as carbon skeletons for amino acid biosynthesis. For example, glutamate biosynthesis in isoleucine and glycine catabolism pathways was supported by the supply of 2-oxoglutarate from the TCA cycle (Figure 5.4). As with isoleucine, the production of glutamate, a branch point in nitrogen metabolism, allowed for the production of many other amino acids.

Growth under carbon-limited conditions using free phloem compositional constraints was characterised by a markedly low respiration rate in sink organs, suggesting an improvement in carbon use efficiency (Table 5.1). The generation of acetyl-CoA from threonine contributed to this. Under normal physiological conditions in sink organs, acetyl-CoA is produced from the oxidation of sucrose (Stein and Granot, 2019; Colombié et al., 2015; Biais et al., 2014). Through glycolysis, pyruvate is generated and is decarboxylated by pyruvate dehydrogenase to yield acetyl-CoA. However, this conversion also results in the loss of assimilated carbon as carbon dioxide. Generating acetyl-CoA through acetate-coA ligase thus reduces respiratory carbon losses in sink organs. Model simulations predicted 49% of the acetyl-CoA pool to be provided by threonine catabolism, with isoleucine catabolism providing another 45% (Figure 5.6). A small flux through pyruvate dehydrogenase was predicted in the plastid, supporting 6% of acetyl-CoA production. No flux through the mitochondrial isoform was reported. This is a significant reduction from the predictions using the fixed phloem composition model, where 99% of the

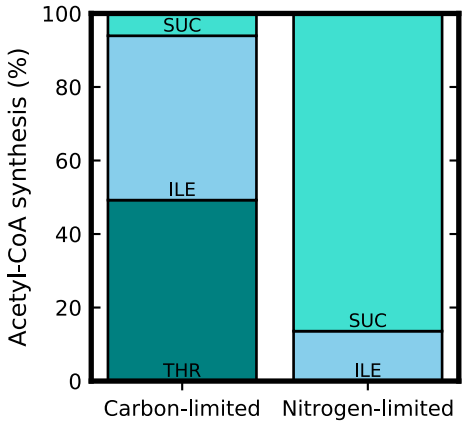

Figure 5.6: Model predictions for acetyl-CoA synthesis under two different modes of resource limitation in sink organs (root and stem) using the free phloem composition constraint. ILE, isoleucine catabolism; SUC, sucrose catabolism; THR, threonine catabolism.

acetyl-CoA pool was provided by pyruvate dehydrogenase.

Overall, model predictions indicate three different functions for threonine in sink organs. Firstly, threonine acted as a carbon carrier by generating 2-oxoglutarate and acetyl-CoA for amino acid and fatty acid biosythesis. Secondly, threonine acted as a nitrogen carrier by providing nitrogen for glutamate production. And thirdly, threonine acted as an energy carrier by providing malate to the TCA cyle and also generating reducing power through aldehyde dehydrogenase. Though the potential energy yield of threonine degradation is significantly lower than that of glucose (18 ATP/threonine versus 32 ATP/glucose), the benefits afforded by its nitrogen and carbon carrying capacity make threonine an efficient resource to fuel heterotrophic metobolism (Hildebrandt et al., 2015). Carbon-conserving features of the pathway contribute to this further during carbon-limited growth.

Sucrose as a carbon carrier

Though greatly reduced compared to physiologically observed values, sucrose uptake into sink organs was still predicted even when there was no constraint on the composition of the phloem metabolites. Downstream products of sucrose

degradation were used to generate cellulose, fructose, and starch for biomass production. Sucrose itself also contributed to biomass production.

Sucrose degradation was predicted to be mediated by SuSy, generating fructose and UDP-glucose. Fructose entered plastidial glycolysis at the level glyceraldehyde-3-phosphate, generating 6% of the reducing power supply. Substrate-level phosphorylation only generated 1% of the ATP supply. The ultimate fate of carbon moving through glycolysis was to provide phosphoenolpyruvate and pyruvate as carbon skeletons for amino acid biosynthesis, and to provide acetyl-CoA for fatty acid biosynthesis to a smaller extent (Figure 5.4). UDP-glucose entered the plastidial OPPP, generating 17% of the reducing power supply. Similarly to plastidial glycolysis, the ultimate fate of carbon through the OPPP was for use in amino acid biosynthesis, via the production ribose-5-phosphate and erythrose-4-phosphate. Overall, model predictions indicate that despite a decrease in the C/N balance of the phloem under free constraints, sucrose was still required as a carrier of carbon and reducing power.

5.2.4 Optimal resource partitioning under nitrogen limitation

Compared to model predictions under carbon-limited conditions, the optimal phloem composition under nitrogen-limited conditions had a higher preference for sucrose (41%) and aspartate transport (14%; Figure 5.2). Isoleucine transport was reduced (8%), and threonine was only transported in trace amounts (2%). In fact, 36% of the phloem was composed of metabolites that were transported in trace amounts and used solely for biomass production, including glucose and 12 amino acids (asparagine, arginine, cysteine, glycine, histidine, lysine, phenylalanine, proline, threonine, tryptophan, tyrosine, and valine).

Figure 5.7 shows the predicted fates for aspartate, isoleucine, and sucrose in

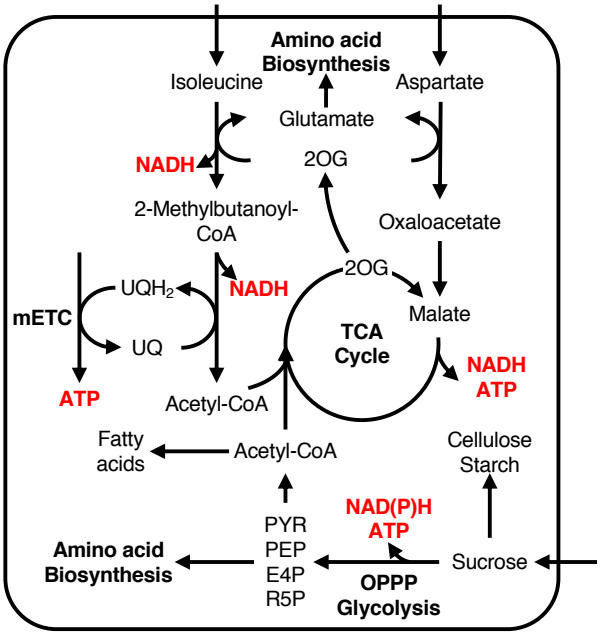

Figure 5.7: Model predictions for the fate of aspartate, isoleucine, and sucrose in sink organs (root and stem) following import from the phloem using the free phloem constrain under nitrogen-limited growth conditions. Aspartate and isoleucine entered amino acid catabolism pathways to generate energy, carbon skeletons, and other amino acids. Sucrose provided energy through the OPPP, glycolysis, the TCA cycle, and the mETC. Processes generating ATP and reducing power are highlighted in red. Carbon skeletons for amino acid biosynthesis were also provided by sucrose degradation. 2OG, 2-oxoglutarate; E4P, erythrose-4-phosphate; mETC, mitochondrial electron transport chain; OPPP, oxidative pentose phosphate pathway; PEP, phosphoenolpyruvate; PYR, pyruvate; R5P, ribose-5-phosphate; TCA, tricarboxylic acid; UQ, ubiquinone; UQH_2, ubiquinol.

nitrogen-limited sink organs. Similar to predictions under carbon-limited conditions, BCAA catabolism pathways were active, generating glutamate for amino acid biosynthesis, providing electrons to the mETC, producing reducing power (6% of the total pool), and feeding acetyl-CoA into the TCA cycle (Figure 5.5). This indicates that the nitrogen and energy carrying properties of isoleucine are also beneficial in low nitrate conditions.

However, the proportion of acetyl-CoA generated by isoleucine catabolism was greatly reduced (14% compared to 45%; Figure 5.6). Instead, sucrose degradation by SuSy, and the subsequent oxidation of hexoses through glycolysis and pyruvate dehydrogenase, generated 86% of the acetyl-CoA pool (Figure 5.6). Sucrose-derived acetyl-CoA was used to fuel the TCA cycle, generating 47% of the reducing power

pool, and also to support fatty acid biosynthesis in the plastid. Flux through glycolysis also supplied 15% of the ATP pool via substrate-level phosphorylation and 32% of the reducing power pool (Figure 5.5). Similar to growth under carbon limitation, hexoses were also diverted to the OPPP for the generation of reducing power (11%) and the production of precursors for amino acid biosynthesis. A large proportion of the reducing power produced by sucrose degradation was used to provide electrons to the mETC, which generated 79% of the ATP supply. Overall, this suggests that sucrose was the principal source of energy in sink organs under nitrogen-limited conditions. High fluxes through pyruvate dehydrogenase for acetyl-CoA production indicates a higher tolerance for respiratory carbon loss in sink organs compared to growth under carbon limitation (Figure 5.6) and that sucrose remains an efficient source of energy when carbon is not the primary driver of growth.

As many of the amino acids demanded for protein synthesis were imported directly from the phloem, fewer amino acid biosynthetic pathways were predicted to be active. However, aspartate was deaminated by aspartate transaminase to produce glutamate and oxaloacetate (Figure 5.7). Malate dehydrogenase then converted oxaloacetate to malate, which entered the TCA cycle in mitochondria. The subsequent generation of 2-oxoglutarate provided the carbon skeleton required for glutamate synthesis by aspartate transaminase. Glutamate was used to synthesise various other amino acids, including alanine, glutamine, leucine, and serine. Aspartate was thus being used as a nitrogen and carbon carrier.

5.2.5 Experimental characterisation of phloem content under different nitrate-supply regimes

Model predictions suggest different optimal patterns of resource partitioning under carbon-limited and nitrogen-limited conditions. To assess whether plants modulate

their phloem contents in response to environmental conditions, I experimentally characterised the metabolite profiles of leaf petiole phloem exudates in tomato plants grown under two different nitrate treatments: high (14 mM) and low (0.1 mM). Plants were exposed to these treatments for one week before exudates were collected at 45 DAS. Figure 5.8 shows the final height of plants on the day of sample collection. There was a significant difference in plant height between the two groups (t = 2.45, p = 0.03), with low nitrate-treated plants being 12% shorter, indicating that the degree of nutrient limitation was sufficient to elicit phenotypic differences.

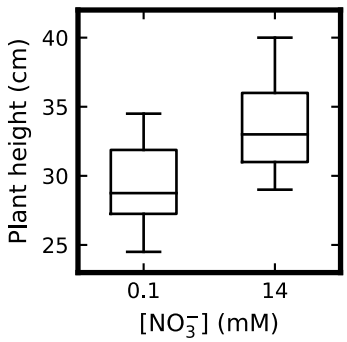

Figure 5.8: The effect of an altered nitrate supply (one week exposure) on the growth of tomato plants. There was a statistically significant difference in mean plant height between the two treatments (t = 2.45, p = 0.03). n = 10.

In both treatments, the phloem metabolite composition was dominated by sucrose (75±8% for high nitrate, and 66±10% for low nitrate; Figure 5.9). The remainder of the phloem consisted mainly of hexoses (fructose and glucose), and only a small proportion of amino acids was detected (7±5% for high nitrate, and 3±2% for low nitrate). These findings are in good agreement with a previous characterisation of phloem contents in tomato, where the following composition was reported: 76% sucrose, 8% fructose, 6% glucose, and 9% amino acids (Walker and Ho, 1977). A large-scale phloem metabolite profiling study also reported the mean relative content of sucrose to be 71% of the phloem across 14 plant species

(Wilkinson and Douglas, 2003).

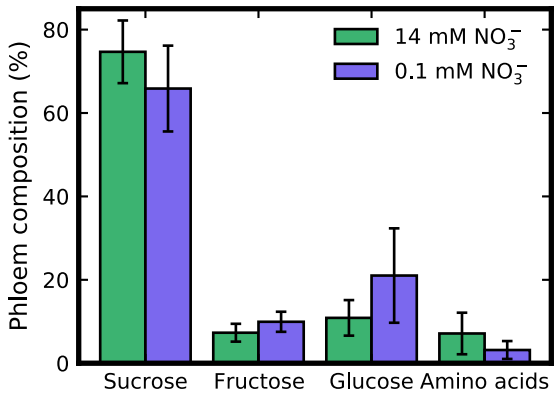

Figure 5.9: Metabolite content of leaf phloem exudate measured at 45 days after sowing in tomato cv. Moneymaker grown under two different nitrate regimes. There were no statistically significant differences in the relative abundance of any metabolite group between the two treatments as determined by *t*-tests. Data are the mean±SD (n = 4).

11 amino acids were detected in both sample groups (Figure 5.10). Glutamine and glutamate were the two most commonly detected amino acids, and collectively contributed to 47±12% of the phloem amino acid pool under the high nitrate treatment, and 39±12% in low nitrate treatment. This is in good agreement with a previous characterisation of amino acid content in tomato phloem, where glutamine and glutamate collectively contributed to 46% of the phloem (Valle et al., 1998). High levels of glutamine and glutamate in phloem amino acid pools have also been reported in a range of other plant species (Wilkinson and Douglas, 2003; Karley et al., 2002; Winter et al., 1992; Riens et al., 1991).

Phloem content has been shown to vary greatly between species, over the diel cycle, over plant development, and across growing seasons (Gessler et al., 2008; Wilkinson and Douglas, 2003; Karley et al., 2002; Pate et al., 1998; Winter et al., 1992). Shifts in phloem composition have also been reported in response to a range of environmental stimuli, including salinity, drought, and potassium supply (Pérez-Alfocea et al., 2000; Girousse et al., 1996; Mengel and Haeder, 1977). However, no explicit assessment of nitrogen availability on phloem transport has

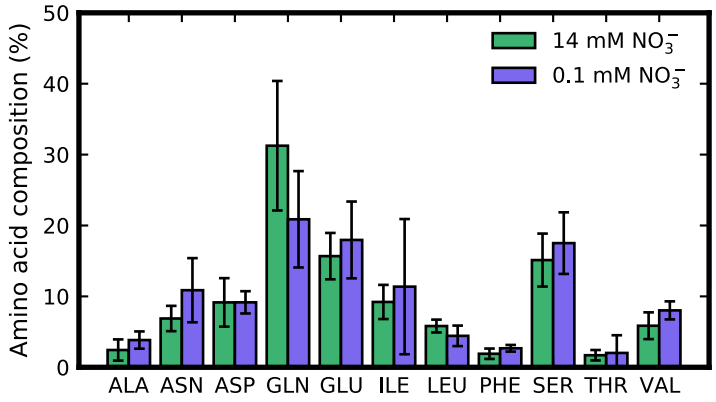

Figure 5.10: Amino acid content of leaf phloem exudate measured at 45 days after sowing in tomato cv. Moneymaker grown under two different nitrate regimes. There were no statistically significant differences in the relative abundance of any amino acid between the two treatments as determined by *t*-tests. Amino acids are abbreviated using their respective three-letter codes. Data are the mean±SD (n = 4).

been conducted yet. In this study, statistical analysis showed that there were no significant differences between the relative contents of sucrose, fructose, glucose, or amino acids in the two nitrate treatments (Table 5.2). Nor were significant differences found between the relative abundances of the 11 amino acids (Table 5.2). Overall, this indicates that the C/N balance of assimilate transport through the phloem was not affected by nitrate availability.

It should be noted that plants were only subjected to the two different nitrate treatments for a week before phloem exudate samples were collected. Prior to this, all plants were grown in nutrient rich conditions. Under excess nitrate supply, plants have been reported to store nitrate in leaf vacuoles for future remobilisation under more limiting conditions (Chen et al., 2004; Harada et al., 2004). The interpretation of the results presented here should be taken with this caveat in mind. Future assessments of the impact of nitrogen availability on phloem content should also include assessments of the overall nitrogen status of the plant (e.g. leaf nitrogen content) to account for nitrogen storage and remobilisation.

Table 5.2: Statistical analysis of phloem metabolite composition in tomato cv. Moneymaker grown under two different nitrate regimes. Data mean and standard deviation (SD) for sucrose, fructose, glucose, and total amino acids are expressed as percentages of total phloem content. Values for individual amino acids are expressed as percentages of total amino acid content. Student *t*-test analysis revealed no significant differences in the mean of any metabolite between the two treatments (n = 4).

Metabolite	14 mM NO_3^-		0.1 mM NO_3^-		t	p
	Mean	SD	Mean	SD		
Sucrose	74.68	7.51	65.87	10.29	1.38	0.21
Fructose	7.32	2.14	9.94	2.41	-1.63	0.15
Glucose	10.88	4.26	21.02	11.32	-1.68	0.14
Amino acids	7.13	4.98	3.17	2.14	1.46	0.19
Alanine	2.44	1.50	3.84	1.22	-1.32	0.24
Asparagine	6.88	1.78	10.87	4.53	-1.64	0.15
Aspartate	9.15	3.42	9.16	1.57	-0.004	1.00
Glutamate	15.68	3.27	17.96	5.42	-0.72	0.50
Glutamine	31.25	9.13	20.88	6.80	1.82	0.12
Isoleucine	9.21	2.41	11.37	9.54	-0.31	0.79
Leucine	5.82	0.91	4.44	1.45	1.57	0.18
Phenylalanine	1.91	0.73	2.68	0.47	-1.77	0.13
Serine	15.12	3.74	17.51	4.34	-0.84	0.44
Threonine	1.70	0.74	2.02	2.50	-0.23	0.84
Valine	5.86	1.89	8.03	1.27	-1.90	0.11

5.3 Discussion

In this chapter, the optimality constraint of FBA was used identify optimal resource allocation patterns for improved vegetative growth in tomato. The analysis focused on carbon and nitrogen transport through the phloem, and revealed potential benefits for increased amino acid transport, including routes for minimising respiration costs in sink organs, efficient nitrogen transport, and energy provision through catabolism pathways.

5.3.1 Respiratory carbon loss

Compared to improving photosynthetic carbon gain, reducing respiratory carbon loss is much less well-studied as a target for improving crop yield due to its complex nature, which affects almost all aspects of plant physiology (Amthor et al.,

2019). However, up to 60% of carbon assimilated through photosynthesis is lost through respiration in crop plants (Amthor et al., 2019; Cannell and Thornley, 2000). Improving the energetic efficiencies of both growth respiration and NGAM processes thus presents itself as an attractive target for improving plant growth, where increased carbon flux towards biomass gain can be achieved. Recently, Amthor et al. (2019) presented a list of possible targets for reducing excessive ATP consumption in plants, including slowing down the turnover rates for protein and membranes (Ishihara et al., 2017). For example, replacing amino acid residues particularly vulnerable to glycation can reduce the rate of protein damage, and engineering an alternative pathway for thiamin synthesis to bypass thiazole synthase activity, a suicidal enzyme that can only catalyse its reaction once, has been predicted to reduce NGAM costs by up to 10% (Soboleva et al., 2017; Hanson et al., 2018). Suppressing flux through futile cycles was also suggested, such as the simultaneous degradation and synthesis of sucrose, and fructose-6-phosphate and fructose-1,6-bisphosphate cycling in glycolysis (Geigenberger and Stitt, 1991; Hill and ap Rees, 1993). However, futile cycles often perform regulatory roles and provide a route for energy dissipation under stress, so these additional functions should be taken into account when devising targeting strategies (Adolfsen and Brynildsen, 2015; Samoilov et al., 2005; Stitt, 1998).

The efficiency of growth respiration can also be improved by relocating and rescheduling metabolic activity to the leaf during the day (Amthor et al., 2019; Shaw and Cheung, 2018; Cheung et al., 2014). Model predictions for optimal growth in this chapter also support the idea that there is an excess of energy in the leaf under illumination, allowing the light-dependent reactions to efficiently generate reducing power and ATP. Under normal physiological conditions, nitrate assimilation through the activities of NR, NiR, GOGAT, and GS was predicted to consume up to 60% of the reducing power and 7% of ATP in sink organs (Chapter 4).

Allowing the model to dictate the site of nitrate assimilation resulted in a total shift towards leaf-based assimilation, greatly reducing growth respiration costs in sink organs (Table 5.1). This indicates that it is more energetically efficient to transport nitrate to leaves, and to subsequently export amino acids to sink organs, than it is transport sucrose to sink organs as a source of energy and carbon skeletons for amino acid biosynthesis (Shaw and Cheung, 2018). Increased nitrogen availability in leaves has also been linked to improved photosynthesis, so relocating nitrate assimilation could also provide benefits through synergy with carbon metabolism (Zhang et al., 2015).

The model also predicted a novel target for reducing respiratory carbon loss. Through threonine catabolism, sink organs could generate acetyl-CoA for the TCA cycle and biosynthetic pathways without any carbon loss (Figure 5.4). This pathway bypasses pyruvate dehydrogenase activity, through which pyruvate is decarboxylated to release carbon dioxide. Pyruvate dehydrogenase requires thiamin-diphosphate as a cofactor, but cellular thiamin-diphosphate pools have been reported to fluctuate greatly owing to its labile nature. The maintenance of a steady acetyl-CoA supply under thiamin-diphosphate starvation and stress conditions has recently been proposed as the function of an elusive pyruvate dehydrogenase bypass in plants (Joshi et al., 2019). However, the bypass requires pyruvate decarboxylase activity, which releases respiratory carbon. Generating acetyl-CoA from threonine could guarantee a study supply under thiamin-diphosphate-deficiency, whilst reducing carbon loss at the same time.

5.3.2 Arginine as an efficient nitrogen carrier

Arginine functions as an important organic nitrogen store in many plant species, and high levels of free arginine have been reported in a range of sink organs, including roots and underground storage organs (Winter et al., 2015; Rennenberg

et al., 2010; Bausenwein et al., 2001; Nordin and Näsholm, 1997). Developing *Glycine max* embryos can have as much as 62% of their free amino acid pool made up of arginine (Micallef and Shelp, 1989). Arginine is also a precursor for the synthesis of plant developmental and stress signalling molecules, including polyamines and nitric oxide, which may also underlie its accumulation in plant tissues (Winter et al., 2015). Arginine is an efficient carrier of nitrogen due to its nitrogen-rich structure and enzymatic reactions are available to allow it to be exploited as a source of nitrogen in sink organs (Figure 5.3). Out of the 20 proteinogenic amino acids, arginine has the highest nitrogen:carbon ratio. This allows plants to store organic nitrogen, whilst minimising carbon that needs to be dedicated towards it.

5.3.3 Increased amino acid transport

Nitrogen has been long-established as a major determinant for plant growth, and many efforts have been made to target inorganic nitrogen uptake by roots and nitrate assimilation for improved NUE (Fernie et al., 2020; Tegeder and Masclaux-Daubresse, 2018; Thomsen et al., 2014; Masclaux-Daubresse et al., 2010). However, model predictions identified significant shifts in the C/N balance of assimilate transport via the phloem for optimal plant growth. Specifically, amino acid transport was preferred over sucrose from source leaves to sinks (Figure 5.2). The partitioning of nitrogen between organs and nitrogen transport from sources to sinks as targets for improving crop yield remains relatively unexplored, though some promising progress has been made. For example, expressing transgenic yeast S-methylmethionine permease 1, which loads a methionine-derivative into the phloem, in pea leaves increased total plant growth, seed yield, and also the protein content of seeds (Tan et al., 2010). In another study, a *push and pull* approach was used to increase both phloem loading in leaves and loading into pea embryo of amino acids (Zhang et al., 2015). The overexpression of a broad-range amino acid

transporter in both sieve element-companion cell complexes in leaves and seed cotyledon epidermal cells increased phloem amino acid content, seed yield, NUE, and total plant growth. Improved NUE in transgenic lines in a range of nitrogen regimes has also been confirmed compared to the wild type (WT; Perchlik and Tegeder, 2017). Overall, these results support the model prediction that increasing the amino acid content of the phloem would be beneficial to crop yield, and provide evidence of amino acid transport as a bottleneck for plant growth.

Model predictions also indicated an increased role for amino acids as a respiratory substrate in sink organs (Figures 5.4 and 5.7). In particular, isoleucine catabolism generated a substantial proportion of the energy supply in roots and stems, whilst also transporting nitrogen from source leaves (Hildebrandt et al., 2015). Under carbon starvation, fluxes through degradation pathways for BCAA and lysine, all of which can provide electrons directly to the mETC via ubiquinone, are elevated (Araújo et al., 2011; Ishizaki et al., 2005). Proteins can thus act as reserve energy stores under stress conditions, despite being energetically less efficient that carbohydrates. BCAA catabolism has also been shown to be important for maintaining cellular activity under other stress conditions, such as drought (Pires et al., 2016). During the normal life cycle of plants, amino acid catabolism pathways are commonly active during leaf senescence, when carbon and nitrogen are remobilised to sink tissues. In a well-controlled process, up to 80% of leaf nitrogen can be recycled, but up to only 30% of carbon is remobilised out of the leaf, as plants cannot hydrolyse cellulose (Havé et al., 2017). The role of BCAA catabolism in providing energy has been implicated in senescing leaves, but how much this contributes to the overall energy supply remains to be determined (Watanabe et al., 2013).

5.3.4 Implementing model predictions *in planta*

Using technological advances in molecular biology and an improved knowledge of plant genetics, the manipulation of specific pathways has become relatively facile to achieve. Model-guided predictions for improved metabolic behaviour should be implemented in a highly-targeted manner *in planta* to assess their effect on plant growth. The proposed strategies include relocating nitrate assimilation to the leaf, increasing amino acid biosynthesis in leaves, increasing the transport of amino acids through the phloem, and increasing flux through amino acid catabolism pathways in sink organs. As WholePlantMetabolism v1 represents metabolism in a generalised C_3 plant, it can be assumed that these engineering targets would be beneficial to a wide range of plant species. However, in plants with large starch storage organs, such as potato, rice, and wheat, significant rates of carbon transport through the phloem may still be required.

Relocating nitrate assimilation to the leaf

The balance between shoot and root nitrate assimilation shows large interspecies variations; for example, temperate cereals and legumes show a preference for root-based assimilation, but tropical annuals prefer shoot-based assimilation (Andrews, 1986). However, most species carry out at least a moderate degree of root-based nitrate assimilation. To relocate nitrate assimilation to the leaf, NR expression in the root can simply be knocked down. Knocking down NiR may also provide additional benefits by reducing the energy expenditure in producting this large protein (Amthor et al., 2019). No additional intervention may be necessary to ensure that nitrate assimilation is restricted to the day in leaves as NR activity is directly regulated by light and proceeds at a reduced rate in darkness (Lillo, 2008; Lillo and Appenroth, 2001). It is worth noting that Hänsch et al. (2001) observed that tobacco mutants deficient in root nitrate reductase had smaller shoots and

roots and slower growth rates compared to the WT. The accumulation of nitrate, glutamine, hexoses, and sucrose were also significantly altered between tissues. Together, the observed effects on growth and C/N balances indicate that further factors may influence the practicality of relocating nitrate assimilation.

Increasing amino acid biosynthesis in source leaves

The amino acid contents of the phloem have been reported to correlate strongly with leaf cytosolic pools (Valle et al., 1998; Winter et al., 1992; Riens et al., 1991). As the primary products of nitrate assimilation in leaves, glutamate and glutamine (and to a lesser extend, aspartate and asparagine) show a high level of abundance in leaves (Amthor et al., 2019). Accordingly, Figure 5.10 shows the high relative abundances of these amino acids in the phloem. A high level of serine was also detected. Winter et al. (1992) observed that the relationship between leaf cytosol and phloem amino acid composition was maintained throughout the diel cycle, so serine and glycine concentrations in the phloem increased during the day in response to photorespiratory activity. Thus, the biosynthesis of amino acids in leaf tissues is the main driver of phloem amino acid composition.

In this chapter, increased aspartate transport was predicted to be beneficial under nitrogen limitation (Figure 5.7). However, the ultimate goal of improving plant growth is for its application to crop species grown in an agricultural setting, where fertiliser use ensures an adequate supply of nitrogen. The specific strategies proposed here focus on arginine, isoleucine, and threonine instead (Figures 5.3 and 5.4). Hildebrandt et al. (2015) also identified high energy yields from the oxidation of tyrosine, other BCAAs, lysine, and proline; future analysis should review the benefits of using them as an energy source in sink organs.

Amino acid biosynthesis pathways are normally active in leaves to support protein synthesis and export to the phloem (Balotf et al., 2016; Hildebrandt et al., 2015;

Joshi et al., 2010). Several amino acids are also precursors for various secondary metabolites, including anthocyanins, glucosinolates, and phenylpropanoids (Pott et al., 2019; Tzin and Galili, 2010; Halkier and Gershenzon, 2006). However, flux through the specific biosynthetic pathways for arginine, isoleucine, and threonine should be increased to promote their production in leaves. The enzymes in these pathways are well characterised, and should be targeted for overexpression using leaf-specific promoters (Alotaibi et al., 2018; Xue et al., 2018; Winter et al., 2015; Binder et al., 2007; Song et al., 2000). For example, overexpressing aspartate kinase, a constituent enzyme in the threonine biosynthesis pathway, resulted in high levels of threonine accumulation in tobacco leaves (Hacham et al., 2008). In another study, lysine accumulation was enhanced by the concurrent overexpression of biosynthetic enzymes and the downregulation of lysine catabolism (Kirma et al., 2012; Zhu and Galili, 2004). However, the repression of amino acid catabolism pathways may disrupt nitrogen remobilisation processes during leaf senescence (Lim et al., 2007).

Increasing source-to-sink transport of amino acids

Amino acids from source leaves can either enter the phloem column through symplastic or apoplastic transport routes. Most crop plants have been found to prefer the latter, requiring an active step to mediate metabolite transport from the apoplast into phloem sieve element-companion cell complexes (Yao et al., 2020; Tegeder and Masclaux-Daubresse, 2018; Tegeder, 2014). Various members of the AAP transporter family are expressed in leaf phloem tissues and are thought to mediate amino acid loading into the phloem (Tegeder, 2012). Some AAPs show high specificity for certain amino acids (e.g. *AAP3* for arginine and lysine), whereas other have a broad range of substrate specificities (Perchlik and Tegeder, 2017; Santiago and Tegeder, 2016; Zhang et al., 2015). To improve amino acid phloem

loading, AAPs overexpression under the control of phloem-specific promoters using should be implemented (Guo et al., 2004; Haritatos et al., 2000; Yin et al., 1997).

Amino acid loading into sink cells also presents a potential area for improvement (Zhang et al., 2015). Along with AAPs, cationic acid transporter proteins have also been implicated in amino acid import in sink organs (Tegeder and Masclaux-Daubresse, 2018). For example, Arabidopsis *aap1* mutants produced seeds with reduced nitrogen content and protein levels (Sanders et al., 2009). Various sink-specific promoters have been identified, including those for flowers, fruits, seeds, roots, and tubers, and can be used for sink-specific overexpression of amino acid transporters to facilitate amino acid import (Lim et al., 2012; Wu et al., 2011; El-Mezawy et al., 2009; Rocha-Sosa et al., 1989).

Inducing amino acid catabolism pathways in sink organs

In order to facilitate their catabolism, the expression of genes encoding enzymes involved in arginine, isoleucine, and threonine catabolism would need to be up-regulated as these genes are generally not expressed in non-senescing tissues (Hildebrandt et al., 2015). Whatever engineering strategy is taken, considerations should be made to ensure that catabolic pathways do not deplete sink organs of amino acids pools for protein synthesis. Compared to amino acid biosynthesis, amino acid catabolism remains relatively unexplored (Hildebrandt et al., 2015). For example, only the first three reactions in the isoleucine degradation pathway have been identified in plants (Binder, 2010). The remaining steps leading to acetyl-CoA production have been inferred from homology to animal and yeast systems, and other indirect evidence. Increasing the activity through the first enzymatic step in BCAA catabolism (BCAA transaminase) by overexpression may be sufficient to increase isoleucine breakdown in sink organs. BCAA transaminase also partici-

pates in BCAA synthesis, but the mitochondrial isoform (BCAT2) has been linked to degradation so may be a suitable target (Angelovici et al., 2013). Nonetheless, future studies should aim to further characterise BCAA degradation enzymes in plants.

In constrast, arginine degradation is well characterised owing to its central position in the nitrogen metabolic network. Overexpressing arginase has been shown to reduce free arginine pools in Arabidopsis and also result in improved pathogen defence responses (Brauc et al., 2012).

Though other routes for threonine breakdown exist in plants (threonine deaminase and threonine dehydrogenase), threonine aldolase, which catalyses the production of glycine and acetaldehyde from threonine, has been shown to be critical to threonine metabolism (Joshi et al., 2006). Threonine aldolase mutants exhibited a 50-fold increase in threonine accumulation, and a 50% decrease in glycine pools. Overexpressing threonine aldolase in sink organs could increase flux through threonine catabolism. However, acetaldehyde generated as part of the pathway could produce toxicity effects as it has a high tendency to form adducts with proteins and DNA, impairing their function (Tsuji et al., 2003; Zhang et al., 1997; Perata et al., 1992). From the nutritional perspective, acetaldehyde is also toxic to humans (mutagenic and carcinogenic), and is not fit for consumption (Waris et al., 2020, 2018; Brooks and Schuebel, 2017). Overexpressing aldehyde dehydrogenase to ensure the rapid breakdown of acetaldehyde to non-toxic acetate could also be beneficial.

5.4 Conclusions

In this chapter, WholePlantMetabolism v1 was used to explore the possible solution space for improving growth, focussing on assimilate transport through the phloem. Model predictions identified (1) an increased role for amino acid catabolism in sink

organs, both as a method for reducing respiratory carbon loss and also energy production, (2) various amino acids as efficient carriers of carbon and nitrogen, and (3) significantly different optimal resource partitioning patterns for growth under carbon and nitrogen limitation. Overall, promising targets for improving plant growth were suggested, and the strategies proposed in this work should be implemented using precise genetic engineering techniques to assess their efficacy *in planta*. Though it should be noted that optimal model solutions were generated based solely on reaction stoichiometry and enzyme/transporter availability.

6 | Optimal biomass partitioning for improved fruit yield

6.1 Introduction

As fruits constitute a large sink organ, much of the research on optimising tomato fruit production has focused on manipulating source-sink interactions (Glanz-Idan and Wolf, 2020; Fukushima et al., 2018; Sonnewald and Fernie, 2018; Bénard et al., 2015; Bermúdez et al., 2014; Osorio et al., 2014; Jiang et al., 2013; Park et al., 2012; Kang et al., 2011; Pérez-Alfocea et al., 2010; Bénard et al., 2009; Dong et al., 2008; Heuvelink, 1995a; Russell and Morris, 1983). Many of these have identified assimilation partitioning between vegetative and reproductive organs as a key determinant of crop yield. For example, SPA is a DnaJ chaperone-related protein involved in carbon partitioning. SPA-silenced tomato mutants produced larger fruits and had increased fruit number per plant compared to the WT (Bermúdez et al., 2014). SPA localised to thylakoid membranes in photosynthetic tissues, and carbohydrate levels in leaves were reduced, suggesting an increase in carbon transport from source leaves to fruit sinks. In another example, the balance between the initiation of reproductive and vegetative phytomers was fine-tuned by modulating plant hormone levels (Park et al., 2014; Jiang et al., 2013). Modelling predictions have also revealed the relationship between fruit set probability and source:sink ratios, indicating a pay-off between investments in the development of new leaves versus fruit growth (Kang et al., 2011). Many agronomically important traits in tomato

have been investigated extensively, including fruit nutritional quality, fruit ripening, and disease resistance and abiotic stress resistance (Li et al., 2018b; Zsögön et al., 2018; Snowden et al., 2015; Abuqamar et al., 2009; Frusciante et al., 2007; Cuartero and Fernández-Muñoz, 1998; Oeller et al., 1991). Overall, manipulating biomass partitioning between organs presents an attractive target for improving tomato fruit production. However, this has not been systematically explored at the metabolic level, and hence it remains unclear what is the ideal balance between vegetative and reproductive growth for maximal fruit yield.

Tomato fruit growth is characterised by dynamic shifts in metabolite content between distinct stages of maturation (Quinet et al., 2019; Karlova et al., 2014; Carrari and Fernie, 2006). For example, tomato is climacteric, meaning that fruits undergo a respiratory burst and increase ethylene production prior to ripening (Alexander and Grierson, 2002). Ripening is also characterised by increased lycopene and carotenoid content, the degradation of starch carbon stores, increased accumulation of sugars, and tissue softening. To capture the reprogramming of fruit metabolism over development, stoichiometric fruit models use dynamic biomass compositions as the objective function in a multiphase framework (Shameer et al., 2020; Colombié et al., 2017, 2015). Using this set-up, Shameer et al. (2020) were able to predict accurate metabolite levels throughout fruit development, and also elucidate the role of starch as a source of energy to fuel late fruit development when assimilate import from the phloem is greatly reduced. The model also identified solute accumulation for osmotically-driven cell expansion as a significant energy drain.

In this chapter, the WholePlantMetabolism v1 model was extended to include fruit metabolism. In order to simulate the dynamic shifts in fruit metabolic activity over development, the model structure was adapted to include metabolic detail at the individual organ level (Quinet et al., 2019). A model mechanism for initiating

new organs along the plant main stem (leaf, fruit, and stem models) was developed, and model growth predictions were validated against a tomato growth dataset. The improved model (WholePlantMetabolism v2) was used to identify optimal patterns of biomass partitioning between plant organs for optimal fruit yield.

6.2 Results

6.2.1 Model extension: plant organ development

This section describes how I constructed WholePlantMetabolism v2 by building on WholePlantMetabolism v1 to account for the development of new fruit and leaf organs along the main stem and their metabolism.

Phytomer appearance

Organs are organised along the main stem in phytomer units, with each unit composed of a leaf, the stem itself, and sometimes a truss of fruits. The rate of phytomer appearance (also referred to as the phyllochron) is controlled by temperature and responds linearly to thermal time (Fleisher et al., 2006). New organs are initiated in the model according to phyllochron length, and the cumulative temperature on each day is calculated as the difference between mean daily temperature and a species-specific base temperature below which development halts. The model also requires the structure of each phytomer as input parameters (i.e. whether the phytomer contains a leaf, stem, or fruit). At the structural level, the initiation of a new organ results in the creation of a model object recording its age, mass, and position along the main stem.

In the validation dataset, the phyllochron in tomato was found to be 33.4 °Cd (Figure 4.1). As plants were grown under constant temperature (23.9 °C), this equated to a phyllochron of 2.4 days in absolute time, using a tomato-specific base temperature (10 °C; Dong et al., 2008; Heuvelink and Marcelis, 1989). Leaves and

stems were present on all phytomers, and fruits were present on the 10th and 13th phytomers.

Multi-leaf metabolic model

At the metabolic level, separate organ-specific models are only initiated and coupled to the whole-plant metabolic stoichiometric model for new leaves and fruits. As the stem is assumed to not exhibit significant shifts in its metabolic function over development, the entire shoot main stem is modelled as one metabolic compartment. The modelling approach used for reproductive metabolism in fruits is discussed separately later in Section 6.2.2.

For each leaf, a diel leaf model was coupled to the whole-plant metabolic network via the vascular metabolite common pool. Young leaves are metabolic sinks and rely on assimilate supply from other source leaves. However, leaves transition from sink to source status over development once they have established sufficient photosynthetic capacity of their own. As a result, leaf models contain both phloem import and export reactions. The model was free to choose between these two reactions, allowing it to dictate the sink-to-source transition of each leaf. The minimisation of the total sum of fluxes objective in pFBA ensured that these two reactions would not operate simultaneously in a single leaf in a futile cycle.

As with WholePlantMetabolism v1, constraints are applied to RuBisCO carboxylase and photon uptake fluxes by scaling the maximum rates using the mass of each leaf. Additionally, as the model does not have a metabolic compartment explicitly modelling cotyledons, the contribution to photosynthetic activity by cotyledons are instead attributed to the lowest active leaf along the main stem. The validation dataset also reported a lower SLA during reproductive growth compared to vegetative growth (Figure 4.4). After the appearance of fruits, the maximum RuBisCO carboxylation and photon uptake rates are recalculated using this SLA

value to account for changes in leaf thickness throughout development.

The model requires the maximum leaf lifespan as an input parameter to model leaf senescence. On each day of growth, the age of each leaf is checked to determine if it has reached the maximum leaf lifespan; if it has, fluxes through all the reactions in that particular leaf are constrained to zero.

As with WholePlantMetabolism v1, NGAM requirements are scaled according to leaf mass and distributed between the day and night phases according to the photoperiod.

Biomass partitioning

As before, biomass partitioning between different vegetative organ types is constrained by calculating the ratio of absolute growth rates using scaling exponents (α) and existing organ masses (M). The distribution of biomass amongst different organs of the same type (leaf or stem in this case) is calculated based on their individual relative growth demand, taking into account organ age (θ) and position along the main stem (λ). Firstly, growth data of individual leaves and stem portions were used to generate generalised growth functions at the individual organ level. Determinate organ growth is most commonly modelled using a sigmoidal function ($\sigma(\theta)$):

$$\sigma(\theta) = \frac{a}{1 + e^{-b \cdot (\theta - c)}}, \tag{6.1}$$

where a, b, c are constants (Voorend et al., 2014; Yin et al., 2003). The growth rate can then be resolved by taking the first order differential of the fitted function in the form

$$\sigma'(\theta) = \frac{a \cdot b \cdot e^{-b \cdot (\theta - c)}}{(e^{-b \cdot (\theta - c)} + 1)^2}. \tag{6.2}$$

Figure 6.1a-b shows fitted growth rate curves for leaves and stems at different phytomer ranks as a function of organ age derived from growth data in the valida-

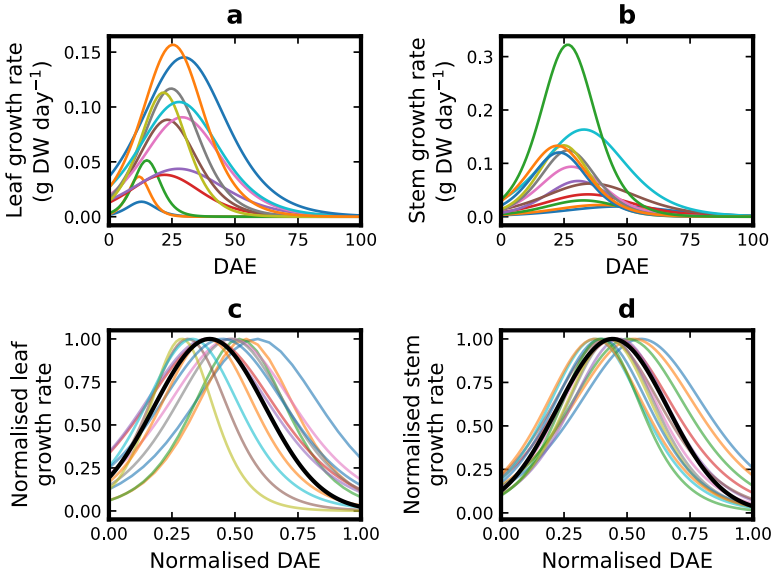

Figure 6.1: Generation of generalised growth rate functions for leaf and stem growth at the individual organ level derived from experimental data. First order derivatives of fitted sigmoidal functions to tomato **(a)** leaf and **(b)** stem growth data at the individual phytomer level as a function of organ age representing daily growth rates. Normalised first order derivatives of fitted sigmoidal functions to tomato **(c)** leaf and **(d)** stem growth data at the individual phytomer level as a function of organ age. Coloured lines represent fits at different phytomer levels. Solid black lines indicate a secondary fit to the combined normalised data at all phytomer levels using a first order derivative sigmoidal function. In WholePlantMetabolism v2, parameters provided by this fitted function are used to dictate biomass partitioning between individual leaves and stems. Original data are presented in Figure 4.2. DAE, days after (organ) emergence; DW, dry weight.

tion dataset. From this, I determined the length of time each organ grows before reaching maturation (the expansion period) as a function of phytomer position ($\theta_e(\lambda)$) by assessing the age at which the growth rate approaches zero. Growth rate curves were normalised in the x-direction using $\theta_e(\lambda)$, and in the y-direction using the maximum growth rate at each phytomer position. Figure 6.1c-d shows the results of fitting $\sigma'(\theta)$ to the normalised data to generate generalised growth rate functions for leaf and stem growth at the individual organ level.

Within the model, the growth demand ($D(\rho, \theta, \lambda)$) of each individual organ is modelled as

$$D(\rho, \theta, \lambda) = \frac{a(\rho) \cdot b(\rho) \cdot e^{-b \cdot (\theta'(\rho,\theta,\lambda) - c(\rho))}}{(e^{-b \cdot (\theta'(\rho,\theta,\lambda) - c(\rho))} + 1)^2}, \tag{6.3}$$

where ρ is organ type (L for leaf, and S for stem). $\theta'(\theta, \lambda)$ is a function to scale

organ age according to its expansion period:

$$\theta'(\rho, \theta, \lambda) = \frac{\theta}{\theta_e(\rho, \lambda)}. \tag{6.4}$$

The growth demand of each organ is scaled to the total growth demand of all organs of the same type to generate its relative growth demand ($D'(\rho, \theta, \lambda)$):

$$D'(\rho, \theta, \lambda) = \frac{D(\rho, \theta, \lambda)}{\sum_{\lambda'=1}^{n(\rho)} D(\rho, \theta, \lambda')}, \tag{6.5}$$

where $n(\rho)$ is the number of organs of type ρ along the shoot main stem. The distribution of biomass among vegetative organs is thus partitioned on day t of growth as

$$\left[\sum_{\lambda=1}^{n(L)} D'(L, \theta, \lambda) \cdot (M_L(t) \cdot \alpha_{M_L/M_R})\right] + \left[\sum_{\lambda=1}^{n(S)} D'(R, \theta, \lambda) \cdot (M_R(t) \cdot \alpha_{M_S/M_R})\right] + M_R(t). \tag{6.6}$$

6.2.2 Model extension: fruit metabolism

The model does not account for inflorescence and assumes that the growth demand of flowers is negligible. For reproductive phytomers, a flowering time delay is included in the model to account for the interval between phytomer appearance and fruit development (10 days in the validation dataset). All the fruits on a truss are collectively modelled using a single fruit metabolic model. Fruit models are coupled to the whole-plant metabolic model through the metabolite common pool. The phloem transport reaction is constrained to only allow for metabolite uptake into fruits to simulate sink behaviour.

Low levels of photosynthetic activity have been reported in tomato fruits early on in fruit development, especially in outer pericarp tissues (Carrara et al., 2001; Piechulla et al., 1987; Farineau and Laval-Martin, 1977). However, chloroplasts quickly become photosynthetically inactive, and become repurposed as chromo-

plasts during development (Osorio et al., 2014; Kahlau and Bock, 2008). Mutants with disrupted chlorophyll biosynthesis pathways in fruits showed no impairments in growth, despite a reduction in photosynthetic activity (Höfgen et al., 1994). Overall, fruits are not net carbon assimilators and photosynthesis does not seem to be a critical determinant for fruit growth. As a result, RuBisCO carboxylase and photon uptake fluxes are constrained to zero in fruit compartments.

As with all other organs, fruit NGAM is simulated by scaling an experimentally observed demand using the fruit's mass as a constraint for generic ATPase and NADPH oxidase reactions (Heuvelink, 1995b).

To capture the shifts in the metabolite profile of tomato fruit throughout growth, a dynamic biomass equation is used to constrain the fruit model. Shameer et al. (2020) characterised the biomass composition of tomato fruit at all important growth stages, from the immature green stage to the ripened red stage. This dataset was used to generate the daily biomass content of fruits, from which the daily relative demand for growth can be calculated and used to constrain the biomass equation (Section 2.1.3). This includes biomass components that are degraded throughout development to fuel growth. Principally, the dataset provided values for cellulose, cell membrane phospholipids, proteinaceous amino acids, soluble amino acids, organic acids, starch, and soluble carbohydrates (Appendix A). Phospholipids were composed of phosphatidic acid, phosphatidyl choline, and phosphatidyl ethanolamine, and their relative abundances were estimated based on characterisations in cherry tomato (Güçlü et al., 1989).

6.2.3 Biomass partitioning towards fruit growth

The conserved allometric scaling patterns observed between vegetative organs are often not reported for reproductive structures (Cheplick, 2005; Niklas and Enquist, 2003). The growth of vegetative mass is essential for plant viability; leaves

function as a source of carbon, roots as a source of nutrients, water, and stability, and stems for above ground structural support. In contrast, the production of reproductive tissues is conditional and does not directly affect plant survivability. There is a high degree of variation between the reproductive strategies of different plant species, and many often show a response to environmental conditions. For example, the rate of fruit-set in tomato has been linked to soil salinity, crop density, light availability, and temperature (Sandri et al., 2002; Adams et al., 2001; Peet and Bartholemew, 1996; van Ieperen, 1996). Consequently, a meta-analysis of 97 growth datasets reported high levels of plasticity (non-linear relationship) or a lack of any relationship between the size of reproductive organs in relation vegetative mass in mutiple species (Weiner et al., 2009). Overall, this suggests that allometric scaling laws do not provide a suitable framework for modelling biomass partitioning to fruits.

WholePlantMetabolism v2 instead simulates growth in fruits using a growth function derived from experimental data. Figure 6.2a shows the result of fitting a sigmoidal function (Equation 6.1) to mass data at the individual fruit level. The mass of an individual fruit at anthesis was extrapolated from this fit (0.00025 g DW) and is used in the model to initiate organ mass for fruits at the start of growth by scaling according to the mean fruit number (7.37 fruits truss^{-1} at the 10th phytomer, and 9.12 fruits truss^{-1} at the 13th phytomer). Figure 6.2b shows the first order derivative of the sigmoidal fit to growth data, which equates to the daily fruit growth rate. In the model, this relationship is used to fix the rate of biomass production in fruit models as a function of fruit number ($F_n(\lambda)$) and organ age:

$$\sigma'(\theta) \cdot F_n(\lambda). \tag{6.7}$$

As the fruit growth rate is applied as a hard constraint, in contrast to vegetative organs where only the relative demand is constrained, the model effectively assumes

that plants prioritise reproductive growth over vegetative growth once fruits have been initiated.

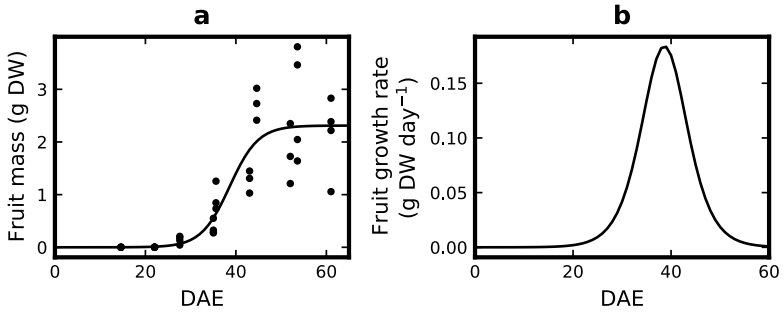

Figure 6.2: Generation of a generalised fruit growth rate function at the individual fruit level. **(a)** Sigmoidal function (line) fitted to individual fruit growth data (symbols) in tomato as a function of organ age. **(b)** First order derivative of the sigmoidal function representing the daily fruit growth rate. In WholePlantMetabolism v2, parameters provided by this fitted function are used to dictate the growth of fruits. DAE, days after (organ) emergence; DW, dry weight.

6.2.4 Growth predictions

With the described model extensions, WholePlantMetabolism v2 was used to simulate growth over vegetative and reproductive phases in tomato using input parameters generated by the validation dataset. Figure 6.3 shows model growth predictions for organ growth at the whole plant level. The model was able to predict leaf and fruit growth to a high degree of accuracy (RMSE = 3.33 and RMSE = 4.19 for leaves and fruits, respectively). The predicted final fruit mass was within experimental error, and the predicted final leaf mass was within 2 g DW of experimental error (Figure 6.3a-b). In contrast, model performance was worse for root and stem growth predictions. Accurate growth predictions for the root and stem were generated over the vegetative phase (12–45 DAS), but were underestimated during reproductive growth (> 45 DAS; Figure 6.3c-d). The predicted final root mass was 68% lower than the data mean, and the predicted final stem mass was underestimated by 38%. Nonetheless, the dynamics of root and stem growth predictions were qualitatively similar to the data, with continual

growth throughout both vegetative and reproductive phases.

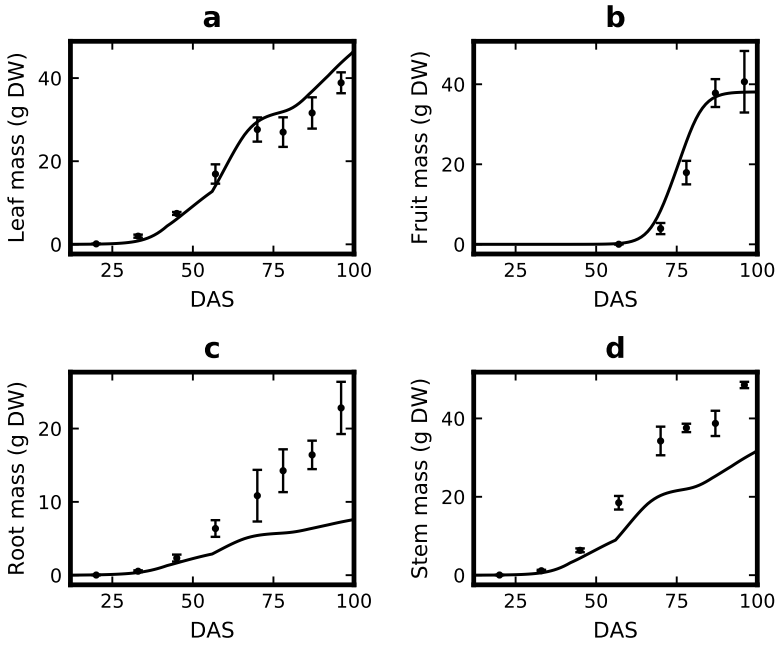

Figure 6.3: Growth predictions (lines) for **(a)** leaf, **(b)** fruit, **(c)** root, and **(d)** stem by WholePlant-Metabolism v2 over 100 days. Data (symbols) are the mean±SD mass of tomato cv. Moneymaker in the validation dataset (n = 3 – 6 plants at each harvest). DAS, days after sowing; DW, dry weight.

At the individual phytomer level, growth predictions for fruit growth at both the 10th and 13th phytomers were in good agreement with the data (Figure 6.4). The predicted final fruit masses at both trusses were within the range of experimental error. This is unsurprising as the model mechanism for fruit growth requires the direct input of daily growth rates as a hard constraint.

Similar to growth predictions at the whole-plant level, growth predictions for leaves at the individual phytomer level also showed good agreement with the data throughout the entire growth period, both qualitatively and quantitatively (Figure 6.5a). This indicates that the biomass partitioning function for vegetative organs accurately captures the competition for growth resources between individual leaves along the plant stem.

In contrast, stem growth predictions at the phytomer level were comparatively poor (Figure 6.5b). As with predictions at the whole-plant level, predictions during

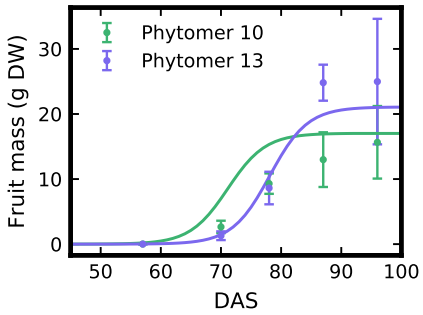

Figure 6.4: Growth predictions (coloured lines) for fruit growth on two different trusses by WholePlantMetabolism v2. Data (coloured symbols) are the mean±SD of tomato cv. Moneymaker fruits in the validation dataset (n = 3 – 5 plants at each harvest). DAS, days after sowing, DW, dry weight.

vegetative growth were in good agreement with the data, but were underestimated during the reproductive phase. Peaks in stem mass at reproductive phytomers (10th and 13th phytomers) resulting from peduncle mass providing support for fruits were observed in the experimental data. The model was unable to capture this dynamic as no explicit mechanism accounting for fruit structural support was included.

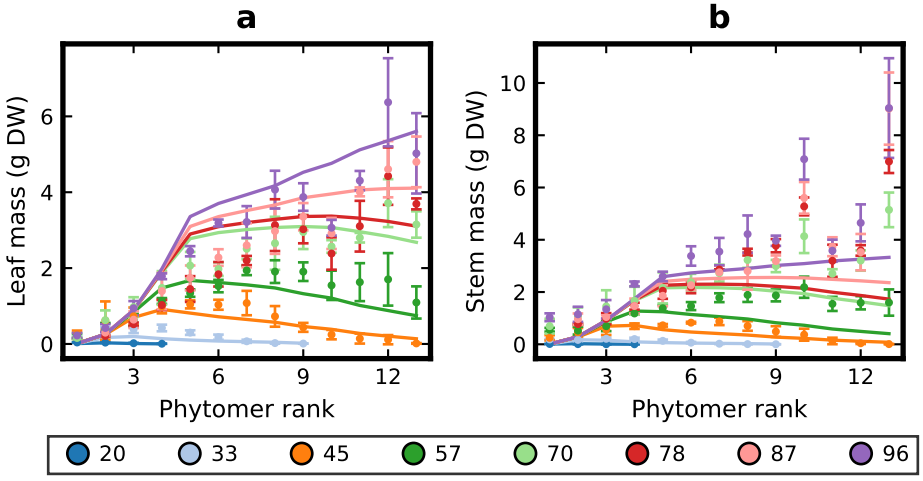

Figure 6.5: Growth predictions (coloured lines) for **(a)** leaf and **(b)** stem growth at the phytomer level by WholePlantMetabolism v2. Data (coloured symbols) are the mean±SD of tomato cv. Moneymaker in the validation dataset (n = 3 – 6 plants at each harvest). The legend indicates the plant harvest date in DAS. DAS, days after sowing, DW, dry weight.

6.2.5 Optimal plant structure for increased fruit yield

In WholePlantMetabolism v2, biomass partitioning between organs is controlled by allometric scaling exponents expressed relative to the root. By varying the scaling exponents for leaf and stem growth, the partitioning of growth to all vegetative organs can be manipulated (e.g. reducing α_L and α_S results in a reciprocal relative increase in α_R. WholePlantMetabolism v2 can thus be used to identify optimal plant structures for improved fruit yields by altering the sink strengths of each organ. To this end, growth was simulated in three different environments: the reference conditions of the validation dataset (320 μmol m^{-2} s^{-1} PPFD, 14 mM nitrate), high light (640 μmol m^{-2} s^{-1} PPFD, 14 mM nitrate), and high nitrate (320 μmol m^{-2} s^{-1} PPFD, 28 mM nitrate). For each simulation, the fixed fruit growth rate was increased incrementally until the model returned infeasible solutions, which indicates that the predicted plant structure did not have sufficient resources to support further growth.

The limits of the scanned parameter space were chosen to diverge no more than 0.2 from experimentally observed values for α_L (0.98) and α_S (1.22). Figure 6.6 shows the final organ masses that could be supported within this space and shows that feasible solutions were restricted along the diagonal plane. The boundaries of this space corresponded most strongly with leaf growth dynamics, which showed the most difference in growth along the same gradient, indicating that carbon source activity exerted the principal control on growth (Figure 6.6a-c). As reported in Chapters 4 and 5, growth under reference conditions was predicted to be carbon-limited. A trade-off between stunted growth resulting from an underinvestment into leaf growth and excessive foliage resulting in reduced light throughout the canopy explains the diagonal form of the solution space. When α_L was low, plants were severely limited in their ability to assimilate carbon. But when a

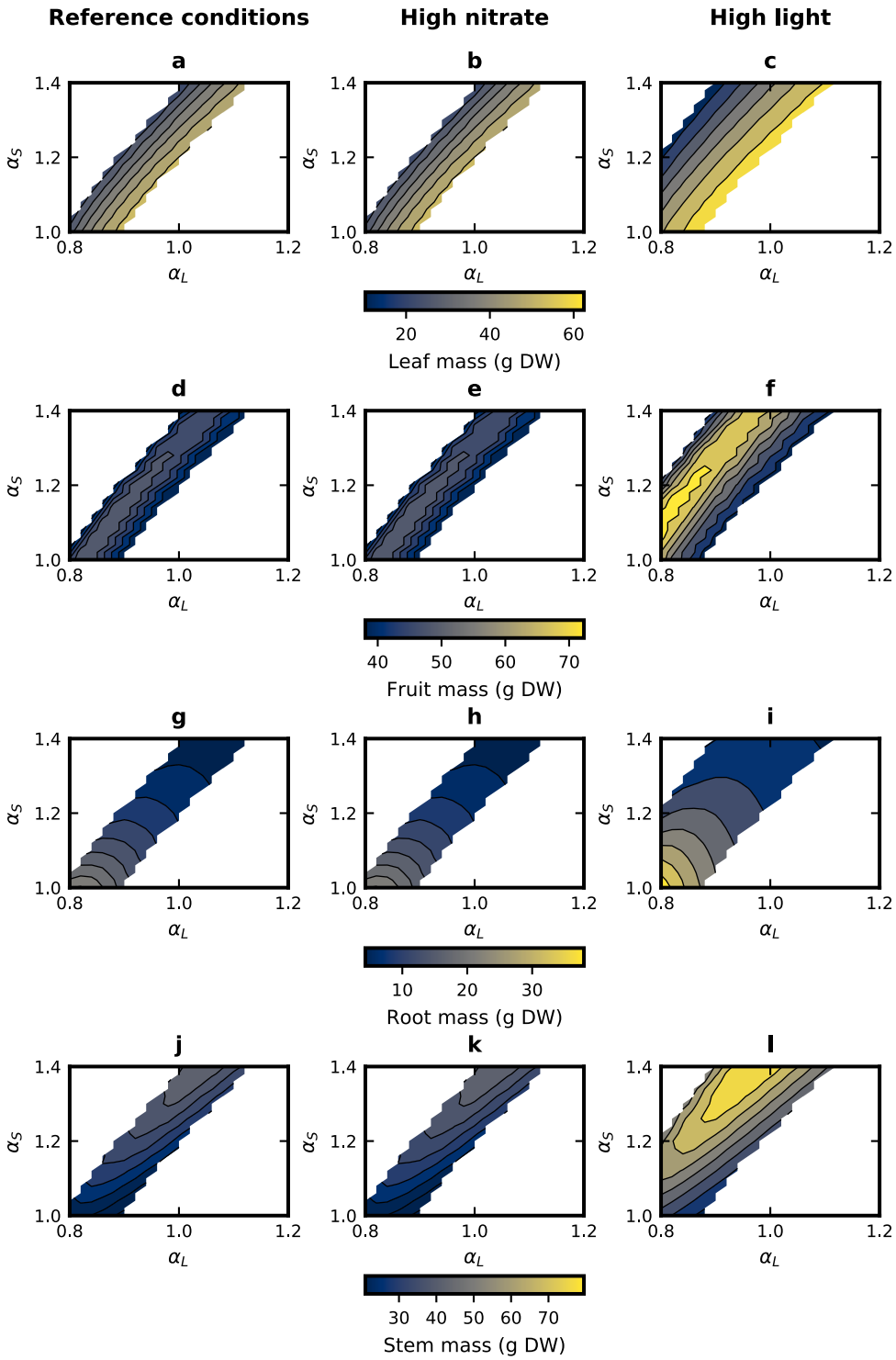

Figure 6.6: Final mass predictions after 100 days of growth for **(a-c)** leaf, **(d-f)** fruit, **(g-i)** root, and **(j-l)** and stem by WholePlantMetabolism v2 using a range of different scaling exponents for leaf (α_L) and stem (α_S) biomass partitioning. Growth was simulated under three different environmental conditions: the reference conditions of the validation dataset (320 µmol m^{-2} s^{-1} PPFD, 14 mM nitrate), high light (640 µmol m^{-2} s^{-1} PPFD, 14 mM nitrate), and high nitrate (320 µmol m^{-2} s^{-1} PPFD, 28 mM nitrate). White portions of plots indicate the infeasible solution space. DW, dry weight.

low α_L value was accompanied with a low α_S value, this equated to an effective increase in α_L. Conversely, when α_L was high, plants had improved carbon source capacities, but excessive leaf growth eventually results in highly reduced light levels within the canopy as predicted by the Monsi-Saeki model (Hirose, 2005). A high α_S also resulted in an effective reduction of α_L as more resources were diverted to support stem growth (Figure 6.6j-l). Increasing the supply of light significantly increased the size of the feasible solution space (Figure 6.6c,f,i,l). The maximum final sizes of all organs were also significantly increased, indicating a higher degree of tolerance towards canopy effects. In contrast, increasing nitrate supply resulted in no improvements in growth and produced model predictions identical to simulations using reference conditions (Figure 6.6b,e,h,k).

Under reference conditions, the model predicted that fruit growth could be increased by 18% compared to the experimental rate without any alteration to vegetative growth processes (Figure 6.6d). This indicates that sink limitation in fruits may be limiting fruit yield, and that targeting metabolic processes in fruits may be a promising strategy. However, manipulating vegetative growth could potentially increase fruit growth further by 30%, suggesting that both vegetative and reproductive growth should be targeted. Under high light availability, the maximum final fruit size was improved further to 72 g DW, equating to a 90% increase in yield (Figure 6.6f).

Under all three environmental conditions, optimal fruit production showed a clear preference for reduced α_L and α_S. This indicates a preference for increased root growth (Figure 6.6g-i) and reduced stem growth (Figure 6.6j-l). The root is functionalised as a source of inorganic nitrogen in the model, so increased root growth will inevitably elevate nitrogen source capacity. However, as the simulations here are for growth under carbon limitation, nitrogen metabolism is highly unlikely to exert strong control on growth. The lack of differences in model

predictions between the reference conditions and high nitrate supply support this further. On the other hand, it is likely that reducing stem growth increases the amount of photoassimilates that can be diverted to fruit growth instead. In fact, data from the validation dataset shows that stems constituted the largest sink in tomato, demanding more than 30% of the plant's dry matter (Figure 6.3). Additionally, as the stem functions purely as a sink in the model, reductions in its growth does not lead to any detrimental effects on carbon or nitrogen source strengths.

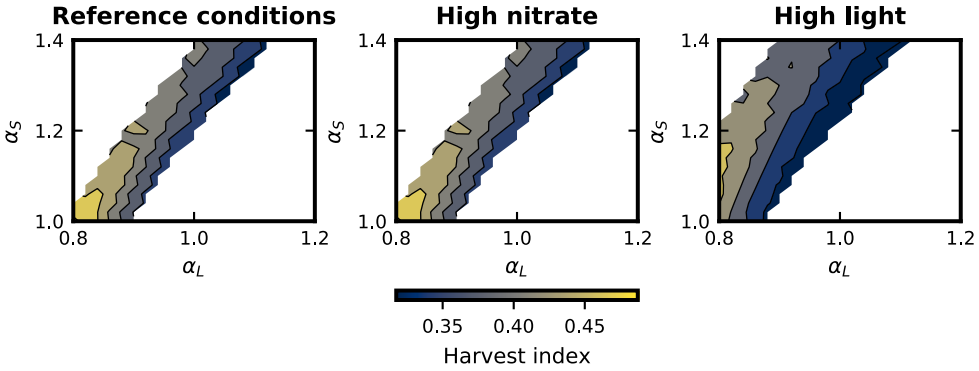

Figure 6.7: Harvest index predictions by WholePlantMetabolism v2 after 100 days of growth using a range of different scaling exponents for leaf (α_L) and stem (α_S) biomass partitioning. Harvest index was calculated as the fraction of above ground dry mass dedicated to fruits. Growth was simulated under three different environmental conditions: the reference conditions of the validation dataset (320 µmol m^{-2} s^{-1} PPFD, 14 mM nitrate), high light (640 µmol m^{-2} s^{-1} PPFD, 14 mM nitrate), and high nitrate (320 µmol m^{-2} s^{-1} PPFD, 28 mM nitrate). White portions of plots indicate the infeasible solution space.

The harvest index is commonly used to measure improvements in crop production efficiency, and is defined as the fraction of the above ground biomass that is harvestable (fruits in tomato). A high harvest index indicates that a plant is optimised for partitioning assimilates into the organ of agricultural interest and that the plant expresses a high degree of resource use efficiency, arising from both plant physiology (e.g. water use, photosynthesis, etc.) and agronomic practises (e.g. fertiliser use, pruning, etc.). As a result of the latter, harvest indexes can vary significantly between studies and growth conditions. For example, the harvest

index for tomato cv. Moneymaker ranges from 0.1 to 0.6 in the literature (Mereb et al., 2020; Renau-Morata et al., 2020; Mayta et al., 2019; Bermúdez et al., 2014). The mean harvest index for tomato plants in the validation set was 0.32±0.04. Figure 6.7 shows the predicted harvest index under the three different conditions. As is the case for optimal fruit growth, similar dynamics are reported here: there is a clear preference for reduced partitioning towards stem growth. However, the effects here are much more pronounced, with the highest harvest indexes reported only for the bottom left corner of the solution space (whereas optimal fruit production is reported for comparatively higher α_L and α_S values). This suggests that while optimal fruit production shows some degree of flexibility, as a wide range of parameters can produce the maximum fruit mass, harvest index has a more restricted optimum.

6.3 Discussion

6.3.1 Model improvements

Many ecophysiological models of photosynthesis at the whole-plant level commonly scale up single leaf models using a big leaf framework, where the metabolic activities of leaves within the canopy are considered together in a combined manner (Holland et al., 2019; Shaw and Cheung, 2018; Zakhartsev et al., 2016; de Oliveira Dal'Molin et al., 2015; Friend et al., 1997; Kull and Jarvis, 1995). This assumes homogeneity between the behaviour of leaves at different phytomer levels, an assumption that greatly reduces the level of parametrisation required for modelling source carbon activity and also computational time. However, the biological reality in leaves differs greatly from this *in silico* depiction, and major differences have been identified between sunlit and shaded leaves within the canopy (Marchiori et al., 2014; Eyles et al., 2013; Crous and Ellsworth, 2004; Hirose, 2005; de Pury

and Farquhar, 1997; Terashima and Hikosaka, 1995; Hirose and Werger, 1987). There is now a large body of evidence supporting the use of multi-layered leaf models in favour of big leaf models (Dai et al., 2004; Friend, 2001; Leuning et al., 1995). Direct comparisons between the two modelling methods have shown that explicitly accounting internal canopy structure greatly improves predictions for net primary production, gross primary production, and evapotranspiration rates (Luo et al., 2018; Song et al., 2013; Raulier et al., 1999).

In this chapter, a mechanism for modelling the initiation and development of organs along the main stem and the partitioning of biomass between them were introduced to WholePlantMetabolism, significantly improving model depictions of leaf metabolism. The transport of assimilates through the phloem from source leaves to sink leaves and the associated energetic costs were accounted for. Modelling leaves at the individual organ level also allowed for predictions of dynamic metabolic behaviours over the course of leaf development. Due to time constraints, I was unable to explore this aspect of the model in more detail, but the current modelling framework generates predictions for sink-to-source transitions in leaves over growth (Chen and Wang, 2008; Harn et al., 1993; Turgeon, 1989). Future analysis of the model could investigate the following aspects of leaf development: the timing of the transition to source status, the effect of the shift from heterotrophic to autotrophic growth on respiratory carbon loss in leaves, and the increasing role of photorespiration in contributing to glycine and serine biosynthesis throughout leaf development (Marchi et al., 2005; Jeong et al., 2004; Meng et al., 2001; Masclaux et al., 2000).

Modelling metabolism at the individual organ-level allows for the dynamic biomass requirements of fruit growth to be simulated. Future applications of the model could be use to determine whether shifts in metabolite demand result in variations in optimal phloem content over fruit development (Chapter 5). For

example, differences in phloem amino acid composition and the sucrose:amino acid ratio have been reported between pre-tuber filling and tuber filling phases in potato (Karley et al., 2002). Model predictions could elucidate the role these changes play in reproductive growth.

6.3.2 Redesigning plant architecture for increased crop yield

Model predictions identified the following features of plant growth as potential targets for optimal fruit production: (1) increased fruit sink activity and (2) reduced stem growth. Recent advances in molecular biology have allowed for the identification of specific genetic targets for these improvements.

Increasing fruit sink strength

The model predicted that without any direct manipulation of vegetative growth, fruit yield could be improved by targeting fruit sink activity alone, suggesting that resource partitioning within tomato may be further optimised (Figure 6.6d). During the domestication of tomato, lines with increased fruit size were selected for; cultivated tomato fruits are on average 500-fold larger than its wild equivalent, and the Giant Heirloom variety shows a 1000-fold increase (Lippman and Tanksley, 2001). As a result, many quantitative trait loci (QTLs) associated with harvest index have been identified through introgression lines established from crosses between wild ancestors and cultivated varieties (Lippman et al., 2007; Schauer et al., 2006; Eshed and Zamir, 1995). The regulation of locule (seed compartment) number has been linked to fruit size and is associated with the QTLs *fas* and *lc* (Lippman and Tanksley, 2001). Increased fruit number also improved the harvest index in tomato. Mutants with increased inflorescence branching (*fab* and *fin*) had enlarged meristems and produced more flowers and fruits per truss compared to the WT (Xu et al., 2015). In tomato, flower initiation is promoted by the hormone

florigen, which itself is repressed by *sp*. Park et al. (2014) isolated a weak allele of *sft* (a florigen gene) by screening chemically-induced mutations, and combined heterozygous mutations to find the optimal balance between vegetative and reproductive growth for increased fruit yield. Homologues of *sft* and *sp* have been identified in many other crops, including soybean, rice, and barley, and should be targeted to identify optimal dosage responses to florigen signalling (Ogiso-Tanaka et al., 2013; Comadran et al., 2012; Liu et al., 2010).

Promisingly, CRISPR/Cas9 technology has been used in two independent studies to show that targeting fruit number, locule number, and the florigen pathway results in the *de novo* domestication of *Solanum pimpinellifolium* (a wild ancestor of tomato), with engineered plants producing more fruits with increased mass (Li et al., 2018a; Zsögön et al., 2018). Overall, this suggests that targeting fruit developmental features for increased reproductive sink strength presents an attractive target for improving crop yield. Future studies should assess whether the harvest index of cultivated tomato varieties can be optimised further using these gene targets.

Reducing stem growth

A major outcome of the Green Revolution was the establishment of dwarf varieties of crop plants with reduced plant height through selective breeding (Sakamoto and Matsuoka, 2004; Hedden, 2003). Yield increases were mostly attributed to increased shoot stability resulting in more structural resistance to wind and weather, and less susceptibility to lodging (the bending of stems resulting in grain rot or difficulty in harvesting), especially in cereal crops. Mechanised harvesting technology has also been greatly optimised towards use on crops with compact shoot architecture. However, model predictions by WholePlantMetabolism v2 indicate another advantage of reducing shoot size: more assimilates can be allocated towards the

production of reproductive organs.

Numerous studies have linked dwarfed phenotypes to the action of gibberellins, a class of plant hormones that promote a range of shoot development processes, including stem elongation, germination, leaf expansion, and flower development (Würschum et al., 2017; Ji et al., 2014; Band and Bennett, 2013; Hedden, 2003; Schomburg et al., 2003; Sasaki et al., 2002; Peng et al., 1999). Gibberellins function by degrading the growth repressor DELLA through the ubiquitin-proteasome pathway. Loss-of-function mutations in gibberellin biosynthesis genes have been identified in many high-yielding dwarf crop varieties established in the Green Revolution (Fleet and Sun, 2005). However, yield improvements from traditional breeding methods have significantly slowed down, leading to efforts to engineer dwarf phenotypes using more precise genome editing methods (Guo et al., 2020; Xue et al., 2020; Wang et al., 2017). Increasing flux through gibberellin catabolism (e.g. overexpression of GA2-oxidases), overexpressing transcription factors repressing gibberellin biosynthesis genes, and encoding gibberellin-insensitive forms of DELLA have successfully reduced plant height and stem internode length in a various of species (Wu et al., 2018; Otani et al., 2013; Fleet and Sun, 2005; Muangprom et al., 2005; Sakamoto et al., 2003, 2001).

Compact shoot architecture has also been identified as a key feature of domesticated tomato varieties, with *S. pimpinellifolium sp* mutants (vegetative growth promoter) showing reduced height (Zsögön et al., 2018). Tomato plants treated with the growth retardand paclobutrazol also showed increased harvest indexes resulting from a 28% reduction in vegetative shoot growth (Gianfagna et al., 1998). Similarly, tomato crop yield and harvest index was increased following treatment with the chemical pruning agent OSO, which prevented the development of side shoots (Gianfagna et al., 1998). Recently, CRISPR/Cas9 genome editing was used to establish a dominant gain-of-function allele for the DELLA protein for dwarfing

phenotype in tomato (Tomlinson et al., 2019). However, its effect on fruit growth and crop yield have yet to be assessed. In another study, cyanobacterial flavodoxin expressed in tomato was reported to alter plant size and increase harvest index, suggesting that targets other than gibberellin signalling may also have high potential (Mayta et al., 2019).

6.3.3 Model limitations

A major limitation of this formulation of the model was the mechanism used to model fruit growth. Owing to the complex nature of reproductive allometry and condition-specific patterns of fruit production, it was not possible to implement a generalised partitioning function for reproductive growth (Weiner et al., 2009; Reekie and Bazzaz, 2005; Cheplick, 2005; Niklas and Enquist, 2003). This problem is common to all plant growth models and future efforts should be made to characterise fruit development better. By constraining growth to a fixed rate, WholePlantMetabolism v2 could not generate flux distributions for optimised fruit growth. However, a suitable workaround to this was found by incrementally increasing the growth rate until infeasibility was reached. Future model versions should also account for other better resolved aspects of fruit growth. For example, several studies have identified species-specific minimum plant sizes for reproductive growth (Weiner et al., 2009; Reekie and Bazzaz, 2005). This size threshold is representative of the resources and qualities a plant must possess before investing in seed production (e.g. photosynthetic capacity, structural integrity, etc.). Future model versions could include a mechanism for fruit abortion for plants of insufficient size.

WholePlantMetabolism v2 also models leaf developmental processes, but senescence is constrained in a relatively crude manner. Metabolic activity in leaves simply ceases at a specified age. In reality, leaf senesce is gradual, and is charac-

terised by the activation of nitrogen remobilisation pathways and a decrease in carbon source activity resulting from chloroplast disassembly (Woo et al., 2019; Havé et al., 2017; Kim et al., 2016). Future model versions should include a decay function for RuBisCO carboxylase activity. The remobilisation of both organic and inorganic nitrogen can be modelled by including pathways for protein degradation, and the metabolite profiles of senescing leaves can be used to constrain the amino acid composition of protein degradation products (Watanabe et al., 2018, 2013; Breeze et al., 2011).

Lastly, model predictions for leaf and fruit growth at the individual phytomer level showed good agreement with the data (Figures 6.4 and 6.5a). However, model performance for root and stem growth were notably worse (Figures 6.3 and 6.5b). A potential cause for the discrepancy in accuracy may arise from that fact that tomato-specific biomass compositions were used for leaf and fruit compartments, but interspecies compositional averages of 24 C_3 species were used for stem and root models, as no tomato-specific data were available (Poorter and Bergkotte, 1992). A similar issue was encountered in Chapter 3 when generating stoichiometric models of sink metabolism in Arabipdopsis, where using Arabipdosis-specific biomass compositions significant improved model performance. Future analysis of WholePlantMetabolism should quantify the composition of different tomato tissues for use as constraints to allow for a similar comparison to be made.

6.4 Conclusions

In this chapter, I developed an improved version of WholePlantMetabolism that accounted for fruit growth, and included metabolic detail at the individual organ level for leaves and fruits. Model predictions were validated by comparison to tomato growth data, and showed a moderate degree of accuracy. By exploring the potential solution space using altered biomass partitioning patterns, model

predictions identified several aspect of plant architecture that could be targeted to improve fruit yield, including increasing fruit sink strength and reducing stem growth.

7 | General discussion

7.1 Summary of results

The goal of this work was to establish a modular, readily adaptable computational framework in which it was possible to account for the full range of metabolic interactions and nutrient flows between plant organs, during development and in response to different growth conditions. Initially, it was hoped that a previously constructed multiscale whole-plant model (the FM), itself constructed by bringing together previously published models, would be a suitable framework with which I could integrate organ-specific FBA models of central metabolism (Chew et al., 2014). However, I found that several aspects of the FM made it unsuitable, including the hard-coding of crucial parameters that would require substantial amounts of recoding to unpick and a carbon-centric view of plant growth that ignored other growth-limiting nutrients, such as nitrogen (Chapter 3).

Instead, I developed a modelling framework (WholePlantMetabolism) with a structure that focussed more heavily on metabolism (Chapter 4). Biomass partitioning between different plant organs was mediated by a novel modelling approach for dictating organ growth based on allometric growth theory, which captured growth dynamics in tomato accurately. Comparisons between metabolic predictions and known plant biochemistry verified that the model was able to capture metabolic behaviour in both source and sink organs accurately. From a computational standpoint, key beneficial features of the model include the use of standardised format

input files that allow environmental conditions, plant phenology, organ-specific biomass compositions, and metabolic constraints to be read into the model. The model structure also generates organ-specific stoichiometric models automatically as new organs appear during growth simulations. These features allow future modellers to easily adapt the model for simulating different growth scenarios and developmental patterns in different species.

The resulting model allowed me to identify optimal modes of nutrient flow that were substantially different to that observed in tomato plants and resulted in substantial predicted increases in both vegetative and fruit growth. More specifically, optimal patterns of nitrogen usage were identified, including the energetic efficiencies associated with leaf-based nitrate assimilation, various amino acid catabolism pathways in sink organs, and the transport of nitrogen-rich amino acids (Chapter 5). Many of these flux modes acted to reduce respiratory carbon loss. Additionally, optimal patterns of biomass partitioning between organs were identified for improved fruit yield (Chapter 6). Analysis of the feasible model solution space revealed various aspects of plant architecture as potential targets, including reducing stem sink strength and increasing fruit sink strength.

7.2 Metabolic models as a tool for studying source-sink interactions

By its very nature, source-sink interactions involve the interaction between multiple tissues types and organs. This necessitates the use of a whole-plant perspective in computational models aiming to investigate such relationships (Shaw and Cheung, 2018; de Oliveira Dal'Molin et al., 2015; Grafahrend-Belau et al., 2013). The modelling framework developed in this work overcomes all of the major limitations present in other whole-plant metabolic models. In short, the WholePlant-Metabolism model is able to simulate growth and metabolism accurately (including

the flow of major plant nutrients), whilst accounting for biological activity in all major organs of the species under consideration, using metabolic predictions as the driver of growth, and allowing for dynamics shifts in growth constraints throughout development. Importantly, growth predictions were also validated using experimental data.

From plant manipulation experiments, it is clear that both source and sink metabolism exert some level of control on growth, and that the balance of this co-limitation is dependent on environmental conditions and development (Section 1.3). Using a multi-organ approach meant that the model accounts for both forms of growth limitation. In contrast to the unconnected approached used in FM-SoFBA-SiFBA, WholePlantMetabolism directly links source supply to sink demand, meaning that the model can concurrently optimise for both source and sink activity. The constraint on the maximum RuBisCO carboxylase flux (as related to empirical measures of the CO_2 assimilation rate) specifies the limits of source capacity, and the steady-state requirement of FBA prevents excessive source activity that exceeds sink demand, effectively accounting for sink limitation. The supply of other resources (e.g. nitrogen) and the respiratory costs of growth and NGAM also impose limits on the growth of sink tissues. With these features, WholePlantMetabolism was able to generate novel insight into source-sink interactions, such as the potential benefits of amino acid catabolism as an energy source in stems and roots, and also to improve our understanding of known biological phenomena, such as the benefits of dwarf phenotypes in improving crop yield.

Efforts were also made to prevent WholePlantMetabolism from being condition-specific. Most importantly, the biomass partitioning mechanism presented in this work is a significant improvement on the condition- and age-specific empirical partitioning coefficients used in other plant growth models (Pullen et al., 2019; Ma et al., 2018; Chew et al., 2014; Dong et al., 2008). The partitioning of assimilates

between organs is constrained by the biophysical relationships between different plant structures as dictated by allometric growth theory (Poorter et al., 2012b; Enquist and Niklas, 2002; Niklas and Enquist, 2002). Additionally, the decision to use thermal time over absolute time to control plant development ensured that the initiation of new phytomers along the plant main stem is not strictly coupled to the phenological timeline of a specific growth condition. The staging of plant phenology by thermal time is known to capture temperature controls on organ initiation and the shift from vegetative to reproductive growth in various species (Valdivia-Mares et al., 2016; Tsimba et al., 2013; Saiyed et al., 2009; Cleland et al., 2007; Granier et al., 2002; Moot et al., 2000; Ketring and Wheless, 1989). Lastly, accounting for growth on the basis of dry mass minimises the impact of variations in water content observed between studies, which is also highly dependent on growth conditions.

Further model flexibility is provided by PlantCoreMetabolism, the stoichiometric model of core metabolism that contains no species-specific reactions, which was used to construct WholePlantMetabolism. Previous applications of PlantCoreMetabolism have shown that it can simulate metabolic activity in a range of organs (source leaf, sink leaf, and fruit) in Arabidopsis, tomato, and *Opuntia* to a high degree of accuracy (Shameer et al., 2020, 2019, 2018). Though constrained for growth in tomato in this study, WholePlantMetabolism is readily applicable to consider the growth and metabolism of other economically important crop plants. For example, the effect of the development of large starch storage organs on optimal carbon and nitrogen partitioning through the phloem in cereal plants and potato can be investigated (Sonnewald and Fernie, 2018; Grafahrend-Belau et al., 2013; Braun and Slewinski, 2009). The generation of these models will be dependent on the availability of species-specific biomass compositions and other physiological constraints on growth. Single-tissue stoichiometric models have already been

constructed for barley, maize, rapeseed, rice, sugarcane, sorghum, soybean, and wheat, and may act as a useful compiled resource for model constraints (Moreira et al., 2019; Bogart and Myers, 2016; Poolman et al., 2013; Hay and Schwender, 2011a; Saha et al., 2011; Grafahrend-Belau et al., 2009). Large organ-specific growth datasets are also available for many species grown in various conditions as plant mass can be measured easily (Enquist and Niklas, 2002; Niklas and Enquist, 2002). The generation of species-specific allometric scaling exponents should therefore not be a significant obstacle to model construction.

For C_4 crops, such as maize, sorghum, and sugarcane, the integration of tissue-specific models is necessary to capture the interactions between different leaf cell types arising from Kranz anatomy. In these plants, carbon source activity is distributed spatially between mesophyll and bundle sheath cells. Various studies have now shown that by using a two-tissue stoichiometric model, applying tissue-specific constraints (e.g. restrict RuBisCO flux to the bundle sheath), and allowing for metabolite transfer between the two cell types to simulate plasmodesmata, FBA can generate accurate flux predictions for all three C_4 subtypes (Shaw and Cheung, 2019; Bogart and Myers, 2016; de Oliveira Dal'Molin et al., 2010b).

The whole-plant modelling approach can also be extended further to model interactions between plants and the microbiome. For example, legumes develop root nodules to host symbiotic rhizobia that fix atmospheric nitrogen and provide ammonia to the plant. Currently, GSMs have been generated for soybean, *M. truncatula* (a leguminous model organism), and also three different rhizobia species (Moreira et al., 2019; Pfau et al., 2018; DiCenzo et al., 2016; Yang et al., 2017; Resendis-Antonio et al., 2007). Recently, a whole-plant metabolic model of the symbiosis between *M. truncatula* and *Sinorhizobium meliloti* (rhizobial bacterium) was constructed, and included compartments for both the shoot and the root, along with five developmentally distinct zones of the root nodule (DiCenzo

et al., 2020). The model was used to identify the energetic costs associated with supporting bacterial nitrogenase flux, the use of ammonia as the main nitrogen export product from rhizobia, and the importance of proton transfers between the two species, illustrating the utility of whole-plant models for characterising source-sink interactions.

Another advantage of using FBA to model plant growth is that it is not driven solely by carbon, as is the case in many other growth models (Chew et al., 2014; Rasse and Tocquin, 2006). The unbiased treatment of all elemental resources means that the limitations imposed by multiple nutrients can be assessed. In this study, the effect of nitrogen limitation on optimal resource partitioning was explored. However, phosphorus limitation is also commonly reported to reduce plant primary productivity (Wang and Wu, 2013; Vitousek et al., 2010). Phosphorus is a constituent part of many important biological molecules (e.g. phospholipids, nucleic acids, ATP, and NAD(P)), and insufficient phosphorus supply hinders cell division and growth (Kavanová et al., 2006). Other nutrients that are essential to plant growth include potassium, calcium, sulphur, and magnesium, all of which are included in the model (Hawkesford and de Kok, 2006; Cakmak, 2005; White and Broadley, 2003; Shaul, 2002). Future model formulations should include biomass components containing these elements to study their limiting effects on growth.

7.3 Limitations of the modelling approach

Whilst many advantages are afforded by using FBA as a modelling approach, there are also some limitations to the method. Principally, FBA does not account for regulatory mechanisms or signalling pathways. Despite this limitation, FBA is consistently able to reproduce accurate flux predictions in a variety of biological contexts. Shameer et al. (2019) posited that the function of regulation at the enzymatic level is to maintain metabolic steady-state, a constraint of FBA. Thus, FBA

accounts for the outcome of regulation even if it does not include its mechanisms.

Biological systems are also assumed in FBA (and other modelling formulations) to have evolved towards a specific goal (the objective function) and for maximal efficiency (the parsimony constraint). For example, the biomass objective function assumes that plants have evolved to optimise resource usage for maximised growth. Whilst this approach has been used successfully in numerous studies, many cellular processes are not in agreement with this assumption, including futile cycles. From a stoichiometric perspective, futile cycles consume energy without contributing actively to growth or providing any net utility. However, experimental evidence suggests that many futile cycles nevertheless do exist and potentially play important regulatory roles, such as increasing the sensitivity of metabolic systems to subtle shifts in substrate concentrations (Nguyen-Quoc and Foyer, 2001; Geigenberger and Stitt, 1991).

Similarly, FBA's efficiency constraint also means that fluxes through energy dissipation mechanisms are unaccounted for by FBA. For example, climacteric is an important metabolic stage in fruit ripening in tomato, and is characterised by a respiratory burst. As it does not fulfil the efficiency requirement of FBA, WholePlantMetabolism cannot predict climacteric without additional constraints. Colombié et al. (2017) demonstrated that by imposing a transitory starch peak constraint during tomato fruit development in an FBA model, the resulting mobilisation of starch stores can produce a burst of respiration. Another extension of FBA, termed cost-weighted flux minimisation, has also been developed to predict non-optimal metabolic routes, including the use of parallel metabolic pathways in different organelles (Cheung et al., 2015). However, the method is computationally expensive and may not be suitable for use on large-scale networks at the whole-plant level.

Additionally, evolution does not necessarily produce optimal solutions, and

biological systems are often stuck in local optima. For example, RuBisCO's active site is promiscuous and has a relatively high affinity for oxygen, leading to respiratory carbon loss through photorespiration (Shih et al., 2016). RuBisCO is therefore often described as a frozen accident as the selection pressures that originally drove its evolution are now no longer present (atmospheric oxygen concentrations have risen). FBA formulations of leaf metabolism thus requires an explicit oxygenase constraint, as is required in the two modelling approaches presented in this work.

Owing to the steady-state constraint, FBA is insensitive to the direction of reversible reactions operating at near-equilibrium, which are often sensitive to the balance of substrate availability. Direct constraints on reaction direction based on experimental observations can be applied to the model, but the accurate measurement of metabolite concentrations in subcellular compartments under specific metabolic states remains difficult.

Lastly, many model constraints were assumed to be constant throughout growth. However, environmental conditions and the stage of plant life history can have significant effects on biological activity. For example, the composition of assimilates in the phloem has been reported to show spatial variations throughout the plant structure and also temporal variations over the developmental timescale, but the lack of a comprehensive dataset in tomato resulted in phloem transport being constrained using an unchanging composition in the model (Karley et al., 2002; Walker and Ho, 1977). Similarly, NGAM respiration rates increase significantly in response to higher temperatures, but are constrained to a fixed value in WholePlantMetabolism (Posch et al., 2019; Maier et al., 1998; Szaniawski and Kielkiewicz, 1982). The same issue applies to biomass composition constraints, the ratio of phloem export flux from source leaves over the diel cycle, and the ratio of nitrate import flux from the xylem into leaves over the diel cycle. Future experimental characterisations of metabolic activity in different growth conditions

will provide a valuable source of model constraints.

7.4 Future directions in whole-plant growth modelling

Accurate flux predictions by FBA require the specification of appropriate reaction constraints. Fortunately, many of these constraints are for external inputs or outputs of the metabolic network, making them relatively easy to measure experimentally (e.g. PPFD, nitrate availability, etc.). On the other hand, some flux constraints are for internal reactions and are more difficult to acquire. For example, the maximum RuBisCO carboxylase flux in WholePlantMetabolism is estimated using an empirical characterisation of leaf carbon assimilation rates in response to light availability in tomato (Nunes-Nesi et al., 2005). These constraints could instead be provided by more mechanistic models of photosynthesis, which take atmospheric carbon dioxide concentration and light availability as inputs (Zhu et al., 2013; Farquhar et al., 1980). Similarly, kinetic models of photosynthesis predict RuBisCO oxygenase flux using atmospheric carbon dioxide and oxygen concentrations as inputs and by accounting for intracellular diffusion pathways of the gases and their rates of utilization and production within the tissue. RuBisCO oxygenase flux, which is modelled using a flux ratio constraint between carboxylase and oxygenase fluxes based on experimental data in WholePlantMetabolism, can also be constrained using predictions by kinetic models. Futhermore, metabolic regulation is explicitly specified in kinetic rate equations, providing a solution to one of FBA's major limitations. However, this comes at the cost of an increased demand for experimentally determined parameter values and increased computational burden to solve non-linear ordinary differential equations.

Model integration at other biological scales should also be pursued. For example, root architecture is highly complex and exhibits intricate branching patterns. 3D

models of root growth can provide detailed predictions for root architecture, which in turn could be used to constrain the surface area available for nutrient uptake from the growth substrate (Leitner et al., 2010; Fang et al., 2009). Some root models can even simulate growth responses to the heterogeneous distribution of nutrients within soil (Postma et al., 2017). This would constitute an improvement on the nutrient uptake constraint in the current version of WholePlantMetabolism, which is based on root dry mass, and does not account for root architecture. Similar improvements can also be made for aboveground structures through integration with 3D models of shoot architecture, allowing for more accurate predictions of light interception (Braghiere et al., 2020; Gibbs et al., 2017; Christophe et al., 2008; Cournède et al., 2008; Yan et al., 2004).

As one of the ultimate goals of constructing multiscale growth models is to use their predictions to inform future efforts to improve crop yield, it may also be necessary to integrate models at the plot, field, regional, and even global scale (Peng et al., 2020). This may allow for a better assessment of the potential additive effects of genetic manipulations and adaptive crop management practices in changing environmental conditions. For example, a recent geospatial assesment of maize and soybean productivity using a simple model of plant physiology, soil quality, and climate revealed that certain phenotypes and agricultural practices can improve crop yield in some locations, but reduce yields in other sites (Sinclair et al., 2020).

Various technical difficulties may also present as obstacles to integrating models at different biological scales. For example, the coupling process between the FM and metabolic models highlighted the importance of true model modularity and the pitfalls of hard-coding model features (Chapter 3). Workarounds were required to ensure time step compatibility between the two models, as an hourly time step was hard-coded in the FM (Chew et al., 2014). The tight coupling between the CDM and the FSPM in FM also meant that the control of growth could not be entirely shifted

to the stoichiometric models, and continued to be quantified solely in terms of carbon. The ability to couple models in a *plug-and-play* manner will facilitate the construction of multiscale models, and allow for additional models to be integrated easily without the need for workarounds on an *ad hoc* basis. Recently, Lang (2019) developed a software package, named yggdrasil, for connecting models in different languages (C, C++, Python, and MATLAB) and scales (biological, temporal, and computational). The framework executes model simulations in parallel, and was designed with coupling flexibility, robust connections, and low latency in mind. Though yggdrasil has yet to be tested extensively, it can potentially allow future modellers to pick and choose the aspects of plant biology that they wish to assess together to provide a cross-scale perspective.

A major advantage of FBA is the low computational investment required to generate flux predictions. FBA optimisations are typically completed within milliseconds to seconds. However, WholePlantMetabolism uses various extensions of FBA that significantly increase the computational time required to simulate growth. For example, the dFBA approach necessitates the use of multiple optimisation steps over the growth period, and pFBA involves looping through the complete reaction list to apply flux minimisation constraints. The large size of the metabolic network at the whole-plant level also adds to the computational power required, though the use of a core metabolic model instead of a GSM alleviates this issue slightly. For example, WholePlantMetabolism v2 at the end of reproductive growth contains more than 25,000 reactions and 23,387 metabolites across 364 subcellular compartments. In comparison, a single tissue GSM of Arabidopsis only contains 2,769 reactions, 2,739 metabolites, and 6 subcellular compartments (Cheung et al., 2013). As a result, the computational time required to execute FBA optimisations was increased from seconds to hours, and even to weeks in the case of parameter scans across the solution space (Chapter 6). The use of high-performance

computing may be a viable solution to reduce simulation time, as an increasing number of academic institutions across the world have now established in-house supercomputing facilities. In contrast to serial processing used in conventional computing, high-performance computing uses parallel processing to divide large tasks into smaller discrete jobs, and executes them simultaneously on different cores on a multi-core processor. Large memory capacities and fast data transfer rates also contribute to high performance. It should be noted that individual simulations of WholePlantMetabolism cannot be divided into discrete jobs as the model optimisation process at each time step explicitly relies on the model solution from the previous time step (dFBA is serial in nature). However, simulations involving running the model multiple times (e.g. parameter scans across the solution space) are easily divisible. Manual code parallelisation may also significantly reduce computational time if supercomputing facilities are not available. The integration of FBA models with non-linear models (e.g. kinetic differential equation models) will necessitate the optimisation of coding efficiency and computational speed further, as non-linear problems are generally computationally expensive to solve.

7.5 Closing remarks

The full potential of multiscale whole-plant models in generating informative insights into plant growth still remains relatively unexplored. Through this work, I hope that I have made a convincing case for why future modellers should continue to pursue the development of new and better models. The world is currently facing environmental problems at an unprecedented scale. I truly hope that the explorations of source-sink interactions presented here may one day provide real world solutions to such pressing problems.

References

Abuqamar, S., Luo, H., Laluk, K., Mickelbart, M. V., and Mengiste, T. (2009). Crosstalk between biotic and abiotic stress responses in tomato is mediated by the *AIM1* transcription factor. *The Plant Journal*, 58(2):347–360.

Acock, B., Charles-Edwards, D. A., and Hand, D. W. (1976). An analysis of some effects of humidity on photosynthesis by a tomato canopy under winter light conditions and a range of carbon dioxide concentrations. *Journal of Experimental Botany*, 27(5):933–941.

Adams, S. R., Cockshull, K. E., and Cave, C. (2001). Effect of temperature on the growth and development of tomato fruits. *Annals of Botany*, 88(5):869–877.

Adolfsen, K. J. and Brynildsen, M. P. (2015). Futile cycling increases sensitivity toward oxidative stress in *Escherichia coli*. *Metabolic Engineering*, 29:26–35.

Ainsworth, E. A., Leakey, A. D., Ort, D. R., and Long, S. P. (2008). FACE-ing the facts: inconsistencies and interdependence among field, chamber and modeling studies of elevated [CO_2] impacts on crop yield and food supply. *New Phytologist*, 179(1):5–9.

Ainsworth, E. A. and Long, S. P. (2005). What have we learned from 15 years of free-air CO_2 enrichment (FACE)? A meta-analytic review of the responses of photosynthesis, canopy properties and plant production to rising CO_2. *New Phytologist*, 165(2):351–372.

Ainsworth, E. A., Rogers, A., Vodkin, L. O., Walter, A., and Schurr, U. (2006). The effects of elevated CO_2 concentration on soybean gene expression. An analysis of growing and mature leaves. *Plant Physiology*, 142(1):135–147.

Albornoz, F., Gebauer, M., Ponce, C., Cabeza, R., Albornoz, F., Gebauer, M., Ponce, C., and Cabeza, R. A. (2018). LeNRT1.1 Improves nitrate uptake in grafted tomato plants under high nitrogen demand. *International Journal of Molecular Sciences*, 19(12):3921.

Alexander, L. and Grierson, D. (2002). Ethylene biosynthesis and action in tomato: a model for climacteric fruit ripening. *Journal of Experimental Botany*, 53(377):2039–2055.

Alexandratos, N. and Bruinsma, J. (2012). *World Agriculture Towards 2030/50. The 2012 Revision*. FAO Document Repository.

Alotaibi, S. S., Sparks, C. A., Parry, M. A., Simkin, A. J., and Raines, C. A. (2018). Identification of leaf promoters for use in transgenic wheat. *Plants*, 7(2):27.

Alper, H., Jin, Y. S., Moxley, J. F., and Stephanopoulos, G. (2005). Identifying gene targets for the metabolic engineering of lycopene biosynthesis in *Escherichia coli*. *Metabolic Engineering*, 7(3):155–164.

Amthor, J. S. (2000). The McCree-de Wit-Penning de Vries-Thornley respiration paradigms: 30 years later. *Annals of Botany*, 86(1):1–20.

Amthor, J. S., Bar-Even, A., Hanson, A. D., Millar, A. H., Stitt, M., Sweetlove, L. J., and Tyerman, S. D. (2019). Engineering strategies to boost crop productivity by cutting respiratory carbon loss. *Plant Cell*, 31(2):297–314.

Andrews, M. (1986). The partitioning of nitrate assimilation between root and shoot of higher plants. *Plant, Cell & Environment*, 9(7):511–519.

Andrews, M., Raven, J. A., and Lea, P. J. (2013). Do plants need nitrate? The mechanisms by which nitrogen form affects plants. *Annals of Applied Biology*, 163(2):174–199.

Angelovici, R., Lipka, A. E., Deason, N., Gonzalez-Jorge, S., Lin, H., Cepela, J., Buell, R., Gore, M. A., and della Penna, D. (2013). Genome-wide analysis of branched-chain amino acid levels in Arabidopsis Seeds. *Plant Cell*, 25(12):4827–4843.

Anoman, A. D., Muñoz-Bertomeu, J., Rosa-Téllez, S., Flores-Tornero, M., Serrano, R., Bueso, E., Fernie, A. R., Segura, J., and Ros, R. (2015). Plastidial glycolytic glyceraldehyde-3-phosphate dehydrogenase is an important determinant in the carbon and nitrogen metabolism of heterotrophic cells in Arabidopsis. *Plant Physiology*, 169(3):1619–1637.

Aranjuelo, I., Sanz-Sáez, Á., Jáuregui, I., Irigoyen, J. J., Araus, J. L., Sánchez-Díaz, M., and Erice, G. (2013). Harvest index, a parameter conditioning responsiveness of wheat plants to elevated CO_2. *Journal of Experimental Botany*, 64(7):1879–1892.

Araújo, W. L., Tohge, T., Ishizaki, K., Leaver, C. J., and Fernie, A. R. (2011). Protein degradation — an alternative respiratory substrate for stressed plants. *Trends in Plant Science*, 16(9):489–498.

Arnold, A. and Nikoloski, Z. (2014). Bottom-up metabolic reconstruction of Arabidopsis and its application to determining the metabolic costs of enzyme production. *Plant Physiology*, 165(3):1380–1391.

Asao, S. and Ryan, M. G. (2015). Carbohydrate regulation of photosynthesis and respiration from branch girdling in four species of wet tropical rain forest trees. *Tree Physiology*, 35(6):608–620.

Baghalian, K., Hajirezaei, M. R., and Schreiber, F. (2014). Plant metabolic modeling: achieving new insight into metabolism and metabolic engineering. *Plant Cell*, 26(10):3847–3866.

Bakshi, A., Moin, M., Madhav, M. S., and Kirti, P. B. (2019). Target of rapamycin, a master regulator of multiple signalling pathways and a potential candidate gene for crop improvement. *Plant Biology*, 21(2):190–205.

Ballicora, M. A., Iglesias, A. A., and Preiss, J. (2004). ADP-glucose pyrophosphorylase: a regulatory enzyme for plant starch synthesis. *Photosynthesis Research*, 79(1):1–24.

Balotf, S., Kavoosi, G., and Kholdebarin, B. (2016). Nitrate reductase, nitrite reductase, glutamine synthetase, and glutamate synthase expression and activity in response to different nitrogen sources in nitrogen-starved wheat seedlings. *Biotechnology and Applied Biochemistry*, 63(2):220–229.

Band, L. R. and Bennett, M. J. (2013). Mapping the site of action of the Green Revolution hormone gibberellin. *Proceedings of the National Academy of Sciences of the United States of America*, 110(12):4443–4444.

Bar-Even, A., Noor, E., Lewis, N. E., and Milo, R. (2010). Design and analysis of synthetic carbon fixation pathways. *Proceedings of the National Academy of Sciences of the United States of America*, 107(19):8889–8894.

Baroja-Fernández, E., Muñoz, F. J., Montero, M., Etxeberria, E., Sesma, M. T., Ovecka, M., Bahaji, A., Ezquer, I., Li, J., Prat, S., and Pozueta-Romero, J. (2009). Enhancing sucrose synthase activity in transgenic potato (*Solanum tuberosum* L.) tubers results in increased levels of starch, ADPglucose and UDPglucose and total yield. *Plant & cell physiology*, 50(9):1651–1662.

Bausenwein, U., Millard, P., Thornton, B., and Raven, J. A. (2001). Seasonal nitrogen storage and remobilization in the forb *Rumex acetosa*. *Functional Ecology*, 15(3):370–377.

Bénard, C., Bernillon, S., Biais, B., Osorio, S., Maucourt, M., Ballias, P., Deborde, C., Colombié, S., Cabasson, C., Jacob, D., Vercambre, G., Gautier, H., Rolin, D., Génard, M., Fernie, A. R., Gibon, Y., and Moing, A. (2015). Metabolomic profiling in tomato reveals diel compositional changes in fruit affected by source-sink relationships. *Journal of Experimental Botany*, 66(11):3391–3404.

Bénard, C., Gautier, H., Bourgaud, F., Grasselly, D., Navez, B., Caris-Veyrat, C., Weiss, M., and Génard, M. (2009). Effects of low nitrogen supply on tomato (*Solanum lycopersicum*) fruit yield and quality with special emphasis on sugars, acids, ascorbate, carotenoids, and phenolic compounds. *Journal of Agricultural and Food Chemistry*, 57(10):4112–4123.

Benes, B., Guan, K., Lang, M., Long, S. P., Lynch, J. P., Marshall-Colón, A., Peng, B., Schnable, J., Sweetlove, L. J., and Turk, M. J. (2020). Multiscale computational models can guide experimentation and targeted measurements for crop improvement. *The Plant Journal*, 103(1):21–31.

Bermúdez, L., de Godoy, F., Baldet, P., Demarco, D., Osorio, S., Quadrana, L., Almeida, J., Asis, R., Gibon, Y., Fernie, A. R., Rossi, M., and Carrari, F. (2014). Silencing of the tomato Sugar Partitioning Affecting protein (SPA) modifies sink strength through a shift in leaf sugar metabolism. *The Plant Journal*, 77(5):676–687.

Bernacchi, C. J., Bagley, J. E., Serbin, S. P., Ruiz-Vera, U. M., Rosenthal, D. M., and Vanloocke, A. (2013). Modelling C_3 photosynthesis from the chloroplast to the ecosystem. *Plant, Cell & Environment*, 36(9):1641–1657.

Biais, B., Benard, C., Beauvoit, B., Colombie, S., Prodhomme, D., Menard, G., Bernillon, S., Gehl, B., Gautier, H., Ballias, P., Mazat, J.-P., Sweetlove, L., Genard, M., and Gibon, Y. (2014). Remarkable reproducibility of enzyme activity profiles in tomato fruits grown

under contrasting environments provides a roadmap for studies of fruit metabolism. *Plant Physiology*, 164(3):1204–1221.

Bialczyk, J. and Lechowski, Z. (1995). Chemical composition of xylem sap of tomato grown on bicarbonate containing medium. *Journal of Plant Nutrition*, 18(10):2005–2021.

Bijlsma, R. J. and Lambers, H. (2000). A dynamic whole-plant model of integrated metabolism of nitrogen and carbon. 2. Balanced growth driven by C fluxes and regulated by signals from C and N substrate. *Plant and Soil*, 220:71–87.

Binder, S. (2010). Branched-chain amino acid metabolism in *Arabidopsis thaliana*. *The Arabidopsis Book*, 8.

Binder, S., Knill, T., and Schuster, J. (2007). Branched-chain amino acid metabolism in higher plants. *Physiologia Plantarum*, 129(1):68–78.

Bogart, E. and Myers, C. R. (2016). Multiscale metabolic modeling of C_4 plants: connecting nonlinear genome-scale models to leaf-scale metabolism in developing maize leaves. *PLoS ONE*, 11(3):e0151722.

Braghiere, R. K., Gérard, F., Evers, J. B., Pradal, C., and Pagès, L. (2020). Simulating the effects of water limitation on plant biomass using a 3D functional-structural plant model of shoot and root driven by soil hydraulics. *Annals of Botany*, 126(4):713–728.

Brauc, S., de Vooght, E., Claeys, M., Geuns, J. M., Höfte, M., and Angenon, G. (2012). Overexpression of arginase in *Arabidopsis thaliana* influences defence responses against *Botrytis cinerea*. *Plant Biology*, 14:39–45.

Braun, D. M. and Slewinski, T. L. (2009). Genetic control of carbon partitioning in grasses: roles of sucrose transporters and tie-dyed loci in phloem loading. *Plant Physiology*, 149(1):71–81.

Braun, D. M., Wang, L., and Ruan, Y. L. (2014). Understanding and manipulating sucrose phloem loading, unloading, metabolism, and signalling to enhance crop yield and food security. *Journal of Experimental Botany*, 65(7):1713–1735.

Brauner, K., Birami, B., Brauner, H. A., and Heyer, A. G. (2018). Diurnal periodicity of assimilate transport shapes resource allocation and whole-plant carbon balance. *The Plant Journal*, 94(5):776–789.

Breeze, E., Harrison, E., McHattie, S., Hughes, L., Hickman, R., Hill, C., Kiddle, S., Kim, Y. S., Penfold, C. A., Jenkins, D., Zhang, C., Morris, K., Jenner, C., Jackson, S., Thomas, B., Tabrett, A., Legaie, R., Moore, J. D., Wild, D. L., Ott, S., Rand, D., Beynon, J., Denby, K., Mead, A., and Buchanan-Wollaston, V. (2011). High-resolution temporal profiling of transcripts during Arabidopsis leaf senescence reveals a distinct chronology of processes and regulation. *Plant Cell*, 23(3):873–894.

Brewitz, E., Larsson, C.-M., and Larsson, M. (1996). Responses of nitrate assimilation and N translocation in tomato (*Lycopersicon esculentum* Mill) to reduced ambient air humidity. *Journal of Experimental Botany*, 47(7):855–861.

Brooks, P. J. and Schuebel, K. (2017). Timeless insights into prevention of acetaldehyde genotoxicity? *Cell Cycle*, 16(4):308–309.

Brown, H. E., Huth, N. I., Holzworth, D. P., Teixeira, E. I., Wang, E., Zyskowski, R. F., and Zheng, B. (2019). A generic approach to modelling, allocation and redistribution of biomass to and from plant organs. *in silico Plants*, 1(1):diy004.

Brown, H. E., Jamieson, P. D., Brooking, I. R., Moot, D. J., and Huth, N. I. (2013). Integration of molecular and physiological models to explain time of anthesis in wheat. *Annals of Botany*, 112(9):1683–1703.

Burgard, A. P., Pharkya, P., and Maranas, C. D. (2003). OptKnock: a bilevel programming framework for identifying gene knockout strategies for microbial strain optimization. *Biotechnology and Bioengineering*, 84(6):647–657.

Cairns, A. J. and Gallagher, J. A. (2004). Absence of turnover and futile cycling of sucrose in leaves of *Lolium temulentum* L.: implications for metabolic compartmentation. *Planta*, 219(5):836–846.

Cakmak, I. (2005). The role of potassium in alleviating detrimental effects of abiotic stresses in plants. *Journal of Plant Nutrition and Soil Science*, 168(4):521–530.

Caldararu, S., Thum, T., Yu, L., and Zaehle, S. (2020). Whole-plant optimality predicts changes in leaf nitrogen under variable CO_2 and nutrient availability. *New Phytologist*, 225(6):2331–2346.

Cannell, M. G. and Thornley, J. H. (2000). Modelling the components of plant respiration: some guiding principles. *Annals of Botany*, 85(1):45–54.

Carrara, S., Pardossi, A., Soldatini, G. F., Tognoni, F., and Guidi, L. (2001). Photosynthetic activity of ripening tomato fruit. *Photosynthetica*, 39(1):75–78.

Carrari, F. and Fernie, A. R. (2006). Metabolic regulation underlying tomato fruit development. *Journal of Experimental Botany*, 57(9):1883–1897.

Cautha, S. C., Gowen, C. M., Lussier, F. X., Gold, N. D., Martin, V. J., and Mahadevan, R. (2013). Model-driven design of a *Saccharomyces cerevisiae* platform strain with improved tyrosine production capabilities. *12th IFAC Symposium on Computer Applications in Biotechnology*, 46(31):221–226.

Chang, Q., Liu, J., Lin, X., Hu, S., Yang, Y., Li, D., Chen, L., Huai, B., Huang, L., Voegele, R. T., and Kang, Z. (2017). A unique invertase is important for sugar absorption of an obligate biotrophic pathogen during infection. *New Phytologist*, 215(4):1548–1561.

Chang, T. G. and Zhu, X.-G. (2017). Source-sink interaction: a century old concept under the light of modern molecular systems biology. *Journal of experimental botany*, 68(16):4417–4431.

Chen, B. M., Wang, Z. H., Li, S. X., Wang, G. X., Song, H. X., and Wang, X. N. (2004). Effects of nitrate supply on plant growth, nitrate accumulation, metabolic nitrate concentration and nitrate reductase activity in three leafy vegetables. *Plant Science*, 167(3):635–643.

Chen, H. J. and Wang, S. J. (2008). Molecular regulation of sink-source transition in rice leaf sheaths during the heading period. *Acta Physiologiae Plantarum*, 30(5):639–649.

Chen, J. and Henson, M. A. (2016). *In silico* metabolic engineering of *Clostridium ljungdahlii* for synthesis gas fermentation. *Metabolic Engineering*, 38:389–400.

Chen, X., Yao, Q., Gao, X., Jiang, C., Harberd, N. P., and Fu, X. (2016). Shoot-to-root mobile transcription factor HY5 coordinates plant carbon and nitrogen acquisition. *Current Biology*, 26(5):640–646.

Cheplick, G. P. (2005). The Allometry of Reproductive Allocation. In *Reproductive Allocation in Plants*, pages 97–128. Elsevier.

Cheung, C. M., Ratcliffe, R. G., and Sweetlove, L. J. (2015). A method of accounting for enzyme costs in flux balance analysis reveals alternative pathways and metabolite stores in an illuminated Arabidopsis leaf. *Plant Physiology*, 169(3):1671–1682.

Cheung, C. Y. M., Poolman, M. G., Fell, D. A., Ratcliffe, R. G., and Sweetlove, L. J. (2014). A diel flux balance model captures interactions between light and dark metabolism during day-night cycles in C_3 and Crassulacean acid metabolism leaves. *Plant Physiology*, 165(2):917–929.

Cheung, C. Y. M., Williams, T. C., Poolman, M. G., Fell, D. A., Ratcliffe, R. G., and Sweetlove, L. J. (2013). A method for accounting for maintenance costs in flux balance analysis improves the prediction of plant cell metabolic phenotypes under stress conditions. *The Plant Journal*, 75(6):1050–1061.

Chew, Y. H., Seaton, D. D., Mengin, V., Flis, A., Mugford, S. T., Smith, A. M., Stitt, M., and Millar, A. J. (2017a). Linking circadian time to growth rate quantitatively via carbon metabolism. *bioRxiv*, page 105437.

Chew, Y. H., Seaton, D. D., and Millar, A. J. (2017b). Multi-scale modelling to synergise plant systems biology and crop science. *Field Crops Research*, 202:77–83.

Chew, Y. H., Wenden, B., Flis, A., Mengin, V., Taylor, J., Davey, C. L., Tindal, C., Thomas, H., Ougham, H. J., de Reffye, P., Stitt, M., Williams, M., Muetzelfeldt, R., Halliday, K. J., and Millar, A. J. (2014). Multiscale digital *Arabidopsis* predicts individual organ and whole-organism growth. *Proceedings of the National Academy of Sciences of the United States of America*, 111(39):E4127–E4136.

Chew, Y. H., Wilczek, A. M., Williams, M., Welch, S. M., Schmitt, J., and Halliday, K. J. (2012). An augmented Arabidopsis phenology model reveals seasonal temperature control of flowering time. *New Phytologist*, 194(3):654–665.

Chiewchankaset, P., Siriwat, W., Suksangpanomrung, M., Boonseng, O., Meechai, A., Tanticharoen, M., Kalapanulak, S., and Saithong, T. (2019). Understanding carbon utilization routes between high and low starch-producing cultivars of cassava through flux balance analysis. *Scientific Reports*, 9(1):1–15.

Choon, Y. W., Mohamad, M. S., Deris, S., Illias, R. M., Chong, C. K., Chai, L. E., Omatu, S., and Corchado, J. M. (2014). Differential bees flux balance analysis with OptKnock for *in silico* microbial strains optimization. *PLoS ONE*, 9(7):e102744.

Christophe, A., Letort, V., Hummel, I., Cournède, P. H., de Reffye, P., and Lecœur, J. (2008). A model-based analysis of the dynamics of carbon balance at the whole-plant level in *Arabidopsis thaliana*. *Functional Plant Biology*, 35(11):1147–1162.

Cleland, E. E., Chuine, I., Menzel, A., Mooney, H. A., and Schwartz, M. D. (2007). Shifting plant phenology in response to global change. *Trends in Ecology and Evolution*, 22(7):357–365.

Colombié, S., Beauvoit, B., Nazaret, C., Bénard, C., Vercambre, G., Le Gall, S., Biais, B., Cabasson, C., Maucourt, M., Bernillon, S., Moing, A., Dieuaide-Noubhani, M., Mazat, J. P., and Gibon, Y. (2017). Respiration climacteric in tomato fruits elucidated by constraint-based modelling. *New Phytologist*, 213(4):1726–1739.

Colombié, S., Nazaret, C., Bénard, C., Biais, B., Mengin, V., Solé, M., Fouillen, L., Dieuaide-Noubhani, M., Mazat, J. P., Beauvoit, B., and Gibon, Y. (2015). Modelling central metabolic fluxes by constraint-based optimization reveals metabolic reprogramming of developing *Solanum lycopersicum* (tomato) fruit. *The Plant Journal*, 81(1):24–39.

Comadran, J., Kilian, B., Russell, J., Ramsay, L., Stein, N., Ganal, M., Shaw, P., Bayer, M., Thomas, W., Marshall, D., Hedley, P., Tondelli, A., Pecchioni, N., Francia, E., Korzun, V., Walther, A., and Waugh, R. (2012). Natural variation in a homolog of *Antirrhinum CENTRORADIALIS* contributed to spring growth habit and environmental adaptation in cultivated barley. *Nature Genetics*, 44(12):1388–1391.

Cortleven, A. and Schmülling, T. (2015). Regulation of chloroplast development and function by cytokinin. *Journal of Experimental Botany*, 66(16):4999–5013.

Cournède, P. H., Mathieu, A., Houllier, F., Barthélémy, D., and de Reffye, P. (2008). Computing competition for light in the GREENLAB model of plant growth: a contribution to the study of the effects of density on resource acquisition and architectural development. *Annals of Botany*, 101(8):1207–1219.

Crous, K. Y. and Ellsworth, D. S. (2004). Canopy position affects photosynthetic adjustments to long-term elevated CO_2 concentration (FACE) in aging needles in a mature *Pinus taeda* forest. *Tree Physiology*, 24(9):961–970.

Cuartero, J. and Fernández-Muñoz, R. (1998). Tomato and salinity. *Scientia Horticulturae*, 78(1-4):83–125.

Dai, Y., Dickinson, R. E., and Wang, Y. P. (2004). A two-big-leaf model for canopy temperature, photosynthesis, and stomatal conductance. *Journal of Climate*, 17(12):2281–2299.

Däschner, K., Couée, I., and Binder, S. (2001). The mitochondrial isovaleryl-coenzyme a dehydrogenase of Arabidopsis oxidizes intermediates of leucine and valine catabolism. *Plant Physiology*, 126(2):601–612.

de Oliveira Dal'Molin, C. G., Quek, L.-E., Palfreyman, R. W., Brumbley, S. M., and Nielsen, L. K. (2010a). AraGEM, a genome-Scale reconstruction of the primary metabolic network in Arabidopsis. *Plant Physiology*, 152(2):579–589.

de Oliveira Dal'Molin, C. G., Quek, L. E., Palfreyman, R. W., Brumbley, S. M., and Nielsen, L. K. (2010b). C4GEM, a genome-scale metabolic model to study C_4 plant metabolism. *Plant Physiology*, 154(4):1871–1885.

de Oliveira Dal'Molin, C. G., Quek, L.-E., Saa, P. A., and Nielsen, L. K. (2015). A multi-tissue genome-scale metabolic modeling framework for the analysis of whole plant systems. *Frontiers in Plant Science*, 6(4):1–12.

de Oliveira Pereira, M., Lyra, G. B., Lyra, G. B., Batista, L. D., de Souza, J. L., Pereira, C. R., and Jorge, M. F. (2019). Extinction coefficient and interception efficiency of the photosynthetic photon flux density in cherry tomato under levels of nitrogen in greenhouse conditions. *Australian Journal of Crop Science*, 13(11):1749–1755.

de Pury, D. G. G. and Farquhar, G. D. (1997). Simple scaling of photosynthesis from leaves to canopies without the errors of big-leaf models. *Plant, Cell & Environment*, 20(5):537–557.

de Schepper, V., de Swaef, T., Bauweraerts, I., and Steppe, K. (2013). Phloem transport: a review of mechanisms and controls. *Journal of Experimental Botany*, 64(16):4839–4850.

Delhon, P., Gojon, A., Tillard, P., and Passama, L. (1995). Diurnal regulation of NO_3^- uptake in soybean plants I. Changes in NO_3^- influx, efflux, and N utilization in the plant during the day/night cycle. *Journal of Experimental Botany*, 46(10):1585–1594.

Delucia, E. H., Sasek, T. W., and Strain, B. R. (1985). Photosynthetic inhibition after long-term exposure to elevated levels of atmospheric carbon dioxide. *Photosynthesis Research*, 7(2):175–184.

DiCenzo, G. C., Checcucci, A., Bazzicalupo, M., Mengoni, A., Viti, C., Dziewit, L., Finan, T. M., Galardini, M., and Fondi, M. (2016). Metabolic modelling reveals the specialization of secondary replicons for niche adaptation in *Sinorhizobium meliloti*. *Nature Communications*, 7(1):1–10.

DiCenzo, G. C., Tesi, M., Pfau, T., Mengoni, A., and Fondi, M. (2020). Genome-scale metabolic reconstruction of the symbiosis between a leguminous plant and a nitrogen-fixing bacterium. *Nature Communications*, 11(1):1–11.

Dong, Q., Louarn, G., Wang, Y., Barczi, J. F., and de Reffye, P. (2008). Does the structure-function model GREENLAB deal with crop phenotypic plasticity induced by plant spacing? A case study on tomato. *Annals of Botany*, 101(8):1195–1206.

Driever, S. M., Simkin, A. J., Alotaibi, S., Fisk, S. J., Madgwick, P. J., Sparks, C. A., Jones, H. D., Lawson, T., Parry, M. A., and Raines, C. A. (2017). Increased SBPase activity improves photosynthesis and grain yield in wheat grown in greenhouse conditions. *Philosophical Transactions of the Royal Society B: Biological Sciences*, 372(1730):20160384.

Ebrahim, A., Lerman, J. A., Palsson, B. O., and Hyduke, D. R. (2013). COBRApy: COnstraints-Based Reconstruction and Analysis for Python. *BMC Systems Biology*, 7(1):74.

El-Mezawy, A., Wu, L., and Shah, S. (2009). A seed coat-specific promoter for canola. *Biotechnology Letters*, 31(12):1961–1965.

Enquist, B. J. and Niklas, K. J. (2002). Global allocation rules for patterns of biomass partitioning. *Science*, 295(5559):1517–1520.

Eshed, Y. and Zamir, D. (1995). An introgression line population of *Lycopersicon pennellii* in the cultivated tomato enables the identification and fine mapping of yield-associated QTL. *Genetics*, 141(3):1147–1162.

Eyles, A., Pinkard, E. A., Davies, N. W., Corkrey, R., Churchill, K., O'Grady, A. P., Sands, P., and Mohammed, C. (2013). Whole-plant versus leaf-level regulation of photosynthetic responses after partial defoliation in *Eucalyptus globulus* saplings. *Journal of Experimental Botany*, 64(6):1625–1636.

Fang, S., Yan, X., and Liao, H. (2009). 3D reconstruction and dynamic modeling of root architecture in situ and its application to crop phosphorus research. *The Plant Journal*, 60(6):1096–1108.

Fangmeier, A., Chrost, B., Högy, P., and Krupinska, K. (2000). CO_2 enrichment enhances flag leaf senescence in barley due to greater grain nitrogen sink capacity. *Environmental and Experimental Botany*, 44(2):151–164.

FAO (1997). *FAOSTAT Statistical Database*. FAO.

Farineau, J. and Laval-Martin, D. (1977). Light versus dark carbon metabolism in cherry tomato fruits. *Plant Physiology*, 60(6):877–880.

Farquhar, G. D., von Caemmerer, S., and Berry, J. A. (1980). A biochemical model of photosynthetic CO_2 assimilation in leaves of C_3 species. *Planta*, 149(1):78–90.

Feller, C., Favre, P., Janka, A., Zeeman, S. C., Gabriel, J. P., and Reinhardt, D. (2015). Mathematical modeling of the dynamics of shoot-root interactions and resource partitioning in plant growth. *PLoS ONE*, 10(7):e0127905.

Fernie, A. R., Bachem, C. W., Helariutta, Y., Neuhaus, H. E., Prat, S., Ruan, Y. L., Stitt, M., Sweetlove, L. J., Tegeder, M., Wahl, V., Sonnewald, S., and Sonnewald, U. (2020). Synchronization of developmental, molecular and metabolic aspects of source-sink interactions. *Nature Plants*, 6:55–66.

Fleet, C. M. and Sun, T. P. (2005). A DELLAcate balance: the role of gibberellin in plant morphogenesis. *Current Opinion in Plant Biology*, 8(1):77–85.

Fleisher, D. H., Shillito, R. M., Timlin, D. J., Kim, S. H., and Reddy, V. R. (2006). Approaches to modeling potato leaf appearance rate. *Agronomy Journal*, 98(3):522–528.

Flores, P., Botella, M. Á., Cerdá, A., and Martínez, V. (2004). Influence of nitrate level on nitrate assimilation in tomato (*Lycopersicon esculentum*) plants under saline stress. *Canadian Journal of Botany*, 82(2):207–213.

Frantz, J. M. and Bugbee, B. (2005). Acclimation of plant populations to shade: photosynthesis, respiration, and carbon use efficiency. *Journal of the American Society for Horticultural Science*, 130(6):918–927.

Friend, A. D. (2001). Modelling canopy CO_2 fluxes: are 'big-leaf' simplifications justified? *Global Ecology and Biogeography*, 10(6):603–619.

Friend, A. D., Stevens, A. K., Knox, R. G., and Cannell, M. G. (1997). A process-based, terrestrial biosphere model of ecosystem dynamics (Hybrid v3.0). *Ecological Modelling*, 95(2-3):249–287.

Frusciante, L., Carli, P., Ercolano, M. R., Pernice, R., Di Matteo, A., Fogliano, V., and Pellegrini, N. (2007). Antioxidant nutritional quality of tomato. *Molecular Nutrition and Food Research*, 51(5):609–617.

Fu, Y., Yi, H., Bao, J., and Gong, J. (2015). LeNRT2.3 functions in nitrate acquisition and long-distance transport in tomato. *FEBS Letters*, 589(10):1072–1079.

Fukushima, A., Hikosaka, S., Kobayashi, M., Nishizawa, T., Saito, K., Goto, E., and Kusano, M. (2018). A systems analysis with 'simplified source-sink model' reveals metabolic reprogramming in a pair of source-to-sink organs during early fruit development in tomato by led light treatments. *Frontiers in Plant Science*, 9(1439):1–17.

Gardeström, P. and Igamberdiev, A. U. (2016). The origin of cytosolic ATP in photosynthetic cells. *Physiologia plantarum*, 157(3):367–379.

Gauthier, P. P., Bligny, R., Gout, E., Mahé, A., Nogués, S., Hodges, M., and Tcherkez, G. G. (2010). In folio isotopic tracing demonstrates that nitrogen assimilation into glutamate is mostly independent from current CO_2 assimilation in illuminated leaves of *Brassica napus*. *New Phytologist*, 185(4):988–999.

Gaxiola, R. A., Palmgren, M. G., and Schumacher, K. (2007). Plant proton pumps. *FEBS Letters*, 581(12):2204–2214.

Geigenberger, P., Regierer, B., Nunes-Nesi, A., Leisse, A., Urbanczyk-Wochniak, E., Springer, F., van Dongen, J. T., Kossmann, J., and Fernie, A. R. (2005). Inhibition of de novo pyrimidine synthesis in growing potato tubers leads to a compensatory stimulation of the pyrimidine salvage pathway and a subsequent increase in biosynthetic performance. *Plant Cell*, 17(7):2077–2088.

Geigenberger, P. and Stitt, M. (1991). A 'futile' cycle of sucrose synthesis and degradation is involved in regulating partitioning between sucrose, starch and respiration in cotyledons of germinating *Ricinus communis* L. seedlings when phloem transport is inhibited. *Planta*, 185(1):81–90.

Gessler, A., Tcherkez, G., Peuke, A. D., Ghashghaie, J., and Farquhar, G. D. (2008). Experimental evidence for diel variations of the carbon isotope composition in leaf, stem and phloem sap organic matter in *Ricinus communis*. *Plant, Cell & Environment*, 31(7):941–953.

Ghanem, M. E., Albacete, A., Smigocki, A. C., Frébort, I., Pospíilová, H., Martínez-Andújar, C., Acosta, M., Sánchez-Bravo, J., Lutts, S., Dodd, I. C., and Pérez-Alfocea, F. (2011). Root-synthesized cytokinins improve shoot growth and fruit yield in salinized tomato (*Solanum lycopersicum* L.) plants. *Journal of Experimental Botany*, 62(1):125–140.

Gianfagna, T. J., Logendra, L., Durner, E. F., and Janes, H. W. (1998). Improving tomato harvest index by controlling crop height and side shoot production. *Life Support & Biosphere Science : International Journal of Earth Space*, 5(2):255–261.

Gibbs, J. A., Pound, M., French, A. P., Wells, D. M., Murchie, E., and Pridmore, T. (2017). Approaches to three-dimensional reconstruction of plant shoot topology and geometry. *Functional Plant Biology*, 44(1):62–75.

Gibeaut, D. M., Cramer, G. R., and Seemann, J. R. (2001). Growth, cell walls, and UDP-glucose dehydrogenase activity of *Arabidopsis thaliana* grown in elevated carbon dioxide. *Journal of Plant Physiology*, 158(5):569–576.

Gibon, Y., Bläsing, O. E., Palacios-Rojas, N., Pankovic, D., Hendriks, J. H., Fisahn, J., Höhne, M., Günther, M., and Stitt, M. (2004). Adjustment of diurnal starch turnover to short days: depletion of sugar during the night leads to a temporary inhibition of carbohydrate utilization, accumulation of sugars and post-translational activation of ADP-glucose pyrophosphorylase in the following light period. *The Plant Journal*, 39(6):847–862.

Gibon, Y., Pyl, E. T., Sulpice, R., Lunn, J. E., Höhne, M., Günther, M., and Stitt, M. (2009). Adjustment of growth, starch turnover, protein content and central metabolism to a decrease of the carbon supply when *Arabidopsis* is grown in very short photoperiods. *Plant, Cell & Environment*, 32(7):859–874.

Gilliham, M. and Tester, M. (2005). The regulation of anion loading to the maize root xylem. *Plant Physiology*, 137(3):819–828.

Girousse, C., Bournoville, R., and Bonnemain, J. L. (1996). Water deficit-induced changes in concentrations in proline and some other amino acids in the phloem sap of alfalfa. *Plant Physiology*, 111(1):109–113.

Glanz-Idan, N. and Wolf, S. (2020). Upregulation of photosynthesis in mineral nutrition-deficient tomato plants by reduced source-to-sink ratio. *Plant Signaling and Behavior*, 15(2).

Glass, A. D., Britto, D. T., Kaiser, B. N., Kinghorn, J. R., Kronzucker, H. J., Kumar, A., Okamoto, M., Rawat, S., Siddiqi, M. Y., Unkles, S. E., and Vidmar, J. J. (2002). The regulation of nitrate and ammonium transport systems in plants. *Journal of Experimental Botany*, 53(370):855–864.

Gong, H. Y., Li, Y., Fang, G., Hu, D. H., Jin, W. B., Wang, Z. H., and Li, Y. S. (2015). Transgenic rice expressing *Ictb* and *FBP*/*Sbpase* derived from cyanobacteria exhibits enhanced photosynthesis and mesophyll conductance to CO_2. *PLoS ONE*, 10(10):e0140928.

Grafahrend-Belau, E., Junker, A., Eschenroder, A., Muller, J., Schreiber, F., and Junker, B. H. (2013). Multiscale metabolic modeling: dynamic flux balance analysis on a whole-plant scale. *Plant Physiology*, 163(2):637–647.

Grafahrend-Belau, E., Schreiber, F., Koschutzki, D., and Junker, B. H. (2009). Flux balance analysis of barley seeds: a computational approach to study systemic properties of central metabolism. *Plant Physiology*, 149(1):585–598.

Granier, C., Massonnet, C., Turc, O., Muller, B., Chenu, K., and Tardieu, F. (2002). Individual leaf development in *Arabidopsis thaliana*: a stable thermal-time-based programme. *Annals of Botany*, 89(5):595–604.

Grünzweig, J. M., Katan, J., Ben-Tal, Y., and Rabinowitch, H. D. (1998). The role of mineral nutrients in the increased growth response of tomato plants in solarized soil. *Plant and Soil*, 206(1):21–27.

Güçlü, J., Paulin, A., and Soudain, P. (1989). Changes in polar lipids during ripening and senescence of cherry tomato (*Lycopersicon esculentum*): relation to climacteric and ethylene increases. *Physiologia Plantarum*, 77(3):413–419.

Guilbaud, C. S., Dalchau, N., Purves, D. W., and Turnbull, L. A. (2015). Is 'peak N' key to understanding the timing of flowering in annual plants? *New Phytologist*, 205(2):918–927.

Guo, H., Chen, X., Zhang, H., Fang, R., Yuan, Z., Zhang, Z., and Tian, Y. (2004). Characterization and activity enhancement of the phloem-specific pumpkin *PP2* gene promoter. *Transgenic Research*, 13(6):559–566.

Guo, W., Chen, L., Herrera-Estrella, L., Cao, D., and Tran, L. S. P. (2020). Altering plant architecture to improve performance and resistance. *Trends in Plant Science*, 25(11):1154–1170.

Guo, W., Chen, S., Hussain, N., Cong, Y., Liang, Z., and Chen, K. (2015). Magnesium stress signaling in plant: just a beginning. *Plant Signaling and Behavior*, 10(3):e992287.

Gutteridge, S. and Pierce, J. (2006). A unified theory for the basis of the limitations of the primary reaction of photosynthetic CO_2 fixation: was Dr. Pangloss right? *Proceedings of the National Academy of Sciences of the United States of America*, 103(19):7203–7204.

Hacham, Y., Matityahu, I., Schuster, G., and Amir, R. (2008). Overexpression of mutated forms of aspartate kinase and cystathionine γ-synthase in tobacco leaves resulted in the high accumulation of methionine and threonine. *The Plant Journal*, 54(2):260–271.

Halkier, B. A. and Gershenzon, J. (2006). Biology and biochemistry of glucosinolates. *Annual Review of Plant Biology*, 57:303–333.

Hänsch, R., Fessel, D. G., Witt, C., Hesberg, C., Hoffmann, G., Walch-Liu, P., Engels, C., Kruse, J., Rennenberg, H., Kaiser, W. M., et al. (2001). Tobacco plants that lack expression of functional nitrate reductase in roots show changes in growth rates and metabolite accumulation. *Journal of Experimental Botany*, 52(359):1251–1258.

Hanson, A. D., Amthor, J. S., Sun, J., Niehaus, T. D., Gregory, J. F., Bruner, S. D., and Ding, Y. (2018). Redesigning thiamin synthesis: prospects and potential payoffs. *Plant Science*, 273:92–99.

Harada, H., Kuromori, T., Hirayama, T., Shinozaki, K., and Leigh, R. A. (2004). Quantitative trait loci analysis of nitrate storage in *Arabidopsis* leading to an investigation of the contribution of the anion channel gene, *AtCLC-c*, to variation in nitrate levels. *Journal of Experimental Botany*, 55(405):2005–2014.

Haritatos, E., Ayre, B. G., and Turgeon, R. (2000). Identification of phloem involved in assimilate loading in leaves by the activity of the galactinol synthase promoter. *Plant Physiology*, 123(3):929–937.

Harn, C., Khayat, E., and Daie, J. (1993). Expression dynamics of genes encoding key carbon metabolism enzymes during sink to source transition of developing leaves. *Plant and Cell Physiology*, 34(7):1045–1053.

Havé, M., Marmagne, A., Chardon, F., and Masclaux-Daubresse, C. (2017). Nitrogen remobilization during leaf senescence: lessons from Arabidopsis to crops. *Journal of Experimental Botany*, 68(10):2513–2529.

Hawkesford, M. J. and de Kok, L. J. (2006). Managing sulphur metabolism in plants. *Plant, Cell & Environment*, 29(3):382–395.

Hawkins, D. M. (2004). The Problem of Overfitting. *Journal of Chemical Information and Computer Sciences*, 44(1):1–12.

Hay, J. and Schwender, J. (2011a). Computational analysis of storage synthesis in developing *Brassica napus* L. (oilseed rape) embryos: flux variability analysis in relation to ^{13}C metabolic flux analysis. *The Plant Journal*, 67(3):513–525.

Hay, J. and Schwender, J. (2011b). Metabolic network reconstruction and flux variability analysis of storage synthesis in developing oilseed rape (*Brassica napus* L.) embryos. *The Plant Journal*, 67(3):526–541.

Hedden, P. (2003). The genes of the Green Revolution. *Trends in Genetics*, 19(1):5–9.

Hendriks, J. H., Kolbe, A., Gibon, Y., Stitt, M., and Geigenberger, P. (2003). ADP-glucose Pyrophosphorylase Is activated by posttranslational redox-modification in response to light and to sugars in leaves of Arabidopsis and other plant species. *Plant Physiology*, 133(2):838–849.

Hendrix, D. L. and Huber, S. C. (1986). Diurnal fluctuations in cotton leaf carbon export, carbohydrate content, and sucrose synthesizing enzymes. *Plant Physiology*, 81(2):584–586.

Hetherington, S. E., Smillie, R. M., and Davies, W. J. (1998). Photosynthetic activities of vegetative and fruiting tissues of tomato. *Journal of Experimental Botany*, 49(324):1173–1181.

Heuvelink, E. (1995a). Dry matter partitioning in a tomato plant: one common assimilate pool? *Journal of Experimental Botany*, 46(8):1025–1033.

Heuvelink, E. (1995b). Dry matter production in a tomato crop: measurements and simulation. *Annals of Botany*, 75(4):369–379.

Heuvelink, E. (1995c). Growth, development and yield of a tomato crop: periodic destructive measurements in a greenhouse. *Scientia Horticulturae*, 61(1-2):77–99.

Heuvelink, E. and Marcelis, L. (1989). Dry matter distribution in tomato and cucumber. *Acta Horticulturae*, 260:149–180.

Hildebrandt, T. M., Nunes Nesi, A., Araújo, W. L., and Braun, H. P. (2015). Amino acid catabolism in plants. *Molecular Plant*, 8(11):1563–1579.

Hill, S. A. and ap Rees, T. (1993). Fluxes of carbohydrate metabolism in ripening bananas. *Planta*, 192(1):52–60.

Hirose, T. (2005). Development of the Monsi-Saeki theory on canopy structure and function. *Annals of Botany*, 95(3):483–494.

Hirose, T. and Werger, M. J. (1987). Maximizing daily canopy photosynthesis with respect to the leaf nitrogen allocation pattern in the canopy. *Oecologia*, 72(4):520–526.

Höfgen, R., Axelsen, K. B., Kannangara, C. G., Schüttke, I., Pohlenz, H. D., Willmitzer, L., Grimm, B., and von Wettstein, D. (1994). A visible marker for antisense mRNA expression in plants: inhibition of chlorophyll synthesis with a glutamate-1-semialdehyde aminotransferase antisense gene. *Proceedings of the National Academy of Sciences of the United States of America*, 91(5):1726–1730.

Holland, B. L., Monk, N. A. M., Clayton, R. H., and Osborne, C. P. (2019). A theoretical analysis of how plant growth is limited by carbon allocation strategies and respiration. *in silico Plants*, 1(1):diz004.

Ishihara, H., Moraes, T. A., Pyl, E. T., Schulze, W. X., Obata, T., Scheffel, A., Fernie, A. R., Sulpice, R., and Stitt, M. (2017). Growth rate correlates negatively with protein turnover in Arabidopsis accessions. *The Plant Journal*, 91(3):416–429.

Ishizaki, K., Larson, T. R., Schauer, N., Fernie, A. R., Graham, I. A., and Leaver, C. J. (2005). The critical role of Arabidopsis electron-transfer flavoprotein:ubiquinone oxidoreductase during dark-induced starvation. *Plant Cell*, 17(9):2587–2600.

Jeong, M. L., Jiang, H., Chen, H. S., Tsai, C. J., and Harding, S. A. (2004). Metabolic profiling of the sink-to-source transition in developing leaves of quaking aspen. *Plant physiology*, 136(2):3364–3375.

Ji, S. H., Gururani, M. A., Lee, J. W., Ahn, B. O., and Chun, S. C. (2014). Isolation and characterisation of a dwarf rice mutant exhibiting defective gibberellins biosynthesis. *Plant Biology*, 16(2):428–439.

Jiang, K., Liberatore, K. L., Park, S. J., Alvarez, J. P., and Lippman, Z. B. (2013). Tomato yield heterosis is triggered by a dosage sensitivity of the florigen pathway that fine-tunes shoot architecture. *PLoS Genetics*, 9(12):e1004043.

Jonik, C., Sonnewald, U., Hajirezaei, M. R., Flügge, U. I., and Ludewig, F. (2012). Simultaneous boosting of source and sink capacities doubles tuber starch yield of potato plants. *Plant Biotechnology Journal*, 10(9):1088–1098.

Jordi, W., Schapendonk, A., Davelaar, E., Stoopen, G. M., Pot, C. S., de Visser, R., van Rhijn, J. A., Gan, S., and Amasino, R. M. (2000). Increased cytokinin levels in transgenic P_{SAG12}-*IPT* tobacco plants have large direct and indirect effects on leaf senescence, photosynthesis and N partitioning. *Plant, Cell & Environment*, 23(3):279–289.

Joshi, J., Folz, J., Gregory, J. F., McCarty, D. R., Fiehn, O., and Hanson, A. D. (2019). Rethinking the PDH bypass and GABA shunt as thiamin-deficiency workarounds. *Plant Physiology*, 181(2):389–393.

Joshi, V., Joung, J. G., Fei, Z., and Jander, G. (2010). Interdependence of threonine, methionine and isoleucine metabolism in plants: accumulation and transcriptional regulation under abiotic stress. *Amino Acids*, 39(4):933–947.

Joshi, V., Laubengayer, K. M., Schauer, N., Fernie, A. R., and Jander, G. (2006). Two Arabidopsis threonine aldolases are nonredundant and compete with threonine deaminase for a common substrate pool. *Plant Cell*, 18(12):3565–3575.

Josse, E. M., Simkin, a. J., Gaffé, J., Labouré, a. M., Kuntz, M., and Carol, P. (2000). A plastid terminal oxidase associated with carotenoid desaturation during chromoplast differentiation. *Plant physiology*, 123(8):1427–1436.

Kahlau, S. and Bock, R. (2008). Plastid transcriptomics and translatomics of tomato fruit development and chloroplast-to-chromoplast differentiation: chromoplast gene expression largely serves the production of a single protein. *Plant Cell*, 20(4):856–874.

Kaiser, W. M., Weiner, H., Kandlbinder, A., Tsai, C. B., Rockel, P., Sonoda, M., and Planchet, E. (2002). Modulation of nitrate reductase: some new insights, an unusual case and a potentially important side reaction. *Journal of Experimental Botany*, 53(370):875–882.

Kalt-Torres, W. and Huber, S. C. (1987). Diurnal changes in maize leaf photosynthesis. *Plant physiology*, 83(1987):294–298.

Kang, M., Yang, L., Zhang, B., and de Reffye, P. (2011). Correlation between dynamic tomato fruit-set and sourcesink ratio: a common relationship for different plant densities and seasons? *Annals of Botany*, 107(5):805–815.

Karley, A. J., Douglas, A. E., and Parker, W. E. (2002). Amino acid composition and nutritional quality of potato leaf phloem sap for aphids. *Journal of Experimental Biology*, 205(19):3009–3018.

Karlova, R., Chapman, N., David, K., Angenent, G. C., Seymour, G. B., and De Maagd, R. A. (2014). Transcriptional control of fleshy fruit development and ripening. *Journal of Experimental Botany*, 65(16):4527–4541.

Kavanová, M., Lattanzi, F. A., Grimoldi, A. A., and Schnyder, H. (2006). Phosphorus deficiency decreases cell division and elongation in grass leaves. *Plant Physiology*, 141(2):766–775.

Kelly, G., Moshelion, M., David-Schwartz, R., Halperin, O., Wallach, R., Attia, Z., Belausov, E., and Granot, D. (2013). Hexokinase mediates stomatal closure. *The Plant Journal*, 75(6):977–988.

Ketring, D. L. and Wheless, T. G. (1989). Thermal time requirements for phenological development of peanut. *Agronomy Journal*, 81(6):910–917.

Kim, J., Woo, H. R., and Nam, H. G. (2016). Toward systems understanding of leaf senescence: an integrated multi-omics perspective on leaf senescence research. *Molecular Plant*, 9(6):813–825.

Kimura, S. and Sinha, N. (2008). Tomato (*Solanum lycopersicum*): a model fruit-bearing crop. *Cold Spring Harbor Protocols*, 3(11):pdb–emo105.

Kirma, M., Araújo, W. L., Fernie, A. R., and Galili, G. (2012). The multifaceted role of aspartate-family amino acids in plant metabolism. *Journal of Experimental Botany*, 63(14):4995–5001.

Kitajima, K. (1992). Relationship between photosynthesis and thickness of cotyledons for tropical tree species. *Functional Ecology*, 6(5):582–589.

Klein, D., Morcuende, R., Stitt, M., and Krapp, A. (2000). Regulation of nitrate reductase expression in leaves by nitrate and nitrogen metabolism is completely overridden when sugars fall below a critical level. *Plant, Cell & Environment*, 23(8):863–871.

Koch, T., Heck, K., Schröder, N., Class, H., and Helmig, R. (2018). A new simulation framework for soil-root interaction, evaporation, root growth, and solute transport. *Vadose Zone Journal*, 17(1):170210.

Köhler, B. (2007). Step by step: deciphering ion transport in the root xylem parenchyma. *Plant Signaling and Behavior*, 2(4):303–305.

Köhler, B. and Raschke, K. (2007). Loading of ions into the xylem of the root. In Sattelmacher, B. and Horst, W., J., editors, *The Apoplast of Higher Plants: Compartment of Storage, Transport and Reactions*, pages 181–200. Springer.

Kramer, D. M. and Evans, J. R. (2011). The importance of energy balance in improving photosynthetic productivity. *Plant Physiology*, 155(1):70–78.

Kromdijk, J., Głowacka, K., Leonelli, L., Gabilly, S. T., Iwai, M., Niyogi, K. K., and Long, S. P. (2016). Improving photosynthesis and crop productivity by accelerating recovery from photoprotection. *Science*, 354(6314):857–861.

Kruger, N. J. and Ratcliffe, R. G. (2015). Fluxes through plant metabolic networks: measurements, predictions, insights and challenges. *Biochemical Journal*, 465(1):27–38.

Kuiper, D. (1993). Sink strength: established and regulated by plant growth regulators. *Plant, Cell & Environment*, 16(9):1025–1026.

Kull, O. and Jarvis, P. G. (1995). The role of nitrogen in a simple scheme to scale up photosynthesis from leaf to canopy. *Plant, Cell & Environment*, 18(10):1174–1182.

Ladwig, F., Stahl, M., Ludewig, U., Hirner, A. A., Hammes, U. Z., Stadler, R., Harter, K., and Koch, W. (2012). Siliques Are Red1 from Arabidopsis acts as a bidirectional amino acid transporter that is crucial for the amino acid homeostasis of siliques. *Plant Physiology*, 158(4):1643–1655.

Lang, M. (2019). yggdrasil: a Python package for integrating computational models across languages and scales. *in silico Plants*, 1(1):diz001.

Lastdrager, J., Hanson, J., and Smeekens, S. (2014). Sugar signals and the control of plant growth and development. *Journal of Experimental Botany*, 65(3):799–807.

Leakey, A. D., Ainsworth, E. A., Bernacchi, C. J., Rogers, A., Long, S. P., and Ort, D. R. (2009). Elevated CO_2 effects on plant carbon, nitrogen, and water relations: six important lessons from FACE. *Journal of Experimental Botany*, 60(10):2859–2876.

Lefebvre, S., Lawson, T., Zakhleniuk, O. V., Lloyd, J. C., and Raines, C. A. (2005). Increased sedoheptulose-1,7-bisphosphatase activity in transgenic tobacco plants stimulates photosynthesis and growth from an early stage in development. *Plant Physiology*, 138(1):451–460.

Leitner, D., Klepsch, S., Bodner, G., and Schnepf, A. (2010). A dynamic root system growth model based on L-Systems. *Plant and Soil*, 332(1):177–192.

Leuning, R., Kelliher, F. M., de Pury, D. G., and Schulze, E. D. (1995). Leaf nitrogen, photosynthesis, conductance and transpiration: scaling from leaves to canopies. *Plant, Cell & Environment*, 18(10):1183–1200.

Leuzinger, S., Manusch, C., Bugmann, H., and Wolf, A. (2013). A sink-limited growth model improves biomass estimation along boreal and alpine tree lines. *Global Ecology and Biogeography*, 22(8):924–932.

Li, T., Yang, X., Yu, Y., Si, X., Zhai, X., Zhang, H., Dong, W., Gao, C., and Xu, C. (2018a). Domestication of wild tomato is accelerated by genome editing. *Nature Biotechnology*, 36(12):1160–1163.

Li, Y., Wang, H., Zhang, Y., and Martin, C. (2018b). Can the world's favorite fruit, tomato, provide an effective biosynthetic chassis for high-value metabolites? *Plant Cell Reports*, 37(10):1443–1450.

Lillo, C. (2008). Signalling cascades integrating light-enhanced nitrate metabolism. *Biochemical Journal*, 415(1):11–19.

Lillo, C. and Appenroth, K. J. (2001). Light regulation of nitrate reductase in higher plants: which photoreceptors are involved? *Plant Biology*, 3(5):455–465.

Lim, C. J., Lee, H. Y., Kim, W. B., Lee, B. S., Kim, J., Ahmad, R., Kim, H. A., Yi, S. Y., Hur, C. G., and Kwon, S. Y. (2012). Screening of tissue-specific genes and promoters in tomato by comparing genome wide expression profiles of Arabidopsis orthologues. *Molecules and Cells*, 34(1):53–59.

Lim, P. O., Kim, H. J., and Nam, H. G. (2007). Leaf Senescence. *Annual Review of Plant Biology*, 58:115–136.

Linstrom, P. J. and Mallard, W. G. (2020). *NIST Chemistry WebBook, NIST Standard Reference Database Number 69*. National Institute of Standards and Technology, US.

Lippman, Z. and Tanksley, S. D. (2001). Dissecting the genetic pathway to extreme fruit size in tomato using a cross between the small-fruited wild species *Lycopersicon pimpinellifolium* and *L. esculentum* var. Giant Heirloom. *Genetics*, 158(1):413–422.

Lippman, Z. B., Semel, Y., and Zamir, D. (2007). An integrated view of quantitative trait variation using tomato interspecific introgression lines. *Current Opinion in Genetics and Development*, 17(6):545–552.

Liu, B., Watanabe, S., Uchiyama, T., Kong, F., Kanazawa, A., Xia, Z., Nagamatsu, A., Arai, M., Yamada, T., Kitamura, K., Masuta, C., Harada, K., and Abe, J. (2010). The soybean stem growth habit gene *Dt1* is an ortholog of Arabidopsis *TERMINAL FLOWER1*. *Plant Physiology*, 153(1):198–210.

Liu, D. D., Chao, W. M., and Turgeon, R. (2012). Transport of sucrose, not hexose, in the phloem. *Journal of Experimental Botany*, 63(11):4315–4320.

Long, S. P., Ainsworth, E. A., Leakey, A. D., Nösbsrger, J., and Ort, D. R. (2006). Food for thought: lower-than-expected crop yield stimulation with rising CO_2 concentrations. *Science*, 312(5782):1918–1921.

Long, S. P., Marshall-Colon, A., and Zhu, X.-G. (2015). Meeting the global food demand of the future by engineering crop photosynthesis and yield potential. *Cell*, 161(1):56–66.

López-Calcagno, P. E., Brown, K. L., Simkin, A. J., Fisk, S. J., Vialet-Chabrand, S., Lawson, T., and Raines, C. A. (2020). Stimulating photosynthetic processes increases productivity and water-use efficiency in the field. *Nature Plants*, 6(8):1054–1063.

Lu, M., Snyder, R., Grant, J., and Tegeder, M. (2019). Manipulation of sucrose phloem and embryo loading affects pea leaf metabolism, carbon and nitrogen partitioning to sinks as well as seed storage pools. *The Plant Journal*.

Luo, R., Wei, H., Ye, L., Wang, K., Chen, F., Luo, L., Liu, L., Li, Y., Crabbe, M. J. C., Jin, L., Li, Y., and Zhong, Y. (2009). Photosynthetic metabolism of C_3 plants shows highly cooperative regulation under changing environments: a systems biological analysis. *Proceedings of the National Academy of Sciences of the United States of America*, 106(3):847–852.

Luo, X., Chen, J. M., Liu, J., Black, T. A., Croft, H., Staebler, R., He, L., Arain, M. A., Chen, B., Mo, G., Gonsamo, A., and McCaughey, H. (2018). Comparison of big-leaf, two-big-leaf, and two-leaf upscaling schemes for evapotranspiration estimation using coupled carbon-water modeling. *Journal of Geophysical Research: Biogeosciences*, 123(1):207–225.

Ma, Y., Chen, Y., Zhu, J., Meng, L., Guo, Y., Li, B., and Hoogenboom, G. (2018). Coupling individual kernel-filling processes with source-sink interactions into GREENLAB-Maize. *Annals of Botany*, 121(5):961–973.

Macduff, J. H. and Bakken, A. K. (2003). Diurnal variation in uptake and xylem contents of inorganic and assimilated N under continuous and interrupted N supply to *Phleum pratense* and *Festuca pratensis*. *Journal of Experimental Botany*, 54(381):431–444.

Maier, C. A., Zarnoch, S. J., and Dougherty, P. M. (1998). Effects of temperature and tissue nitrogen on dormant season stem and branch maintenance respiration in a young loblolly pine (*Pinus taeda*) plantation. *Tree Physiology*, 18(1):11–20.

Marcelis, L. (1993). Simulation of biomass allocation in greenhouse crops — a review. *Acta Horticulturae*, 328:49–68.

Marcelis, L. and Heuvelink, E. (2007). Concepts of modelling carbon allocation among plant organs. In Vos, J., Marcelis, L. F. M., de Visser, P. H. B., Struik, P. C., and B, E. J., editors, *Functional-Structural Plant Modelling in Crop Production*, pages 103–111. Frontis.

Marchi, S., Sebastiani, L., Gucci, R., and Tognetti, R. (2005). Sink-source transition in peach leaves during shoot development. *Journal of the American Society for Horticultural Science*, 130(6):928–935.

Marchiori, P. E., Machado, E. C., and Ribeiro, R. V. (2014). Photosynthetic limitations imposed by self-shading in field-grown sugarcane varieties. *Field Crops Research*, 155:30–37.

Marshall-Colon, A., Long, S. P., Allen, D. K., Allen, G., Beard, D. A., Benes, B., von Caemmerer, S., Christensen, A. J., Cox, D. J., Hart, J. C., Hirst, P. M., Kannan, K., Katz, D. S., Lynch, J. P., Millar, A. J., Panneerselvam, B., Price, N. D., Prusinkiewicz, P., Raila, D., Shekar, R. G., Shrivastava, S., Shukla, D., Srinivasan, V., Stitt, M., Turk, M. J., Voit, E. O., Wang, Y., Yin, X., and Zhu, X.-G. (2017). Crops *In Silico*: generating virtual crops using an integrative and multi-scale modeling platform. *Frontiers in Plant Science*, 8:786.

Masakapalli, S. K., Bryant, F. M., Kruger, N. J., and Ratcliffe, R. G. (2014). The metabolic flux phenotype of heterotrophic Arabidopsis cells reveals a flexible balance between the cytosolic and plastidic contributions to carbohydrate oxidation in response to phosphate limitation. *The Plant Journal*, 78(6):964–977.

Masakapalli, S. K., Kruger, N. J., and Ratcliffe, R. G. (2013). The metabolic flux phenotype of heterotrophic Arabidopsis cells reveals a complex response to changes in nitrogen supply. *The Plant Journal*, 74(4):569–582.

Masclaux, C., Valadier, M. H., Brugière, N., Morot-Gaudry, J. F., and Hirel, B. (2000). Characterization of the sink/source transition in tobacco (*Nicotiana tabacum* L.) shoots in relation to nitrogen management and leaf senescence. *Planta*, 211(4):510–518.

Masclaux-Daubresse, C., Daniel-Vedele, F., Dechorgnat, J., Chardon, F., Gaufichon, L., and Suzuki, A. (2010). Nitrogen uptake, assimilation and remobilization in plants: challenges for sustainable and productive agriculture. *Annals of Botany*, 105(7):1141–1157.

Mason, T. G. and Maskell, E. J. (1928). Studies on the transport of carbohydrates in the cotton plant. I. A study of diurnal variation in the carbohydrates of leaf, bark, and wood, and of the effects of ringing. *Annals of Botany*, 42(165):189–253.

Mayta, M. L., Arce, R. C., Zurbriggen, M. D., Valle, E. M., Hajirezaei, M. R., Zanor, M. I., and Carrillo, N. (2019). Expression of a chloroplast-targeted cyanobacterial flavodoxin in tomato plants increases harvest index by altering plant size and productivity. *Frontiers in Plant Science*, 10(1432):1–13.

Meng, Q., Siebke, K., Lippert, P., Baur, B., Mukherjee, U., and Weis, E. (2001). Sink-source transition in tobacco leaves visualized using chlorophyll fluorescence imaging. *New Phytologist*, 151(3):585–595.

Mengel, K. and Haeder, H.-E. (1977). Effect of potassium supply on the rate of phloem sap exudation and the composition of phloem sap of *Ricinus communis*. *Plant Physiology*, 59(2):282–284.

Mereb, E. L., Alves, F. R. R., Rezende, M. H., Oliveira, E. J. d., Carvalho, R. F., and Melo, H. C. D. (2020). Morphophysiological responses of tomato phytochrome mutants under sun and shade conditions. *Revista Brasileira de Botanica*, 43(1):45–54.

Micallef, B. J. and Shelp, B. J. (1989). Arginine metabolism in developing soybean cotyledons. *Plant Physiology*, 90(2):624–630.

Migue, F. E., Maughan, M., Bollero, G. A., and Long, S. P. (2012). Modeling spatial and dynamic variation in growth, yield, and yield stability of the bioenergy crops *Miscanthus* x *giganteus* and *Panicum virgatum* across the conterminous United States. *GCB Bioenergy*, 4(5):509–520.

Millar, A. J., Urquiza, J. U., Freeman, P. L., Hume, A., Plotkin, G. D., Sorokina, O., Zardilis, A., and Zielinski, T. (2019). Practical steps to digital organism models, from laboratory model species to 'Crops *in silico*'. *Journal Of Experimental Botany*, 34(9):2403–2418.

Mintz-Oron, S., Meir, S., Malitsky, S., Ruppin, E., Aharoni, A., and Shlomi, T. (2012). Reconstruction of *Arabidopsis* metabolic network models accounting for subcellular compartmentalization and tissue-specificity. *Proceedings of the National Academy of Sciences of the United States of America*, 109(1):339–344.

Monsi, M. and Saeki, T. (1953). Uber den Lichtfaktor in den Pflanzen-gesellschaf und seine Begeutung fur die Stoffproduktion. *Japanese Journal of Botany*, 14:22–52.

Moot, D. J., Scott, W. R., Roy, A. M., and Nicholls, A. C. (2000). Base temperature and thermal time requirements for germination and emergence of temperate pasture species. *New Zealand Journal of Agricultural Research*, 43(1):15–25.

Moreira, T. B., Shaw, R., Luo, X., Ganguly, O., Kim, H. S., Coelho, L. G. F., Cheung, C. Y. M., and Williams, T. C. R. (2019). A genome-scale metabolic model of soybean (*Glycine max*) highlights metabolic fluxes in seedlings. *Plant Physiology*, 180(4):1912–1929.

Muangprom, A., Thomas, S. G., Sun, T. P., and Osborn, T. C. (2005). A novel dwarfing mutation in a green revolution gene from *Brassica rapa*. *Plant Physiology*, 137(3):931–938.

Mugford, S. T., Fernandez, O., Brinton, J., Flis, A., Krohn, N., Encke, B., Feil, R., Sulpice, R., Lunn, J. E., Stitt, M., and Smith, A. M. (2014). Regulatory properties of ADP-glucose pyrophosphorylase are required for adjustment of leaf starch synthesis in different photoperiods. *Plant Physiology*, 166(4):1733–1747.

Müller, I., Schmid, B., and Weiner, J. (2000). The effect of nutrient availability on biomass allocation patterns in 27 species of herbaceous plants. *Perspectives in Plant Ecology, Evolution and Systematics*, 3(2):115–127.

Müller, P., Li, X. P., and Niyogi, K. K. (2001). Non-photochemical quenching. A response to excess light energy. *Plant Physiology*, 125(4):1558–1566.

Nguyen, T., Bajwa, A. A., Navie, S., O'Donnell, C., and Adkins, S. (2017). Parthenium weed (*Parthenium hysterophorus* L.) and climate change: the effect of CO_2 concentration, temperature, and water deficit on growth and reproduction of two biotypes. *Environmental Science and Pollution Research*, 24(11):10727–10739.

Nguyen-Quoc, B. and Foyer, C. H. (2001). A role for 'futile cycles' involving invertase and sucrose synthase in sucrose metabolism of tomato fruit. *Journal of Experimental Botany*, 52(358):881–889.

Nicolas, M., Munns, R., Samarakoon, A., and Gifford, R. (1993). Elevated CO_2 improves the growth of wheat under salinity. *Functional Plant Biology*, 20(3):349.

Niklas, K. J. (2006). A phyletic perspective on the allometry of plant biomass-partitioning patterns and functionally equivalent organ-categories. *New Phytologist*, 171(1):27–40.

Niklas, K. J. and Enquist, B. J. (2002). Canonical rules for plant organ biomass partitioning and annual allocation. *American Journal of Botany*, 89(5):812–819.

Niklas, K. J. and Enquist, B. J. (2003). An allometric model for seed plant reproduction. *Evolutionary Ecology Research*, 5(1):79–88.

Nölke, G., Houdelet, M., Kreuzaler, F., Peterhänsel, C., and Schillberg, S. (2014). The expression of a recombinant glycolate dehydrogenase polyprotein in potato (*Solanum tuberosum*) plastids strongly enhances photosynthesis and tuber yield. *Plant Biotechnology Journal*, 12(6):734–742.

Nordin, A. and Näsholm, T. (1997). Nitrogen storage forms in nine boreal understorey plant species. *Oecologia*, 110(4):487–492.

Nunes-Nesi, A., Carrari, F., Lytovchenko, A., Smith, A. M. O., Ehlers Loureiro, M., Ratcliffe, R. G., Sweetlove, L. J., and Fernie, A. R. (2005). Enhanced photosynthetic performance and growth as a consequence of decreasing mitochondrial malate dehydrogenase activity in transgenic tomato plants. *Plant Physiology*, 137(2):611–622.

Nunes-Nesi, A., Fernie, A. R., and Stitt, M. (2010). Metabolic and signaling aspects underpinning the regulation of plant carbon nitrogen interactions. *Molecular Plant*, 3(6):973–996.

Oeller, P. W., Min-Wong, L. U., Taylor, L. P., Pike, D. A., and Theologis, A. (1991). Reversible inhibition of tomato fruit senescence by antisense RNA. *Science*, 254(5030):437–439.

Ogiso-Tanaka, E., Matsubara, K., Yamamoto, S., Nonoue, Y., Wu, J., Fujisawa, H., Ishikubo, H., Tanaka, T., Ando, T., Matsumoto, T., and Yano, M. (2013). Natural variation of the *RICE FLOWERING LOCUS T 1* contributes to flowering time divergence in rice. *PLoS ONE*, 8(10):e75959.

Ögren, E. (2000). Maintenance respiration correlates with sugar but not nitrogen concentration in dormant plants. *Physiologia Plantarum*, 108(3):295–299.

Okumoto, S. and Pilot, G. (2011). Amino acid export in plants: a missing link in nitrogen cycling. *Molecular Plant*, 4(3):453–463.

O'Leary, B. M., Khim Oh, G. G., Lee, C. P., and Harvey Millar, A. (2020). Metabolite regulatory interactions control plant respiratory metabolism via target of rapamycin (TOR) kinase activation. *Plant Cell*, 32(3):666–682.

Omid, A., Malter, D., Peleg, G., and Wolf, S. (2008). Long-distance trafficking of macromolecules in the phloem. *Plant Signaling and Behavior*, 3(4):260–262.

Orth, J. D., Thiele, I., and Palsson, B. O. (2010). What is flux balance analysis? *Nature Biotechnology*, 28(3):245–248.

Osakabe, Y., Arinaga, N., Umezawa, T., Katsura, S., Nagamachi, K., Tanaka, H., Ohiraki, H., Yamada, K., Seo, S.-U., Abo, M., Yoshimura, E., Shinozaki, K., and Yamaguchi-Shinozaki, K. (2013). Osmotic stress responses and plant growth controlled by potassium transporters in Arabidopsis. *The Plant Cell*, 25(2):609–624.

Osorio, S., Ruan, Y.-L., and Fernie, A. R. (2014). An update on source-to-sink carbon partitioning in tomato. *Frontiers in Plant Science*, 5:516.

Ostaszewska, M., Juszczuk, I. M., Kołodziejek, I., and Rychter, A. M. (2014). Long-term sulphur starvation of *Arabidopsis thaliana* modifies mitochondrial ultrastructure and activity and changes tissue energy and redox status. *Journal of Plant Physiology*, 171(7):549–558.

Otani, M., Meguro, S., Gondaira, H., Hayashi, M., Saito, M., Han, D. S., Inthima, P., Supaibulwatana, K., Mori, S., Jikumaru, Y., Kamiya, Y., Li, T., Niki, T., Nishijima, T., Koshioka, M., and Nakano, M. (2013). Overexpression of the gibberellin 2-oxidase gene from *Torenia fournieri* induces dwarf phenotypes in the liliaceous monocotyledon *Tricyrtis* sp. *Journal of Plant Physiology*, 170(16):1416–1423.

Papanatsiou, M., Petersen, J., Henderson, L., Wang, Y., Christie, J. M., and Blatt, M. R. (2019). Optogenetic manipulation of stomatal kinetics improves carbon assimilation, water use, and growth. *Science*, 363(6434):1456–1459.

Park, B. S., Song, J. T., and Seo, H. S. (2011). *Arabidopsis* nitrate reductase activity is stimulated by the E3 SUMO ligase AtSIZ1. *Nature Communications*, 2:400.

Park, S. J., Jiang, K., Schatz, M. C., and Lippman, Z. B. (2012). Rate of meristem maturation determines inflorescence architecture in tomato. *Proceedings of the National Academy of Sciences of the United States of America*, 109(2):639–644.

Park, S. J., Jiang, K., Tal, L., Yichie, Y., Gar, O., Zamir, D., Eshed, Y., and Lippman, Z. B. (2014). Optimization of crop productivity in tomato using induced mutations in the florigen pathway. *Nature Genetics*, 46(12):1337–1342.

Parker, J. L. and Newstead, S. (2014). Molecular basis of nitrate uptake by the plant nitrate transporter NRT1.1. *Nature*, 507(7490):68–72.

Passioura, J. and Ashford, A. (1974). Rapid translocation in the phloem of wheat roots. *Functional Plant Biology*, 1(4):521.

Pate, J., Shedley, E., Arthur, D., and Adams, M. (1998). Spatial and temporal variations in phloem sap composition of plantation-grown *Eucalyptus globulus*. *Oecologia*, 117(3):312–322.

Paul, M. J. and Foyer, C. H. (2001). Sink regulation of photosynthesis. *Journal of Experimental Botany*, 52(360):1383–1400.

Peet, M. M. and Bartholemew, M. (1996). Effect of night temperature on pollen characteristics, growth, and fruit set in tomato. *Journal of the American Society for Horticultural Science*, 121(3):514–519.

Peng, B., Guan, K., Tang, J., Ainsworth, E. A., Asseng, S., Bernacchi, C. J., Cooper, M., Delucia, E. H., Elliott, J. W., Ewert, F., Grant, R. F., Gustafson, D. I., Hammer, G. L., Jin, Z., Jones, J. W., Kimm, H., Lawrence, D. M., Li, Y., Lombardozzi, D. L., Marshall-Colon, A., Messina, C. D., Ort, D. R., Schnable, J. C., Vallejos, C. E., Wu, A., Yin, X., and Zhou, W. (2020). Towards a multiscale crop modelling framework for climate change adaptation assessment. *Nature plants*, 6(4):338–348.

Peng, J., Richards, D. E., Hartley, N. M., Murphy, G. P., Devos, K. M., Flintham, J. E., Beales, J., Fish, L. J., Worland, A. J., Pelica, F., Sudhakar, D., Christou, P., Snape, J. W., Gale, M. D., and Harberd, N. P. (1999). 'Green revolution' genes encode mutant gibberellin response modulators. *Nature*, 400(6741):256–261.

Perata, P., Vernieri, P., Armellini, D., Bugnoli, M., Tognoni, F., and Alpi, A. (1992). Immunological detection of acetaldehyde-protein adducts in ethanol-treated carrot cells. *Plant Physiology*, 98(3):913–918.

Perchlik, M. and Tegeder, M. (2017). Improving plant nitrogen use efficiency through alteration of amino acid transport processes. *Plant Physiology*, 175(1):235–247.

Péret, B., Clément, M., Nussaume, L., and Desnos, T. (2011). Root developmental adaptation to phosphate starvation: better safe than sorry. *Trends in Plant Science*, 16(8):442–450.

Pérez-Alfocea, F., Albacete, A., Ghanem, M. E., and Dodd, I. C. (2010). Hormonal regulation of source-sink relations to maintain crop productivity under salinity: a case study of root-to-shoot signalling in tomato. *Functional Plant Biology*, 37(7):592–603.

Pérez-Alfocea, F., Balibrea, M. E., Alarcón, J. J., and Bolarín, M. C. (2000). Composition of xylem and phloem exudates in relation to the salt-tolerance of domestic and wild tomato species. *Journal of Plant Physiology*, 156(3):367–374.

Peyhardi, J., Caraglio, Y., Costes, E., Lauri, P. É., Trottier, C., and Guédon, Y. (2017). Integrative models for joint analysis of shoot growth and branching patterns. *New Phytologist*, 216(4):1291–1304.

Pfau, T., Christian, N., Masakapalli, S. K., Sweetlove, L. J., Poolman, M. G., and Ebenhöh, O. (2018). The intertwined metabolism during symbiotic nitrogen fixation elucidated by metabolic modelling. *Scientific Reports*, 8(1):1–11.

Pharkya, P., Burgard, A. P., and Maranas, C. D. (2003). Exploring the overproduction of amino acids using the bilevel optimization framework OptKnock. *Biotechnology and Bioengineering*, 84(7):887–899.

Piechulla, B., Glick, R. E., Bahl, H., Melis, A., and Gruissem, W. (1987). Changes in photosynthetic capacity and photosynthetic protein pattern during tomato fruit ripening. *Plant Physiology*, 84(3):911–917.

Pires, M. V., Pereira Júnior, A. A., Medeiros, D. B., Daloso, D. M., Pham, P. A., Barros, K. A., Engqvist, M. K., Florian, A., Krahnert, I., Maurino, V. G., Araújo, W. L., and Fernie, A. R. (2016). The influence of alternative pathways of respiration that utilize branched-chain amino acids following water shortage in Arabidopsis. *Plant Cell and Environment*, 39(6):1304–1319.

Poolman, M. G., Kundu, S., Shaw, R., and Fell, D. A. (2013). Responses to light intensity in a genome-scale model of rice metabolism. *Plant Physiology*, 162(2):1060–1072.

Poolman, M. G., Miguet, L., Sweetlove, L. J., and Fell, D. A. (2009). A genome-scale metabolic model of Arabidopsis and some of its properties. *Plant Physiology*, 151(3):1570–1581.

Poorter, H. and Bergkotte, M. (1992). Chemical composition of 24 wild species differing in relative growth rate. *Plant, Cell & Environment*, 15(2):221–229.

Poorter, H., Bühler, J., van Dusschoten, D., Climent, J., and Postma, J. A. (2012a). Pot size matters: a meta-analysis of the effects of rooting volume on plant growth. *Functional Plant Biology*, 39(11):839–850.

Poorter, H., Niklas, K. J., Reich, P. B., Oleksyn, J., Poot, P., and Mommer, L. (2012b). Biomass allocation to leaves, stems and roots: meta-analyses of interspecific variation and environmental control. *New Phytologist*, 193(1):30–50.

Posch, B. C., Kariyawasam, B. C., Bramley, H., Coast, O., Richards, R. A., Reynolds, M. P., Trethowan, R., Atkin, O. K., and Raines, C. (2019). Exploring high temperature responses of photosynthesis and respiration to improve heat tolerance in wheat. *Journal of Experimental Botany*, 70(19):5051–5069.

Postma, J. A., Kuppe, C., Owen, M. R., Mellor, N., Griffiths, M., Bennett, M. J., Lynch, J. P., and Watt, M. (2017). OpenSimRoot: widening the scope and application of root architectural models. *New Phytologist*, 215(3):1274–1286.

Pott, D. M., Osorio, S., and Vallarino, J. G. (2019). From central to specialized metabolism: an overview of some secondary compounds derived from the primary metabolism for their role in conferring nutritional and organoleptic characteristics to fruit. *Frontiers in Plant Science*, 10(835):1–19.

Pourtau, N., Jennings, R., Pelzer, E., Pallas, J., and Wingler, A. (2006). Effect of sugar-induced senescence on gene expression and implications for the regulation of senescence in Arabidopsis. *Planta*, 224(3):556–568.

Pullen, N., Zhang, N., Dobon Alonso, A., and Penfield, S. (2019). Growth rate regulation is associated with developmental modification of source efficiency. *Nature Plants*, 5:148–152.

Quinet, M., Angosto, T., Yuste-Lisbona, F. J., Blanchard-Gros, R., Bigot, S., Martinez, J. P., and Lutts, S. (2019). Tomato fruit development and metabolism. *Frontiers in Plant Science*, 10(1554):1–23.

Radrich, K., Tsuruoka, Y., Dobson, P., Gevorgyan, A., Swainston, N., Baart, G., and Schwartz, J. M. (2010). Integration of metabolic databases for the reconstruction of genome-scale metabolic networks. *BMC Systems Biology*, 4(114):1–16.

Ranathunge, K., El-Kereamy, A., Gidda, S., Bi, Y. M., and Rothstein, S. J. (2014). *AMT1;1* transgenic rice plants with enhanced NH_4^+ permeability show superior growth and higher yield under optimal and suboptimal NH_4^+ conditions. *Journal of Experimental Botany*, 65(4):965–979.

Rasse, D. P. and Tocquin, P. (2006). Leaf carbohydrate controls over Arabidopsis growth and response to elevated CO_2: an experimentally based model. *New Phytologist*, 172(3):500–513.

Raulier, F., Bernier, P. Y., and Ung, C. H. (1999). Canopy photosynthesis of sugar maple (*Acer saccharum*): comparing big-leaf and multilayer extrapolations of leaf-level measurements. *Tree Physiology*, 19(7):407–420.

Reda, M. (2015). Response of nitrate reductase activity and *NIA* genes expression in roots of *Arabidopsis hxk1* mutant treated with selected carbon and nitrogen metabolites. *Plant Science*, 230:51–58.

Reekie, E. G. and Bazzaz, F. A. (2005). *Reproductive Allocation in Plants*. Elsevier.

Reekie, E. G., MacDougall, G., Wong, I., and Hicklenton, P. R. (1998). Effect of sink size on growth response to elevated atmospheric CO_2 within the genus *Brassica*. *Canadian Journal of Botany*, 76(5):829–835.

Regierer, B., Fernie, A. R., Springer, F., Perez-Melis, A., Leisse, A., Koehl, K., Willmitzer, L., Geigenberger, P., and Kossmann, J. (2002). Starch content and yield increase as a result of altering adenylate pools in transgenic plants. *Nature Biotechnology*, 20(12):1256–1260.

Reich, P. B., Hobbie, S. E., and Lee, T. D. (2014). Plant growth enhancement by elevated CO_2 eliminated by joint water and nitrogen limitation. *Nature Geoscience*, 7(12):920–924.

Reid, R. and Hayes, J. (2003). Mechanisms and control of nutrient uptake in plants. *International Review of Cytology*, 229:73–114.

Renau-Morata, B., Carrillo, L., Cebolla-Cornejo, J., Molina, R. V., Martí, R., Domínguez-Figueroa, J., Vicente-Carbajosa, J., Medina, J., and Nebauer, S. G. (2020). The targeted overexpression of *SlCDF4* in the fruit enhances tomato size and yield involving gibberellin signalling. *Scientific Reports*, 10(1):1–14.

Rennenberg, H., Wildhagen, H., and Ehlting, B. (2010). Nitrogen nutrition of poplar trees. *Plant Biology*, 12(2):275–291.

Resendis-Antonio, O., Reed, J. L., Encarnación, S., Collado-Vides, J., and Palsson, B. (2007). Metabolic reconstruction and modeling of nitrogen fixation in *Rhizobium etli*. *PLoS Computational Biology*, 3(10):1887–1895.

Riens, B., Lohaus, G., Heineke, D., and Heldt, H. W. (1991). Amino acid and sucrose content determined in the cytosolic, chloroplastic, and vacuolar compartments and in the phloem sap of spinach leaves. *Plant Physiology*, 97(1):227–233.

Rocha-Sosa, M., Sonnewald, U., Frommer, W., Stratman, M., Schell, J., and Willmitzer, L. (1989). Both developmental and metabolic signals activate the promoter of a class I patatin gene. *The EMBO Journal*, 8(1):23–29.

Rohwer, J. M. (2012). Kinetic modelling of plant metabolic pathways. *Journal of Experimental Botany*, 63(6):2275–2292.

Roitsch, T. and González, M. C. (2004). Function and regulation of plant invertases: sweet sensations. *Trends in Plant Science*, 9(12):606–613.

Rosche, E., Blackmore, D., Tegeder, M., Richardson, T., Schroeder, H., Higgins, T. J., Frommer, W. B., Offler, C. E., and Patrick, J. W. (2002). Seed-specific overexpression of a potato sucrose transporter increases sucrose uptake and growth rates of developing pea cotyledons. *The Plant Journal*, 30(2):165–175.

Ruan, Y. L. (2014). Sucrose metabolism: gateway to diverse carbon use and sugar signaling. *Annual Review of Plant Biology*, 65:33–67.

Ruan, Y. L. and Patrick, J. W. (1995). The cellular pathway of postphloem sugar transport in developing tomato fruit. *Planta: An International Journal of Plant Biology*, 196(3):434–444.

Russell, C. R. and Morris, D. A. (1983). Patterns of assimilate distribution and source-sink relationships in the young reproductive tomato plant (*Lycopersicon esculentum* mill.). *Annals of Botany*, 52(3):357–363.

Saha, R., Suthers, P. F., and Maranas, C. D. (2011). *Zea mays i*RS1563: a comprehensive genome-scale metabolic reconstruction of maize metabolism. *PLoS ONE*, 6(7):e21784.

Saiyed, I. M., Bullock, P. R., Sapirstein, H. D., Finlay, G. J., and Jarvis, C. K. (2009). Thermal time models for estimating wheat phenological development and weather-based relationships to wheat quality. *Canadian Journal of Plant Science*, 89(3):429–439.

Sakamoto, T., Kobayashi, M., Itoh, H., Tagiri, A., Kayano, T., Tanaka, H., Iwahori, S., and Matsuoka, M. (2001). Expression of a gibberellin 2-oxidase gene around the shoot apex is related to phase transition in rice. *Plant Physiology*, 125(3):1508–1516.

Sakamoto, T. and Matsuoka, M. (2004). Generating high-yielding varieties by genetic manipulation of plant architecture. *Current Opinion in Biotechnology*, 15(2):144–147.

Sakamoto, T., Morinaka, Y., Ishiyama, K., Kobayashi, M., Itoh, H., Kayano, T., Iwahori, S., Matsuoka, M., and Tanaka, H. (2003). Genetic manipulation of gibberellin metabolism in transgenic rice. *Nature Biotechnology*, 21(8):909–913.

Samoilov, M., Plyasunov, S., and Arkin, A. P. (2005). Stochastic amplification and signaling in enzymatic futile cycles through noise-induced bistability with oscillations. *Proceedings of the National Academy of Sciences of the United States of America*, 102(7):2310–2315.

Sanders, A., Collier, R., Trethewy, A., Gould, G., Sieker, R., and Tegeder, M. (2009). AAP1 regulates import of amino acids into developing Arabidopsis embryos. *The Plant Journal*, 59(4):540–552.

Sandri, M. A., Andriolo, J. L., Witter, M., and dal Ross, T. (2002). High density of defoliated tomato plants in protected cultivation and its effects on development of trusses and fruits. *Horticultura Brasileira*, 20(3):485–489.

Santiago, J. P. and Tegeder, M. (2016). Connecting source with sink: the role of Arabidopsis AAP8 in phloem loading of amino acids. *Plant Physiology*, 171(1):508–521.

Sasaki, A., Ashikari, M., Ueguchi-Tanaka, M., Itoh, H., Nishimura, A., Swapan, D., Ishiyama, K., Saito, T., Kobayashi, M., Khush, G. S., Kitano, H., and Matsuoka, M. (2002). A mutant gibberellin-synthesis gene in rice: new insight into the rice variant that helped to avert famine over thirty years ago. *Nature*, 416(6882):701–702.

Sato, S., Tabata, S., Hirakawa, H., Asamizu, E., Shirasawa, K., Isobe, S., Kaneko, T., Nakamura, Y., Shibata, D., Aoki, K., Egholm, M., Knight, J., Bogden, R., Li, C., Shuang, Y., Xu, X., Pan, S., Cheng, S., Liu, X., Ren, Y., Wang, J., Albiero, A., dal Pero, F., Todesco, S., van Eck, J., Buels, R. M., Bombarely, A., Gosselin, J. R., Huang, M., Leto, J. A., Menda, N., Strickler, S., Mao, L., Gao, S., Tecle, I. Y., York, T., Zheng, Y., Vrebalov, J. T., Lee, J., Zhong, S., Mueller, L. A., Stiekema, W. J., Ribeca, P., Alioto, T., Yang, W., Huang, S., Du, Y., Zhang, Z., Gao, J., Guo, Y., Wang, X., Li, Y., He, J., Li, C., Cheng, Z., Zuo, J., Ren, J., Zhao, J., Yan, L., Jiang, H., Wang, B., Li, H., Li, Z., Fu, F., Chen, B., Han, B., Feng, Q., Fan, D., Wang, Y., Ling, H., Xue, Y., Ware, D., Richard McCombie, W., Lippman, Z. B., Chia, J. M., Jiang, K., Pasternak, S., Gelley, L., Kramer, M., Anderson, L. K., Chang, S. B., Royer, S. M., Shearer, L. A., Stack, S. M., Rose, J. K., Xu, Y., Eannetta, N., Matas, A. J., McQuinn, R., Tanksley, S. D., Camara, F., Guigó, R., Rombauts, S., Fawcett, J., van de Peer, Y., Zamir, D., Liang, C., Spannagl, M., Gundlach, H., Bruggmann, R., Mayer, K., Jia, Z., Zhang, J., Ye, Z., Bishop, G. J., Butcher, S., Lopez-Cobollo, R., Buchan, D., Filippis, I., Abbott, J., Dixit, I. R., Singh, M., Singh, A., Pal, J. K., Pandit, A., Singh, P. K., Mahato, A. K., Dogra, V., Gaikwad, K., Sharma, T. R., Mohapatra, T., Singh, N. K., Causse, M., Rothan, C., Noirot, C., Bellec, A., Klopp, C., Delalande, C., Berges, H., Mariette, J., Frasse, P., Vautrin, S., Zouine, T. M., Latché, A., Rousseau, C., Regad, F., Pech, J. C., Philippot, M., Bouzayen, M., Pericard, P., Osorio, S., del Carmen, A. F., Monforte, A., Granell, A., Fernandez-Muñoz, R., Conte, M., Lichtenstein, G., Carrari, F., de Bellis, G., Fuligni, F., Peano, C., Grandillo, S., Termolino, P., Pietrella, M., Fantini, E., Falcone, G., Fiore, A., Giuliano, G., Lopez, L., Facella, P., Perrotta, G., Daddiego, L., Bryan, G., Orozco, B. M., Pastor, X., Torrents, D., van Schriek, M. G., Feron, R. M., van Oeveren, J., de Heer, P., Da Ponte, L., Jacobs-Oomen, S., Cariaso, M., Prins, M., van Eijk, M. J., Janssen, A., van Haaren, J. J., Hwan, J. S., Kim, J., Kwon, S. Y., Kim, S., Koo, D. H., Lee, S., Clouser, C., Rico, A., Hallab, A., Gebhardt, C., Klee, K.,

Jöcker, A., Warfsmann, J., Göbel, U., Kawamura, S., Yano, K., Sherman, J. D., Fukuoka, H., Negoro, S., Bhutty, S., Chowdhury, P., Chattopadhyay, D., Datema, E., Smit, S., Schijlen, E. G., van de Belt, J., van Haarst, J. C., Peters, S. A., van Staveren, M. J., Henkens, M. H., Mooyman, P. J., Hesselink, T., van Ham, R. C., Jiang, G., Droege, M., Choi, D., Kang, B. C., Kim, B. D., Park, M., Kim, S., Yeom, S. I., Lee, Y. H., Choi, Y. D., Li, G., Gao, J., Liu, Y., Huang, S., Fernandez-Pedrosa, V., Collado, C., Zuñ Iga, S., Wang, G., Cade, R., Dietrich, R. A., Rogers, J., Knapp, S., Fei, Z., White, R. A., Thannhauser, T. W., Giovannoni, J. J., Botella, M. A., Gilbert, L., Gonzalez, F. R., Goicoechea, J. L., Yu, Y., Kudrna, D., Collura, K., Wissotski, M., Wing, R., Meyers, B. C., Gurazada, A. B., Green, P. J., Mathur, S., Vyas, S., Solanke, A. U., Kumar, R., Gupta, V., Sharma, A. K., Khurana, P., Khurana, J. P., Tyagi, A. K., Dalmay, T., Mohorianu, I., Walts, B., Chamala, S., Barbazuk, W. B., Li, J., Guo, H., Lee, T. H., Wang, Y., Zhang, D., Paterson, A. H., Wang, X., Tang, H., Barone, A., Chiusano, M. L., Ercolano, M. R., D'Agostino, N., Di Filippo, M., Traini, A., Sanseverino, W., Frusciante, L., Seymour, G. B., Elharam, M., Fu, Y., Hua, A., Kenton, S., Lewis, J., Lin, S., Najar, F., Lai, H., Qin, B., Shi, R., Qu, C., White, D., White, J., Xing, Y., Yang, K., Yi, J., Yao, Z., Zhou, L., Roe, B. A., Vezzi, A., D'Angelo, M., Zimbello, R., Schiavon, R., Caniato, E., Rigobello, C., Campagna, D., Vitulo, N., Valle, G., Nelson, D. R., de Paoli, E., Szinay, D., de Jong, H. H., Bai, Y., Visser, R. G., Lankhorst, R. K., Beasley, H., McLaren, K., Nicholson, C., Riddle, C., and Gianese, G. (2012). The tomato genome sequence provides insights into fleshy fruit evolution. *Nature*, 485(7400):635–641.

Schauer, N., Semel, Y., Roessner, U., Gur, A., Balbo, I., Carrari, F., Pleban, T., Perez-Melis, A., Bruedigam, C., Kopka, J., Willmitzer, L., Zamir, D., and Fernie, A. R. (2006). Comprehensive metabolic profiling and phenotyping of interspecific introgression lines for tomato improvement. *Nature Biotechnology*, 24(4):447–454.

Scheible, W. R., Krapp, A., and Stitt, M. (2000). Reciprocal diurnal changes of phosphoenolpyruvate carboxylase expression and cytosolic pyruvate kinase, citrate synthase and NADP-isocitrate dehydrogenase expression regulate organic acid metabolism during nitrate assimilation in tobacco leaves. *Plant, Cell & Environment*, 23(11):1155–1167.

Schellenberger, J., Que, R., Fleming, R. M. T., Thiele, I., Orth, J. D., Feist, A. M., Zielinski, D. C., Bordbar, A., Lewis, N. E., Rahmanian, S., Kang, J., Hyduke, D. R., and Palsson, B. (2011). Quantitative prediction of cellular metabolism with constraint-based models: The COBRA Toolbox v2.0. *Nature Protocols*, 6(9):1290–1307.

Scheunemann, M., Brady, S. M., and Nikoloski, Z. (2018). Integration of large-scale data for extraction of integrated *Arabidopsis* root cell-type specific models. *Scientific Reports*, 8(1):7919.

Schläpfer, P., Zhang, P., Wang, C., Kim, T., Banf, M., Chae, L., Dreher, K., Chavali, A. K., Nilo-Poyanco, R., Bernard, T., Kahn, D., and Rhee, S. Y. (2017). Genome-wide prediction of metabolic enzymes, pathways, and gene clusters in plants. *Plant Physiology*, 173(4):2041–2059.

Schneider, C. A., Rasband, W. S., and Eliceiri, K. W. (2012). NIH Image to ImageJ: 25 years of image analysis. *Nature Methods*, 9(7):671–675.

Schomburg, F. M., Bizzell, C. M., Lee, D. J., Zeevaart, J. A., and Amasino, R. M. (2003). Overexpression of a novel class of gibberellin 2-oxidases decreases gibberellin levels and creates dwarf plants. *Plant Cell*, 15(1):151–163.

Schwarz, D., Thompson, A. J., and Kläring, H.-P. (2014). Guidelines to use tomato in experiments with a controlled environment. *Frontiers in Plant Science*, 5:625.

Seleznyova, A. N. and Hanan, J. (2018). Mechanistic modelling of coupled phloem/xylem transport for L-systems: combining analytical and computational methods. *Annals of Botany*, 121(5):991–1003.

Shameer, S., Baghalian, K., Cheung, C. Y. M., Ratcliffe, R. G., and Sweetlove, L. J. (2018). Computational analysis of the productivity potential of CAM. *Nature Plants*, 4(3):165–171.

Shameer, S., Ratcliffe, R. G., and Sweetlove, L. J. (2019). Leaf energy balance requires mitochondrial respiration and export of chloroplast NADPH in the light. *Plant Physiology*, 180(4):1947–1961.

Shameer, S., Vallarino, J. G., Fernie, A. R., Ratcliffe, R. G., and Sweetlove, L. J. (2020). Flux balance analysis of metabolism during growth by osmotic cell expansion and its application to tomato fruits. *The Plant Journal*, 103(1):68–82.

Sharwood, R. E., Ghannoum, O., and Whitney, S. M. (2016). Prospects for improving CO_2 fixation in C_3-crops through understanding C_4-Rubisco biogenesis and catalytic diversity. *Current Opinion in Plant Biology*, 31:135–142.

Shaul, O. (2002). Magnesium transport and function in plants: the tip of the iceberg. *BioMetals*, 15(3):309–323.

Shaw, R. and Cheung, C. Y. M. (2018). A dynamic multi-tissue flux balance model captures carbon and nitrogen metabolism and optimal resource partitioning during Arabidopsis growth. *Frontiers in Plant Science*, 9:884.

Shaw, R. and Cheung, C. Y. M. (2019). A mass and charge balanced metabolic model of *Setaria viridis* revealed mechanisms of proton balancing in C_4 plants. *BMC Bioinformatics*, 20(1):1–11.

Shaw, R. and Cheung, C. Y. M. (2020). Multi-tissue to whole plant metabolic modelling. *Cellular and Molecular Life Sciences*, 77(3):489–495.

Shaw, R. and Kundu, S. (2015). Metabolic plasticity and inter-compartmental interactions in rice metabolism: an analysis from reaction deletion study. *PLoS ONE*, 10(7):e0133899.

Shi, K., Fu, L. J., Dong, D.-K., Zhou, Y. H., and Yu, J. Q. (2008). Decreased energy synthesis is partially compensated by a switch to sucrose synthase pathway of sucrose degradation in restricted root of tomato plants. *Plant Physiology and Biochemistry*, 46(12):1040–1044.

Shih, P. M., Occhialini, A., Cameron, J. C., Andralojc, P. J., Parry, M. A., and Kerfeld, C. A. (2016). Biochemical characterization of predicted Precambrian RuBisCO. *Nature Communications*, 7(1):1–11.

Shipley, B. and Meziane, D. (2002). The balanced-growth hypothesis and the allometry of leaf and root biomass allocation. *Functional Ecology*, 16(3):326–331.

Siebrecht, S., Herdel, K., Schurr, U., and Tischner, R. (2003). Nutrient translocation in the xylem of poplar — diurnal variations and spatial distribution along the shoot axis. *Planta*, 217(5):783–793.

Sievänen, R., Godin, C., de Jong, T. M., and Nikinmaa, E. (2014). Functional-structural plant models: a growing paradigm for plant studies. *Annals of Botany*, 114(4):599–603.

Simkin, A. J., Lopez-Calcagno, P. E., Davey, P. A., Headland, L. R., Lawson, T., Timm, S., Bauwe, H., and Raines, C. A. (2017). Simultaneous stimulation of sedoheptulose 1,7-bisphosphatase, fructose 1,6-bisphophate aldolase and the photorespiratory glycine decarboxylase-H protein increases CO_2 assimilation, vegetative biomass and seed yield in Arabidopsis. *Plant Biotechnology Journal*, 15(7):805–816.

Simkin, A. J., McAusland, L., Headland, L. R., Lawson, T., and Raines, C. A. (2015). Multigene manipulation of photosynthetic carbon assimilation increases CO_2 fixation and biomass yield in tobacco. *Journal of Experimental Botany*, 66(13):4075–4090.

Sinclair, T. R., Soltani, A., Marrou, H., Ghanem, M., and Vadez, V. (2020). Geospatial assessment for crop physiological and management improvements with examples using the simple simulation model. *Crop Science*, 60(2):700–708.

Smart, D. R. and Bloom, A. J. (1988). Kinetics of ammonium and nitrate uptake among wild and cultivated tomatoes. *Oecologia*, 76(3):336–340.

Smidansky, E. D., Clancy, M., Meyer, F. D., Lanning, S. P., Blake, N. K., Talbert, L. E., and Giroux, M. J. (2002). Enhanced ADP-glucose pyrophosphorylase activity in wheat endosperm increases seed yield. *Proceedings of the National Academy of Sciences of the United States of America*, 99(3):1724–1729.

Smidansky, E. D., Martin, J. M., Hannah, L. C., Fischer, A. M., and Giroux, M. J. (2003). Seed yield and plant biomass increases in rice are conferred by deregulation of endosperm ADP-glucose pyrophosphorylase. *Planta*, 216(4):656–664.

Smith, A. M. and Stitt, M. (2007). Coordination of carbon supply and plant growth. *Plant, Cell & Environment*, 30(9):1126–1149.

Snowden, C. J., Thomas, B., Baxter, C. J., Smith, J. A. C., and Sweetlove, L. J. (2015). A tonoplast Glu/Asp/GABA exchanger that affects tomato fruit amino acid composition. *The Plant Journal*, 81(5):651–660.

Soboleva, A., Schmidt, R., Vikhnina, M., Grishina, T., and Frolov, A. (2017). Maillard proteomics: opening new pages. *International Journal of Molecular Sciences*, 18(12):2677.

Song, P., Heinen, J. L., Burns, T. H., and Allen, R. D. (2000). Expression of two tissue-specific promoters in transgenic cotton plants. *Journal of Cotton Science*, 4(4):217–223.

Song, Q., Zhang, G., and Zhu, X.-G. (2013). Optimal crop canopy architecture to maximise canopy photosynthetic CO_2 uptake under elevated CO_2 — a theoretical study using a mechanistic model of canopy photosynthesis. *Functional Plant Biology*, 40(2):109–124.

Sonnewald, U. and Fernie, A. R. (2018). Next-generation strategies for understanding and influencing source-sink relations in crop plants. *Current Opinion in Plant Biology*, 43:63–70.

South, P. F., Cavanagh, A. P., Liu, H. W., and Ort, D. R. (2019). Synthetic glycolate metabolism pathways stimulate crop growth and productivity in the field. *Science*, 363(6422):eaat9077.

Stein, O. and Granot, D. (2019). An overview of sucrose synthases in plants. *Frontiers in Plant Science*, 10:95.

Stitt, M. (1986). Limitation of photosynthesis by carbon metabolism. *Plant Physiology*, 81(4):1115–1122.

Stitt, M. (1990). Fructose-2,6-bisphosphate as a regulatory molecule in plants. *Annual Review of Plant Physiology and Plant Molecular Biology*, 41(1):153–185.

Stitt, M. (1998). Pyrophosphate as an energy donor in the cytosol of plant cells: an enigmatic alternative to ATP. *Botanica Acta*, 111(3):167–175.

Stitt, M. (1999). Nitrate regulation of metabolism and growth. *Current Opinion in Plant Biology*, 2(3):178–186.

Stitt, M. and Krapp, A. (1999). The interaction between elevated carbon dioxide and nitrogen nutrition: the physiological and molecular background. *Plant, Cell & Environment*, 22(6):583–621.

Stitt, M., Lunn, J., and Usadel, B. (2010). Arabidopsis and primary photosynthetic metabolism — more than the icing on the cake. *The Plant Journal*, 61(6):1067–1091.

Stitt, M., Muller, C., Matt, P., Gibon, Y., Carillo, P., Morcuende, R., Scheible, W.-R., and Krapp, A. (2002). Steps towards an integrated view of nitrogen metabolism. *Journal of Experimental Botany*, 53(370):959–970.

Streb, S. and Zeeman, S. (2012). Starch metabolism in Arabidopsis. *The Arabidopsis Book*, 10.

Sun, A., Dai, Y., Zhang, X., Li, C., Meng, K., Xu, H., Wei, X., Xiao, G., Ouwerkerk, P. B., Wang, M., and Zhu, Z. (2011). A transgenic study on affecting potato tuber yield by expressing the rice sucrose transporter genes *OsSUT5Z* and *OsSUT2M*. *Journal of Integrative Plant Biology*, 53(7):586–595.

Sun, J., Okita, T. W., and Edwards, G. E. (1999). Modification of carbon partitioning, photosynthetic capacity, and O_2 sensitivity in Arabidopsis plants with low ADP-glucose pyrophosphorylase activity. *Plant Physiology*, 119(1):267–276.

Sweetlove, L. J. and Ratcliffe, R. G. (2011). Flux-balance modeling of plant metabolism. *Frontiers in Plant Science*, 2(8):38.

Szaniawski, R. K. and Kielkiewicz, M. (1982). Maintenance and growth respiration in shoots and roots of sunflower plants grown at different root temperatures. *Physiologia Plantarum*, 54(4):500–504.

Taira, M., Valtersson, U., Burkhardt, B., and Ludwig, R. A. (2004). *Arabidopsis thaliana* GLN2-encoded glutamine synthetase is dual targeted to leaf mitochondria and chloroplasts. *Plant Cell*, 16(8):2048–2058.

Tan, Q., Zhang, L., Grant, J., Cooper, P., and Tegeder, M. (2010). Increased phloem transport of S-methylmethionine positively affects sulfur and nitrogen metabolism and seed development in pea plants. *Plant Physiology*, 154(4):1886–1896.

Tegeder, M. (2012). Transporters for amino acids in plant cells: some functions and many unknowns. *Current Opinion in Plant Biology*, 15(3):315–321.

Tegeder, M. (2014). Transporters involved in source to sink partitioning of amino acids and ureides: opportunities for crop improvement. *Journal of Experimental Botany*, 65(7):1865–1878.

Tegeder, M. and Hammes, U. Z. (2018). The way out and in: phloem loading and unloading of amino acids. *Current Opinion in Plant Biology*, 43:16–21.

Tegeder, M. and Masclaux-Daubresse, C. (2018). Source and sink mechanisms of nitrogen transport and use. *New Phytologist*, 217(1):35–53.

Terashima, I. and Hikosaka, K. (1995). Comparative ecophysiology of leaf and canopy photosynthesis. *Plant, Cell & Environment*, 18(10):1111–1128.

Tetyuk, O., Benning, U. F., and Hoffmann-Benning, S. (2013). Collection and analysis of *Arabidopsis* phloem exudates using the EDTA-facilitated method. *Journal of Visualized Experiments*, 10(80):e51111.

Thomsen, H. C., Eriksson, D., Møller, I. S., and Schjoerring, J. K. (2014). Cytosolic glutamine synthetase: a target for improvement of crop nitrogen use efficiency? *Trends in Plant Science*, 19(10):656–663.

Thormählen, I., Ruber, J., von Roepenack-Lahaye, E., Ehrlich, S. M., Massot, V., Hümmer, C., Tezycka, J., Issakidis-Bourguet, E., and Geigenberger, P. (2013). Inactivation of thioredoxin $f1$ leads to decreased light activation of ADP-glucose pyrophosphorylase and altered diurnal starch turnover in leaves of *Arabidopsis* plants. *Plant, Cell & Environment*, 36(1):16–29.

Thornley, J. H. (1972a). A balanced quantitative model for root: shoot ratios in vegetative plants. *Annals of Botany*, 36(2):431–441.

Thornley, J. H. (1972b). A model to describe the partitioning of photosynthate during vegetative plant growth. *Annals of Botany*, 36(2):419–430.

Tomlinson, L., Yang, Y., Emenecker, R., Smoker, M., Taylor, J., Perkins, S., Smith, J., MacLean, D., Olszewski, N. E., and Jones, J. D. (2019). Using CRISPR/Cas9 genome editing in tomato to create a gibberellin-responsive dominant dwarf DELLA allele. *Plant Biotechnology Journal*, 17(1):132–140.

Tsimba, R., Edmeades, G. O., Millner, J. P., and Kemp, P. D. (2013). The effect of planting date on maize: phenology, thermal time durations and growth rates in a cool temperate climate. *Field Crops Research*, 150:145–155.

Tsuji, H., Meguro, N., Suzuki, Y., Tsutsumi, N., Hirai, A., and Nakazono, M. (2003). Induction of mitochondrial aldehyde dehydrogenase by submergence facilitates oxidation of acetaldehyde during re-aeration in rice. *FEBS Letters*, 546(2-3):369–373.

Turgeon, R. (1989). The sink-source transition in leaves. *Annual Review of Plant Physiology and Plant Molecular Biology*, 40(1):119–138.

Tzin, V. and Galili, G. (2010). New Insights into the shikimate and aromatic amino acids biosynthesis pathways in plants. *Molecular Plant*, 3(6):956–972.

Valdivia-Mares, L. E., Zaragoza, F. A., González, J. J. S., and Vargas-Ponce, O. (2016). Phenology, agronomic and nutritional potential of three wild husk tomato species (*Physalis*, Solanaceae) from Mexico. *Scientia Horticulturae*, 200:83–94.

Valle, E. M., Boggio, S. B., and Heldt, H. W. (1998). Free amino acid composition of phloem sap and growing fruit of *Lycopersicon esculentum*. *Plant and Cell Physiology*, 39(4):458–461.

van der Kooij, T. A. W. and de Kok, L. J. (1996). Impact of elevated CO_2 on growth and development of *Arabidopsis thaliana* L. *Phyton — Annales Rei Botanicae*, 36(2):173–184.

van Ieperen, W. (1996). Effects of different day and night salinity levels on vegetative growth, yield and quality of tomato. *Journal of Horticultural Science and Biotechnology*, 71(1):99–111.

Verkroost, A. W. and Wassen, M. J. (2005). A simple model for nitrogen-limited plant growth and nitrogen allocation. *Annals of Botany*, 96(5):871–876.

Vidmar, J. J., Zhuo, D., Siddiqi, M. Y., Schjoerring, J. K., Touraine, B., and Glass, A. D. (2000). Regulation of high-affinity nitrate transporter genes and high-affinity nitrate influx by nitrogen pools in roots of barley. *Plant Physiology*, 123(1):307–318.

Vitousek, P. M., Porder, S., Houlton, B. Z., and Chadwick, O. A. (2010). Terrestrial phosphorus limitation: mechanisms, implications, and nitrogen-phosphorus interactions. *Ecological Applications*, 20(1):5–15.

von Caemmerer, S. (2013). Steady-state models of photosynthesis. *Plant, Cell & Environment*, 36(9):1617–1630.

von Caemmerer, S. and Farquhar, G. D. (1984). Effects of partial defoliation, changes of irradiance during growth, short-term water stress and growth at enhanced $p(CO_2)$ on the photosynthetic capacity of leaves of *Phaseolus vulgaris* L. *Planta*, 160(4):320–329.

Voon, C. P., Guan, X., Sun, Y., Sahu, A., Chan, M. N., Gardeström, P., Wagner, S., Fuchs, P., Nietzel, T., Versaw, W. K., Schwarzländer, M., and Lim, B. L. (2018). ATP compartmentation in plastids and cytosol of *Arabidopsis thaliana* revealed by fluorescent protein sensing. *Proceedings of the National Academy of Sciences of the United States of America*, 115(45):E10778–E10787.

Voorend, W., Lootens, P., Nelissen, H., Roldán-Ruiz, I., Inzé, D., and Muylle, H. (2014). LEAF-E: a tool to analyze grass leaf growth using function fitting. *Plant Methods*, 10(1):1–13.

Walker, A. and Ho, L. (1977). Carbon translocation in the tomato: carbon import and fruit growth. *Annals of Botany*, 41:813–823.

Wang, H., Inukai, Y., and Yamauchi, A. (2006). Root development and nutrient uptake. *Critical Reviews in Plant Sciences*, 25(3):279–301.

Wang, Y. and Wu, W. H. (2013). Potassium transport and signaling in higher plants. *Annual Review of Plant Biology*, 64:451–476.

Wang, Y., Zhao, J., Lu, W., and Deng, D. (2017). Gibberellin in plant height control: old player, new story. *Plant Cell Reports*, 36(3):391–398.

Wang, Z., Xu, Y., Wang, J., Yang, J., and Zhang, J. (2012). Polyamine and ethylene interactions in grain filling of superior and inferior spikelets of rice. *Plant Growth Regulation*, 66(3):215–228.

Waris, S., Habib, S., Tantry, I. Q., Khan, R. H., Mahmood, R., and Ali, A. (2018). Acetaldehyde-induced structural and conformational alterations in human immunoglobulin G: a physicochemical and multi-spectroscopic study. *International Journal of Biological Macromolecules*, 113:701–710.

Waris, S., Patel, A., Ali, A., and Mahmood, R. (2020). Acetaldehyde-induced oxidative modifications and morphological changes in isolated human erythrocytes: an in vitro study. *Environmental Science and Pollution Research*, 27(14):16268–16281.

Watanabe, M., Balazadeh, S., Tohge, T., Erban, A., Giavalisco, P., Kopka, J., Mueller-Roeber, B., Fernie, A. R., and Hoefgen, R. (2013). Comprehensive dissection of spatiotemporal metabolic shifts in primary, secondary, and lipid metabolism during developmental senescence in Arabidopsis. *Plant Physiology*, 162(3):1290–1310.

Watanabe, M., Tohge, T., Balazadeh, S., Erban, A., Giavalisco, P., Kopka, J., Mueller-Roeber, B., Fernie, A. R., and Hoefgen, R. (2018). Comprehensive metabolomics studies of plant developmental senescence. *Methods in Molecular Biology*, 1744:339–358.

Weichert, N., Saalbach, I., Weichert, H., Kohl, S., Erban, A., Kopka, J., Hause, B., Varshney, A., Sreenivasulu, N., Strickert, M., Kumlehn, J., Weschke, W., and Weber, H. (2010). Increasing sucrose uptake capacity of wheat grains stimulates storage protein synthesis. *Plant Physiology*, 152(2):698–710.

Weiner, J., Campbell, L. G., Pino, J., and Echarte, L. (2009). The allometry of reproduction within plant populations. *Journal of Ecology*, 97(6):1220–1233.

White, A. C., Rogers, A., Rees, M., and Osborne, C. P. (2016). How can we make plants grow faster? A source-sink perspective on growth rate. *Journal of Experimental Botany*, 67(1):31–45.

White, P. J. and Broadley, M. R. (2003). Calcium in plants. *Annals of Botany*, 92(4):487–511.

Whitlow, T. H., Bassuk, N. L., Ranney, T. G., and Reichert, D. L. (1992). An improved method for using electrolyte leakage to assess membrane competence in plant tissues. *Plant Physiology*, 98(1):198–205.

Wilkinson, T. L. and Douglas, A. E. (2003). Phloem amino acids and the host plant range of the polyphagous aphid, *Aphis fabae*. *Entomologia Experimentalis et Applicata*, 106(2):103–113.

Winter, G., Todd, C. D., Trovato, M., Forlani, G., and Funck, D. (2015). Physiological implications of arginine metabolism in plants. *Frontiers in Plant Science*, 6(7):534.

Winter, H., Lohaus, G., and Heldt, H. W. (1992). Phloem transport of amino acids in relation to their cytosolic levels in barley leaves. *Plant Physiology*, 99(3):996–1004.

Witte, C. P. (2011). Urea metabolism in plants. *Plant Science*, 180(3):431–438.

Woo, H. R., Kim, H. J., Lim, P. O., and Nam, H. G. (2019). Leaf Senescence: systems and dynamics aspects. *Annual Review of Plant Biology*, 70:347–376.

Wu, A., Hammer, G. L., Doherty, A., von Caemmerer, S., and Farquhar, G. D. (2019). Quantifying impacts of enhancing photosynthesis on crop yield. *Nature Plants*, 5(4):380–388.

Wu, L., El-Mezawy, A., and Shah, S. (2011). A seed coat outer integument-specific promoter for *Brassica napus*. *Plant Cell Reports*, 30(1):75–80.

Wu, Z., Tang, D., Liu, K., Miao, C., Zhuo, X., Li, Y., Tan, X., Sun, M., Luo, Q., and Cheng, Z. (2018). Characterization of a new semi-dominant dwarf allele of *SLR1* and its potential application in hybrid rice breeding. *Journal of Experimental Botany*, 69(20):4703–4713.

Würschum, T., Langer, S. M., Longin, C. F. H., Tucker, M. R., and Leiser, W. L. (2017). A modern Green Revolution gene for reduced height in wheat. *The Plant Journal*, 92(5):892–903.

Xu, C., Liberatore, K. L., Macalister, C. A., Huang, Z., Chu, Y. H., Jiang, K., Brooks, C., Ogawa-Ohnishi, M., Xiong, G., Pauly, M., van Eck, J., Matsubayashi, Y., van der Knaap, E., and Lippman, Z. B. (2015). A cascade of arabinosyltransferases controls shoot meristem size in tomato. *Nature Genetics*, 47(7):784–792.

Xu, G., Fan, X., and Miller, A. J. (2012). Plant nitrogen assimilation and use efficiency. *Annual Review of Plant Biology*, 63:153–182.

Xue, H., Zhang, Y., and Xiao, G. (2020). Neo-gibberellin signaling: guiding the next generation of the Green Revolution. *Trends in Plant Science*, 25(6):520–522.

Xue, M., Long, Y., Zhao, Z., Huang, G., Huang, K., Zhang, T., Jiang, Y., Yuan, Q., and Pei, X. (2018). Isolation and characterization of a green-tissue promoter from common wild rice (*Oryza rufipogon* griff.). *International Journal of Molecular Sciences*, 19(7):2009.

Yadav, U. P., Ayre, B. G., and Bush, D. R. (2015). Transgenic approaches to altering carbon and nitrogen partitioning in whole plants: assessing the potential to improve crop yields and nutritional quality. *Frontiers in Plant Science*, 6(4):275.

Yamamoto, H., Peng, L., Fukao, Y., and Shikanai, T. (2011). An Src homology 3 domain-like fold protein forms a ferredoxin binding site for the chloroplast NADH dehydrogenase-like complex in *Arabidopsis*. *The Plant Cell*, 23(4):1480–1493.

Yan, H. P., Meng, Z. K., de Reffye, P., and Dingkuhn, M. (2004). A dynamic, architectural plant model simulating resource-dependent growth. *Annals of Botany*, 93(5):591–602.

Yang, J., Zhang, J., Wang, Z., Zhu, Q., and Wang, W. (2001). Hormonal changes in the grains of rice subjected to water stress during grain filling. *Plant Physiology*, 127(1):315–323.

Yang, Y., Hu, X. P., and Ma, B. G. (2017). Construction and simulation of the *Bradyrhizobium diazoefficiens* USDA110 metabolic network: a comparison between free-living and symbiotic states. *Molecular BioSystems*, 13(3):607–620.

Yao, X., Nie, J., Bai, R., and Sui, X. (2020). Amino acid transporters in plants: identification and function. *Plants*, 9(8):972.

Yin, L. H., Choon, Y. W., En Chai, L., Chong, C. K., Deris, S., Illias, R. M., and Mohamad, M. S. (2013). Prediction of vanillin production in yeast using a hybrid of continuous bees algorithm and flux balance analysis (CBAFBA). *Studies in Computational Intelligence*, 477:101–116.

Yin, X., Goudriaan, J., Lantinga, E. A., Vos, J., and Spiertz, H. J. (2003). A flexible sigmoid function of determinate growth. *Annals of Botany*, 91(3):361–371.

Yin, Y., Chen, L., and Beachy, R. (1997). Promoter elements required for phloem-specific gene expression from the RTBV promoter in rice. *The Plant Journal*, 12(5):1179–1188.

Yuan, H., Cheung, C. Y., Poolman, M. G., Hilbers, P. A., and van Riel, N. A. (2016a). A genome-scale metabolic network reconstruction of tomato (*Solanum lycopersicum* L.) and its application to photorespiratory metabolism. *The Plant Journal*, 85(2):289–304.

Yuan, H., Cheung, C. Y. M., Hilbers, P. A. J., and van Riel, N. A. W. (2016b). Flux balance analysis of plant metabolism: the effect of biomass composition and model structure on model predictions. *Frontiers in Plant Science*, 7:537.

Zakhartsev, M., Medvedeva, I., Orlov, Y., Akberdin, I., Krebs, O., and Schulze, W. X. (2016). Metabolic model of central carbon and energy metabolisms of growing *Arabidopsis thaliana* in relation to sucrose translocation. *BMC Plant Biology*, 16(1):262.

Zhang, H., Rong, H., and Pilbeam, D. (2007). Signalling mechanisms underlying the morphological responses of the root system to nitrogen in *Arabidopsis thaliana*. *Journal of Experimental Botany*, 58(9):2329–2338.

Zhang, J., Tian, H., Yang, J., and Pan, S. (2018). Improving representation of crop growth and yield in the dynamic land ecosystem model and its application to China. *Journal of Advances in Modeling Earth Systems*, 10(7):1680–1707.

Zhang, L., Garneau, M. G., Majumdar, R., Grant, J., and Tegeder, M. (2015). Improvement of pea biomass and seed productivity by simultaneous increase of phloem and embryo loading with amino acids. *The Plant Journal*, 81(1):134–146.

Zhang, L., Häusler, R. E., Greiten, C., Hajirezaei, M. R., Haferkamp, I., Neuhaus, H. E., Flügge, U. I., and Ludewig, F. (2008). Overriding the co-limiting import of carbon and energy into tuber amyloplasts increases the starch content and yield of transgenic potato plants. *Plant Biotechnology Journal*, 6(5):453–464.

Zhang, M., Nagata, S., Miyazawa, K., Kikuchi, H., and Esashi, Y. (1997). A competitive enzyme-linked immunosorbent assay to quantify acetaldehyde-protein adducts that accumulate in dry seeds during aging. *Plant Physiology*, 113(2):397–402.

Zhu, X. and Galili, G. (2004). Lysine metabolism is concurrently regulated by synthesis and catabolism in both reproductive and vegetative tissues. *Plant Physiology*, 135(1):129–136.

Zhu, X.-G., Long, S. P., and Ort, D. R. (2010). Improving photosynthetic efficiency for greater yield. *Annual Review of Plant Biology*, 61(1):235–261.

Zhu, X.-G., Lynch, J. P., Lebauer, D. S., Millar, A. J., Stitt, M., and Long, S. P. (2016). Plants *in silico*: why, why now and what? — an integrative platform for plant systems biology research. *Plant Cell and Environment*, 39(5):1049–1057.

Zhu, X.-G., Wang, Y., Ort, D. R., and Long, S. P. (2013). *e*-photosynthesis: a comprehensive dynamic mechanistic model of C_3 photosynthesis: from light capture to sucrose synthesis. *Plant, Cell & Environment*, 36(9):1711–1727.

Zsögön, A., Čermák, T., Naves, E. R., Notini, M. M., Edel, K. H., Weinl, S., Freschi, L., Voytas, D. F., Kudla, J., and Peres, L. E. P. (2018). De novo domestication of wild tomato using genome editing. *Nature Biotechnology*, 36(12):1211–1216.

A | Supplementary data

Tables A.1 and A.2 provide detailed summaries of the biomass and phloem compositions, respectively, in Arabidopsis used to constrain reactions in SoFBA and SiFBA in the FM-SoFBA-SiFBA framework.

Tables A.3 and A.4 provide detailed summaries of the biomass and phloem compositions, respectively, in tomato used to constrain WholePlantMetabolism. Table A.5 provides a detailed summary of the dynamic biomass composition used to constrain fruit models in WholePlantMetabolism v2. Due to its large size, Table A.5 is only available electronically and can be retrieved from the Oxford University Research Archive (https://www.ora.ox.ac.uk), Bodleian Libraries, Osney One, Osney Mead, Oxford, OX2 0EW.

Lastly, Figure A.1 shows the water content of leaf, root, stem, and fruit organs measured at each harvest date in the validation dataset (tomato).

Table A.1: The relative abundance of biomass components in Arabidopsis. Various compositions from different sources are shown: *A* refers to cell culture data from Poolman et al. (2009), *B* refers to leaf data from Arnold and Nikoloski (2014), *C* refers to leaf data from de Oliveira Dal'Molin et al. (2015), and *D* refers to root data from de Oliveira Dal'Molin et al. (2015). Data were used to constrain the biomass composition in SiFBA in the FM-SoFBA-SiFBA framework.

Compound	Relative abundance (%)			
	A	B	C	D
Cellulose	29.18	12.15	15.11	24.56
Fatty acids	4.29	4.88	5.93	1.80
Glycerol	1.96	-	-	-
Starch	4.11	9.84	6.84	24.23
Xylan	6.32	-	-	-
Protein amino acids				
Alanine	2.54	7.70	2.77	1.85
Arginine	1.39	2.26	4.27	2.85
Asparagine	1.36	2.25	10.02	6.68
Aspartate	1.36	3.35	4.19	2.79
Cysteine	-	1.04	0.62	0.41
Glutamate	1.64	3.80	10.25	6.83
Glutamine	1.64	1.66	8.93	5.95
Glycine	1.15	9.10	3.52	2.34
Histidine	0.44	1.11	0.67	0.45
Isoleucine	0.92	2.99	1.55	1.03
Leucine	2.00	5.30	3.62	2.41
Lysine	1.43	3.45	1.81	1.21
Methionine	0.61	1.11	0.05	0.03
Phenylalanine	1.32	2.20	2.07	1.38
Proline	-	3.59	0.26	0.17
Serine	2.03	4.90	5.66	3.77
Threonine	1.15	4.34	2.24	1.49
Tryptophan	-	0.55	1.03	0.69
Tyrosine	0.92	1.56	0.78	0.52
Valine	1.74	4.88	2.59	1.72
Soluble metabolites				
Alanine	2.54	-	-	-
Aspartate	0.52	-	-	-
Citrate	1.47	-	-	-
Fructose	-	0.40	1.37	1.27
Fumarate	0.03	2.24	-	-
γ-aminobutyric acid	0.54	-	-	-
Glucose	-	0.62	1.37	1.27
Glutamate	1.77	-	-	-
Glutamine	1.94	-	-	-
Malate	2.39	1.70	-	-
Succinate	0.37	-	-	-
Sucrose	0.78	1.02	2.47	2.28
Minerals				
Calcium	4.90	-	-	-
Magnesium	3.23	-	-	-
Potassium	10.02	-	-	-

Table A.2: The relative abundance of soluble amino acids and carbohydrates in Arabidopsis phloem sap. Values were taken from Wilkinson and Douglas (2003). Data were used to constrain the phloem composition in SoFBA and SiFBA in the FM-SoFBA-SiFBA framework.

Metabolite	Relative abundance (%)
Alanine	3.03
Arginine	0.50
Asparagine	3.16
Aspartate	2.97
Glutamate	3.56
Glutamine	10.38
Glycine	0.22
Histidine	0.13
Isoleucine	0.38
Leucine	0.38
Lysine	0.56
Methionine	0.22
Phenylalanine	0.34
Serine	2.41
Sucrose	68.75
Threonine	1.75
Tryptophan	0.28
Tyrosine	0.19
Valine	0.75

Table A.3: The relative abundance of biomass components in vegetative tissues in tomato. Values for leaf biomass were taken from Yuan et al. (2016a), and values for stem and root biomass were taken from Poorter and Bergkotte (1992). Data were used to constrain the biomass composition in the WholePlantMetabolism model.

Compound	Relative abundance (%)		
	Leaf	Stem	Root
Cellulose	41.42	19.44	24.67
Fatty acids	0.41	2.34	1.70
Starch	11.66	14.33	24.33
Protein amino acids			
Alanine	0.34	2.30	1.86
Arginine	0.07	3.56	2.86
Asparagine	0.06	8.30	6.70
Aspartate	1.73	3.48	2.80
Cysteine	-	0.51	0.42
Glutamate	3.13	8.51	6.87
Glutamine	0.92	7.40	5.97
Glycine	-	2.91	2.35
Histidine	-	0.56	0.45
Isoleucine	0.25	1.27	1.02
Leucine	0.14	2.98	2.40
Lysine	0.02	1.48	1.19
Methionine	0.01	0.03	0.03
Phenylalanine	0.20	1.71	1.39
Proline	5.07	0.21	0.17
Serine	1.33	4.67	3.68
Threonine	4.08	1.86	1.50
Tryptophan	0.76	0.78	0.57
Tyrosine	0.04	0.65	0.57
Valine	0.30	2.08	1.70
Soluble metabolites			
Fructose	7.14	2.28	1.27
Glucose	16.36	2.28	1.27
Sucrose	4.54	4.10	2.29

Table A.4: The relative abundance of soluble amino acids and carbohydrates in tomato phloem sap. Values were taken from Valle et al. (1998) and Walker and Ho (1977). Data were used to constrain the phloem composition in the WholePlantMetabolism model.

Metabolite	Relative abundance (%)
Alanine	0.40
Arginine	0.04
Aspargine	0.16
Aspartate	0.63
Cysteine	0.04
Fructose	8.25
γ-aminobutyric acid	0.24
Glucose	7.22
Glutamate	1.29
Glutamine	2.51
Glycine	0.07
Histidine	0.04
Isoleucine	0.18
Leucine	0.21
Lysine	0.23
Methionine	0.04
Phenylalanine	0.59
Proline	0.04
Serine	0.41
Sucrose	76.29
Threonine	0.72
Tryptophan	0.04
Tyrosine	0.04
Valine	0.29

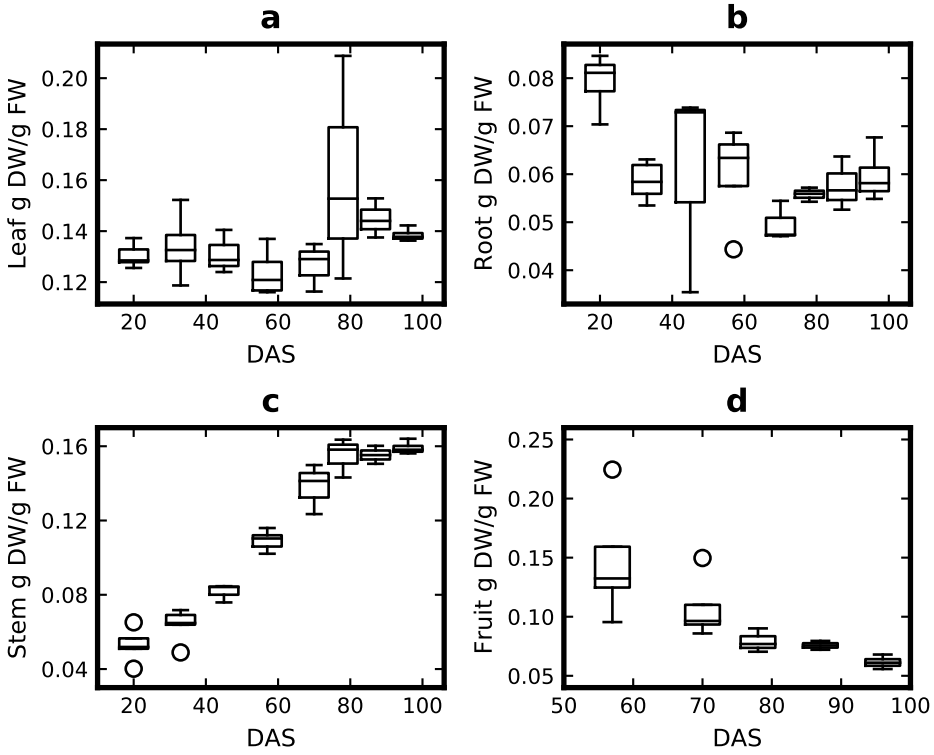

Figure A.1: Variations in water content in different tomato organs measured in the validation dataset: **(a)** leaf, **(b)** root, **(c)** stem, and **(d)** fruit. ANOVA tests revealed that the water content of root, stem, and fruit organs showed significant variations between harvests/over plant development. Only leaf water content remained constant throughout the growth period. DAS, days after sowing; DW, dry weight; FW, fresh weight.

B | Model code

The code for the two models presented in this thesis (FM-SoFBA-SiFBA and Whole-PlantMetabolism) can be retrieved from the Oxford University Research Archive (https://www.ora.ox.ac.uk), Bodleian Libraries, Osney One, Osney Mead, Oxford, OX2 0EW. The models are also hosted at https://github.com/taritkonuntakiet/dphil-fba-models, where a brief explanation of how to simulate the models is also provided. Note that software and packages required by the models are not provided.